A CONSTRAINED SHORT TENSION TEST

FOR PLANE STRESS FRACTURE

TOUGHNESS TESTING OF

THIN MATERIALS

By

KALRAV BUCH

Bachelor in Mechanical Engineering
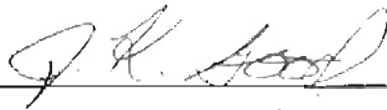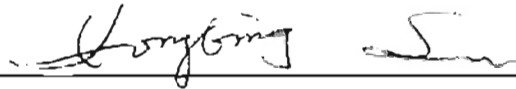
Gujarat University

Amdavad, India

1994

A CONSTRAINED SHORT TENSION TEST

FOR PLANE STRESS FRACTURE

TOUGHNESS TESTING OF

THIN MATERIALS

Thesis Approved:

_____
Thesis Advisor

_____

_____

_____
Dean of the Graduate College

This work is dedicated to
two 'G'iants in my life,
Ikaka,
and
Jerry Dale.

ACKNOWLEDGMENTS

TABLE OF CONTENTS

LIST OF TABLES

LIST OF FIGURES

NOMENCLATURE

$2a_0$	Initial crack length
Δa	Crack extension
B and t	Thickness of the test specimen
C	Constant
E	Modulus of elasticity
G	(i) Energy release rate, (ii) Sheet grammage
2H	Height of the test specimen
J_i	J-integral value for crack initiation
Jp	J-integral value for crack propagation
K_{IC}	Mode-I plane strain fracture toughness
K_C	Plane stress fracture toughness
K_{1e}	Apparent stress intensity (Feddersen approach)
K_0	Initiation fracture toughness
K_{plat}	Plateau fracture toughness
K and K_I	Stress intensity factor
K_R	Crack growth resistance
K_G	Crack driving force
L	Ligament length
P	Tensile load on the test specimen

2W	Width of the test specimen
W_f	Total work of fracture
w_f	Specific work of fracture
w_e	Specific essential work of fracture
w_p	Non-essential, or plastic work of fracture
σ_c	Critical stress value for the test specimen
σ_x	Stress along x-axis
σ_y	Stress along y-axis
σ_{ys}	Yield stress
σ_{gross}	Gross stress value for the test specimen
σ_{net}	Net stress value for the test specimen
ν	Poisson's ratio
CST	Constrained short tension
LEFM	Linear elastic fracture mechanics
MD	Machine direction
CD	Cross direction

CHAPTER 1

INTRODUCTION TO FRACTURE TESTING OF THIN MATERIALS

1.1 Background and motivation

Fracture toughness is the resistance of a material to the propagation of a pre-existing flaw or crack. It determines the flaw-carrying ability of the material. Resistance to cracking under tensile loading is an important property of thin materials, as defects and runnability of thin materials (such as web materials) influence economics of manufacturing, other processing operations and end use. Ongoing research efforts attempt to find a connection between web breaks, web defects, and measurable properties of such materials. Here, the generic term 'thin materials' includes papers, polymer films, metallic sheets, foils, and textiles. The processes used to manufacture such thin materials introduce morphological characteristics that cannot be reproduced in bulk samples of the same. Therefore, a fracture test for thin materials is very important. Whereas fracture testing of bulk materials in plane strain is relatively well developed and standardized [1], the fracture of thin materials has been less widely studied. There is no standard method of plane stress fracture toughness (K_c) testing of thin materials such as papers and polymer films.

Currently used practices to measure the resistance to crack propagation are questionable. Most polymer film tests are generally adopted from paper testing methods [2-4]. The traditional trouser leg tear test (Elmendorf test) for measuring polymer film toughness results in mixed-mode failure, and does not

1

give a value of the desired mode I fracture toughness [5]. The resistance of paper to crack propagation is currently measured by the Elmendorf or Brecht-Imset tear tests [2,3]. During paper manufacturing, printing and many converting operations, however, crack propagation failures are due to stresses applied in the plane of the sheet [6-8]. In-plane mechanical properties, therefore, should be more relevant to end use than out-of-plane tear tests [5,9-12]. The modes of crack propagation in a thin material under the action of in-plane and out-of-plane forces are shown in Figure 1.1, for better understanding of this argument.

A fifteen month long investigation on newsprint showed that breaks in a pressroom (pressroom runnability) can be correlated with in-plane strength property of paper (fracture resistance), but not with Elmendorf tearing resistance [13]. A separate investigation supported the same opinion [14]. It is surprising that established practices disregard such an observation.

The need for better mechanical reliability of microelectronics packaging and better experimental and data-recording procedures have encouraged measurement of in-plane fracture toughness of thin materials [15-17]. However, the test methods for measuring the in-plane fracture toughness of thin materials are complex and unsatisfactory [11,19-23]. Valid plane stress fracture toughness testing has to follow many constraints. Plane stress fracture toughness (K_c), being thickness dependent, is not a material constant with general validity like plane strain fracture toughness (K_{Ic}). Plane stress fracture testing methods depend on the load-elongation behavior of the material. Some typical
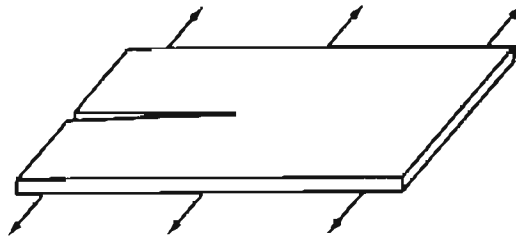
(a)
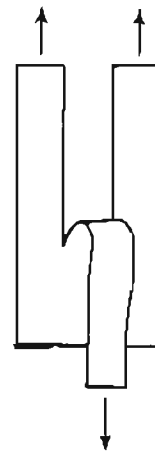
(b) 'Trouser' tear   (c) 'Tongue' tear

Figure 1.1: The modes of crack propagation in a thin material under the action of (a) in-plane, and (b), (c) out-of-plane forces.

stress/strain curves for polymer films are shown in Figure 1.2 to represent certain types of load-elongation behavior.

Current test methods favor Single Edge Notched Tensile (SENT) or Double Edge Notched Tensile (DENT) geometry and a small specimen size for in-plane fracture toughness testing. The nonsingular term σ in the stress field equations for a cracked plate in uniaxial tension indicates that the stress σ_x along the edges of the crack is compressive and of the order of the applied longitudinal tensile stress σ_y [22,23]. In thin materials, this compressive stress causes buckling of the specimen segment adjacent to crack. One can easily demonstrate this buckling by manually pulling a sheet of paper with a central transverse tear. Buckling can affect slow crack growth and residual strength [22,24]. Anti-buckling devices are used by all test methods to prevent the local *buckling of the specimen* near the crack. Figure 1.3 illustrates the crack buckling problem and the use of anti-buckling guides. The adjustment of these anti-buckling plates is critical. Too small a clearance between plates and the specimen results in friction between the specimen and the anti-buckling plates, causing inaccuracies in the estimation of the stress-intensity factor. If the clearance is too large, buckling occurs and the stress-intensity factor is not the same as given by the standard solutions [19,20]. Additionally, an edge crack does not provide a very good check over whether the specimen is pulled in a single plane or not. Plane stress fracture testing favors use of large, center cracked specimens [22,23].
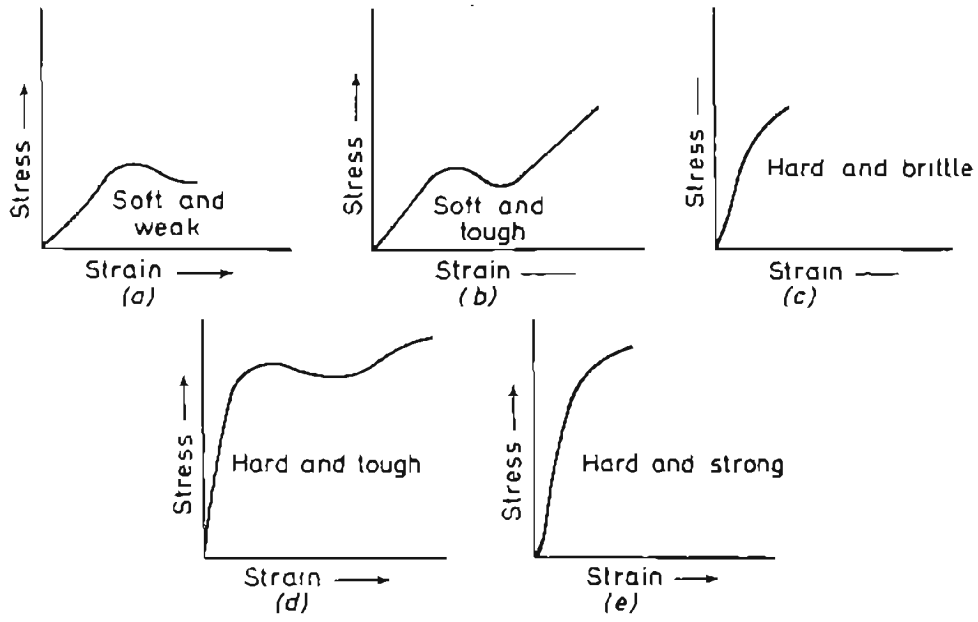
Figure 1.2: Typical stress/strain curves obtained with polymer films [4].

(a)   (b)
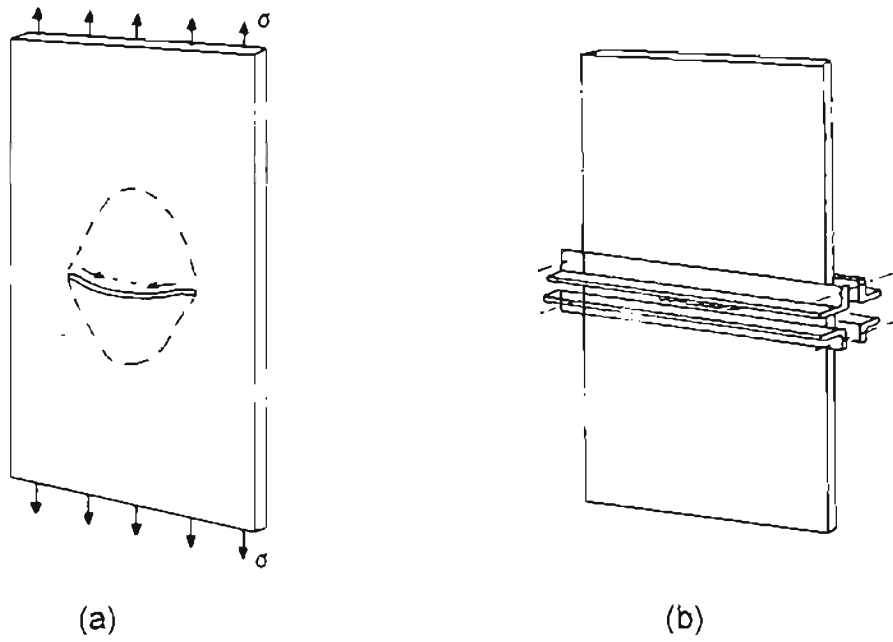
Figure 1.3: (a) Crack buckling, and (b) the use of anti-buckling guides [22]

Table 1.1 lists the mode I fracture toughness values for Kapton 100 HN and 300 HN polyimide film specimens of SENT and CST (constrained short tension) geometries, as reported in the literature [5,15,16,19,20]. Disagreement among these values is easily observed. Table 1.2 and 1.3, adopted from a standard handbook of film properties, are representative of currently available and used mechanical properties data [25]. As observed from Table 1.2, nothing is mentioned about the fracture toughness of Kapton polyimide film, while Table 1.3 reports out-of-plane tear strength values for Ube Upilex polyimide film. These tables illustrate that the measurement of plane stress fracture toughness (K_c) in thin materials is not routine.

Table 1.1: Fracture toughness values for Kapton 100 HN and 300 HN polyimide films as reported in the literature.

Kapton 100 HN polyimide film				
Specimen geometry	SENT	SENT	SENT	CST
Specimen thickness	25 μm	25 μm	25 μm	25 μm
Fracture toughness K_c, MPa $\sqrt{m}$				
Initiation K_c	1.67 ± 0.11	Limiting K_c	1.65 ± 0.14	2.88
Plateau K_c	3.64 ± 0.23	5.3	N.A.	5.0
Reference	[5]	[15]	[16]	[20]

Kapton 300 HN polyimide film		
Specimen geometry	SENT	CST
Specimen thickness	75 μm	75 μm
Fracture toughness K_c, MPa $\sqrt{m}$		
Initiation K_c	Limiting K_c	2.96
Plateau K_c	7.5	4.66
Reference	[15]	[19,20]

Table 1.2: Mechanical properties of DuPont company Kapton polyimide film [25]

	Kapton Type-V	Kapton Type-K	Kapton Type-E
Sample thickness	0.076 mm	0.076 mm	0.076 mm
Modulus of Elasticity (MPa)	2756	4341	5512
Ultimate Elongation (%)	80	80	40

Table 1.3: Mechanical properties of Ube Upilex polyimide film [25].

	UBE Upilex R	UBE Upilex S
Sample thickness	0.025 mm	0.025 mm
Density (g/cm^3)	1.39	1.47
Test Temperature (°C)	25	25
Modulus of Elasticity - MD (MPa)	3728	8190
Tensile strength - MD (MPa)	245	392
Strength @ 5% elongation -- MD (MPa)	118	255
Ultimate elongation -- MD (%)	130	30
Tear strength, propagated, Elmendorf - MD (g/mm)	750	330
Folding endurance (cycles)	100,000	100,000
Co-efficient of friction --kinematic, film to film	0.4	0.4

1.2 A new biaxial stress test method for mode I fracture testing of thin materials

Recently, a simple constrained short tension (CST) test that makes use of Poisson's effect to induce a transverse tensile stress that helps to prevent buckling has been developed by some researchers [19-21]. It offers the following attractive features:

- Thin materials can be tested without the use of anti-buckling devices.

- Large centrally notched specimens are used, the preferred mode for plane stress fracture toughness testing.

- Linear Elastic Fracture Mechanics (LEFM) and J-integral are applicable.

- Accurate measurement of crack length is unnecessary for the determination of fracture toughness.

- Biaxial loading does not affect the fracture toughness or crack growth rate as long as the plastic zone is dominated by the K-field [26].

The only limitation is the constraint related to the specimen size and geometry. The size of the specimen is limited by the height, and not by the width. Finite empirical relationships between height, width and the crack size of the specimen have been suggested in the literature [19-21]. Further work is required to establish minimum size requirements.

1.3 Objectives

The objective of this study is to explore the scope of the CST test for mode I fracture of thin materials. Specifically,

(1) To design and to make a CST test grip fixture to hold the short and wide specimens in a single plane without slip when loaded in tension. Also, to develop fixture attachments and accessories to facilitate easy specimen handling, alignment of clamps and uniform grip pressure.

(2) To develop an experimental apparatus and a test procedure for fracture testing of thin materials. To optimize test variables such as crosshead speed, preload, grip pressure.

(3) To compare the CST test with the practices in mode I fracture testing of thin materials.

(4) To explore geometrical and size constraints and their effects on the fracture toughness data.

(5) To investigate the crack growth behavior during the CST test conditions.

The specimens of different sizes and geometries, made of a variety of materials, such as metal foils and shim stocks, copier paper, waxed paper, PET (polyethylene terephthalate), polypropylene, polyester and polyethylene films will be utilized during the exploratory phase of research. The use of a CST specimen will be investigated for testing thin materials whose fracture characteristics can be described by LEFM. All the testing will be carried out on the Instron series 4202 (Electromechanical) universal testing system operating at a constant crosshead speed. An XY recorder and a PC based data acquisition

system will be used for recording the load-elongation data. To relate the crack extension to the load-elongation data, a complete test run will be videotaped. Effects of variables such as strainrate, viscoelasticity, temperature and humidity will not be investigated in this study.

CHAPTER 2

REVIEW OF LITERATURE

2.1 General remarks

Plane stress problems are more complicated than plane strain problems, especially because the plane stress behavior is still insufficiently understood [22]. Plane stress fracture properties are very sensitive to specimen size and geometry, and the test methodology. Much of the present understanding of the plane stress behavior of materials can be attributed to earlier fracture studies of aircraft sheet structures. The very useful theoretical contributions of those studies include R curve analysis, analysis of Feddersen, and thickness model of Anderson [22,23]. LEFM could effectively analyze the aircraft sheet structures (typically 3 to 4 mm thick) made of aluminum alloys, which limited further theoretical development for materials described by plane stress ductile fracture. Two very useful approaches for plane stress ductile fracture, J-integral and "essential work of fracture" were developed later. The J-integral is a well-established fracture criterion [27-29]. The use of essential work of fracture approach has been very popular in recent paper and polymer film fracture studies [10-12, 30-33]. This approach is briefly discussed in the succeeding section. The remaining of this chapter provides a concise account of plane stress fracture toughness testing studies of metals, papers, and polymers.

2.2 Essential work of fracture (EWF) approach

The development of essential work of plane stress ductile fracture can be credited to Broberg [34,35] and Cotterell et al. [36,37]. Broberg suggested that the non-elastic region at the tip of the crack should be divided into two regions (Figure 2.1):

(1) End region – where fracture process takes place, and

(2) Outer region – where screening plastic deformation is necessary to accommodate the large strains in the end region.

In the case of ductile fracture in thin sheets, the end region can be identified with necking. The work performed in this end region is known as "essential work of fracture". It can be considered autonomous and a candidate for the status of a material constant [36]. The plastic deformation and the associated work performed in the outer region will depend on the particular geometry of the specimen and is not an autonomous material constant.

In LEFM, if the plastic region at the tip of the crack is small, the work of fracture per unit area is $G = K^2/E$ (for plane stress). In ductile materials only a proportion of this work flows to the end region. If the proportion remains constant, as it may for long cracks in large sheets under similar loading conditions, the LEFM approach can be used. However, if the plastic region is not small compared with the crack length, or the geometry of the loading varies, the proportion of the work flowing to the end region is not constant and the LEFM approach is inadequate.
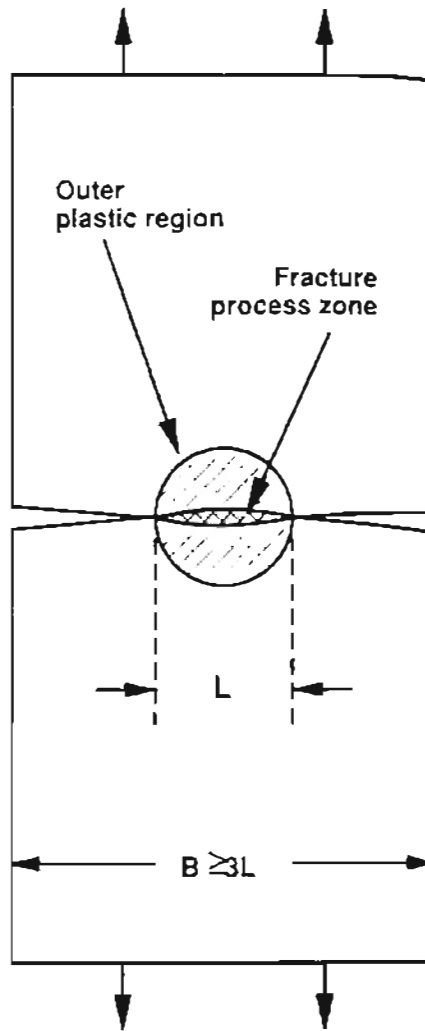
Figure 2.1: The fracture process zone and the outer plastic region of DENT specimen

Broberg [35] suggested that as the crack grows, the screening action of the outer plastic region increases, reducing the proportion of the total energy released that reaches the end region. This concept explains stable sub-critical crack growth without a change in the fracture mechanism.

Attempts to relate crack opening displacement (COD) with the essential work of fracture were also mentioned, however Cotterell et al. proposed a more direct measurement of the essential work [36]. The fracture studies of the same proved deeply double edge notched (DENT) specimens to be the most useful in separating the essential work of fracture from the total fracture work. The fracture theory of DENT specimens developed by Cotterell et al. is briefly presented here.

If a DENT specimen yields completely before fracture, the plastic region is almost circular with the ligament length L as a diameter (Figure 2.2). Assuming that the specific essential work (i.e., essential work per unit fracture area) remains constant,

essential work, $w_e \propto$ ligament length, L,

and

non-essential work, $w_p \propto L^2$,

the total work of fracture (W_f) can be written as,

$$W_f = Lt\, w_e + L^2 w_p \dots\dots\dots\dots\dots\dots\dots\dots\dots\dots\dots\dots\dots\dots\dots\dots\dots\dots\dots\dots(2.1)$$

where, t is the specimen thickness.

Therefore, the specific work of fracture (w_f) is,

$$w_f = W_f/Lt = w_e + L w_p \dots\dots\dots\dots\dots\dots\dots\dots\dots\dots\dots\dots\dots\dots\dots\dots\dots\dots\dots(2.2)$$
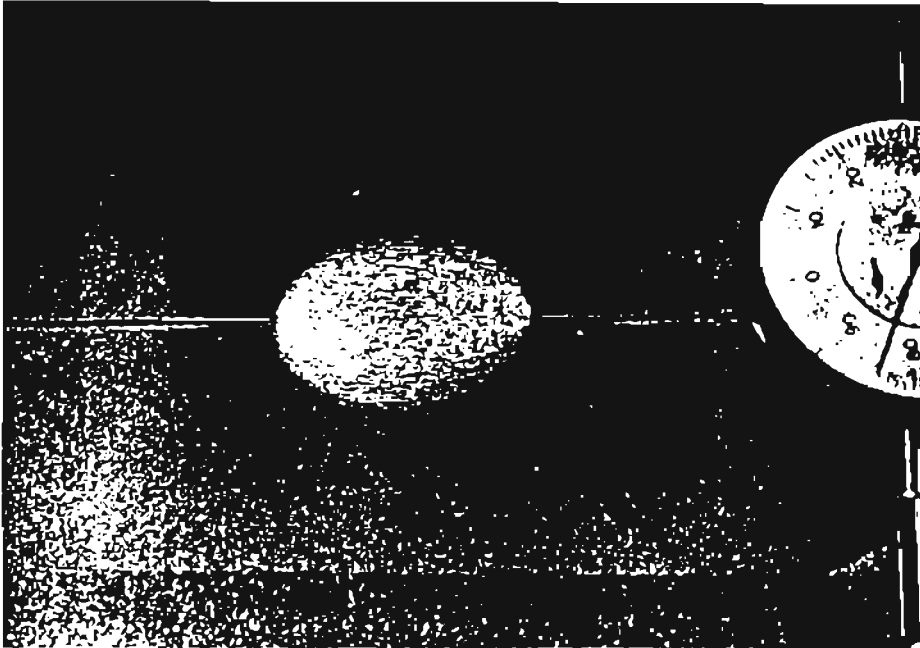
(a) Plastic region in a DENT specimen. The region is detected by the use of a brittle lacquer. The camera angle is 45° to the sheet for clarity. The circular dial gauge face is shown for comparison [36].
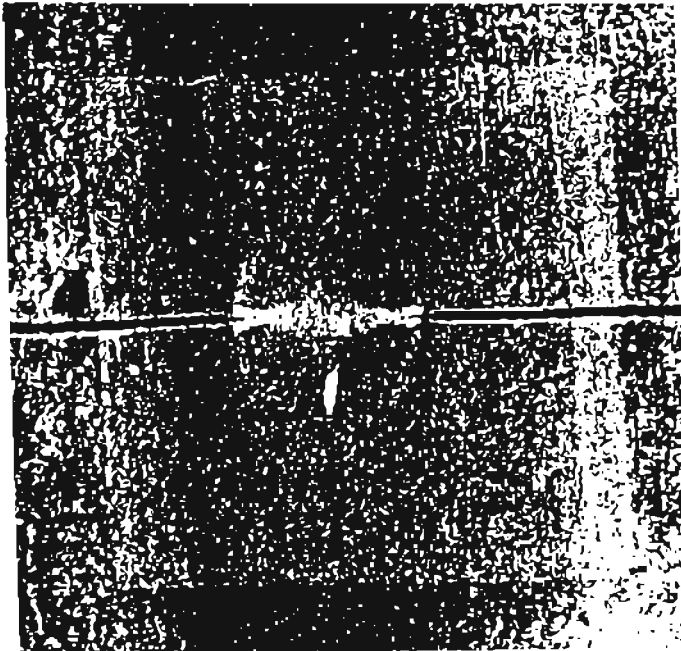
(b) Transverse strain in plastic region [36].

Figure 2.2: Circular plastic region of the DENT specimen with the ligament length, L, as a diameter.

Equation (2.2) represents a straight line with a positive intercept which is the specific essential work, (w_e), if the specific work of fracture is plotted against the ligament length L. Figure 2.3 is a collection of load-elongation curves and the specific work of fracture against ligament length plots for various materials from the literature. Equation (2.2) is valid only if there is complete yielding of the ligament before crack initiation and the ligament is in a state of plane stress. Therefore, Cotterell et al. suggested an upper and lower limit to the ligament length L for which equation (2.2) is valid. The lower limit is governed by the sheet thickness and is of the order L > 5t. The upper limit is determined by the size of the plastic region ahead of a crack in a large sheet, unless buckling occurs at the large length/thickness ratio. The ligament length, L, should not be larger than the plastic region. Thus, LEFM gives an upper limit. The ligament length must lie between the limits

$$\frac{1}{\pi}\left(\frac{K}{\sigma_y}\right)^2 > L > 5t \quad \dots\dots\dots\dots\dots\dots\dots\dots\dots\dots\dots\dots\dots\dots\dots\dots\dots\dots\dots\dots\dots\dots\dots\dots\dots(2.3)$$

The specific essential work of fracture (w_e) has been claimed by all workers to be independent of the specimen size and geometry and recognized as the fracture toughness of the material [10, 11, 30-33, 36, 37]. Like K_c, the specific essential work, w_e, is a function of the specimen thickness. 'w_e' increases with the specimen thickness [36]. In their modified analysis later, Cotterell et al. [37] identified w_e with J-integral values for crack initiation (J_i) and propagation (J_p).

17
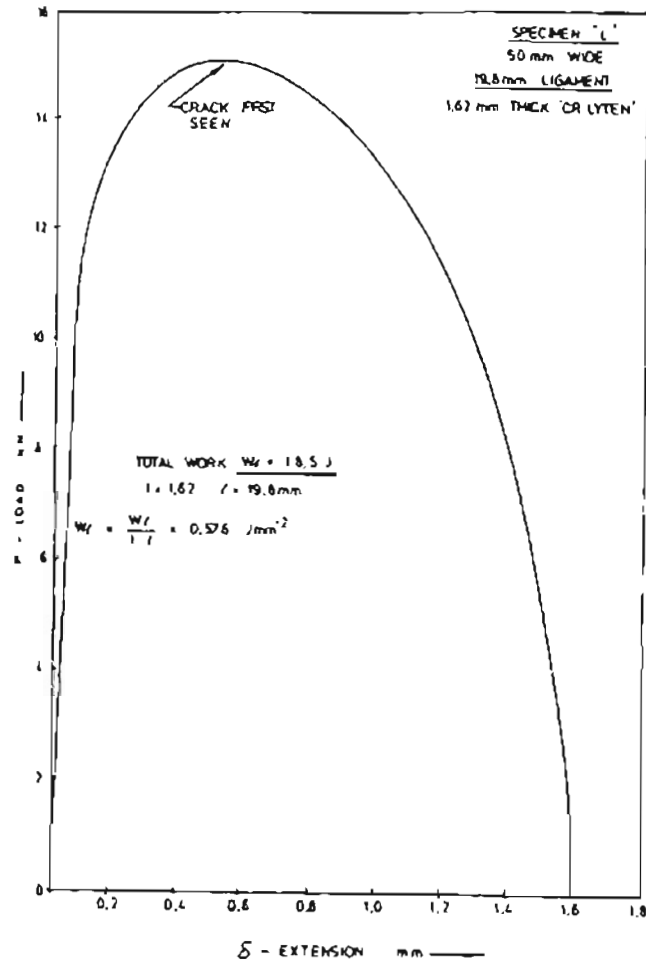
Figure 2.3.1 (a): Load-elongation curve for a cold rolled low alloy steel (16 gauge) DENT specimen [36].
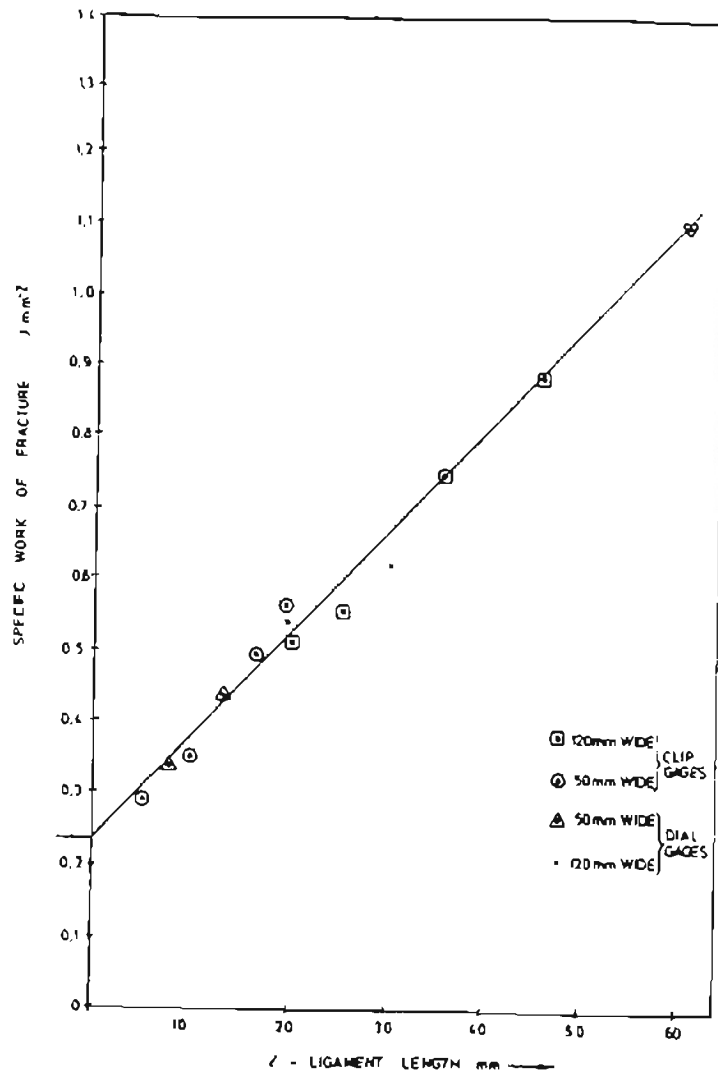
Figure 2.3.1 (b): Specific work of fracture against ligament length for a cold rolled low alloy steel (16 gauge). The linear relationship gives a positive intercept at zero ligament length, which is interpreted as the specific essential work, w_e [36].

19
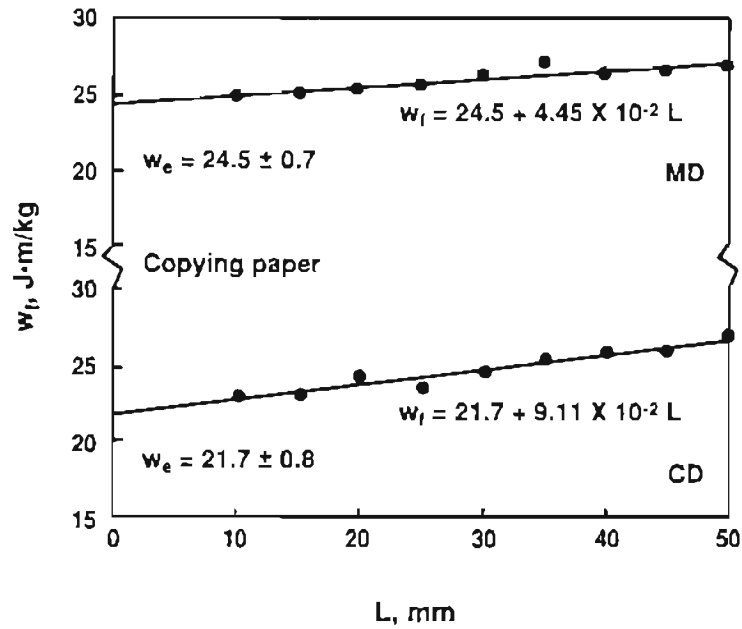
Figure 2.3.2: Work of fracture against ligament length for copying paper in MD and CD. The DENT specimen length was 150 mm, with typically, L/B = 0.3 [10].
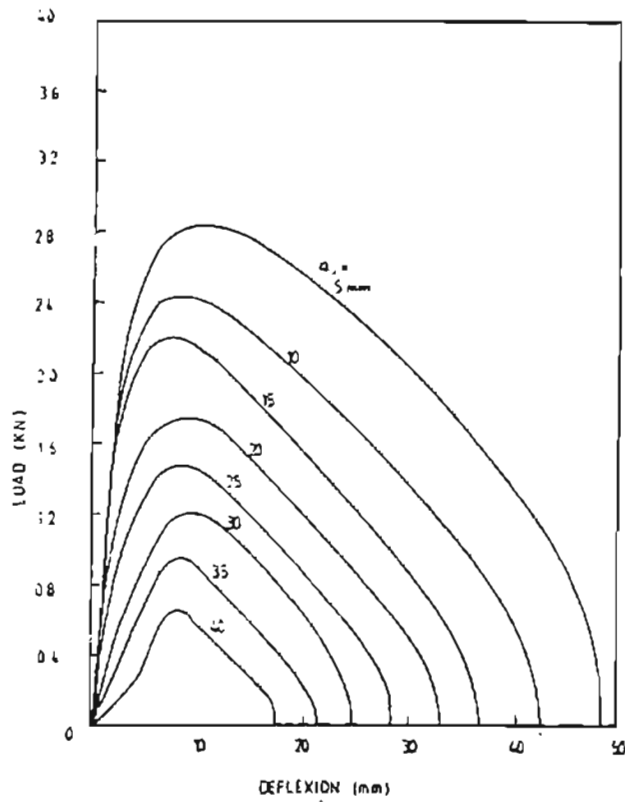
Figure 2.3.3 (a) Load-elongation curves for ductile tearing in SENT specimen for Ertalene HD 1000 (ultrahigh-molecular-weight polyethylene) for various initial crack sizes [30].
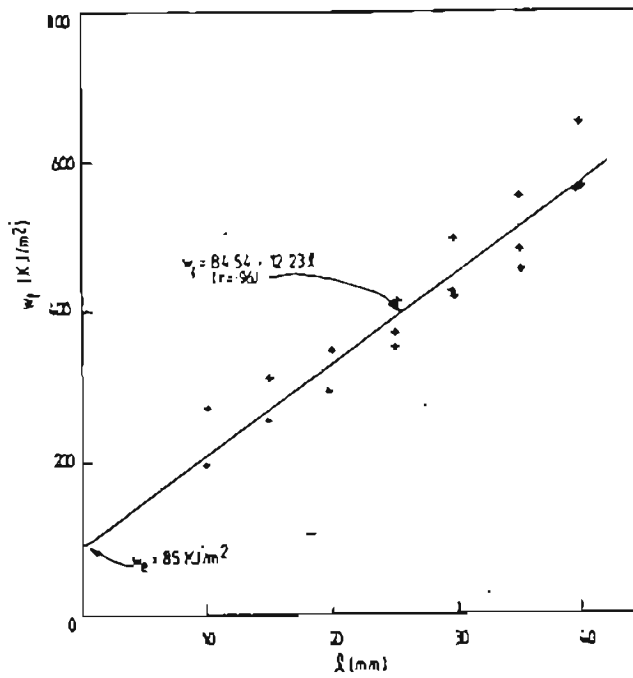
Figure 2.3.3 (b): A plot of the total specific fracture work against ligament length for SENT specimen for Ertalene HD 1000. Values for SENT specimens were found in reasonably good agreement with the DENT samples for the same material. [30].

(a)

(b)
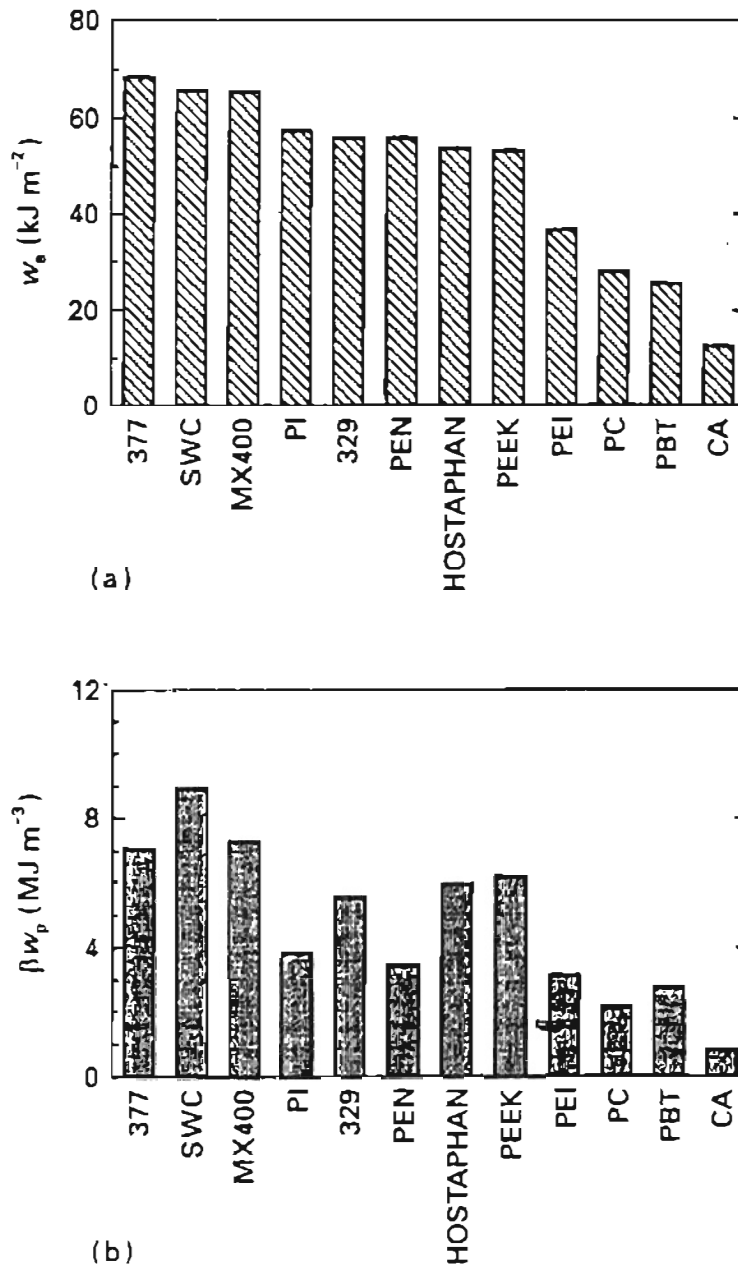
Figure 2.3.4: Barcharts comparing (a) essential work of fracture, w_e, values, and (b) plastic 'non-essential' work for various films studied in [33]. 377, 329, SWC and MX400 are PET films, PI is polyimide, PEN is polyethylene naphthalate, PEEK is poly(ether-ether ketone), PC is polycarbonate, CA is cellulose acetate, PEI is polyetherimide. From barcharts, CA has the lowest w_e. The plastic work is highest for PET and PEEK films.

2.3 Plane stress fracture toughness testing of metals

The plane stress behavior of high strength metals characterized by LEFM has been investigated and reported well [22]. Recent efforts are focused towards the improvement of test methodology [38,39]. One such effort reports comparison of R-curve methodologies for ranking the toughness of developmental aluminum alloys over a wide range of fracture toughness/strength combinations [38]. It should be noted, here, that the focus of investigation of these fracture studies was a metal sheet, sufficiently thick (3-4 mm) and stiff to support its own weight. Therefore, though general observations and the plane stress theory hold, specific details do not apply to paper and polymer film testing practices. In the latter cases, problems like buckling, out-of-plane deformation, and slip, become extremely important and influence the experimental approach followed.

The fracture studies of Cotterell et al. [36,37], are attempts to establish the specific essential work of plane stress ductile fracture as a fundamental material property. Cotterell et al. used materials such as cold rolled low alloy steel and half hard commercial aluminum, to investigate ductile fracture. Their work established that only DENT and modified deeply double edge notched (MDENT) specimen geometries are successful in yielding useful specific essential work of fracture measurements. The center cracked tension (CCT) specimens were found to have a region of compressive stress causing buckling. On the other hand, the single edge notched tension (SENT) specimens became eccentrically loaded so that there was no compressive stress region. The bigger

problem with SENT specimens was the deformation by rotation which caused

the loading geometry to change as fracture progressed and the geometric

similarity could not be maintained [37].

2.4 Plane stress fracture toughness testing of papers

Paper is a pliable material used for writing, packaging, and a variety of

specialized purposes. Paper consisting of a web of pulp fibers (normally from

wood or other vegetable fibers), usually formed from an aqueous slurry on a wire

or screen, and held together by hydrogen bonding. Paper may also contain a

variety of additives and fillers. Paper materials are classified as paper (newsprint,

stationary, tissue, bags, towels, napkins, etc.) or paperboard (linerboard,

corrugating media, tubes, drums, milk cartons, recycled board used in shoe and

cereal boxes, roofing felt, fiberboard, etc.) The industry typically divides paper

into broad categories based on the types of fibers used in paper and the weight

of the paper [8].

Before the 1920s, the influence of scientific testing on pulp and paper was

minimal. Perhaps this is because, for much of its history, paper has been treated

as a unique material, and physical tests developed in the industry did not

address basic engineering properties [9]. Qualitative tests that evaluated

products by appearance, feel and other subjective observations commonly

judged the quality of a product. There are a variety of examples of the

inappropriate application of test methods and dubious interpretation of test data.

Test methods are sometimes applied to types of samples for which they were

not optimized or designed. According to Marks [40], we know less about the

basic strength and elastic properties of paper than almost any other common structural material.

Recently, the mechanical properties of paper have been the subject of intense scrutiny in industrial, academic and governmental research laboratories that specialize in paper and pulp research.

Reference [40] provides a detailed explanation on criteria for meaningful measurements in the mechanical testing of paper. The effects of temperature and moisture content on the mechanical properties of the paper are highly significant. Paper is a very good desiccant and rapidly removes moisture from the air if the equilibrium moisture content falls below that for the surrounding environment. Moisture acts as a plasticizer, producing almost immediate changes in structure and properties. As paper takes on moisture, its properties change and, in effect it becomes a new material. Even moisture on the technician's hands can change the behavior of the specimen. The influence of temperature and moisture variation on the paper properties is interactive. Three important points should be noted [40]:

(1) Paper properties will change dramatically with small changes in relative humidity and larger changes in temperature.

(2) Temperature and relative humidity must be carefully controlled in the test laboratory.

(3) Paper specimens must be adequately conditioned before a test.

TAPPI Standard T402os-70 [2] prescribes requirements for conditioning of paper specimens prior to a test. Preconditioning is necessary because paper

exhibits moisture hysteresis. That is, the equilibrium moisture content at standard conditions will be greater if the paper is exposed to high humidity prior to conditioning than if it enters the conditioning environment from a low humidity. It is advisable to maintain a log of temperature and humidity fluctuation within the test environment. A good record of humidity conditions can be helpful in locating the cause of anomalies in test results and, perhaps, even for making corrections in the data. At very high humidity levels (80-95% RH), the specimen softens so much that it is difficult to fasten the gage to the paper in such a manner that it will not influence the behavior of the paper. A noncontacting optical strain measuring system seems to be a promising solution however, as yet, no suitable method is available for routine laboratory use. If extremely wet webs are held vertically, water migrates under gravity and affects the load-elongation properties. Seth et al. [41] developed a new method for preparing wet webs and measuring their strength over a wide range of moisture contents. Instead of comparing the wet web properties at constant moisture content, Seth et al. measured web properties at similar conditions of specimen preparation. This practice reduced the number of variables to control and gave useful results. A deterministic criterion for quality and a concept of failure envelopes for comparing different furnishes were presented for useful characterization of the web strength. The mentioned requirements make the mechanical testing of paper a highly specialized activity.

The arguments favoring the use of in-plane mechanical properties of paper over the out-of-plane tear properties have already been discussed in

Chapter 1. To add one more, the tear strength of the machine-made paper is reported to be the same in the machine direction (MD) and cross direction (CD), although the tensile strength varies considerably in these directions [8]. One can reason that the out-of-plane properties fail to consider the anisotropic nature of the paper materials. The concept of in-plane fracture testing of paper is relatively new. The essential work of fracture (EWF) has been successfully adopted for the paper materials by Seth et al. [10-12]. Reference [10] provides a brief account of the various approaches investigated for plane stress fracture testing of paper. Seth et al. believe that neither the J-integral nor the crack tip opening displacement (CTOD) method provides a simple and unambiguous measure of the plane stress fracture toughness of paper with laboratory size specimens. Important observations from the investigations of Seth et al. [10-12] are noted below:

- Pulp strength or the reinforcing potential of a pulp is affected by beating or refining the pulp. Beating or refining increases the degree of bonding between the fibers and, therefore, increases the density, tensile strength, and elastic modulus of the sheet. However, for most softwood pulps, the tearing resistance decreases with bonding at moderate to high degrees of bonding.

- Elmendorf tearing resistance decreases with bonding after an initial increase. However, fracture toughness continues to increase before it levels off at high degrees of bonding (Figure 2.4)
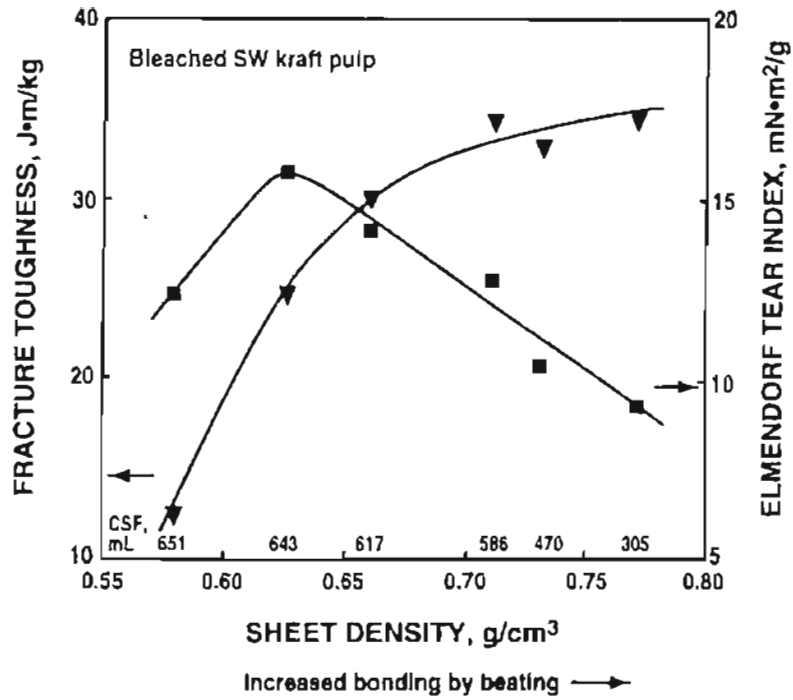
Figure 2.4: While the out-of-plane Elmendorf tear index for softwood pulps decreases with increased bonding in the sheet, the in-plane fracture toughness continues to increase [12].

- A papermaker should refine a pulp to optimize tensile strength, extensibility, elastic modulus and fracture toughness and ignore any loss in the out-of-plane Elmendorf tearing resistance.

- While coarse fibers have a high Elmendorf tear index, fine fibers have superior in-plane properties.

- The extensibility of a paper sheet is a function of the extensibility potential of the fibers and the ability of the fiber network to utilize it, i.e., it also depends on the tensile strength of the sheet. If the sheet is weak and fails prematurely, the extensibility of the fibers is not utilized. Therefore, having a high sheet tensile strength is important for high fracture toughness.

- Since the paper is rough and porous, its thickness (t) is uncertain and is replaced by sheet grammage (G) in calculating the specific essential work of fracture $w_f = W_f/LG$, where G is the sheet grammage. This is equivalent to expressing results as work of fracture per unit area divided by the material density.

- For SW TMP (Softwood thermomechanical pulp) paper sheets and newsprints, the slope of the straight line was found to be nearly zero (Figure 2.5). The entire work of fracture was the essential work, and none was dissipated outside the fracture process zone. Therefore, the EWF approach is suggested primarily for tough ductile paper sheets. In low toughness brittle papers, such as newsprint, it may be difficult to have the ligament yield completely before fracture or to have stable crack growth.
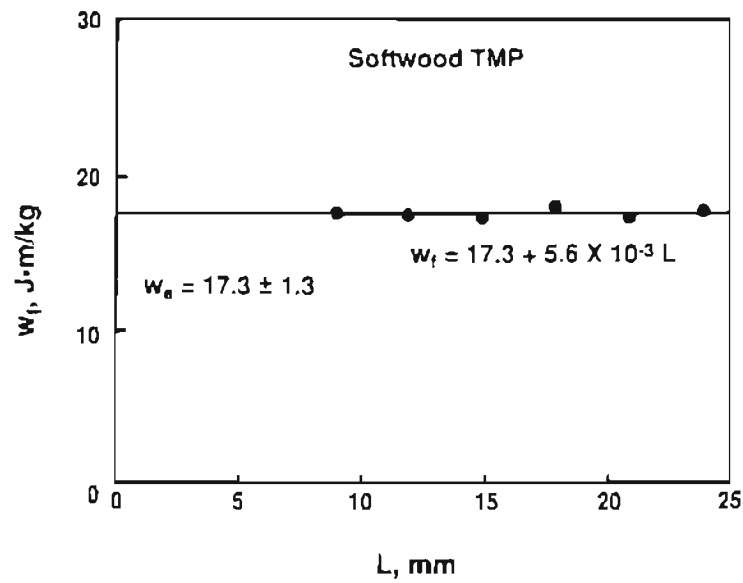
Figure 2.5: Work of fracture against ligament length for softwood TMP (Thermomecahnical pulp) handsheets. The slope is nearly zero. the entire work of fracture is the essential work, w_e [10].

- For metals, the plane stress work of fracture, w_e, depends on sheet thickness, as the specimen necks before fracture [36]. However, paper fails by different mechanisms, for example, bond and fiber breakage, and fiber pull out. The dependence of 'w_e' on the sheet thickness is not suggested.

- The difference in 'w_f' measurements with and without antibuckling plates was less than 5%.

- The EWF based test method though simple is time consuming. However, specimen cutting, notching, testing and data handling can be automated to save time.

A novel tenacity© fracture toughness test was developed by Broek et al.[42]. Tenacity is defined as a material property that provides a measure of the strength of webs containing flaws and, thus, of runnability. The most attractive feature of this test is the adequacy of any specimen size. The minimum size requirements are also reported based on extensive testing. Important conclusions of this investigation were:

- Flaws were more important than web strength. Holes were detrimental to flaws, while light spots and patches were not. The first step then is to reduce the amount of defects.

- Since defects cannot be entirely avoided, increasing web strength is one way to reduce web breaks.

- Tensile strength and tenacity correlated well for specific grades of paper. Tensile strength strongly correlated with the web breaks. A 10% increase in

32

tensile strength resulted in an increase of runnability (defined as the length between breaks) by 26%.

Recently, Tanaka et al. [43] reported the use of thermography for the in-plane fracture toughness testing of paper. A series of DENT specimens prepared from the handsheets made of commercially available bleached kraft pulp were fracture tested. The results showed that thermography with a close-up lens successfully allows the detailed observation of heat generation around the notch tips during the course of in-plane fracture toughness testing. No stress concentration causing plastic deformation occurred within the test specimen except in the area around the ligament The final deformation zone became circular in shape just before the complete fracture and seemed to correspond to the outer plastic region in the EWF method (which supports Cotterell et al.'s analysis [36], Figure 2.2). After the maximum load point to specimen failure is reached, the maximum temperature point was found to move towards the inside, suggesting a stable crack growth from the notch tip.

2.5 Plane stress fracture toughness testing of polymer films

General

A convenient, and widely accepted, definition of polymer (or plastic) film is that film comprises material up to 250 μm (0.01 inch) in thickness whereas thicknesses above that figure refer to sheet. Much of polymer film is used at thicknesses ranging from less than 20 μm to about 65 μm. Identifying rigid material as sheet and flexible material as film can turn out to be misleading.

Materials such as unplasticized PVC or cellulose nitrate are fairly rigid even at thicknesses down to 70 or 80 μm (around 0.003 in) whereas low density polyethylene is not really rigid even at thicknesses around 300 μm (0.012 inch).

The first commercially successful polymer film was cellulose nitrate. It had some excellent properties such as clarity, strength, resistance to moisture, and dimensional stability but it also had one serious drawback, flammability. In the late 19th century, the production of regenerated cellulose was a very important development in films. First applications for regenerated cellulose were as decorative wrappings for luxury or semi-luxury goods. The development of heat sealable and moisture-proof grades by means of coatings expanded the use as a protective wrapper. Cellulose acetate film was developed first, in 1909 as a 'safety' photographic film because of the dangers attached to the use of cellulose nitrate. Since then it has developed as a wrapping film where 'breatheability' is required, as in fresh produce packaging and in print lamination for the covers of journals, maps, etc., and in the manufacture of window cartons. Regenerated cellulose remained the unchallenged leader up to about 1950 since cellulose acetate was too expensive for the large tonnage packaging uses. The first film to challenge the supremacy of cellulose film was polyethylene but other more recent, films such as polypropylene, PVC and polyethylene terephthalate (PET) have also either eroded cellulose film's markets or developed new ones of their own [4]. If one takes a look at the recent fracture studies of polymer films [5, 15-17, 19-21, 43, 45, 46], they include polyimide, polyethylenes, PET, polyvinyl chloride (PVC), polycarbonate, poly(ether-ether ketone) (PEEK), polystyrene,

cellulose acetate(CA), and poly(n-Pentyl-n-Alkylsilanes). Of all these, polyimide

films have been the most widely studied. Polyimide films can maintain their

physical, electrical, and mechanical properties over a 'wide' temperature range.

These make polyimide a very useful industrial material. Applications include

electronic and microelectronics components (circuit boards, insulators, flexible

cables), automotive components, medical devices (prostheses, circuitry in bio-

implants), as coatings, adhesives, films and fiber. However, one limitation to its

use is the low fracture toughness of polyimide [20].

In certain aspects, the deformation of polymeric materials strongly

resembles metals. Polymers become increasingly deformable with increasing

temperature. Also, the extent of polymer deformation is found to vary with time,

temperature, stress and microstructure, consistent with parallel observations for

metals [44]. Viscoelasticity, anisotropy, plasticity, necking rupture, and

workhardening are the fundamental factors influencing fracture testing

methodology and data (Figure 2.6) [18].

In what follows, recent trends and issues in fracture testing of polymer

films are discussed briefly.

Fracture behavior of polymer films

Cho et al. [17] strongly support understanding the mechanical properties

of polymers on a molecular level. In their work, they note related theoretical

attempts, and study the relationship between fracture behavior and the degree of

molecular order measured by the packing coefficient, in thin polyimide films. It

was found that the tear energy showed a maximum value as the packing

Viscoelasticity *(All plastics are viscoelastic, but to various degrees)*	Anisotropy *(Most specimens are anisotropic, but to various degrees)*	Plasticity, Necking Rupture and Work Hardening *· (Beyond the yield point the material is likely to be irrevocably different from the original)*
Effect on test procedure:	Effect on test procedure:	Effect on test procedure:
Specimens may distort at and near grips, and where extensometers are attached. Clamping forces relax progressively with passage of time (except with hydraulic grips).	Specimens under test may deform in irregular ways and break at points other than those of minimum cross-section. Specimens may fail at or near grips unless special precautions are taken.	Strain gauges and clip-on extensometers unlikely to function properly. Slip at grips possible. Inspection of specimen during slow extension and/or after failure is essential.
Effect on results:	Effect on results:	Effect on results:
Force-deformation relationship incorporates time-dependence of material, and is sensitive to deformation rate. Derived moduli have to be fully defined.	Moduli and strengths may be higher or lower than expectation due to anisotropy induced by flow-geometry.	Post-yield deformation likely to be inhomogeneous. Force-deformation relationship beyond the yield-point cannot readily be converted into a stress-strain relationship: any such conversion will be imprecise, strain has to be redefined. Numerical data should be qualified by description of specimen state at rupture.

Figure 2.6: Influence of the inherent nature of polymers on fracture testing methodology and data [18].

coefficient increased. Above the critical packing coefficient, the films became so brittle that the tear energy decreased. Also, the tear energy increased as the flexibility of polyimide films cured at low temperature was different at both sides of the film, substrate-side and air side, whereas, this heterogeneous fracture behavior disappeared in films cured at high temperature. These results suggested the formation of the local molecular order in the film near the surface of the substrate at low curing temperature and it advanced in the direction of the opposite side as curing temperature increased. Polyimide films with low degree of local molecular order and high chain mobility were deformed by crazing with shear yielding. Other polyimides with a high degree of local molecular order and high chain mobility showed only shear yielding.

Time-dependent fracture

Popelar et al. [15] made a maiden attempt toward quantifying the time-dependent fracture in thin polyimide films due to slow crack growth. They tested SENT specimens of Kapton polyimide films at room temperature to develop and validate an analysis model. They presented log scale data correlating the crack growth rate in both the MD and the CD. Popelar et al. [15] found it difficult to initiate crack growth perpendicular to the machine direction and to obtain reproducible data. The crack growth rate was found to depend very strongly upon the stress intensity factor; i.e., small changes in the stress intensity factor produce large changes in the crack growth rate. This made it impossible to develop a correlation for the time for initiation of crack growth. The glass transition temperature; i.e., the demarcation between glassy behavior for lower

temperatures and rubbery behavior at higher temperatures, for Kapton polyimide films is in excess of 350°C. The observed brittle-type failure at room temperature (22°C) implied that the fracture of Kapton polyimide films may be approximated as being controlled by a critical value of the stress intensity factor (Table 1.1). The results also showed a modest decrease of fracture resistance with decreasing film thickness. The crack growth rate for the same stress intensity factor increased substantially with decreasing film thickness.

Essential work of fracture (EWF) approach for polymer films

Essential work of fracture (EWF) approach has been successfully implemented for ductile polymer films, as mentioned before [30-33]. Observations similar to metals and papers are reported. Cotterell et al. [30] investigated linear polyethylenes, as an extension of their work on sheet metals. It is suggested that the specific essential work of fracture, w_e, is a better method than the J_R curve to determine the equivalent J_c. Levita et al. [31] studied thickness effects on the specific essential work of fracture of rigid PVC. They used the EWF approach to test sheets of rigid PVC of different thickness (2 to 10 mm). Two values of the specific EWF were measured depending on whether large ($L/t \geq 3$ to 5, plane stress conditions dominant) or small ligaments (plane strain conditions dominant) are considered. For larger ligament lengths, w_e depended on the sheet thickness. For smaller ligaments, no thickness effect was observed. The critical J values were found to be independent of thickness and close to those of 'w_e' for the smaller ligaments. The EWF method offers an advantage of not requiring monitoring of the advancement of the starter crack.

This makes it useful in toughness testing of semiductile polymers, in which halting the test to mark the actual position of the crack tip is arduous [31]. Kocsis et al. [32] report use of infra-red thermography (IT) for fracture testing of biaxial-oriented filled PET film. Once again, use of in-plane properties over out-of-plane (mode III) is justified. Hashemi et al. [33] tested a wide range of polymeric films. The variation of specific total work of fracture within the plane stress region was found to be a linear function of the ligament length. the transition from a pure plane stress region to mixed mode region (when net section stress $\sigma > 1.15\sigma_y$) occurred at ligament length values much greater than 5B, where B is the specimen thickness. Thereby, Cotterell's lower limit for the ligament length (equation 2.3) is shown not valid for polymeric films.

Residual stress analysis

Klemann et al. [5] report a well-developed test methodology using a residual stress analysis. The method is applicable to brittle films and films of moderate ductility. Trycite biaxially oriented polystyrene films were used during the development of the test methodology. Kapton polyimide films were tested for comparison with results of Hinkley and Mings [16]. Figure 2.7 is the residual strength curve for the final set of Trycite data for SEN geometry. The applicability of the Feddersen analysis is evidenced by the excellent fit over the entire range of crack lengths. The thickness model of Anderson is used for determination of the stress state. For Kapton polyimide films, the results were shown to agree with those of Hinkley and Mings [16]. Fracture process zones for Kapton polyimide film are shown in figure 2.8 [5,16]. No crazing was observed as with
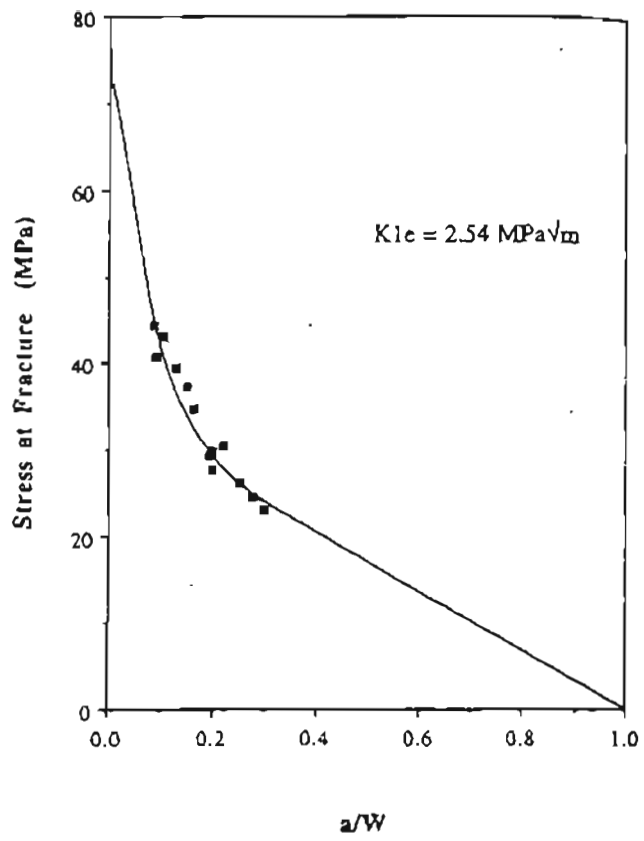
Figure 2.7: Effective fracture toughness of SEN Trycite [5].

(a) Process zone of Trycite bi-axially oriented polystyrene films. Bi-axial orientation enhances strength and ductility. A large duckbill-shaped yield zone can be seen formed ahead of the crack tip [5].
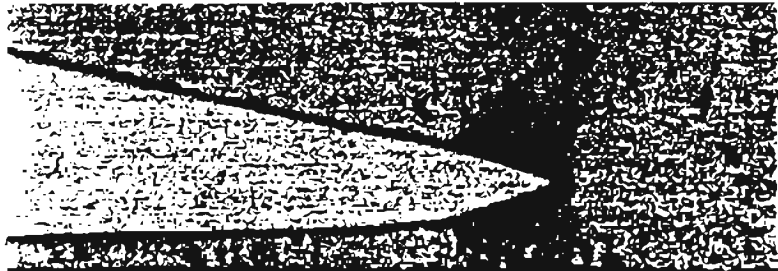
(b) Process zone of Kapton polyimide film. The yielded material that the crack tip had cut through is visible as a black fringe on the crack faces [5]. Cotterell et al. noted this as 'cold drawing' [20].

Figure 2.8: Fracture process zones of various polymer films
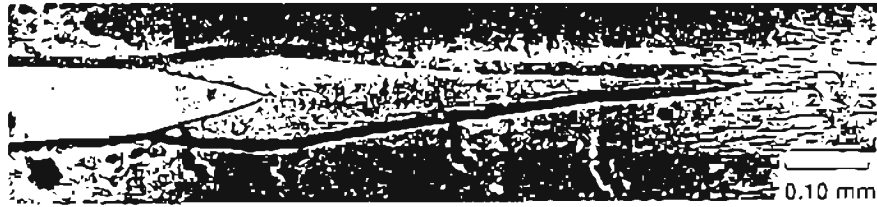
(c) Fully developed deformation zone in notched LARC-TPI film. A thin necked region bordered by a ridge dense lines which are presumably crazes can be seen. Short cracks (crazes) perpendicular to the tensile direction are also present at considerable distances from the primary crack [16].
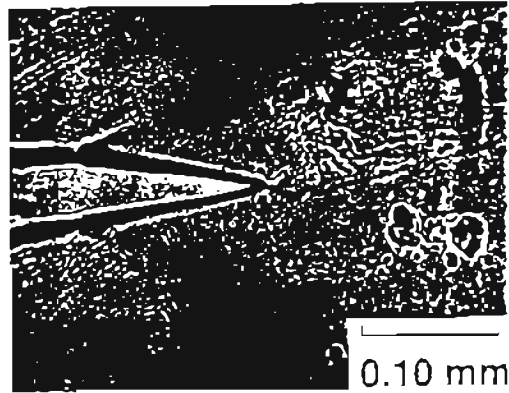
(d) Process zone in a polyamide-imide film. No crazing is observed [16].
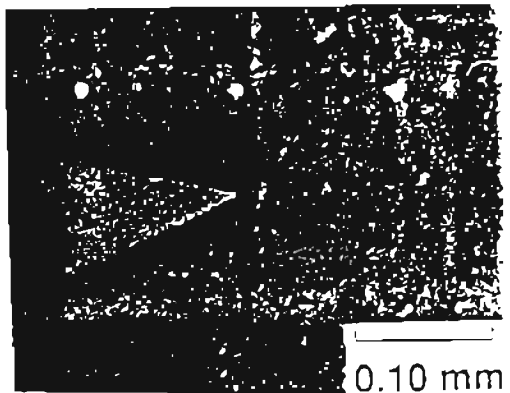
(e) Process zone in Kapton polyimide film. No crazing is observed [16].

Figure 2.8 (contd.): Fracture process zones of various polymer films

other films (polystyrene and LARC-TPI). Both studies [5,16] found that the deformation zone for Kapton polyimide film is not well defined and difficult to observe,

Stress intensity factor approach

A well-reported work of Hinkley and Mings [16] investigates aromatic polyimide films. Film specimens, 1.3 cm wide and 5 cm long were tested to failure in a miniature tensile frame constructed on the stage of an optical microscope. The crosshead was driven by a d.c. gear motor at 0.185 cm/min. Each specimen was supported on lightweight cardboard and cut with a slicing motion to create the edge notch. Antibuckling guides were used for some experiments and no differences in initiation loads were seen between tests with and without guides. Important observations from this study are noted below [16]:

- The razor notching procedure produced a sharp crack which could be seen to open as the specimen was loaded. Further increases in load led to slight crack blunting until, suddenly, crack propagation began, apparently simultaneously with the development of a necked-down crack tip deformation zone. The load at which crack propagation begun depended strongly on the initial crack length.

- For polyimide films, the failure loads were typically 150-230% of the initiation load (Figure 2.9).
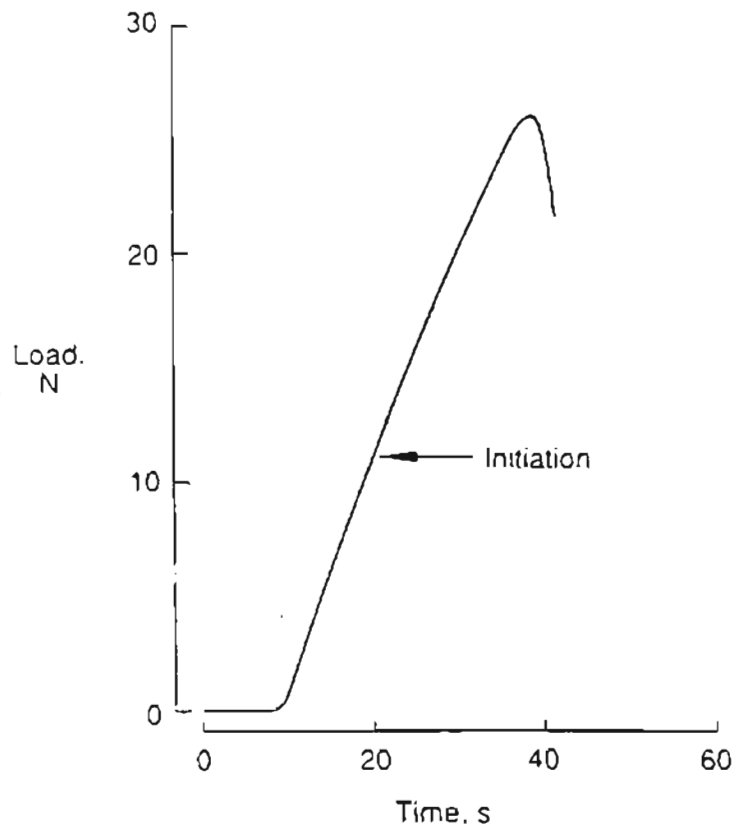
Figure 2.9: Load-time record for single–edge-notched tensile strip of LARC-TPI (thermoplastic polyimide). Initial crack length = 0.5 mm [16]. Note that the specimen is not pre-loaded. It shows some 'slack' in the beginning of curve

J-integral analysis

Klemann et al. [45] reports a J-integral analysis of the ductile tearing of thin films of poly(n-butyl-n-pentylsilane) and poly(n-propyl-n-pentylsilane) using an Instron tensile testing machine and SENT specimens. The critical values of J for fracture initiation, J_{Ic} were found to be significantly higher than the plane stress, G_{IC} values obtained with a residual stress analysis using the same apparatus and testing procedure. Hashemi et al. [46] recommends use of J-integral methods for materials having higher toughness such as linear low density polyethylene (LLDPE).

The constrained short tension (CST) test

Recently Tielking [21] developed a simple constrained short tension (CST) test. Attractive features of this test are listed in chapter 1. Tielking [21] used this geometry to obtain J_R-curves for polyethylene films. Cotterell et al. [19,20] adopted the CST test methodology for testing thin materials whose fracture characteristics can be described by LEFM. The CST test geometry is suitable for measurement of the plane stress fracture toughness K_C, the crack growth resistance, fatigue, or time dependent fracture.

Cotterell et al. [19,20] tested DuPont Kapton polyimide film 100 HN, 200 HN, 300 HN and 500 HN. The specimens were 210 mm wide by 30 mm high. Central notches of total length of 19.5-26.5 mm were cut, perpendicular to the machine direction with a surgical knife to obtain a sharp tip. The specimens were loaded at a strain rate of 1 mm/min (0.04 inch/min) at a temperature of 22°C. The Poisson's ratio was assumed to be 0.35 as stated by the manufacturer.

Finite element results suggested that, for a specimen under the following size constraints,

1. Half width, W > 5H, where H is the half height of the specimen (figure 2.10),

2. Half crack length, a > 0.8H, and

3. 2a < W

--stress intensity factor is independent of the crack length. For above-mentioned inequalities and Poisson's ratios in the range 0.3 to 0.5, the stress intensity factor is given to better than 1% by the approximate expression,

$$\frac{K_R}{\sigma_{gross}[H(1-v^2)]^{1/2}} = \frac{1}{(C-\frac{a}{w})}$$

....(2.4)

σ_{gross} is the gross stress given by,

$$\sigma_{gross} = \frac{P}{B(2W)}$$ ....(2.5)

where P is the tensile load on the test specimen, and B is the thickness of the test specimen.

v is the Poisson's ratio,

H the half-height,

W the half-width,

and the constant,

C = 1 + (0.3154 - 0.7666v^2) (H/W)

The stress intensity factors were plotted against the crack extension to give the K_R-curves shown in Figure 2.11. The results were found to be

46
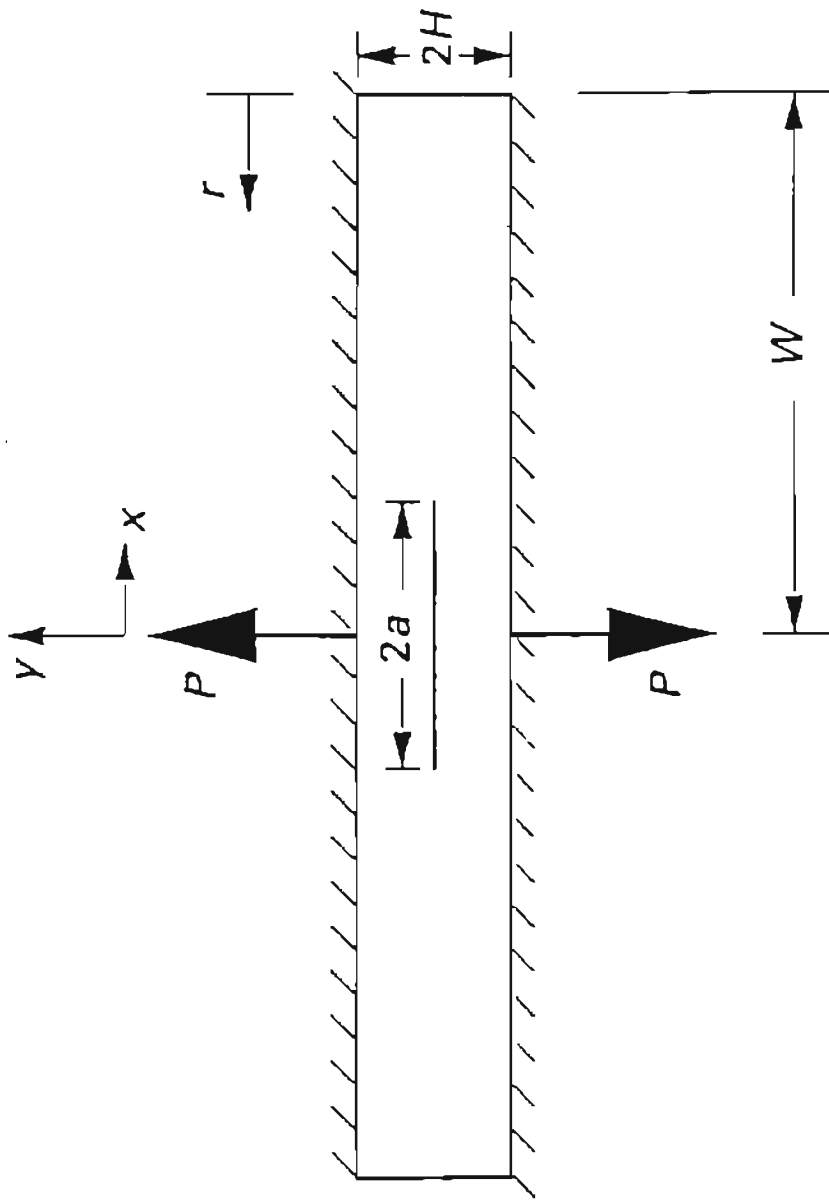
Figure 2 10: Schematic representation of the constrained short tension specimen [19].

independent of the initial crack length. Correction for the plastic zone was found to be negligible. The exponential curve fit, $K_R = A + B\Delta a^n$, where Δa is the crack extension, gave a good fit to the crack growth resistance (Figure 2.11).

The K_R-curves (Figure 2.11) show that the polyimide films possess considerable crack growth resistance within a range of the order of 2 mm and the plateau fracture toughness is sensitive to the film thickness with the thinnest film displaying the highest toughness. The initiation values of the fracture toughness were proved to be more difficult to estimate accurately.
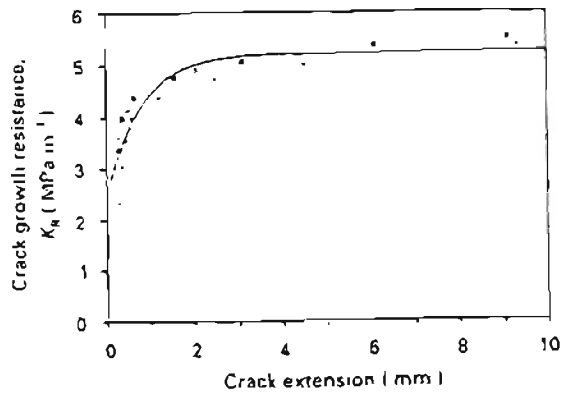
(a) Crack growth resistance curve for Kapton 100 HN polyimide film; symbols, experimental data;(_____) exponential curve of the best fit.
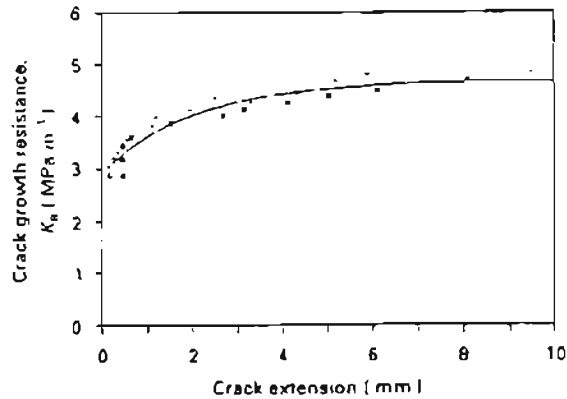
(b) Crack growth resistance curve for Kapton 200 HN polyimide film; symbols, experimental data;(_____) exponential curve of the best fit.
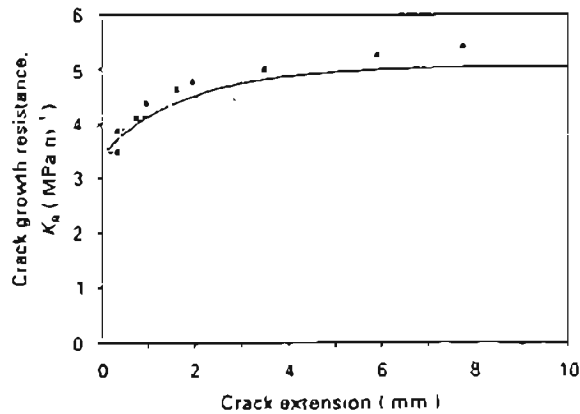
(c) Crack growth resistance curve for Kapton 300 HN polyimide film; symbols, experimental data;(_____) exponential curve of the best fit.

Figure 2.11: Crack growth resistance curves for Kapton polyimide film

49

CHAPTER 3

TEST METHODOLOGY

3.1 Development of CST test grip fixture

It is difficult to uniformly clamp a wide sheet of very thin materials, such as polymer film along its width and to maintain uniform stress in the plane of sheet. The important design requirements to be met by the grip fixtures for plane stress fracture testing of very thin materials, such as papers, polymer films, and metallic foils are [18-21]:

1. The grips must have faces that prevent the materials from slipping. The grip face material should not deform under load.

2. The grips must have sufficient bending stiffness so that the deflection of the grips under load is minimal.

3. Ease of specimen preparation:

   • Specimens of different height, width, and thickness should be tested without major modifications.

   • Quick and easy gage length (height) setting and center crack location.

   • End tabs should not be required.

Seth et al. [11] used a pair of line type clamps mounted on two guide rods with low friction bearings (Figure 3.1) for the fracture testing of paper materials. The clamps were mounted on the Instron universal testing instrument. the clamping members were a rod and a flat plate, both of steel. The uniformity of

50
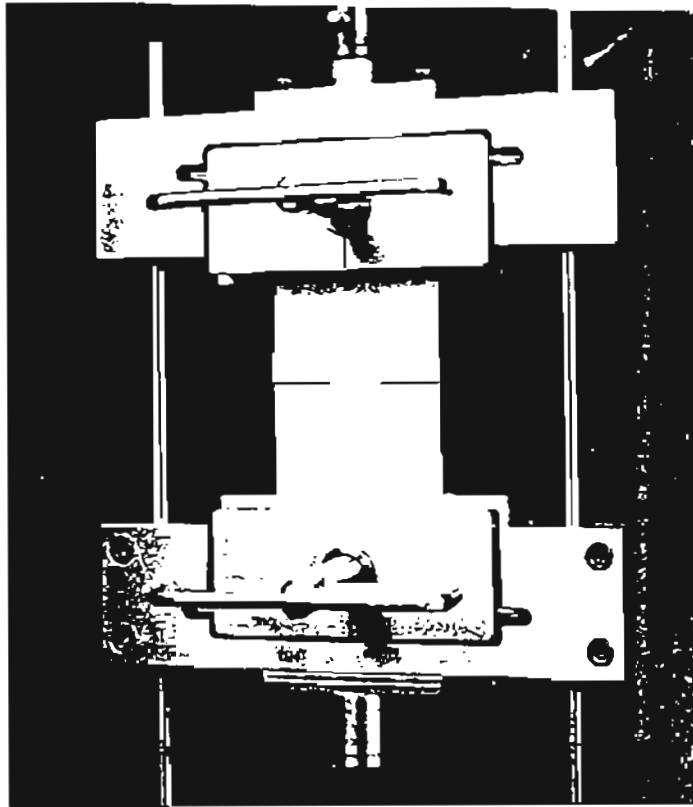
Figure 3.1 Line-type clamps for testing fracture specimens of paper materials [11]

clamping was tested by clamping hard on aluminum foil, and by examining the indentation line.

Figure 3.2 shows the CST test grip fixture used by Cotterell et al. [19]. They used 120 grade silicon carbide paper to face the grips. The grips are housed in a heavy C-shaped fixture which has high bending stiffness, and tightened onto the polymer film specimen by six set screws.

Tielking [21] developed a fixture to test polymer film specimen having width of 254 mm (10 in) and height of 76.2 mm (3 in) (Figure 3.3). The width was limited by the width of a commercial environmental chamber used for low temperature testing. The quick connect-disconnect feature of this design allows the gage length to be set outside the environmental chamber. This is done in an external fixture (not shown in Figure 3.3) that positions the grips at the desired gage length while the set screws on the channel clamps are tightened. The top and bottom grips, with a film specimen between, are then carefully carried to the environmental chamber. The top grip quickly attaches to the two large hooks, and the bottom grip is clamped by the vice grips. Tielking [21] used silicone rubber facing on the grips to hold the film at test temperatures as low as -80°C.

The CST test grip fixture designed for this work is a combination of design features suggested by Cotterell et al. [19], and Tielking [21].

Figures 3.4-3.7 show details of the CST test grip fixture designed and manufactured for this work. Important components and features are described below.
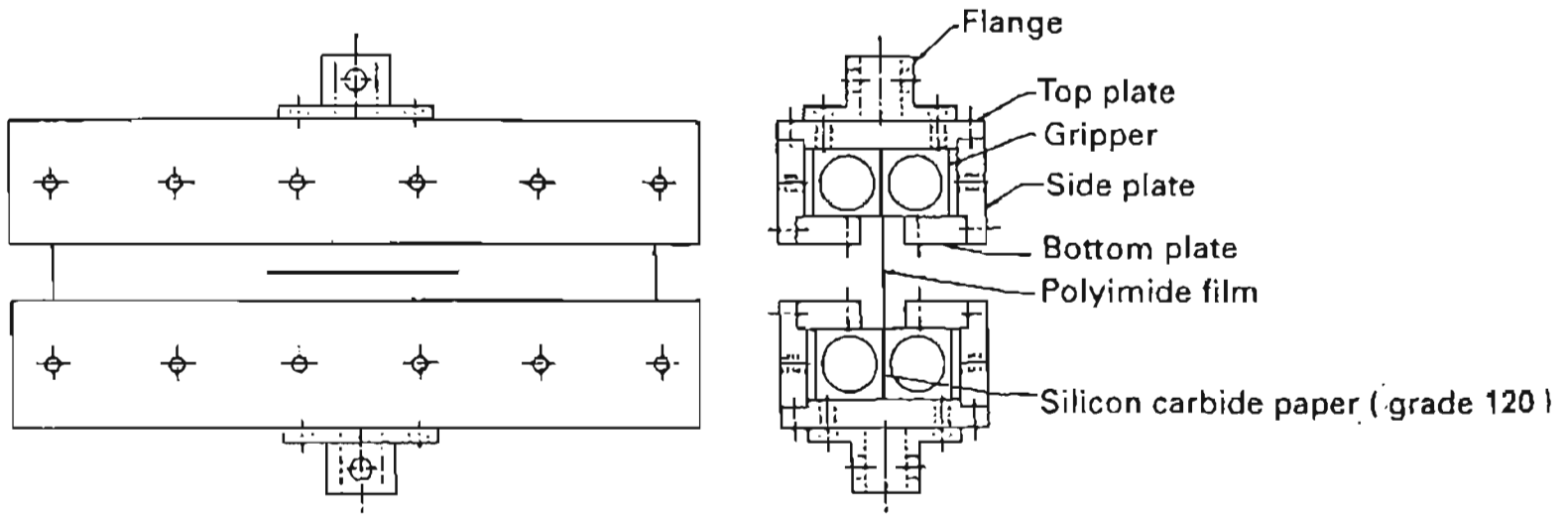
Figure 3.2: Details of the CST test grip fixture developed by Cotterell et al. [19].
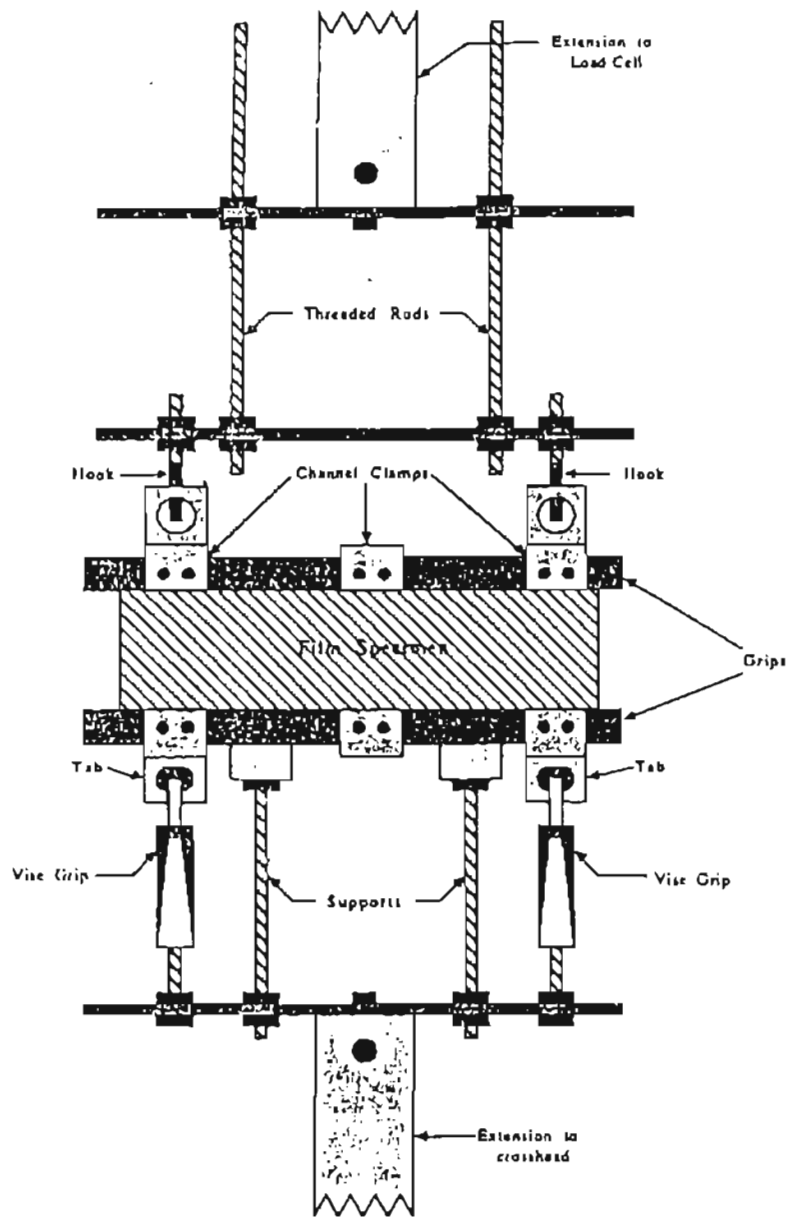
Quick-connect grip fixture –front view
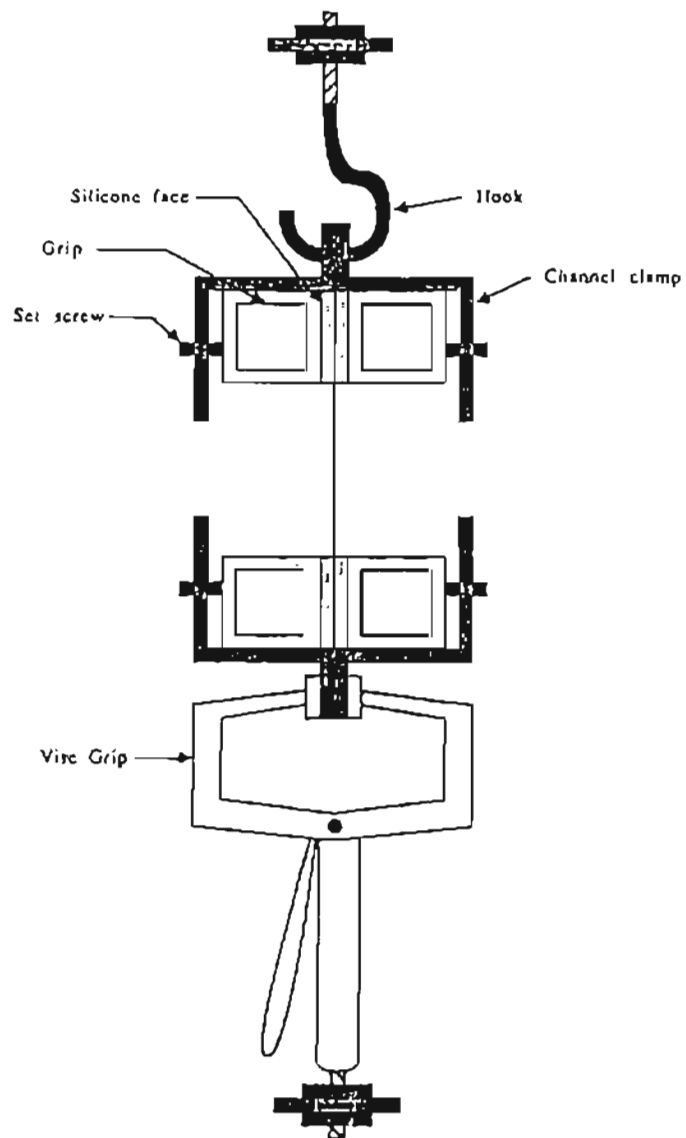
Quick-connect grip fixture –side view

Figure 3.3: Tielking's quick-connect grip fixture [21].
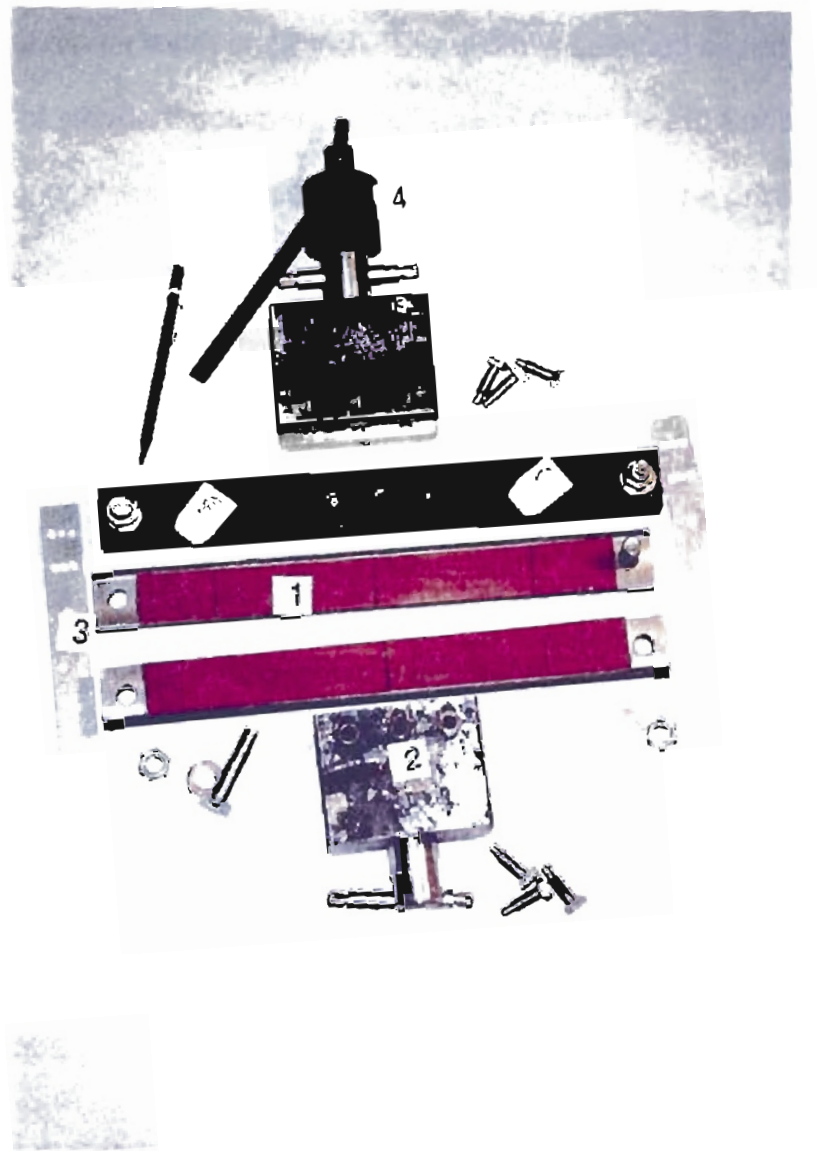
Figure 3.4: Details of the CST test grip fixture developed for this work

1. Grip plates with gasket rubber faces.
2. C-type fixtures.
3. Holding plates.
4. Instron load cell connector

(a) **Plate grips** (Figure 3.5)

A set of plate grips was designed and manufactured to test a specimen having a maximum width of 12 inch. The width is selected based on the availability of standard polymer film roll sizes (6 and 12 in). Specimens as narrow as 4 inch can be tested successfully using the same grips. The sheet height is chosen to ensure that the crack growth will occur in a biaxial stress field. The grips are faced by a 0.09 in thick gasket rubber. The rubber facings are glued to the machined surfaces using contact cement. The grips and C-type fixtures, are made of steel.

(b) **C-type fixtures** (Figure 3.6)

The upper C-type fixture is attached to the load cell using a pin type connector. The lower C-type fixture with similar design features is connected to the fixed end of the tensile testing machine. The upper C-type fixture is free to hang in a plane perpendicular to that of a specimen. The lower one is fixed. The bolts in the back of the fixtures are for supporting and locating the grips. The clamping force on the grip plates is provided by the longer bolts in the front.

(c) **Holding plates** (Figures 3.6, and 3.7)

The aluminum (6061-T6) holding plates have a set of drilled holes positioned to match the specimen height requirements. These plates allow the setting of height, and center crack location between the grips, outside the C-type fixtures, and therefore, externally to the tensile testing machine (Figure 3.7).
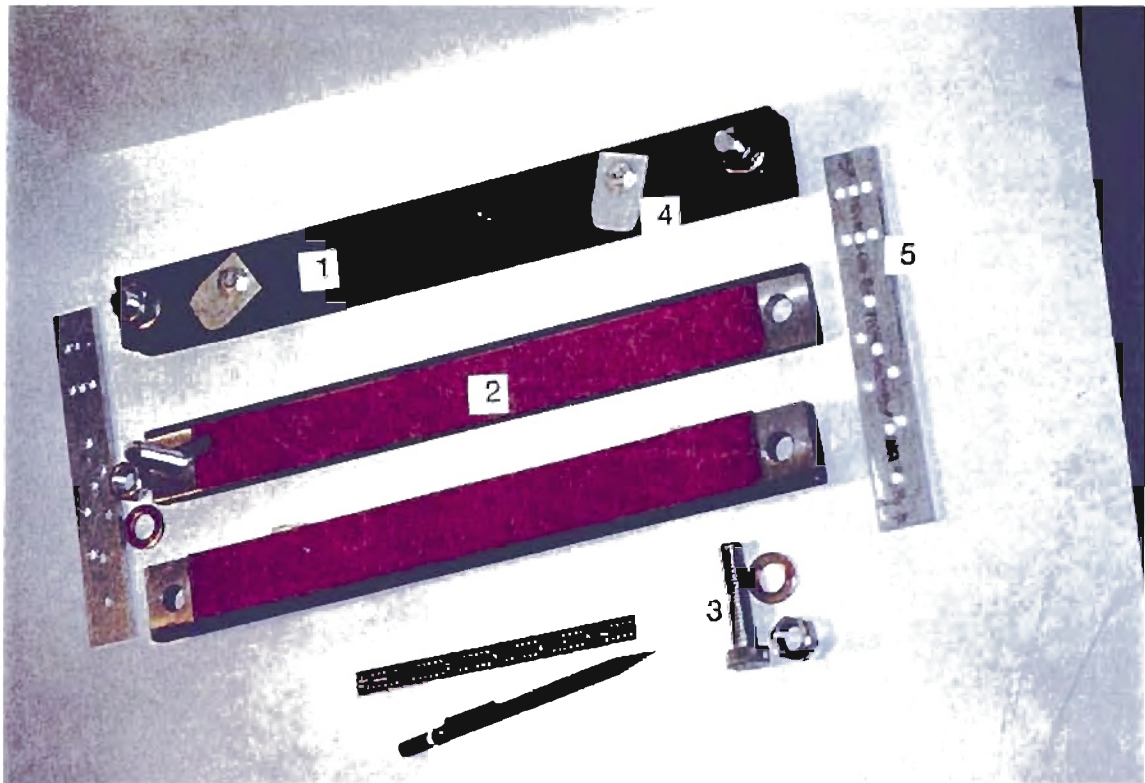
Figure 3.5: Grip plates and holding plates.

1. The top grip is shown in assembled condition. The three drilled holes on the outer surfaces provide   easy clamping and precise alignment of grip plates in the C-type fixture.
2. The bottom grip. A small shoulder is machined at one end of the grip plates to prevent the pull out of rubber facings by stronger test specimens.
3. Grip bolts.
4. Holding plate clamps.
5. Holding plates.
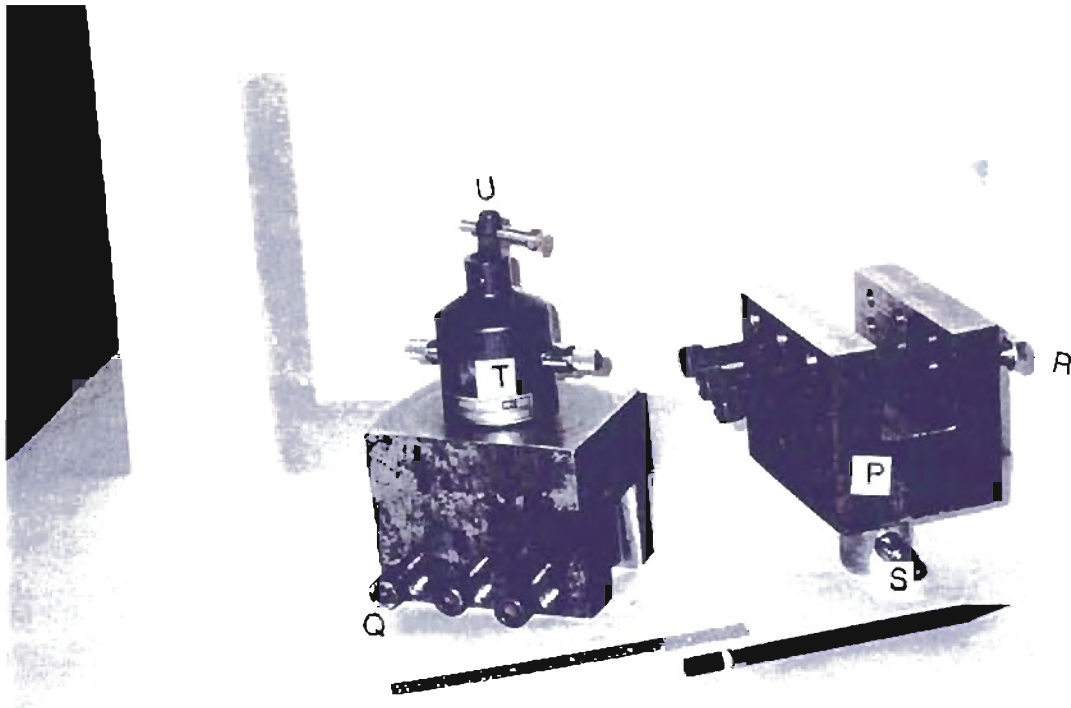
Figure 3.6: C-type fixtures and components.

P. The lower C-type fixture
Q. Clamping bolts.
R. Support and location bolts
S. Pin connector
T. Instron load cell connector.
U. Spherical joint in the load cell connector aids self-alignment of the CST test grip fixture.

Figure 3.7: Holding plates allow the setting of height, and center crack location between the grips, outside the C-type fixtures, and therefore, externally to the tensile testing machine.

S. ICI polyester film (92 gauge) specimen

Troubleshooting the CST test grip fixture and related problems

The development of the working CST test grip fixture is a process of elimination. Serious problems include slip, misalignment, and poor specimen and crack location. Although problems are to a greater extent, specific to the testing machine, the various elements of the specimen-machine interaction that affect the overall operation efficiency in the fracture testing of very thin materials are summarized in Figure 3.8.

Interpretation of load-time records is one effective way of tracking problems. A load-time recording is a 'signature' of the events occurred during a complete test run. In this fracture testing, load-time records form raw data. The accuracy of the entire work depends on the accuracy of these records. Figure 3.9 provides a general collection of faulty techniques and errors in the derivation of raw data and property values in force-deformation testing of materials. Some interesting problems and their solutions are discussed below.

Problem 1: Slip and deforming grip faces

During an exploratory phase of the research, grip plates were faced by a 120 grade silicon carbide paper. The 'peak load before fracture' values for different specimen geometries and materials were not available at that time. Weaker materials (thin gauge, peak loads < 50 lb.) showed considerable slippage. Abrasion marks indicating slip were always found on the gripped area of the specimen. Stronger materials (thicker gauge, peak loads > 50 lb.), when loaded in tension, pulled grip faces out of the grips altogether. Later, gasket rubber facings were used, which solved the slippage problem completely.

Misalignment of Specimens with Respect to Axis of Loading.	Insecure or Over-zealous Clamping.	Imperfect Specimens: Poor Surface Finish Asymmetry.
Caused by:	Caused by:	Caused by:
Extraneous friction.	Unsuitable specimen profiles.	Inappropriate moulding or machining techniques.
Careless clamping of specimen.	Unsuitable grips.	
Asymmetrical specimens.	Careless laboratory technique.	
Resulting in:	Resulting in:	Resulting in:
Non-axial stressing, leading to errors in modulus measurements and underestimates of strength (premature failure).	Slip of specimens in grips, leading to errors on strain or elongation measurements.	Premature failure, embrittlement.
	Distortion of specimens in or near grips, leading to errors on strain or elongation measurements and possible premature failure.	Non-axial stressing.

Figure 3.8: Sources of experimental error in the specimen-machine system [18].

Imperfections in Raw Data.	Errors in Raw Data.	Errors in the Translation of Raw Data into Stresses, Strains, Moduli, Strengths, etc.
Caused by:	Caused by:	Caused by:
Inappropriate Choice of Sensors and Data-Processing Facility:	Injudicious Deployment and Mounting of Strain Sensors:	Reduction in cross-sectional area.
Unsuitable response time.	Incorrect positioning.	Inhomogeneous strains
Unsuitable sensitivity.	Insecure attachment.	
	Constraining attachment.	
Resulting in:	Resulting in:	Resulting in:
Events on the force-deformation curve unregistered or distorted, natural vibrations in the whole system registered as noise. Overall loss of precision and accuracy, reading errors at one extreme, guillotined signal at the other.	Detected response includes extraneous forces, displacements. Sensor movement relative to specimen, therefore erroneous register of actual displacement. Constraint/modification of the local displacements in the specimen.	Difficulties and errors in the conversion of force-deformation into stress-strain. Naive interpretation of force-displacement curves.

Figure 3.9: Faulty techniques and errors in the derivation of raw data and property values [18].

However, a 200 gauge PET film once pulled out the rubber faces too. This problem was successfully countered by modifying the grip plate design. A small shoulder of half the thickness of rubber facings (0.045 in) was introduced in each of the grip plates to prevent the pull out (Figure 3.7). No grip face deformation was observed after this, even at peak loads as high as 450 lb.

Problem 2: The 'two peak' problem

As mentioned before, a center-cracked specimen provides a very good check over the fracture testing conditions. During earlier test runs, center cracked specimens showed uneven crack growth. Initially, the crack propagated equally in both the directions (LHS and RHS). Suddenly, the crack growth became faster on the left hand side. The specimens fractured completely on the left hand side, when the right hand side of the crack had not propagated more than 40% of the ligament length. On a load-time record, this generated a 'two peak' curve shown in Figure 3.10. The first peak describes the peak load before the specimen fracture on the left hand side, and the second one on the right hand side. The following four causes were identified as sources of this problem:

(1) High displacement rate (crosshead speed)

(2) Poor crack location

(3) Uneven grip pressure

(4) Misalignment

The first three causes were easy to counter. The crosshead speed was reduced to a fixed value of 0.04 in/min (1 mm/min) as a result of considerable experimentation and checking values reported in the literature. The grip pressure
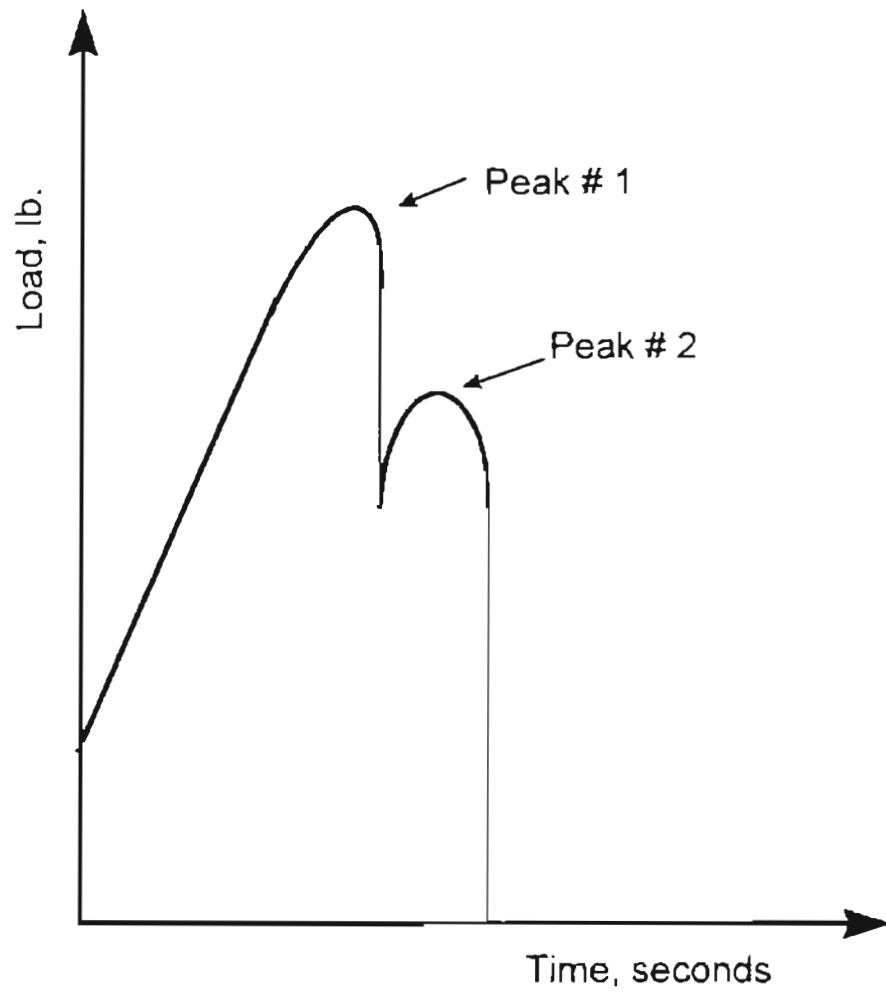
Figure 3.10: 'Two peak' problem (schematic)

was optimally adjusted by determining a torque value using a torque wrench to tighten the grip, and clamping bolts. The crack location technique was improved by the use of cardboard templates and scribing limiting marks on the specimens. The misalignment problem was the most difficult to solve. This required a redesign of grip plates, and careful tracking of the other sources of misalignment such as, a load cell mounting plate, and C-type fixtures.

Problem 3: The 'wave pattern' problem

During final test runs on polyester films, a wave-type pattern was observed on the load-time records (Figure 3.11). This pattern repeated itself at about 50 lb. of load for each test run for which peak loads to fracture were larger than 50 lb. The repeatability of the pattern made it easier to detect the source of error which was the fixture rigidity. The lower C-type fixture was found moving slightly upwards around the noted load value. It was rigidly connected to the lower fixed end of the testing machine to eliminate the problem (Figure 3.12).

3.2 Complete fracture testing apparatus

The complete fracture testing apparatus for the plane stress fracture testing of very thing materials require:

(1) An electromechanical tensile testing machine with a variable displacement rate.

(2) Load cells of different maximum load capacities.

(3) A CST test grip fixture as described in section 3.1.

(4) Means of recording load-time data – an XY recorder or a PC based data acquisition system.
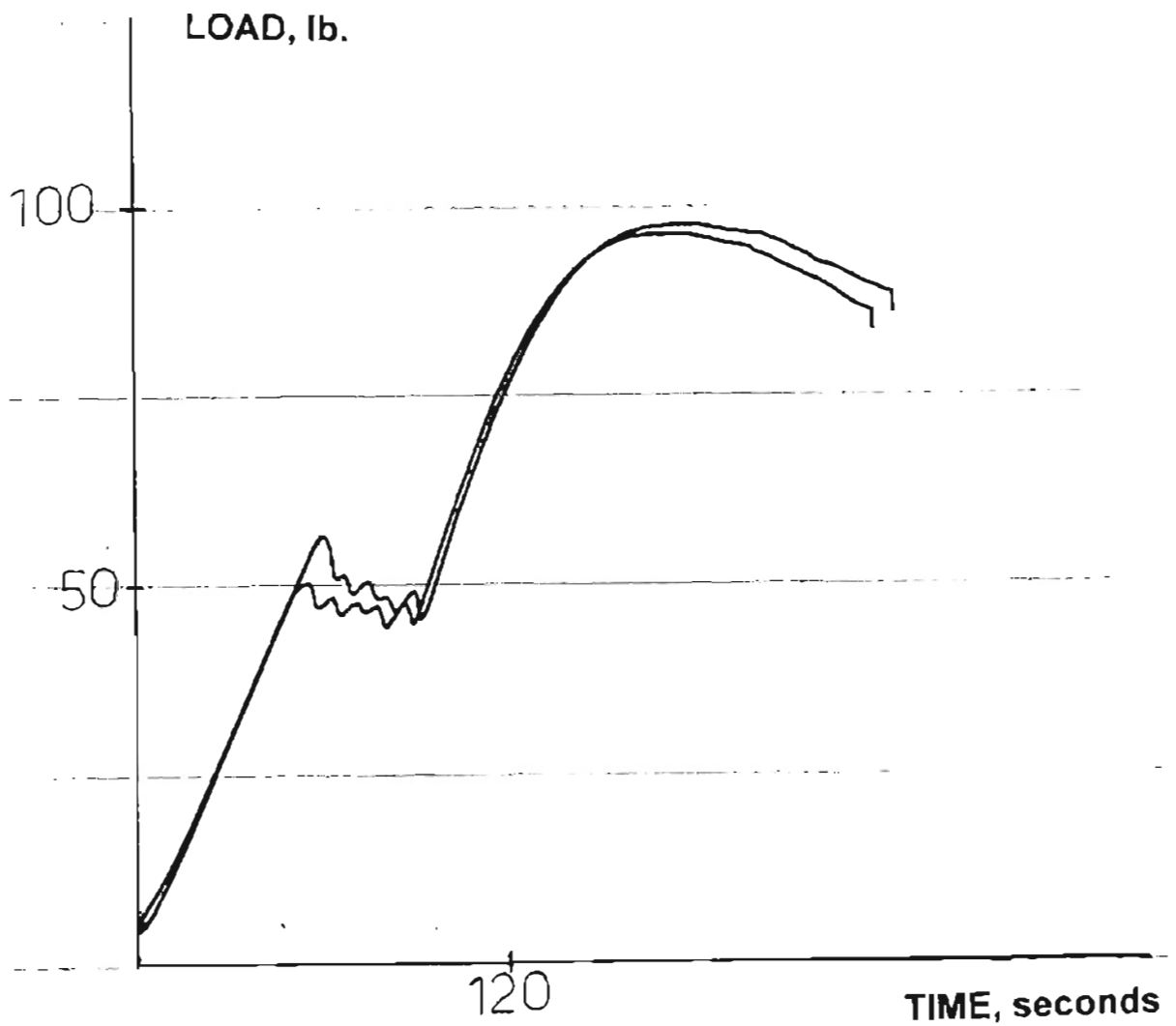
Figure 3.11: A load-time record with a 'wave-type' pattern at load values around 50 lb. The data shown is for two test runs on 92 gauge ICI polyester film specimens tested in MD (2W = 8.0 inch, 2H = 1.25 inch, and $2a_0$ = 1.0 inch). As seen, the pattern repeats itself at about same load values, which helped in detecting the source of error.
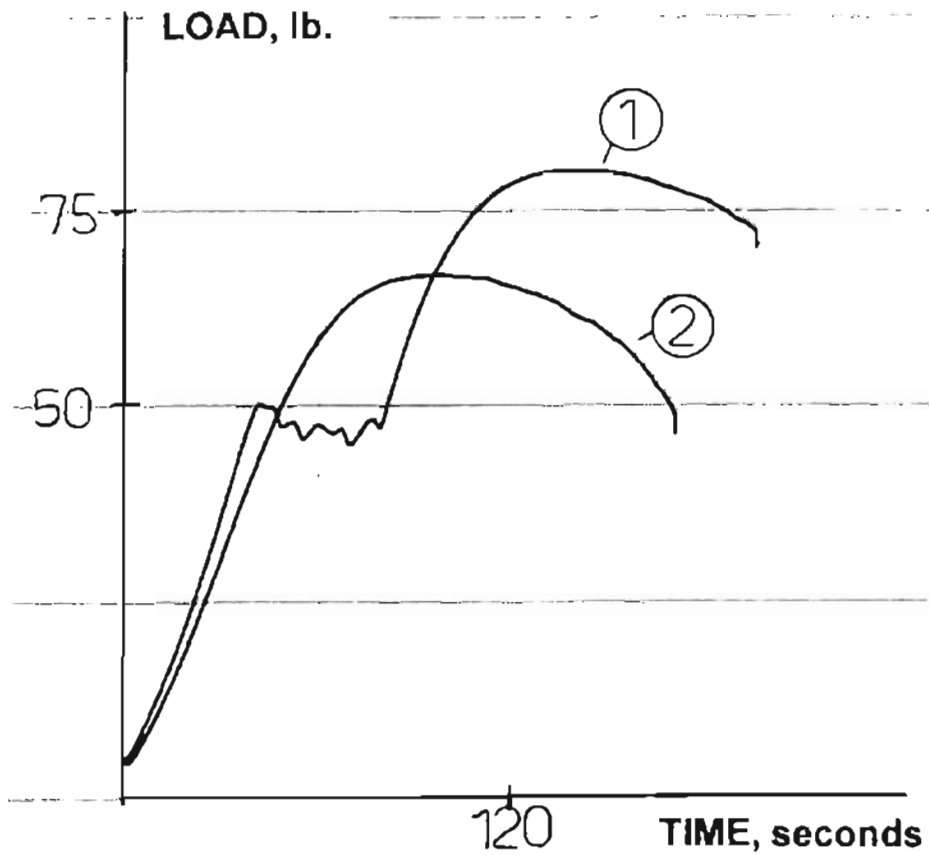
Figure 3.12: By improving the rigidity of the lower C-type fixture, the wave-pattern problem was eliminated.

1. Load-time record for 92 gauge ICI polyester film specimen tested in MD $(2W = 8.0, 2H = 1.25, \text{ and } 2a_0 = 2.0 \text{ inch})$.
2. Load-time record for 92 gauge ICI polyester film specimen tested in MD $(2W = 8.0, 2H = 1.25, \text{ and } 2a_0 = 3.0 \text{ inch})$.

(5) Means of recording the crack extension data – a camcorder with high

   magnification lens, or a precision close up lens still photography camera.

(6) Means of relating the crack extension data to the load-time data – an LCD

   (Liquid Crystal Display) multimedia projector or an image capturing software

   and hardware, using a PC.

The fracture testing apparatus developed by Klemann et al. [5] is among

the best (Figure 3.13). Fracture testing was conducted on an Instron model 1125

tensile testing machine with either a 50 lb. or a 1 lb. load cell and a crosshead

displacement rate of 0.0508 cm/min (0.02 inch/min) at 23°C and 50% RH. The

gage length of the SENT specimen was 5.08 am (2.0 inch). A Javelin MOS solid-

state camera connected to an Olympus SZH optical microscope and a VCR were

used to record the tests. A Fiberlite high-intensity illuminator was placed behind

the specimen in order to provide enough light for the microscope. Magnifications

of 15 to 50X were used; crack lengths were measured at the low magnifications,

and fracture initiation data were taken at the high magnifications. The output load

of the Instron was sent to an Apple Macintosh computer equipped with a

National Instruments data acquisition board. Using Labview II data analysis

software, the load cell voltages were converted to a tensile stress reading. The

computer screen was videotaped and inset in the corner of the picture with a

Multivision video mixer, thus giving an instantaneous readout of the stress for

each frame. A schematic of the testing apparatus is shown in Figure 3.13. The

video was analyzed on a Macintosh computer equipped with a video grabber

using the Image Processing software. The image analysis system facilitated
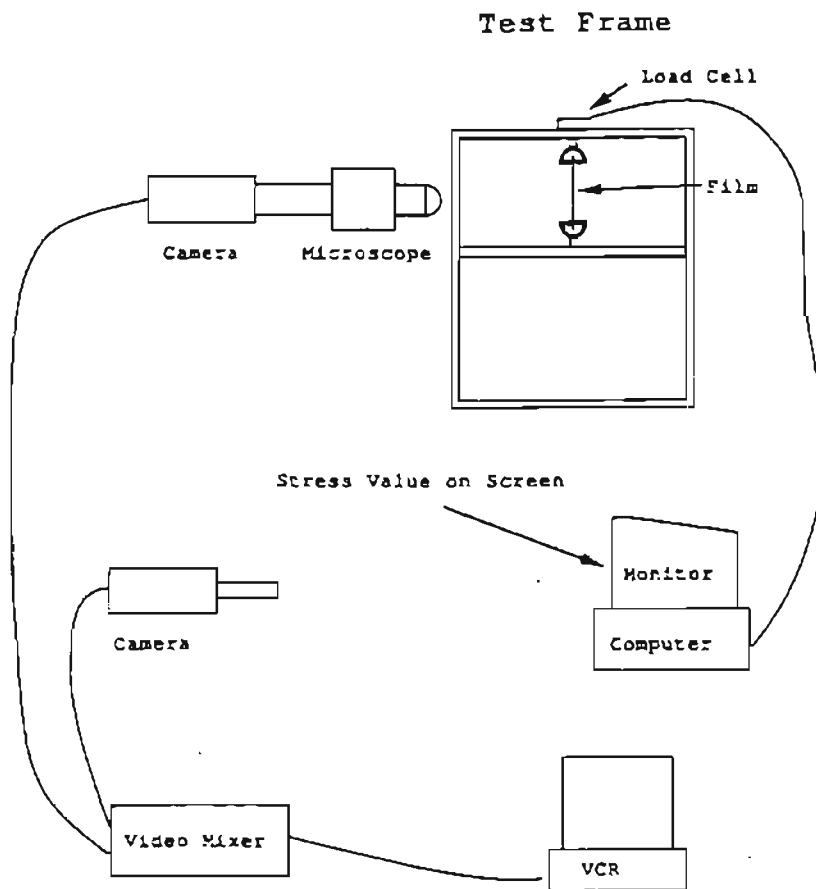
Figure 3.13: Schematic of apparatus for fracture testing developed by Klemann et al. [5].

determination of stress, strain, and crack lengths frame-by-frame, and also allowed precise determination of the stress level at which crack growth initiated.

Tielking [21] made use of separate data acquisition and single camera video imaging facilities. He reports videotaping of a complete test run on a polyethylene film. Although LDPE film is highly transparent, it is possible to adjust the lighting so that the precut crack is clearly seen in the video image. A dark background is found effective for this. The camera is set so that both ends of the crack are visible, with room for crack growth to be recorded. High band 8 mm (Hi8) video tape is used. Image capturing system similar to that reported by Klemann et al. [5] is used. Initially, images are captured at 5 sec intervals, for 2 minutes. This sequence includes the crack growth initiation even. Images are then captured at 30 sec intervals for the remaining 4 minutes of the test.

The fracture testing apparatus developed for this work is shown in Figures 3.14, and 3.15. The apparatus consists of the following:

(1) Instron model 4202 electromechanical universal testing machine. The important specifications are listed in Table 3.1.

(2) A 100 lb. and 2000 lb. Instron load cells. A 2000 lb. load cell is calibrated at 10% and 20% of its full capacity to operate at load values of 200 lb., and 400 lb. respectively.

(3) A PC based data acquisition system. National Instruments data acquisition board and LabView data analysis software are used for this facility.

(4) A SOLTEC XY recorder. A4 size precision ruled grid paper is used for plotting load-time records.

Table 3.1: Important performance specifications of Instron model 4202 electromechanical universal testing machine [47].

Specification	
Testing area	Below the moving crosshead
Capacity	10 kN, 1000 kg, 2250 lb.
Load range - using interchangeable load cells	0.1 N to 10 kN, 10 g to 1000 kg, 0.022 lb. to 2250 lb.
Load weighing system accuracy at digital readout or analog output (@ 25°C)	±0.5% of reading to 1/10 of load cell capacity. ±1% of reading to 1/50 of load cell capacity. ±1 count on the display accuracy
Position measurement (no load)	±0.1 mm (0.004 inch) or ±0.15% of displacement
Position measurement repeatability (no load)	±0.05 mm (0.002 inch)
Crosshead speed range	0.5 to 500 mm/min (0.02 to 20 in/min)
Crosshead speed accuracy	±0.2% of setting over full speed range averaged over 100 mm (4 inch).
Return and jog speed	500 mm/min (20 inch/min)
Machine stiffness (including drive belts, components, and frame)	28 kN/mm (160000 lb./inch)
Crosshead travel (excluding grips and fixtures)	1170 mm (46.1 inch)
Testing space Lateral: Front to back:	412 mm (16.2 in) Unlimited
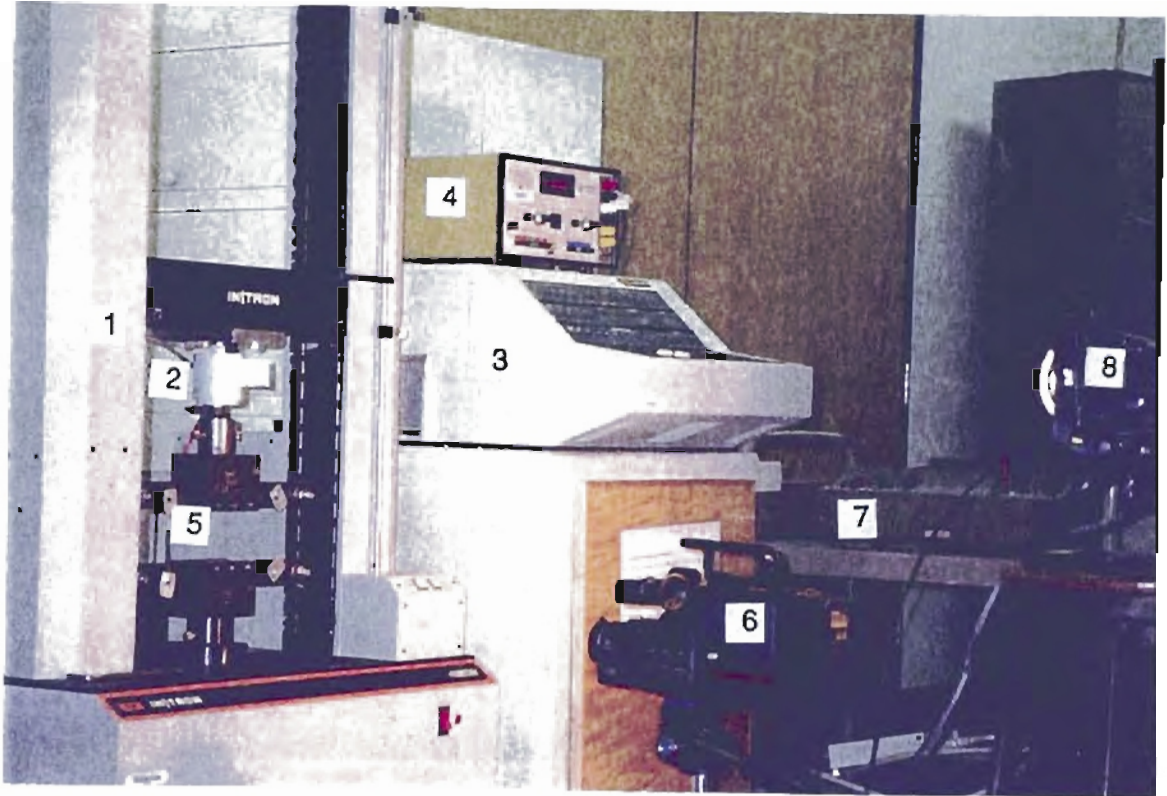
Figure 3.14: Fracture testing apparatus developed for this work.

1. Instron model 4202 electromechanical universal testing machine.
2. A 100 lb. load cell.
3. Control console for Instron 4202.
4. Strain indicator panel used for load measurements with the 100 lb. load cell.
5. CST test grip fixture.
6. Canon VM-E708 camcorder.
7. Soltec XY recorder.
8. Halogen light used for background lighting (not used in the position shown).
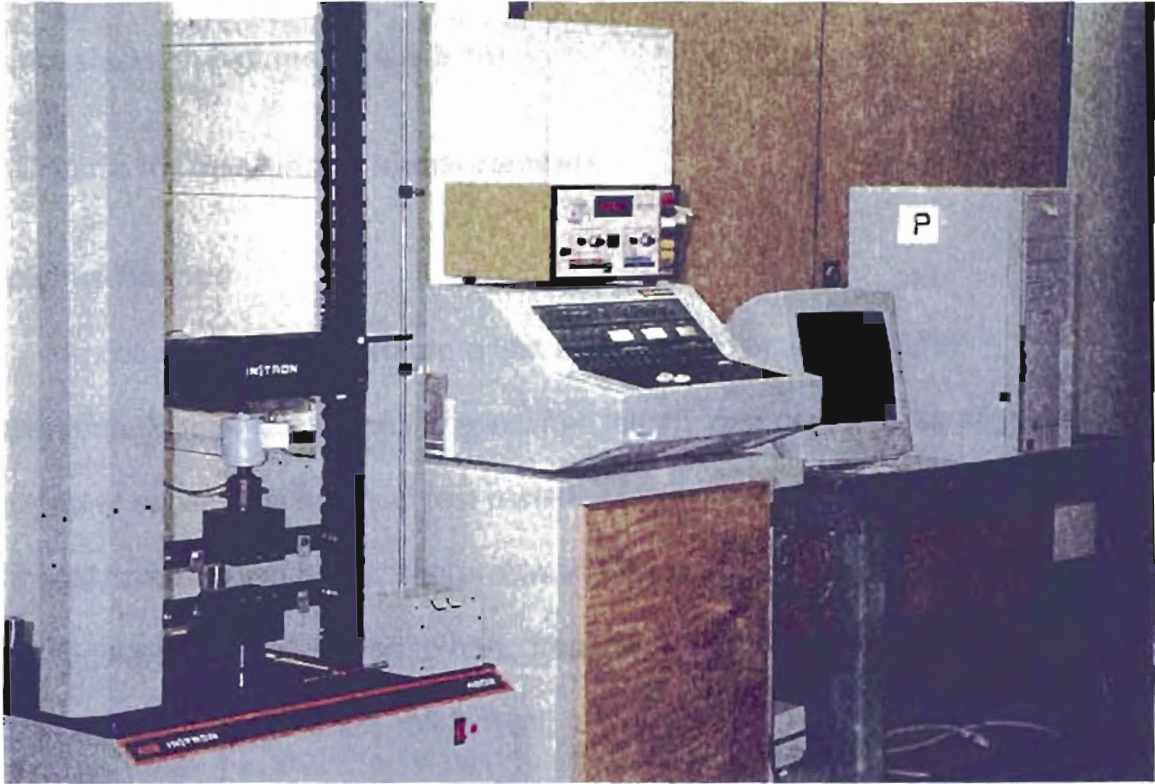
Figure 3.15. Fracture testing apparatus with a PC based data acquisition system.

P. PC based data acquisition system with a National Instruments data acquisition board (not shown) and Labview data analysis software.

(5) A Canon VM-E708 , 8 mm video camera and recorder [48]. SONY 8 mm,

metal MP videotape is used for recording test runs.

(6) Sharpvision LCD multimedia projector (not shown in Figures 3.14 & 3.15).

(7) SNAPPY snapshot hardware and software for a PC based image capturing

(not shown in Figures 3.14 & 3.15).

3.3 Criteria for meaningful measurements

Applying the load

Application of load to fracture test specimens demands careful

preparation. Minute differences in specimen length, grip pressure, or alignment

can lead to substantial errors in test results. Means such as universal joints,

spherical compression seats, and preloading are commonly used [40]. The

upper C-type fixture is allowed to hang freely in the plane perpendicular to that of

the specimen to promote self -alignment.

All test specimens are preloaded to 5 lb. Preloading removes 'slack' in the

load-time record (Figure 2.9 & 3.16), and improves the repeatability of test

results.

Measuring the load

Determining the magnitude of the applied load is, in terms of instruments

availability, one of the easiest and most precise aspects of the fracture testing

process. Use of precision testing machine, load cells and an XY recorder is

made. By eliminating the anti-buckling plates, the source of friction forces in load

measurements is countered.
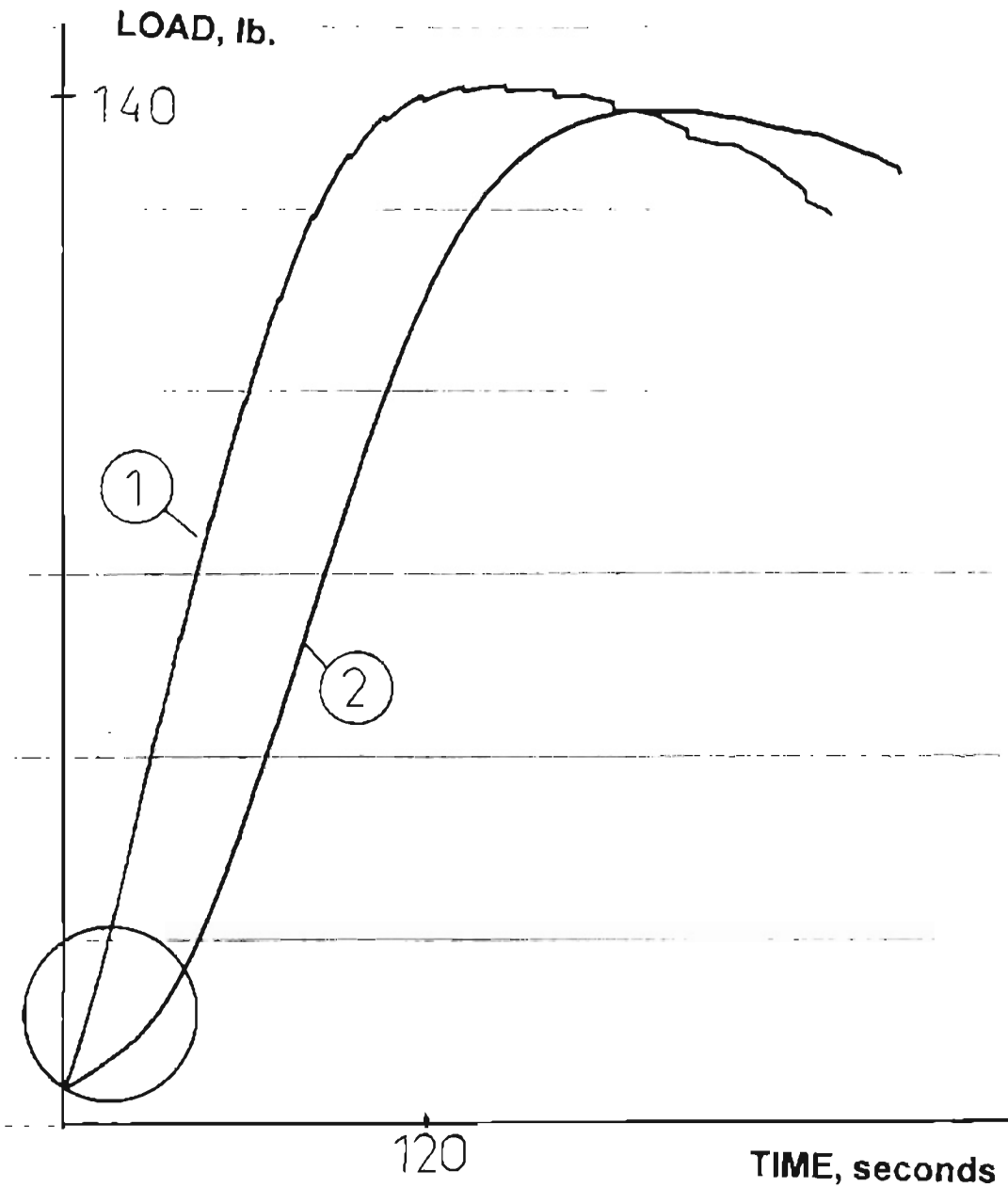
Figure 3.16: Load-time record # 2, showing 'slack' in the circled area.

1. Load-time record for 92 gauge ICI polyester film specimen tested in MD
(2W = 12.0, 2H = 2.0, and $2a_0$ = 1.0 inch).
2. Load-time record for 92 gauge ICI polyester film specimen tested in MD
(2W = 12.0, 2H = 2.0, and $2a_0$ = 1.5 inch).

Measuring deformation

The gages that measure deformation independently on the body of the specimen are not generally used by current polymer film, and paper testing practices. Rather, it is a common practice to measure deformation of the clamps through which the load is applied. For this work, time data based on the crosshead displacement measurements obtained directly from the machine's control console, are considered fairly accurate. The potential for slippage in the clamps, and the fact that the strain in the area of the clamps is, in general, not the same as it is on the body of the specimen, introduce sources of error [40]. However, the slippage problem is completely eliminated (section 3.1). No other suitable technique for time/deformation measurements is considered.

Scaling

The linear portion of the load-deformation curve should be at least 5 cm long in order to accurately measure the slope and coordinates for determination of the elastic region [40]. The horizontal or deformation scale should be generous enough to allow one to accurately determine the proportional limit.

Introducing a sharp center crack

The permissible bluntness of the crack tip depends on material properties, and has to be determined from experiments [22]. If the bluntness of the crack tip is sufficient to raise the stress, σ_i for the crack initiation above the fracture stress, σ_c, this simulation of the crack is not valid (Figure 3.17). In general, sharper cracks are required for materials of lower toughness [22]. Each test specimen is
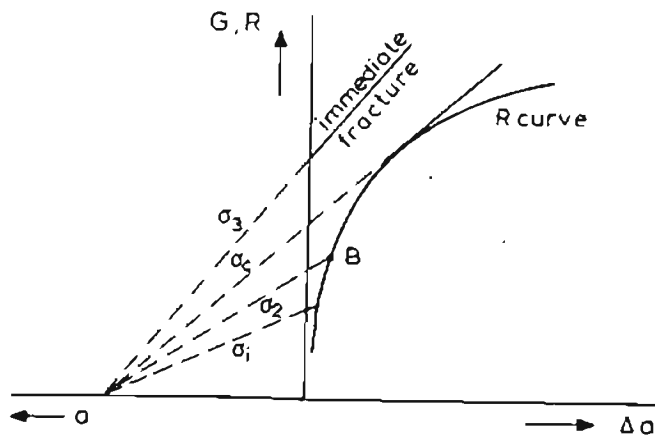
Figure 3.17: Blunt crack tips in plane stress testing [22].

σ_i is the initiation stress. If stress is raised to σ_2 due to bluntness of the crack tip, the simulation is permissible. However, if bluntness raises stress, σ_3 above that of the critical stress σ_c, immediate fracture occurs.

supported on a lightweight cardboard and the center crack of required size is cut with a slicing motion and light hand pressure, using a precision knife.

3.4 Testing procedure

The testing procedure is elaborated in this section. The sequence of activities detailed here is important.

(1) Test specimens are created by cutting large sheets of a polymer film from the rolls, as supplied by the manufacturer (Figures 3.18 - 3.20). Stiff cardboard templates are used for a quick and precise cutting of test specimens, and for creating center cracks in them (Figure 3.21). Polymer film test specimens are marked using a ball point pen. A pen with a sharp point which indents the surface of the film, should not be used. Metallic foils are more sensitive to surface indentation and marked using a soft sketch pen point. Center lines, center crack marks, and crack growth limiting marks for a total of 1 inch crack growth, are drawn on the test specimens.

(2) Pretest preparations: Instron 4202 electromechanical testing machine's power supply is turned on. The load cell must be allowed to 'warm up' for 15 minutes before operation, for accurate measurements [47]. Crosshead travel limit stops are set as per testing requirements. A spring seat arrangement is mounted on the lower C-type fixture. A Soltec XY recorder, or PC based data acquisition system, and a Canon camcorder are set for data recording. The camcorder is arranged so that both the ends of crack are visible, with a room for crack growth (1 inch) to be monitored. Background lighting is arranged to
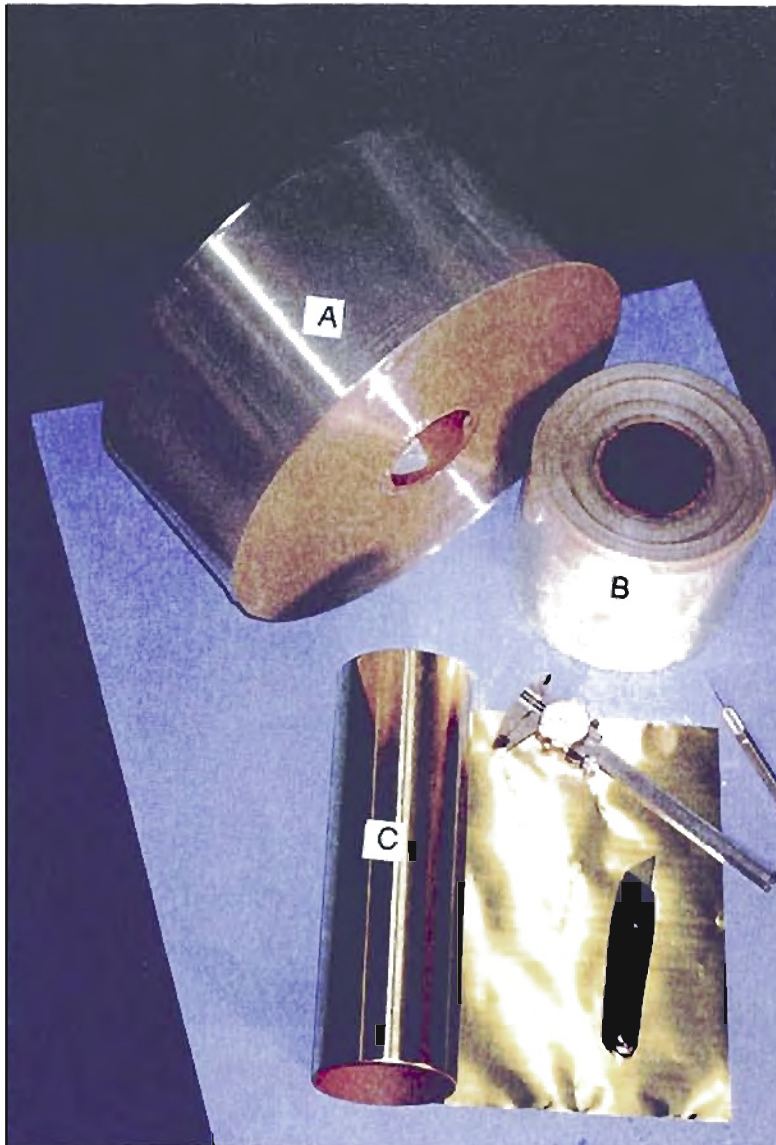
Figure 3.18: Rolls of test materials as supplied by the manufacturer.

A. ICI 48 gauge polyester film.
B. ICI 200 gauge polyester film.
C. Brass shim stock (0.001 inch thick)
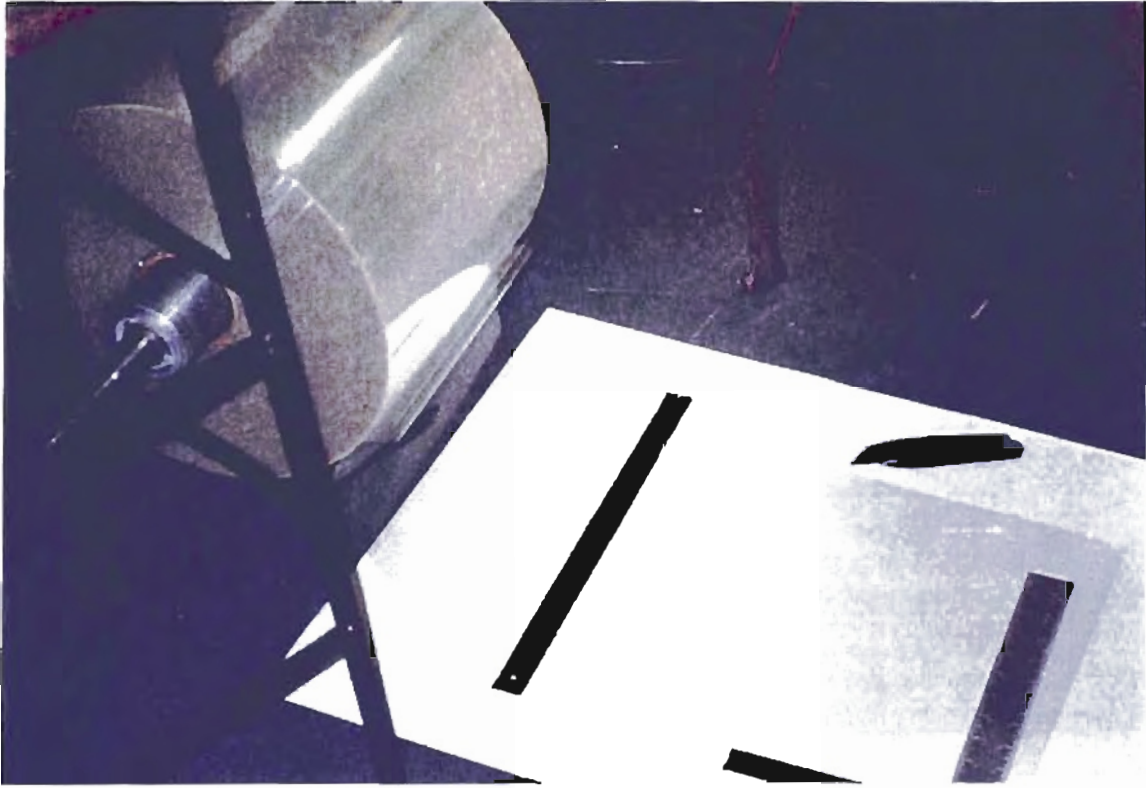
Figure 3 19: Large sheets (about 15 x 12 inch) are cut from the film roll. ICI 92 gauge, 12 inch wide polyester film is shown in the figure.
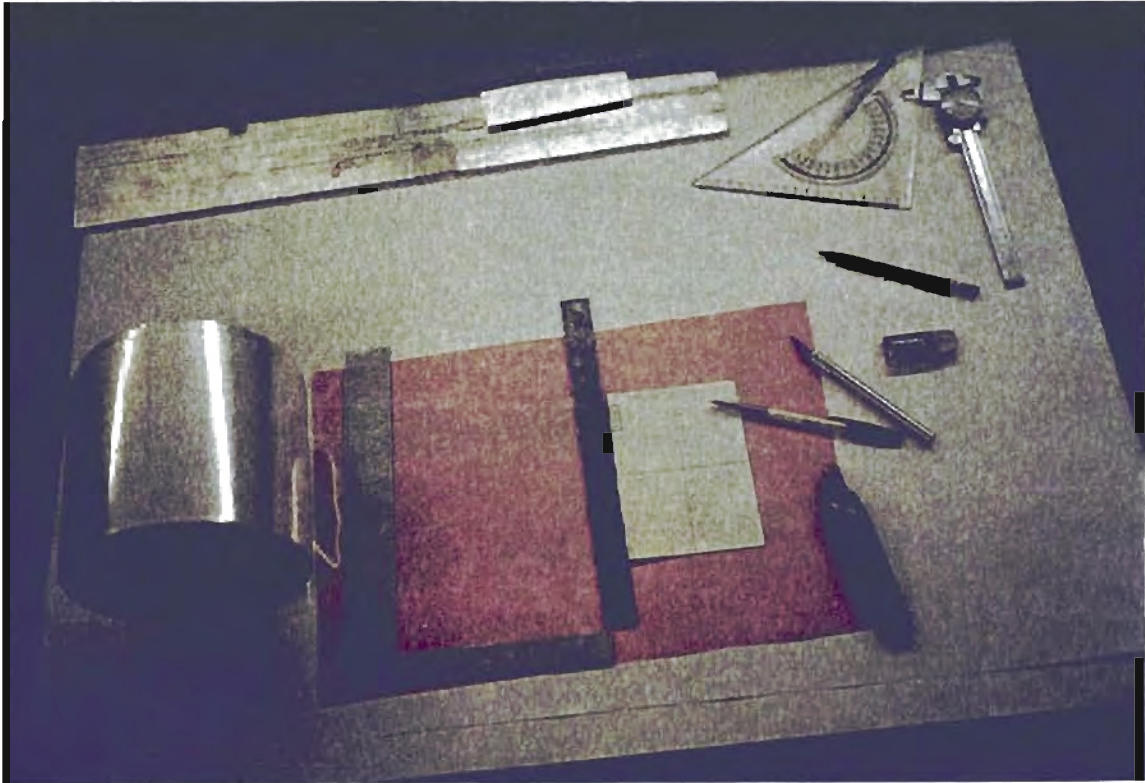
Figure 3.20: Test specimens of exact size requirements are cut directly using cardboard templates, from the smaller film rolls. ICI 200 gauge, 6 inch wide polyester film is shown in the figure.
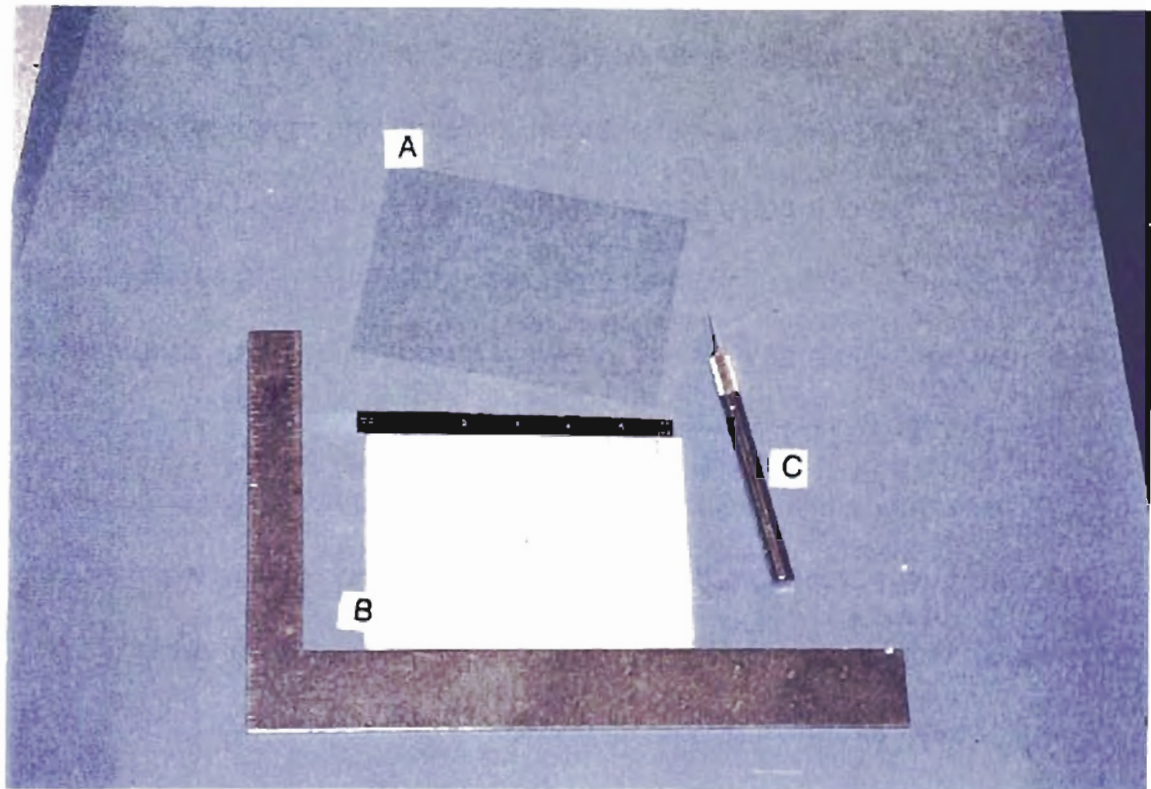
Figure 3.21: Creating test specimens.

A. 6 x 4.25 inch, 92 gauge (0.00092 inch), MD, ICI polyester film specimen. As 3 inch of the specimen height is gripped, the effective specimen height is 1.25 inch.
B. Stiff cardboard template.
C. Precision knife.

clearly observe a growing crack in transparent polymer film specimens (Figure 3.22).

(3) Specimen preparation: The top and bottom grips are positioned apart for the desired specimen height using the holding plates. The test specimen is then carefully positioned and aligned on the lower grip faces. the upper grip faces are then placed on the film. The holding plates are inserted in the location pins to fix the height and the position of the film specimen. The grip bolts are tightened to a fixed torque value predetermined using a torque wrench. The holding plates are moderately clamped onto the grip plates. The top and bottom grips, with the specimen between, are then carefully lifted with the help of clamped holding plates and carried to the Instron 4202. The grip assembly is placed on the spring seat (Figure 3.23). The spring seat arrangement aids in connecting the top grip to the upper C-type fixture and minimizes handling abuse. The top grip is clamped to the upper C-type fixture. The crosshead is moved up and the spring seat is removed. The crosshead is then moved down and the bottom grip is clamped to the lower C-type grip fixture. The grip or clamping pressure is then optimally adjusted to the same torque value as for the grip bolts (about 40 lb. force, depending on materials to be tested). The number of screw turns can be used as a thumb rule in routine. The holding plates are unclamped from the grips and removed. The test specimen is then, preloaded to 5 lb. to remove 'slack'.

(4) Data recording: The operation of Soltec XY recorder, or PC based data acquisition system, and Canon camcorder is synchronized to relate the load-
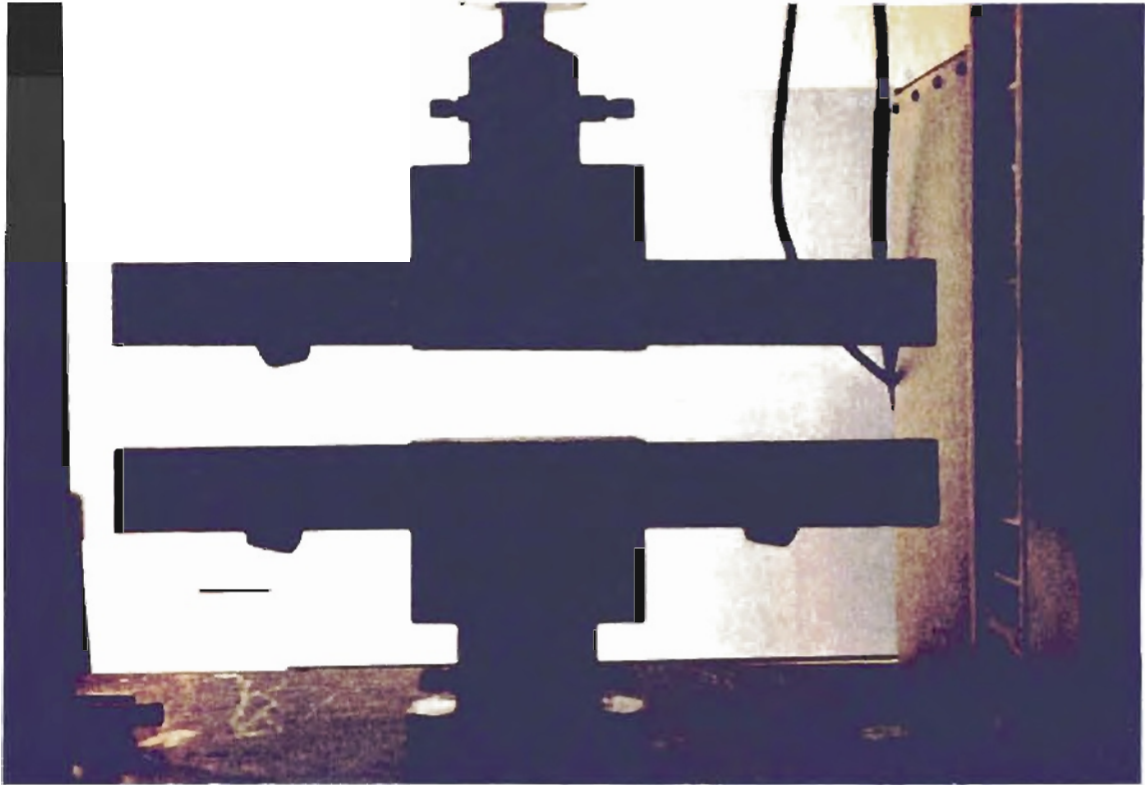
Figure 3.22: Background lighting arrangement for CST fracture testing, using a halogen light. In the figure, only the edges of completely fractured specimen are seen. Using high shutter speed (1/1000), it is possible to record crack growth in a transparent polymer film with a camcorder
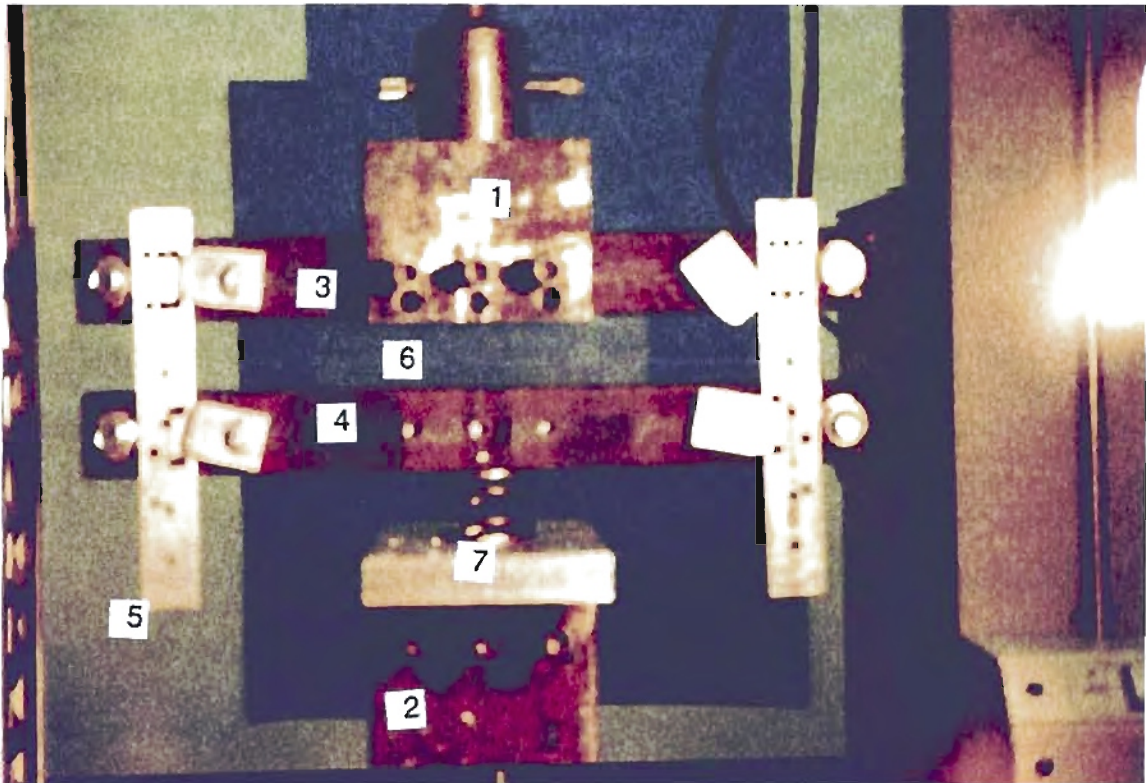
Figure 3.23: Spring seat arrangement for the CST test grip fixture

1. Upper C-type fixture.
2. Lower C-type fixture.
3. Top grip.
4. Bottom grip.
5. Holding plates.
6. CST test specimen.
7. Spring seat arrangement.

time data with the crack extension data. The test is originated by moving the Instron crosshead up at a fixed displacement rate of 0.04 inch/min. All testing is done at room temperature (23°C). The crack growth is monitored and recorded. when the crack extends to the limiting marks, the crosshead movement is stopped. The crack growth measurements are made later using a Sharpvision LCD multimedia projector. 5X to 15X magnification of the original crack sizes is obtained through the projection. A PC based image capturing using SNAPPY snapshot hardware and software, is also tried.

3.5 Data collection plan

The focus of this study is to explore geometrical constraints of the CST test. The data collection plan is developed keeping the following requirements in perspective.

- The finite elements results of Cotterell et al. [19] suggest following constraints for the CST test specimen to obtain useful results:

  (i) Half width, $W > 5H$, where H is the half height (Figure 2.10). A typical specimen tested by Cotterell et al. [19,20] had $W = 10H$.

  (ii) Initial crack length, $2a_0 > 0.8H$.

  (iii) Poisson's ratios for the test materials should be in the range of 0.3 to 0.5.

  (iv) $H > 14r_y$, where r_y is the radius of plastic zone.

- The Feddersen analysis poses the following screening requirements for valid plane stress fracture testing [22]:

(i) Critical stress, $\sigma_c < \dfrac{2}{3}\ \sigma_{ys}$, where σ_{ys} is the yield stress.

(ii) Initial crack length, $2a < \dfrac{2W'}{3}$, $2W$ being the width of specimen.

The geometrical constraints mentioned above, are intentionally violated for some of the test specimens. More test runs are planned for specimen geometries anticipated to give better data. The final test runs are made on ICI polyester films of 48 (0.00048 inch), 92 (0.00092 inch), and 200 (0.002 inch) gauges. The film rolls are available in standard widths of 6 inch and 12 inch. The Poisson's ratio value is assumed to be 0.4 for polyester films. Table 3.2 presents the data collection plan followed for this work.

Table 3.2: Data collection plan for the CST testing

Test run No.	Specimen width (2W) inch	Specimen height (2H) inch	Initial crack lengths (2a$_0$) inch	Test material and conditions
1	4.0	0.8	0.8, 1.2, and 2.0	Narrow, nonstandard width, polyester 92 gauge MD specimens
2	6.0	0.8	0.8, 1.0, 1.5, 2.0, and 3.0	Standard width, polyester 48 gauge MD specimens
3	6.0	0.8	1.0, 1.5, 2.0, 2.4, and 3.0	Standard width, polyester 92 gauge MD specimens
4	6.0	0.8	0.8, 1.0, 1.5, 2.0, and 3.0	Standard width, polyester 200 gauge MD specimens
5	6.0	1.25	1.0, and 2.0	Polyester 92 gauge MD specimens
6	6.0	2.0	1.6, and 2.0	Polyester 92 gauge MD specimens
7	8.0	0.8	0.8, 1.0, 2.0, 2.5, and 3.0	Nonstandard width, polyester 92 gauge MD specimens
8	8.0	1.25	1.0, 2.0, and 3.0	Nonstandard width, polyester 92 gauge MD specimens
9	8.0	2.0	1.0, and 2.0	Nonstandard width, polyester 92 gauge MD specimens
10	8.00	3.0	2.0	Nonstandard width, polyester 92 gauge MD specimens

Test run No.	Specimen width (2W) inch	Specimen height (2H) inch	Initial crack lengths ($2a_0$) inch	Test material and conditions
11	12.00	0.8	0.8, 1.5, 2.0, 3.0, and 4.0	Standard width, polyester 92 gauge MD specimens
12	12.0	1.25	1.0, 1.5, 2.0, and 4.0	Standard width, polyester 92 gauge MD specimens
13	12.0	1.25	1.0, 1.5, 2.0, and 4.0	Standard width, polyester 92 gauge CD specimens
14	12.0	2.00	1.0, 1.5, and 2.0	Standard width, polyester 92 gauge MD specimens
15	12.0	3.0	2.0	Standard width, polyester 92 gauge MD specimens

(Table 3.2, continued from the previous page)

3.6 Determination of K_C using K_R-curves

The effect of slow stable crack growth can be characterized by the use of R-curves. An R-curve is a plot of the crack growth resistance as a function of effective crack extension, Δa. In literature, and in practice, the R-curve is no longer considered in terms of G and R [23]. Instead, the stress intensity factor concept has found wide spread application and the energy balance parameters G and R may be simply converted to stress intensities via the relation $K = \sqrt{EG}$.

A schematic R-curve in terms of K_G and K_R is shown in Figure 3.24. In this diagram, there are three important points [23]:

1. K_0 is the point of initial crack extension.

2. K_C is the critical stress intensity (instability point).

3. K_{plat} is the plateau level of the K_R-curve.

K_0 has been shown experimentally to be independent of specimen thickness and to have a constant value for a particular material [23].

For K_C, however, there is a strong effect of specimen thickness. Thinner specimens give higher K_C values and exhibit more slow stable crack growth, since K_0 remains constant.

K_{plat} also depends strongly on specimen thickness. This parameter is not a generally accepted feature of the K_R-curve. A number of authors consider the existence of K_{plat} to be due to specimen finite geometry effects, and that the K_R-curve for very wide specimens would attain a constant non-zero slope rather than a plateau level [23].
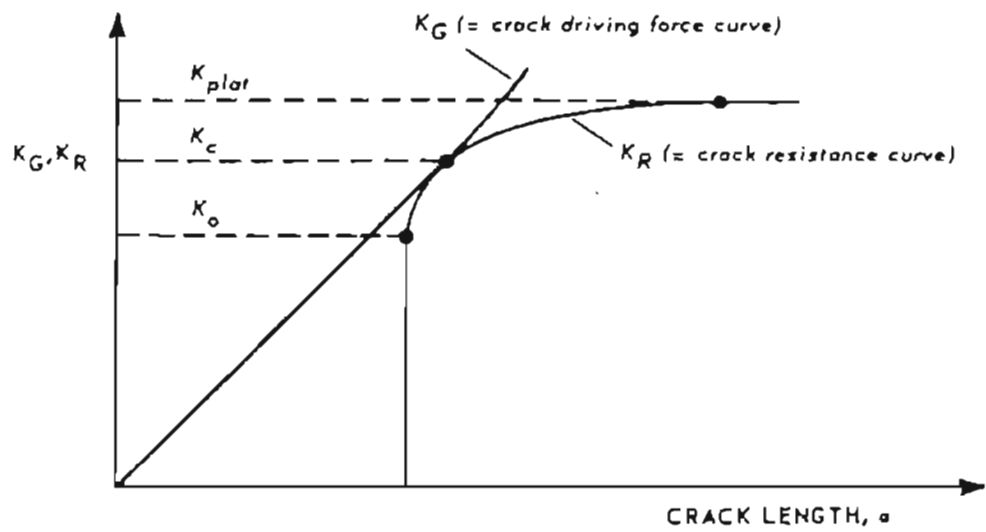
Figure 3.24: The R-curve in terms of stress intensity factor notation [23].

K_R-curves are independent of initial crack length, a_0. However, K_C is approximately constant for only a limited range of crack lengths. The relation between K_R-curve and K_C testing is summarized schematically in Figure 3.25. The shape of the K_C-K_0 curve in Figure 3.25 (b) is due to two effects which partly oppose each other. First, moving the K_R-curve along the crack length axis tends to raise the (K_G, K_R) tangency points. Second, the K_G line becomes markedly curved for longer initial crack lengths, owing to the influence of finite specimen width on the stress intensity factor. Increasing curvature of the K_G lines tends to lower the (K_G, K_R) tangency points [23].
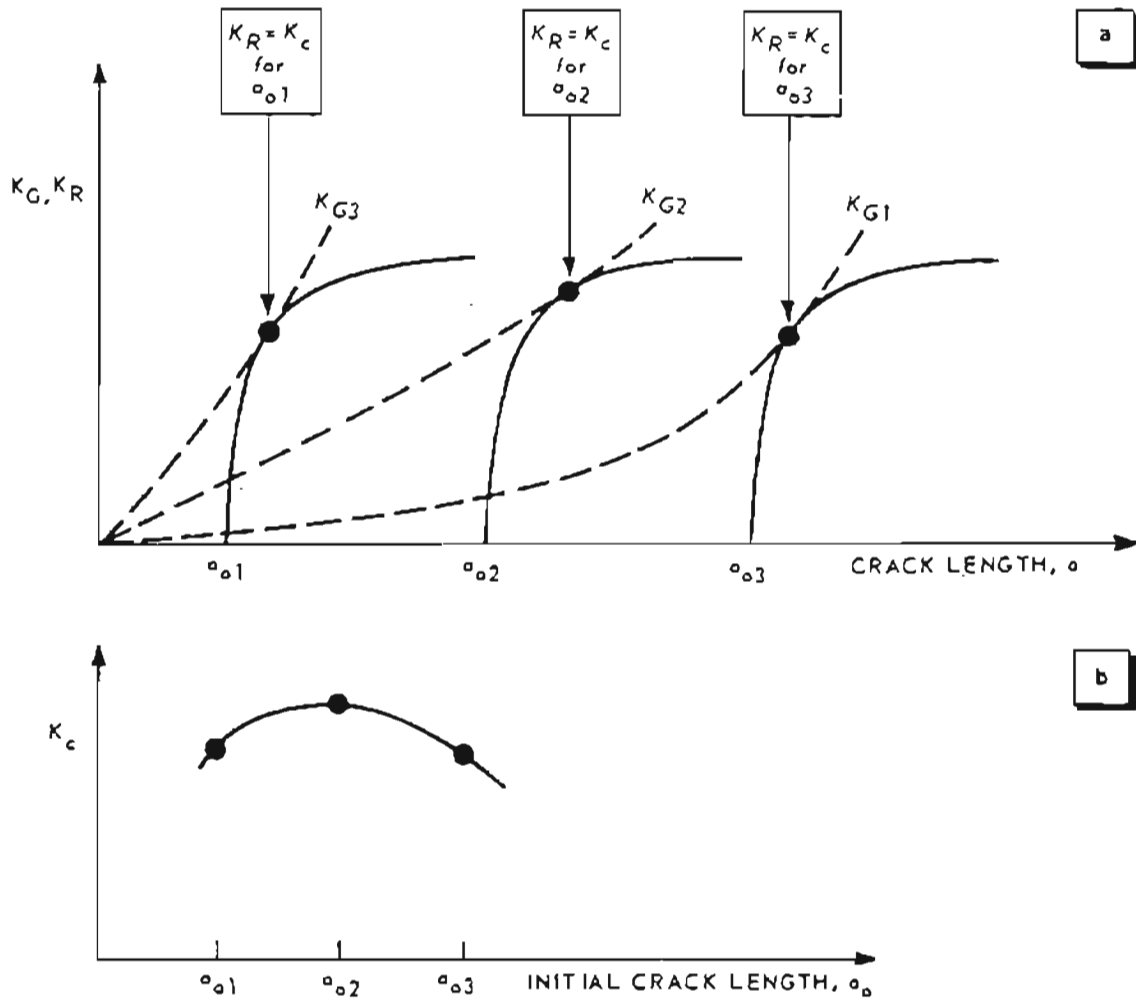
Figure 3.25: Use of K_R-curves for determining K_C as a function of initial crack length [23].

CHAPTER 4

RESULTS AND DISCUSSION

4.1 Load-time records

Load-time records of the test runs were obtained using an XY recorder.
Examples are shown in Figures 4.1-4.8. For the equivalent test specimens,
preloaded to 5 lb., the repeatability of load readings was found better than ±2 lb.
Thinner gauge (48, and 92 gauge) film rolls had edge waviness and crazes. An
attempt was made to utilize the defect-free area of the film while preparing test
specimens. Scaling was optimized, based on the time taken for the observed
crack growth (horizontal scale), and the peak load values reached during the test
runs (vertical scale). Important observations are listed here:

- For test specimens of the same width, height, gage, and material, the peak
load values were observed to decrease with an increase in initial crack
lengths.

- The peak load values for polyester films, were found to be approximately
120-150% of the crack initiation load values.

- For the test runs no. 12 and 13 (refer to Table 3.2), almost similar load-time
records are obtained for like specimens tested in MD, and CD. Load-time
records for CD test specimens showed a slightly increased slope in the linear
region (Figures 4.3-4.5). This behavior is explained by the biaxial orientation
of polyester films. Orientation of film by stretching it under heat is widely
applied to plastic films to improve clarity, impact strength, and barrier
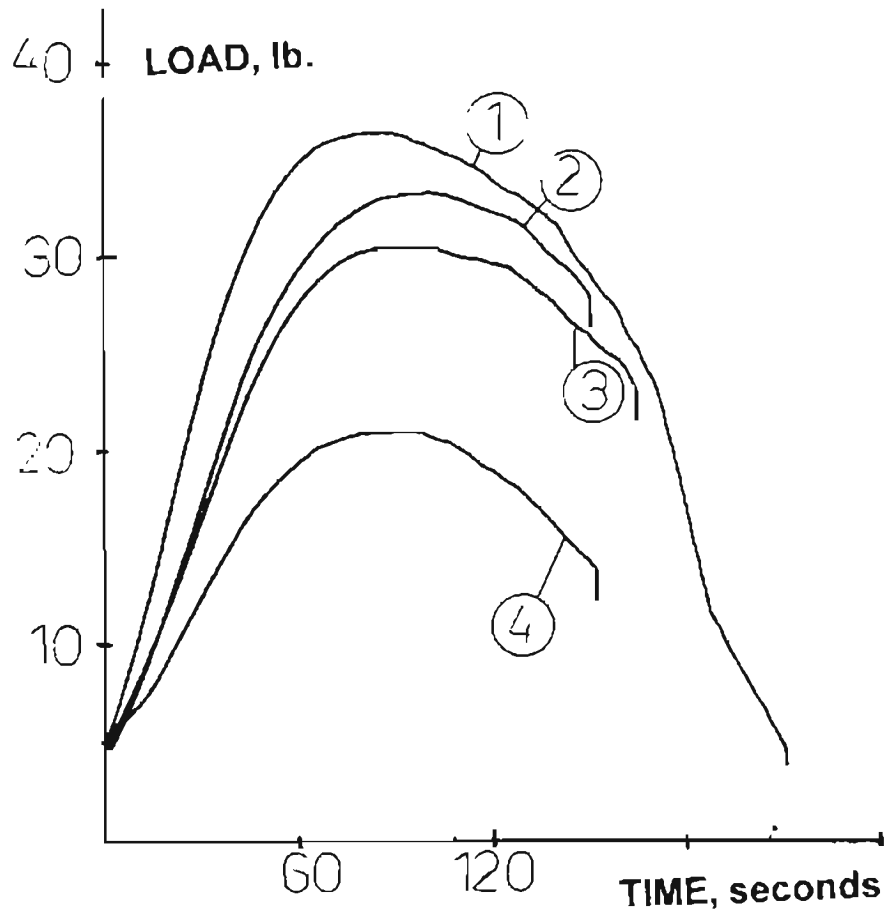
Figure 4.1: Load-time records for 48 gauge ICI polyester film specimens having different initial crack lengths ($2a_0$), tested in MD. (2W = 6.0, 2H = 0.8 inch).

1. $2a_0$ = 1.0 inch
2. $2a_0$ = 1.5 inch
3. $2a_0$ = 2.0 inch
4. $2a_0$ = 3.0 inch
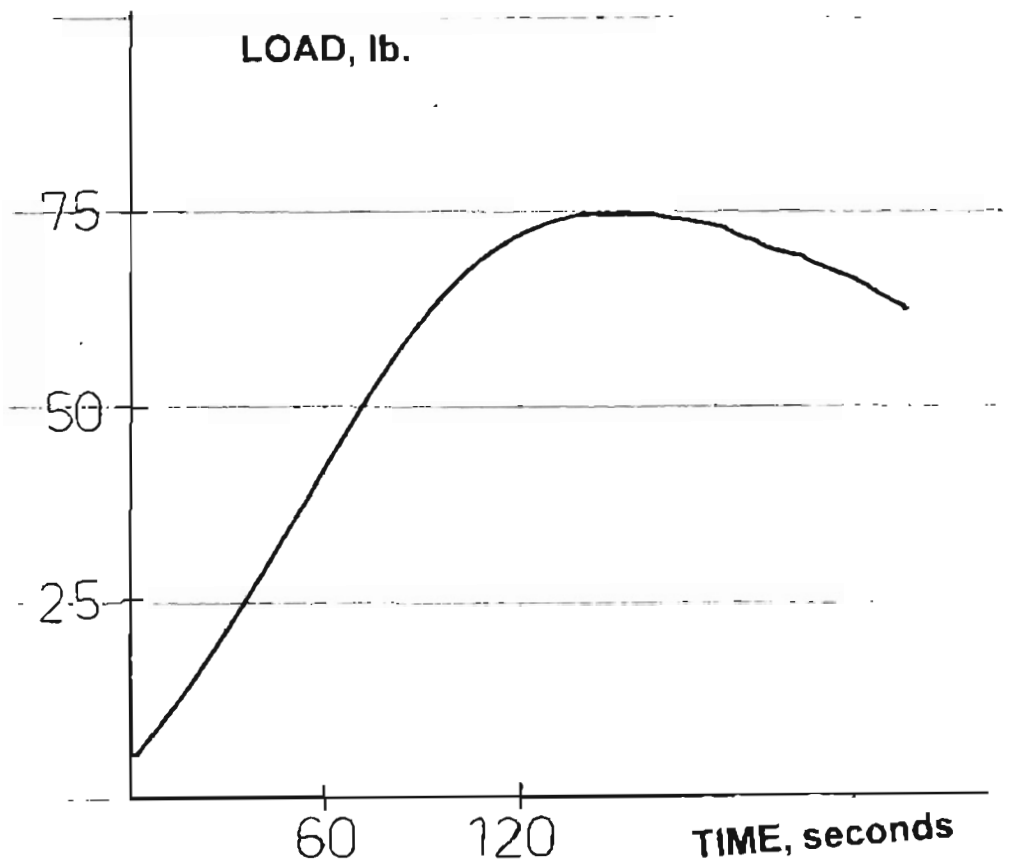
Figure 4.2: Load-time record for 92 gauge ICI polyester film specimen tested in MD (2W = 8.0, 2H = 3.0, and $2a_0$ = 2.0 inch).
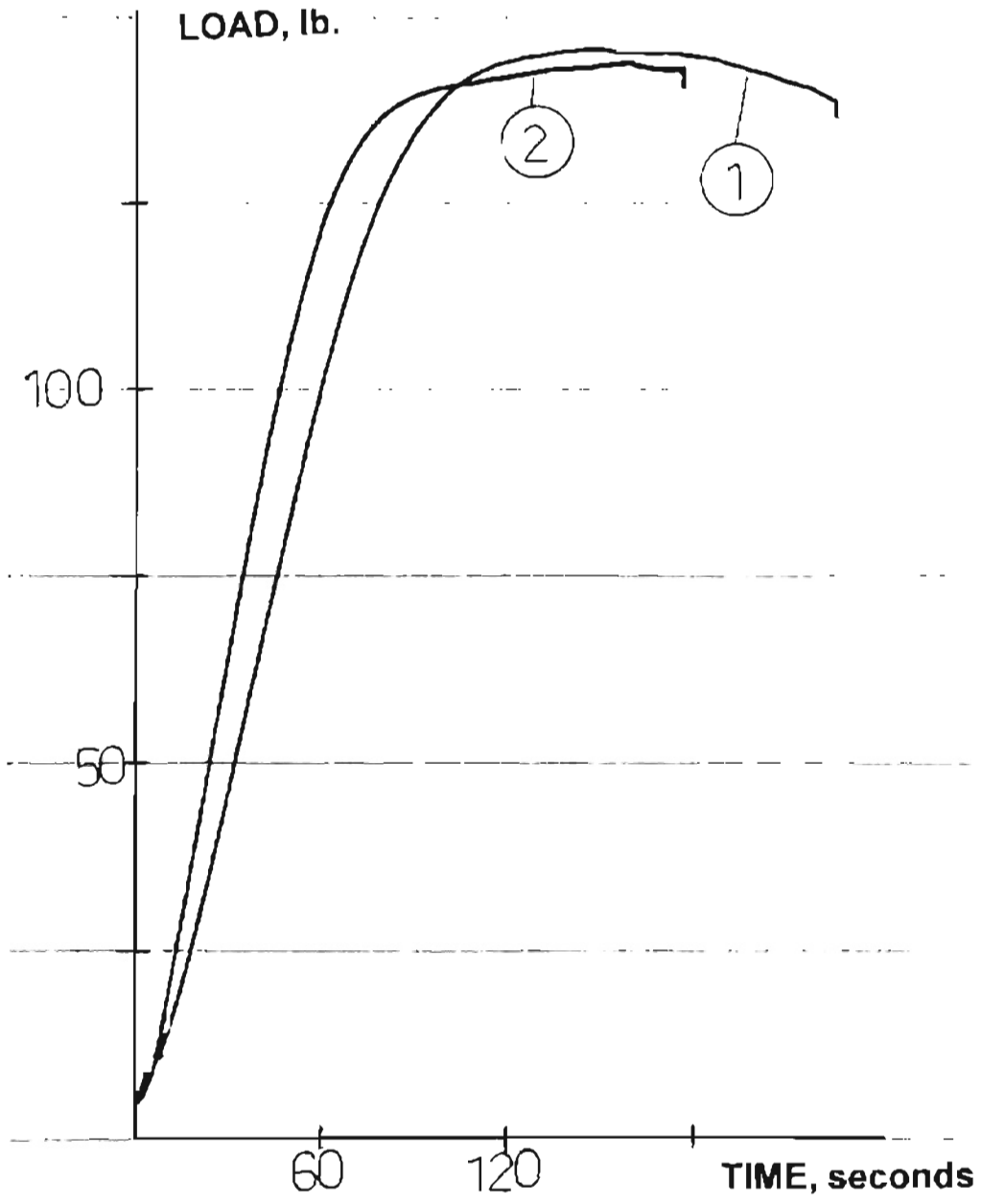
Figure 4.3: Load-time records for 92 gauge ICI polyester film specimens tested in, 1. MD, and 2. CD (2W = 12.0, 2H = 1.25, and $2a_0$ = 1.5 inch).
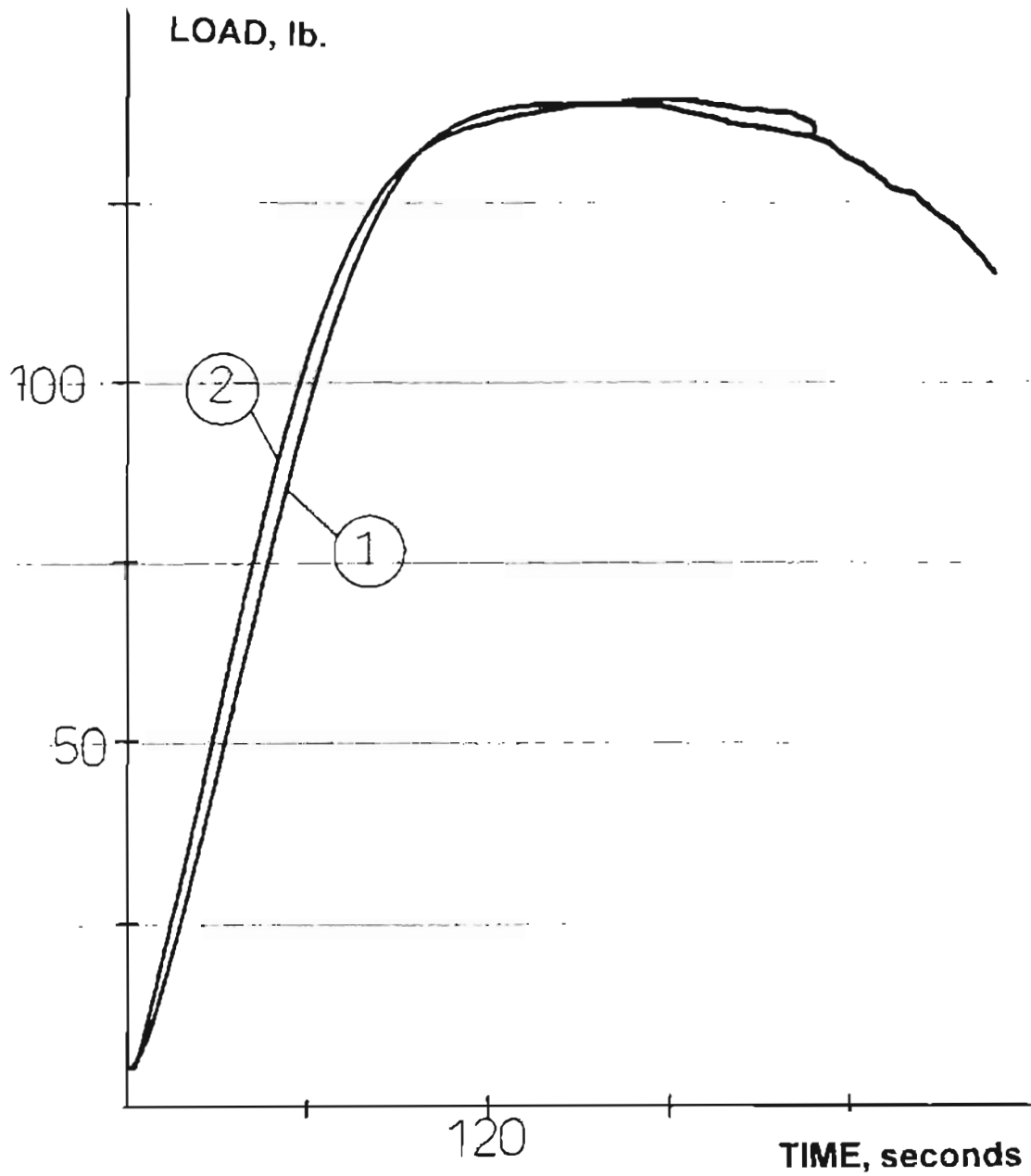
Figure 4.4: Load-time records for 92 gauge ICI polyester film specimens tested in, 1. MD, and 2. CD (2W = 12.0, 2H = 1.25, and $2a_0$ = 2.0 inch).
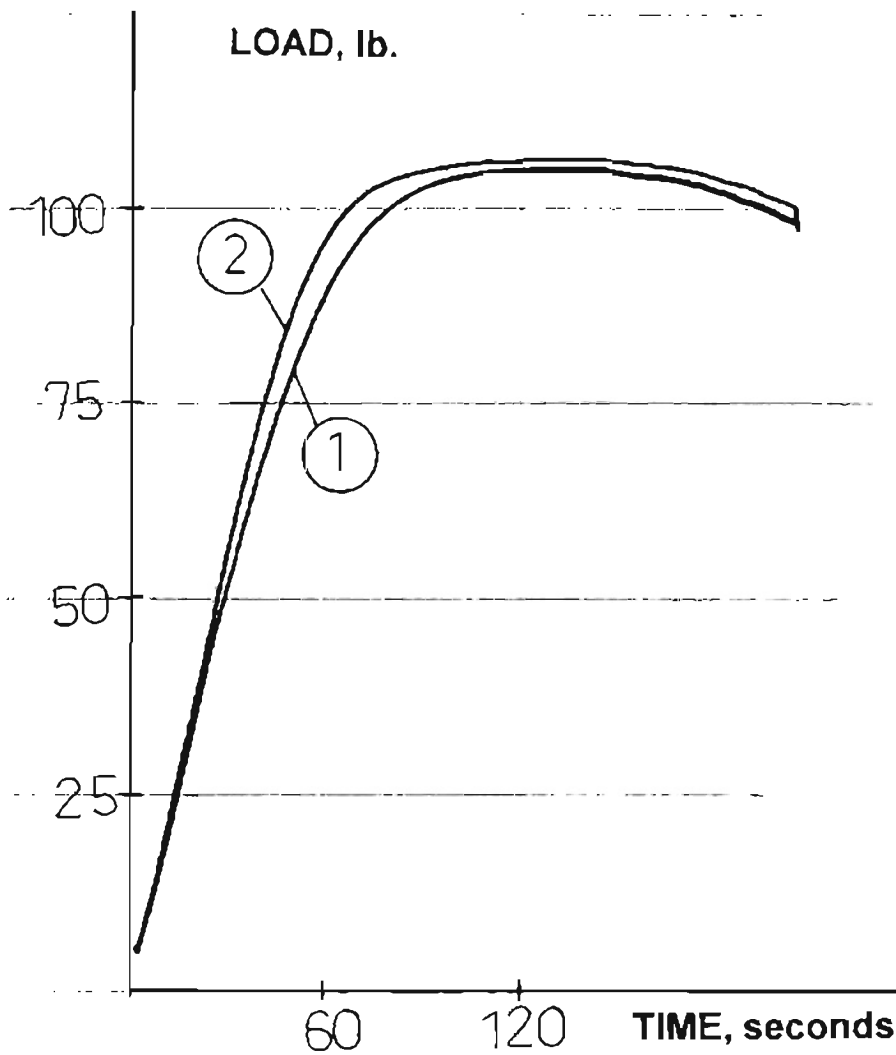
Figure 4.5: Load-time records for 92 gauge ICI polyester film specimens tested in, 1. MD, and 2. CD (2W = 12.0, 2H = 1.25, and $2a_0$ = 4.0 inch).
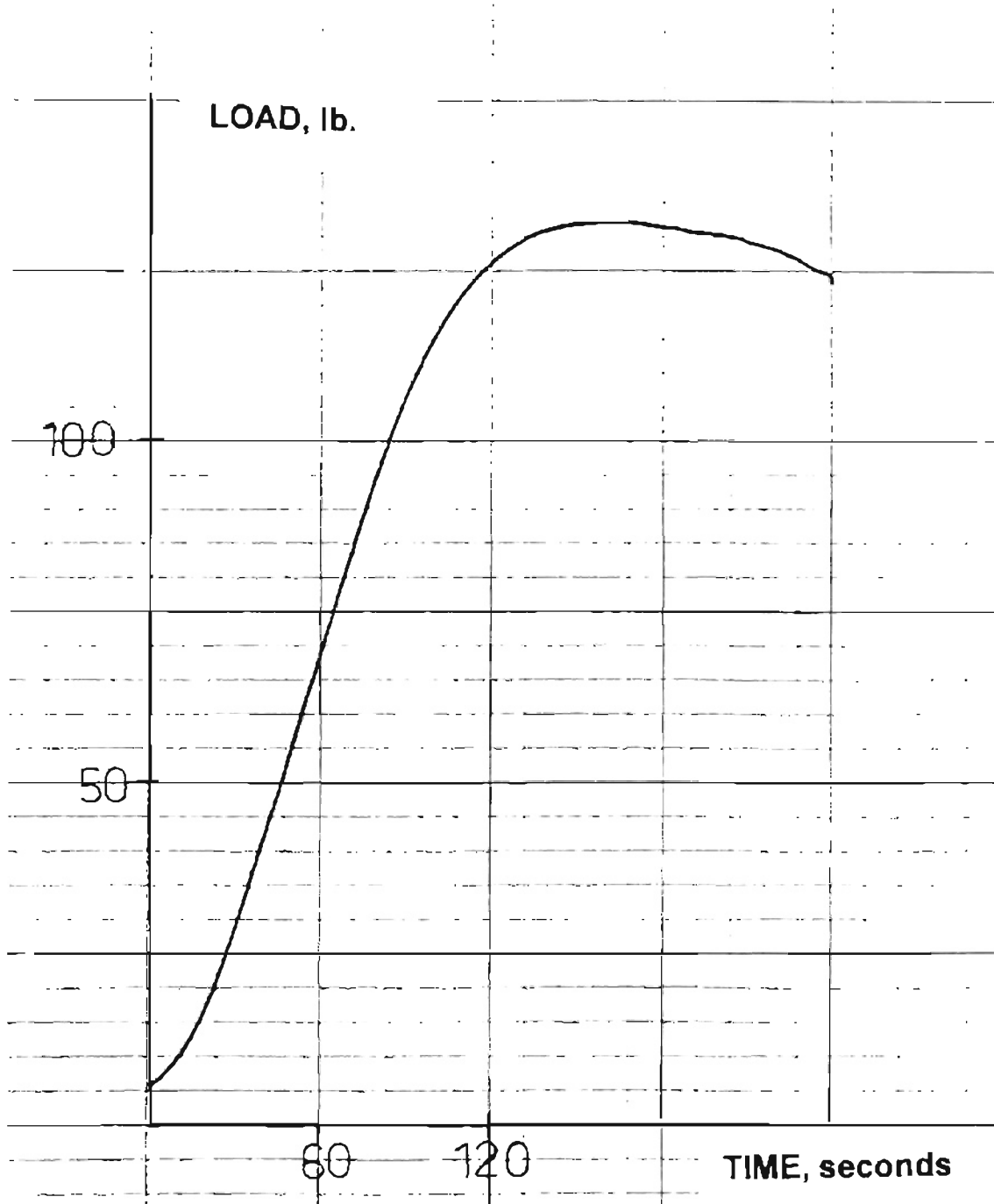
Figure 4.6: Load-time record for 92 gauge ICI polyester film specimen tested in MD (2W = 12.0, 2H = 2.0, and $2a_0$ = 2.0 inch).
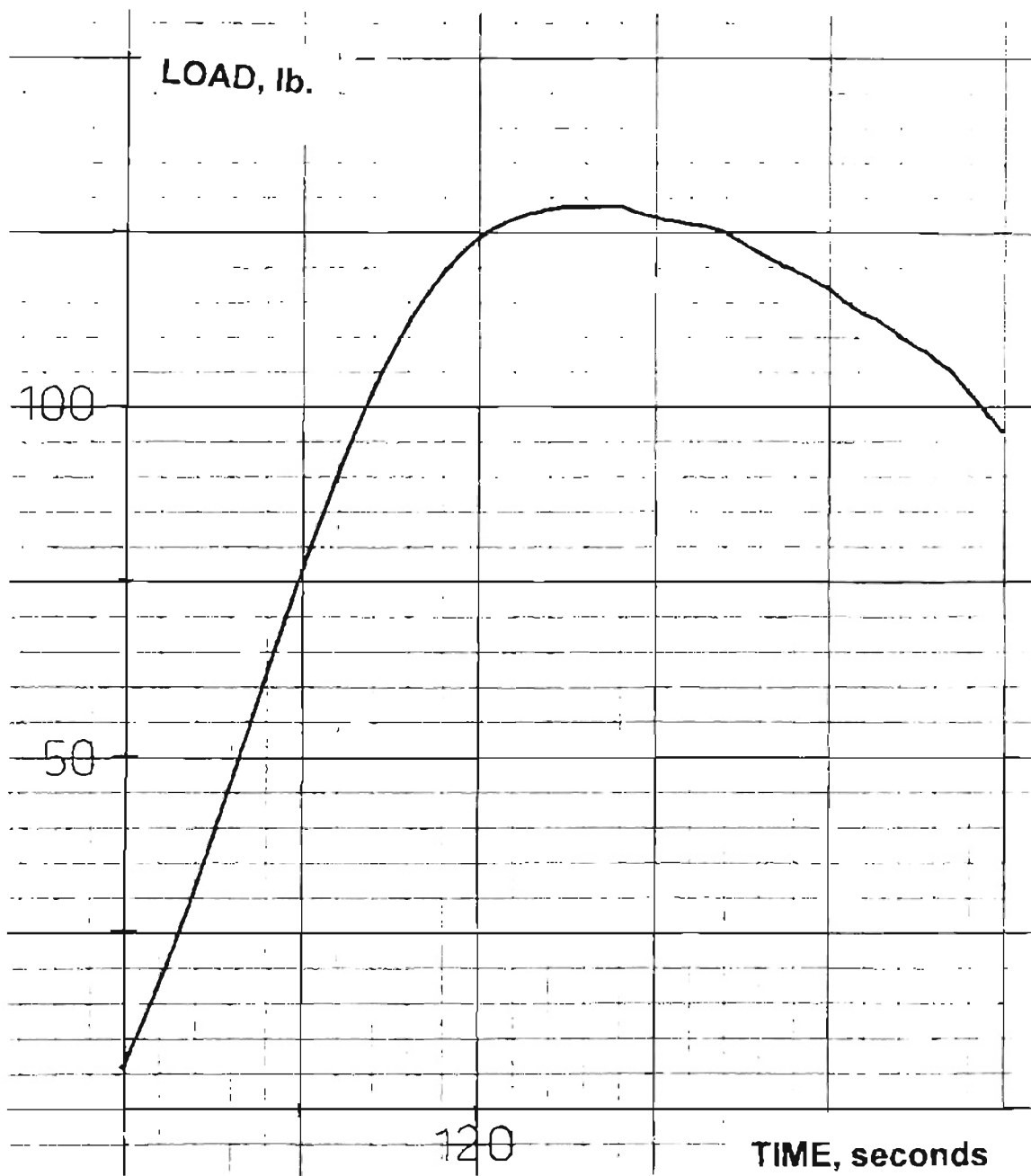
Figure 4.7: Load-time record for 92 gauge ICI polyester film specimen tested in MD (2W = 12.0, 2H = 3.0, and 2a$_0$ = 2.0 inch).
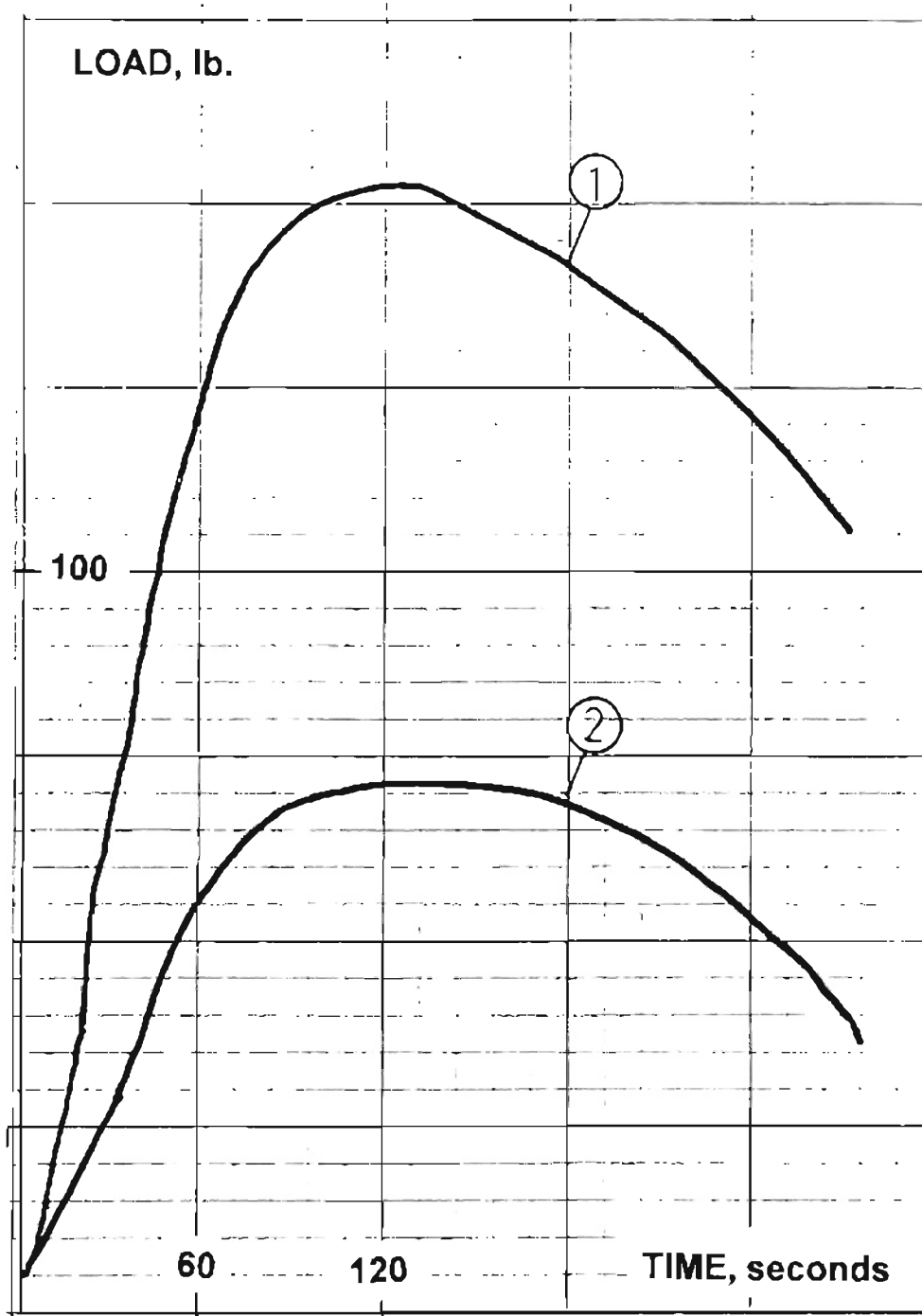
Figure 4.8: Load-time records for ICI polyester film specimens of 92 and 200 gauge thickness, tested in MD (2W = 6.0, 2H = 0.8, and $2a_0$ = 1.0 inch).

1. 200 gauge (0.002 inch) specimen
2. 92 gauge (0.00092 inch) specimen

properties [4]. When biaxially oriented (i.e. oriented in two directions at right angles), the film is quite tough. From the load-time records obtained. The 92 gauge polyester film seem to have similar draw ratios in MD, and in CD.

4.2 Crack extension measurements and crack growth behaviors

Using a multimedia LCD projector, the prerecorded test runs were projected on a flat white screen. As the crack initiation event was neared, the crack sizes (2a) were measured at every 6 seconds intervals, until the peak load value for the particular specimen was reached. After crossing the peak load value, the measurements were made at every 12 seconds. From the beginning of the test to the point when about one inch of total crack growth had taken place, the test runs lasted from 3 to 4 minutes. The projection method provided 5 to 15X magnification of the original crack sizes. This made the process of measurement fast, and easy.

Attempts to perform image capturing using a PC, and hence crack extension measurements, were not so successful. Even under the best resolution settings, the loss of picture quality was unavoidable. The illumination of the cracked region of the test specimen, and hence, the lighting arrangements for these experiments, were inadequate for image capturing. The size of the plastic zone was assumed to be negligible. No attempts were made to measure the crack tip radius, from the crack extension data recorded, as it was difficult to obtain accurate measurements

It was difficult to identify the instant of initial crack growth. At the best, about 3 to 4 crack size measurements were possible within 0.1 inch of the initial crack growth (Figures 4.12-4.26).

The crack growth behavior observed was stable for all the test runs. All the test specimens showed the total of one inch of crack growth within a maximum drop of 10 lb. in the load values, from the peak load values observed, with the wider and thicker gage specimens showing the same, very near to the peak load values. It should be noted that the crack propagation across the ligament will not be co-linear it the specimen is not in plane stress. The schematics of four different kind of crack growth behaviors observed during the CST fracture testing, are shown in Figure 4.9. The test specimens, which did not show the crack growth along the center line were not considered in plane stress. This was true mostly for the polyester film specimens having W/H < 5. Uneven clamping, misalignment and poor specimen preparation could also contribute to the non-linear crack growth. Almost all the test specimens not satisfying W/H > 4.00, showed the crack buckling and visible creases. An 'elliptical depression zone' surrounding the growing crack was observed in these specimens. Detection of undesirable buckling was made by periodic partial unloading of the test specimen, as described in the test record evaluation procedure of ASTM E 561 [50] (Figures 4.10, and 4.11). The initial part of the test record should have a linear portion which can be substantially retraced upon partial unloading. Should buckling or friction problems develop at some later
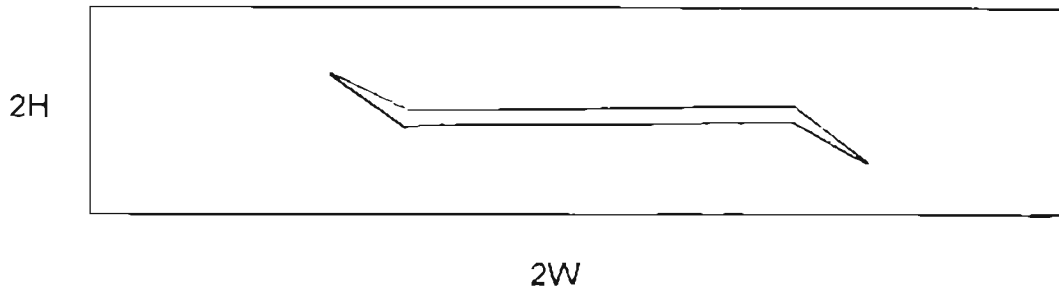
(a) A specimen showing non-linear crack growth under CST test conditions.
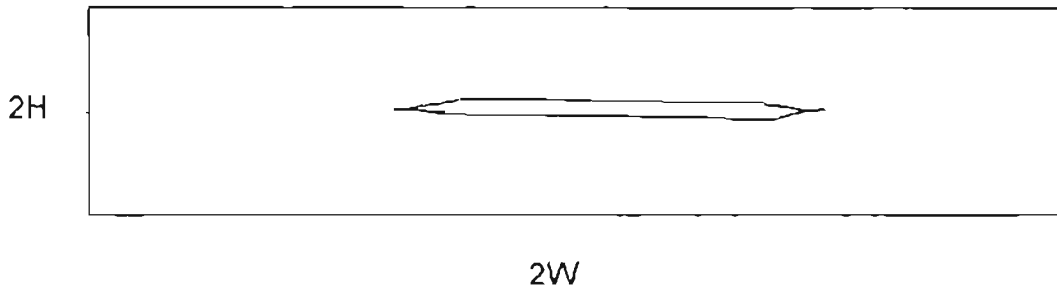
(b) A specimen showing co-linear crack growth, and therefore, plane stress behavior under CST test conditions.
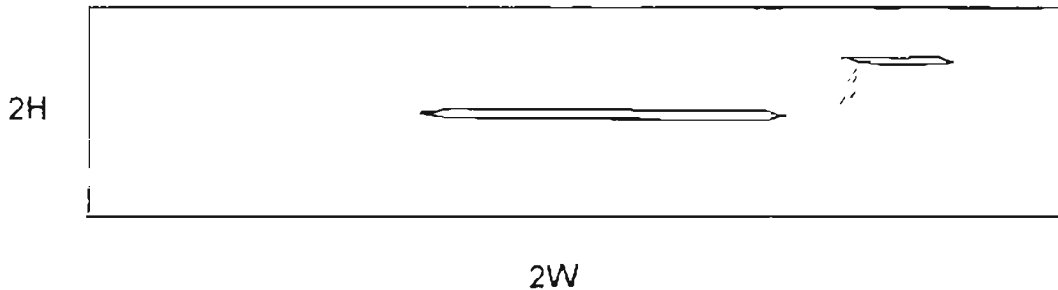
(c) A specimen showing the occurrence of a second crack at random location. This maybe explained by defects present in the film roll, from which the specimens were prepared.
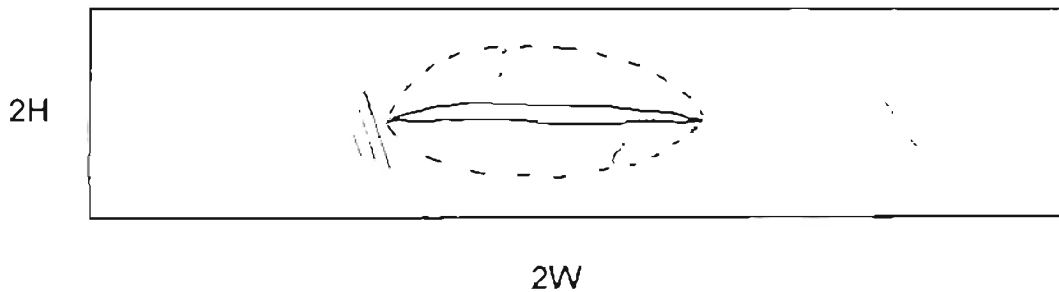
(d) A specimen showing out-of-plane buckling, and creases.

Figure 4.9: Schematics of crack growth behavior observed during the CST testing.
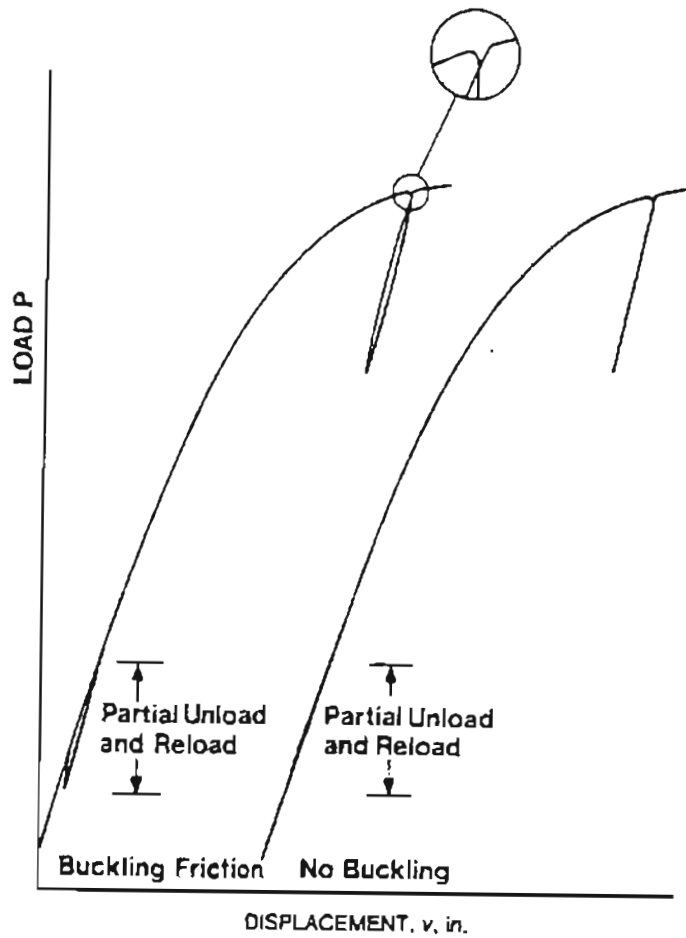
Figure 4.10: Detection of crack buckling from the load-displacement record of the center cracked specimen [50].
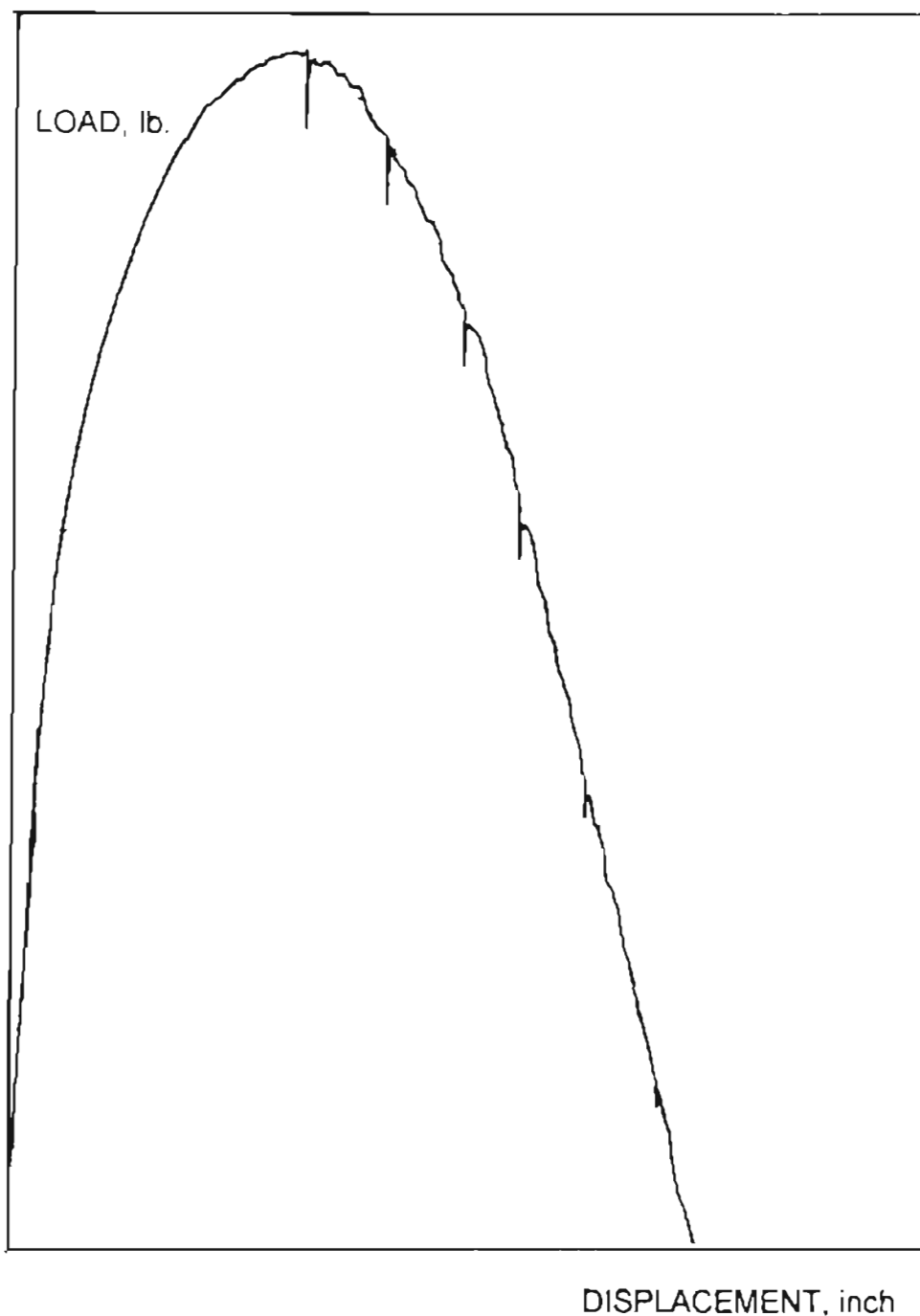
Figure 4.11: Detection of buckling and friction problems for aluminum foil specimen (2W = 8.0, 2H = 1.25, and 2a0 = 5.0 inch). Peak load = 36.3 lb., Max. displacement = 0.091 inch.

As observed, no buckling problems were identified.

stage in the test, the unloading and reloading slopes will tend to diverge as shown in Figure 4.10.

No crazing, and cold drawing as in Kapton films [20], were observed with the polyester film test specimens.

4.3 Estimating K_0 and K_c of polyester film specimens using K_R curves

Construction of the plots

K_R-curves, and K_c estimates for ICI polyester film test specimens are shown in Figures 4.12-4.26. The order of the presentation, is as outlined in the data collection plan of Table 3.2.

Stress intensity factors were calculated using expressions (2.4) and (2.5). Load values, P, for calculating the gross stress, σ_{gross}, were obtained from the load-time record of the particular test specimen. The crack extension data and the load data were synchronized. The stress intensity factors were plotted against the crack extension to construct K_R-curves, as shown in the Figures 4.12-4.26. According to the standard practice for R-curve determination for metallic materials [50], while R-curve (or K_R-curve) can be developed with as few as four or five data points, ten to fifteen give improved confidence, and tougher materials require more data points. Here, the K_R-curves for polyester films are constructed using at least ten data points obtained within 1 inch of total crack growth.

In the case of polyester film test specimens, the exponential curve,

$K_R = A + B\Delta a^n$, as suggested by Cotterell et al. [19,20], was found to give a good

fit for $\Delta a < 0.3$ inch. To obtain this curve fit, the following steps were followed.

$$K_R = A + B\Delta a^n \dots\dots\dots\dots\dots\dots\dots\dots\dots\dots\dots\dots\dots\dots\dots\dots\dots\dots\dots(4.1)$$

where A,B, and n are constants.

When the crack extension $\Delta a = 0$,

$K_R = A$.

The equation of the curve can be rewritten as,

$K_R - A = B\Delta a^n$,

or

$$\log(K_R - A) = n \log(\Delta a) + \log B \dots\dots\dots\dots\dots\dots\dots\dots\dots\dots\dots\dots\dots\dots\dots(4.2)$$

--which is an equation of the straight line, $y = mx + c$. Using linear

regression, the best fitting straight line to the data points generated by (4.2), was

found (For all test results shown here, $0.85 \le r^2 \le 1.00$, where r^2 is the correlation

coefficient.) The n and B were calculated from the slope, and the intercept of this

line respectively. By doing this, the maximum value of the load observed at

$\Delta a = 0$, established the initiation fracture toughness, K_0 (which is constant, A). As

mentioned before, it was difficult to identify the instant of the initial crack growth

exactly. The initiation fracture toughness value reported here, should be

considered as an upper limit for the particular test specimen.

To establish (K_G, K_R) tangency points, the K_G lines were assumed to be

straight lines for the entire range of initial crack lengths $(2a_0)$ investigated here. It

should be noted that, this assumption is valid only for the crack growth

resistance, and crack driving force curves for the load controlled method. The

110

load control method involves rising load tests with crack driving force (K_G) curves like those shown in Figures 3.24 and 3.25. Under rising load conditions, the crack extends gradually to a maximum of Δa, when unstable crack growth occurs at K_C, which is determined by the tangency point between K_R-curve, and one of the lines representing a crack driving force curve, $K_G = f(P, \sqrt{a}, \frac{a}{W})$ [23].

Assuming a K_G curve to be a straight line, could result in higher estimates of K_C, for the specimens with larger initial crack lengths. An accurate expression for the K_G curve can be developed using finite element analysis. For all the test results shown in Figures 4.12-4.26, the K_G lines were made approximately tangent to the exponential curve of the best fit, $K_R = A + B\Delta a^n$. This could shift a K_C estimate, higher or lower, depending on the errors in the experimental data, and the goodness of the curve fit. It should be noted that the K_G line establishing a point of tangency is a geometrical construction, passing through the points $(2a_0, 0)$, and (K_G, K_R). The range of possible variation in the K_C value for a particular test specimen is discussed later.

The precision of K_R-curve data is a complex synergistic function of the precision and accuracy of the instrumentation used, set up of the test fixtures, and the performance of the test. The latter is a matter of care and skill which has been addressed in a detailed manner in Chapter 3.

Additionally, a K_R-curve is not a single valued quantity, but a series of quantities dependent on crack growth. Hence, K_R-curves are not easily analyzed by statistical methods. Bias cannot be evaluated because there exists no

111

reference value by which it is possible to identify a value of K_R at all of the possible levels of the effective crack growth, Δa [50].

Because of the reasons discussed above, K_C values presented here, should be treated as estimates, and should not be considered exact. The overall spread of K_R data is illustrated in Figures 4.14.6, 4.15.6, and 4.23.5, for the test runs 3, 4, and 12 (Table 3.2).

Figure 4.12: K_R-curves for test run no. 1.

Figure 4.12.1: Crack growth resistance curve for a 92 gauge polyester film specimen.

Figure4.12.2: Crack growth resistance curve for a 92 gauge polyester film specimen.

K_R, ksi (inch)$^{1/2}$

K_c

Specimen geometry:
2W = 4.0 inch
2H = 0.8 inch
$2a_0$ = 1.2 inch

K_G

◆ Experimental data

—— Exponential curve of the best fit

-1.2   -0.8   -0.4   0   0.4   0.8   1.2

Crack length, inch

Crack extension, inch
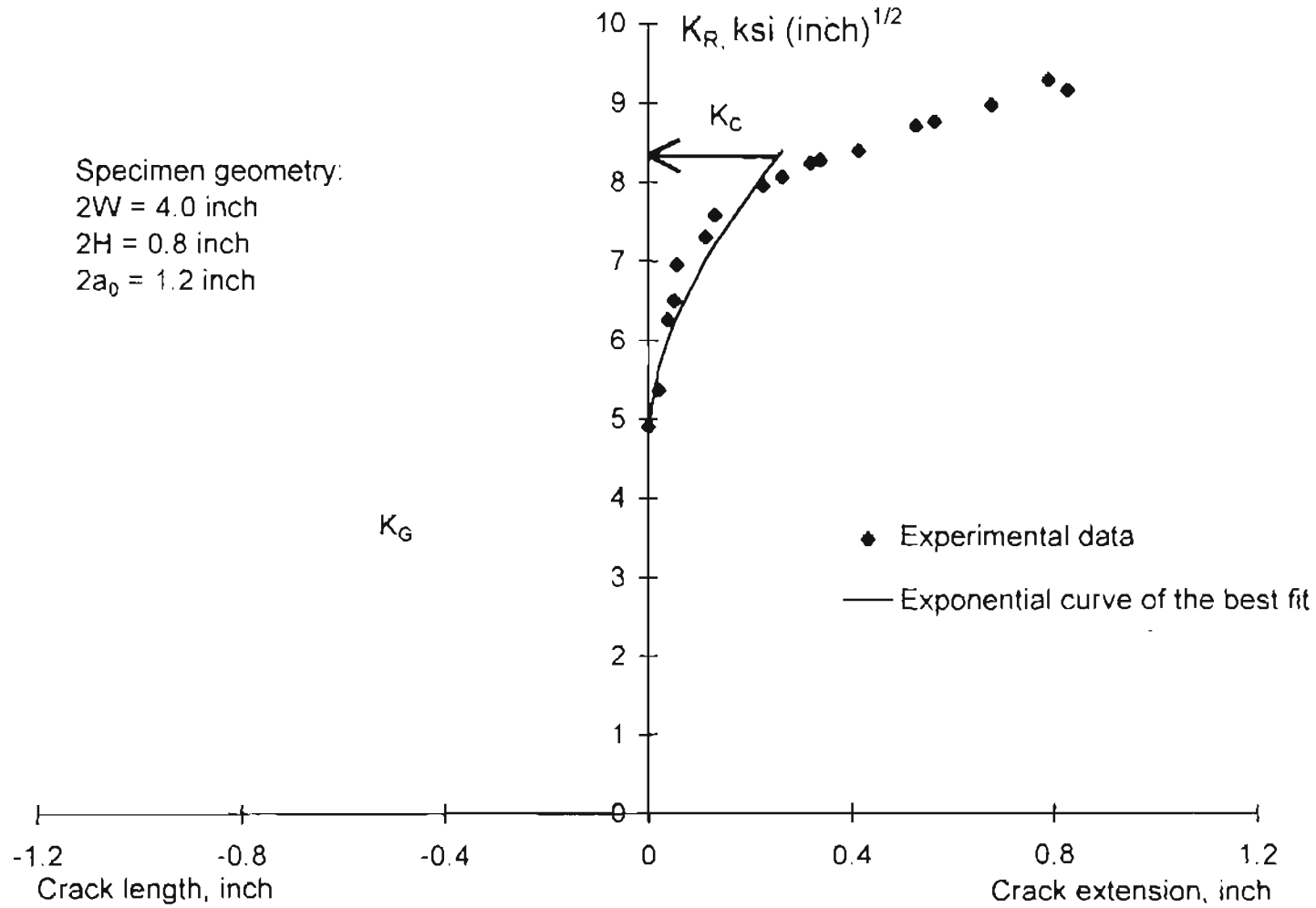
Figure 4.12.3: Crack growth resistance curve for a 92 gauge polyester film specimen.

Figure 4.13: K_R-curves for test run no. 2.

Figure 4.13.1: Crack growth resistance curve for a 48 gauge polyester film specimen.

Specimen geometry:
2W = 6.0 inch
2H = 0.8 inch
$2a_0$ = 0.8 inch

K_R, ksi $(inch)^{1/2}$

K_C

K_G

6.0

0.8 — 0.8

◆ Experimental data

— Exponential curve of the best fit

-0.8   -0.4   0   0.4   0.8
Crack length, inch   Crack extension, inch

Figure 4.13.2: Crack growth resistance curve for a 48 gauge polyester film specimen.

Figure 4.13.3: Crack growth resistance curve for a 48 gauge polyester film specimen.

Specimen geometry:
2W = 6.0 inch
2H = 0.8 inch
$2a_0$ = 1.5 inch

6.0

0.8 ──────── 1.5

K_R, ksi (inch)$^{1/2}$

K_C

K_G

◆ Experimental data

── Exponential curve of the best fit

-1.5   -1.1   -0.7   -0.3   0.1   0.5   0.9

Crack length, inch

Crack extension, inch

Figure 4.13.4: Crack growth resistance curve for a 48 gauge polyester film specimen.

Specimen geometry:
2W = 6.0 inch
2H = 0.8 inch
$2a_0$ = 2.0 inch

Figure 4.13.5: Crack growth resistance curve for a 48 gauge polyester film specimen.

Specimen geometry:
2W = 6.0 inch
2H = 0.8 inch
$2a_0$ = 3.0 inch

6.0
0.8   3.0

◆ Experimental data

—— Exponential curve of the best fit

K_R, ksi (inch)$^{1/2}$

K_C

K_G

Crack length, inch

Crack extension, inch

Figure 4.14: K_R-curves for test run no. 3.

Figure 4.14.1: Crack growth resistance curve for a 92 gauge polyester film specimen.

Specimen geometry:
2W = 6.0 inch
2H = 0.8 inch
$2a_0$ = 1.0 inch

K_R, ksi (inch)$^{1/2}$

K_C

K_G

6.0

0.8

1.0

◆ Experimental data

— Exponential curve of the best fit

Crack length, inch

Crack extension, inch

Figure 4.14.2: Crack growth resistance curve for a 92 gauge polyester film specimen.

Specimen geometry:
2W = 6.0 inch
2H = 0.8 inch
$2a_0$ = 1.5 inch

K_R ksi $(inch)^{1/2}$

K_C

K_G

- ◆ Experimental data
- —— Exponential curve of the best fit

6.0

0.8

1.5

Crack length, inch

Crack extension, inch

Figure 4.14.3: Crack growth resistance curve for a 92 gauge polyester film specimen.

K_R, ksi (inch)$^{1/2}$

K_C

K_G

Specimen geometry:
2W = 6.0 inch
2H = 0.8 inch
$2a_0$ = 2.0 inch

6.0

0.8

2.0

The exponential curve fit
agrees well within 0.3 inch
of the initial crack growth
only.

◆ Experimental data

—— Exponential curve of the best fit

Crack length, inch

Crack extension, inch

Figure 4.14.4: Crack growth resistance curve for a 92 gauge polyester film specimen.

Specimen geometry:
2W = 6.0 inch
2H = 0.8 inch
$2a_0 \approx 2.4$ inch

◆ Experimental data

—— Exponential curve of the best fit

K_R, ksi $(inch)^{1/2}$

K_C

K_G

Crack length, inch

Crack extension, inch

127

Figure 4.14.5: Crack growth resistance curve for a 92 gauge polyester film specimen.

Specimen geometry:
$2W = 6.0$ inch
$2H = 0.8$ inch
$2a_0 = 3.0$ inch

♦ Experimental data

— Exponential curve of the best fit
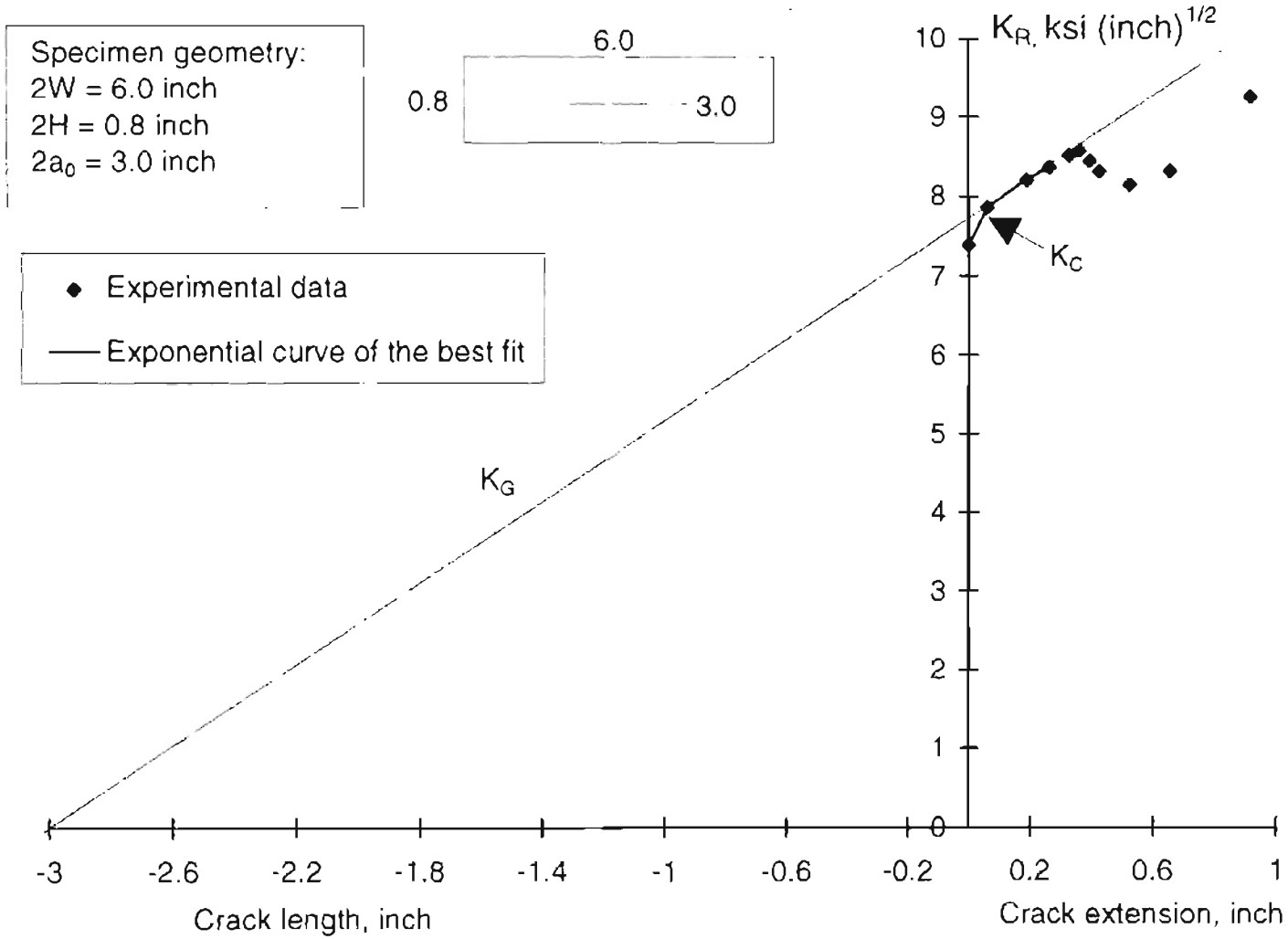
Figure 4.14.6: Crack growth resistance curve for 92 gauge polyester film specimens wiith different initial crack lengths (2a)
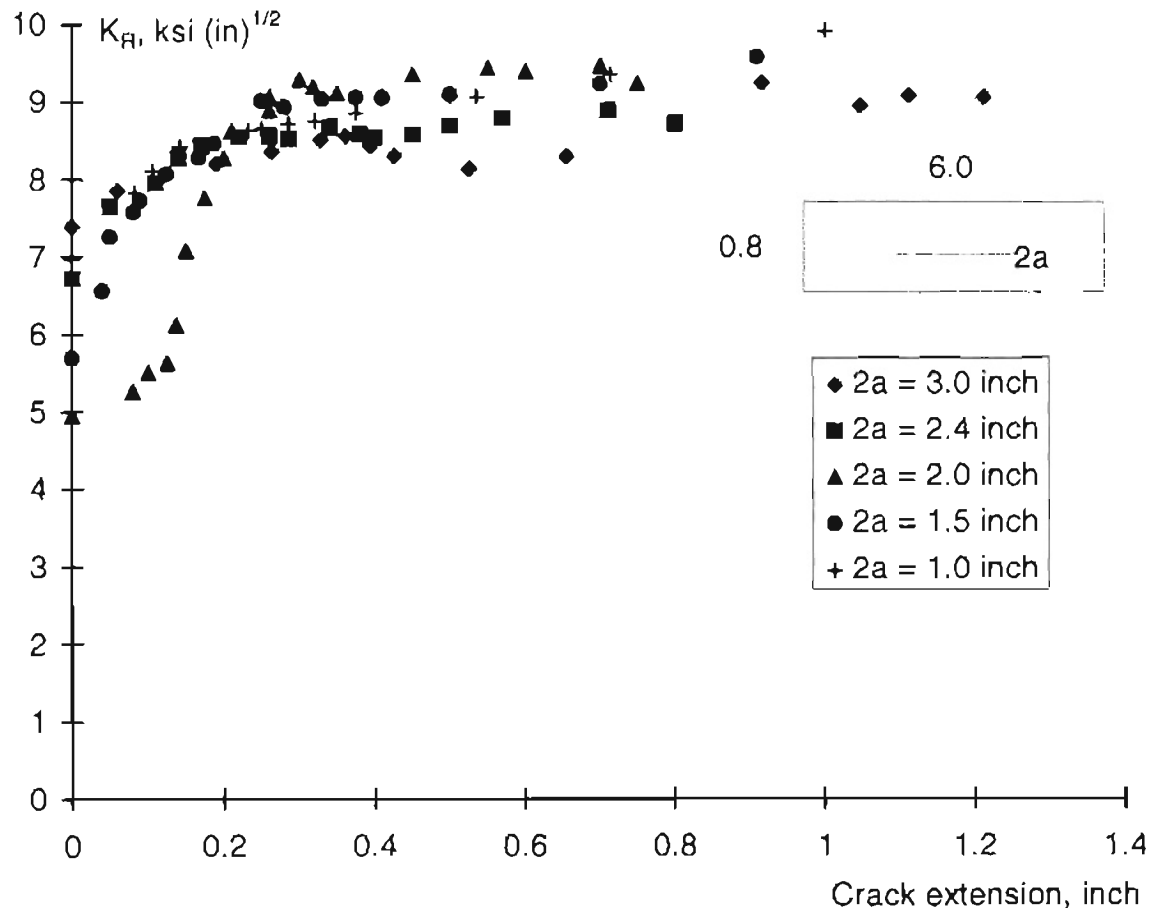
Figure 4.15: K_R-curves for test run no. 4.

Figure 4.15.1: Crack growth resistance curve for a 200 gauge polyester film

Specimen geometry:
2W = 6.0 inch
2H = 0.8 inch
$2a_0$ = 0.8 inch

6.0

0.8   0.8

K_R, ksi $(inch)^{1/2}$

12

10

8

K_c

6

4

K_G

2

0

-0.8   -0.4   0   0.4   0.8   1.2

Crack length, inch   Crack extension, inch

♦ Experimental data

— Exponential curve of the best fit
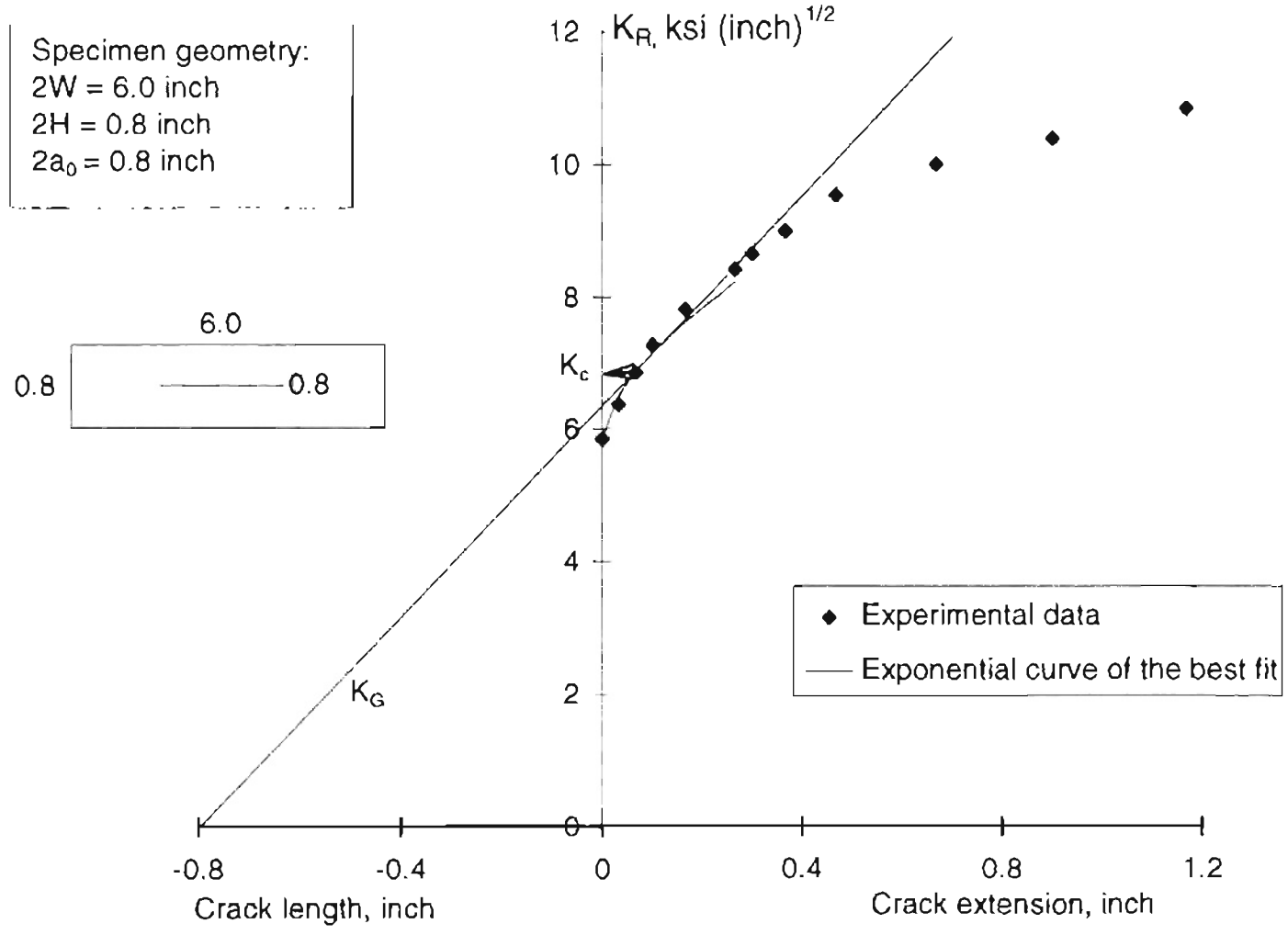
Figure 4.15.2: Crack growth resistance curve for a 200 gauge polyester film

K_R, ksi (inch)$^{1/2}$

K_G

K_C

Specimen Geometry:
2W = 6.0 inch
2H = 0.8 inch
$2a_0$ = 1.0 inch

- ◆ Experimantal data
- — Exponential curve of the best fit

Crack length, inch

Crack extension, inch

132
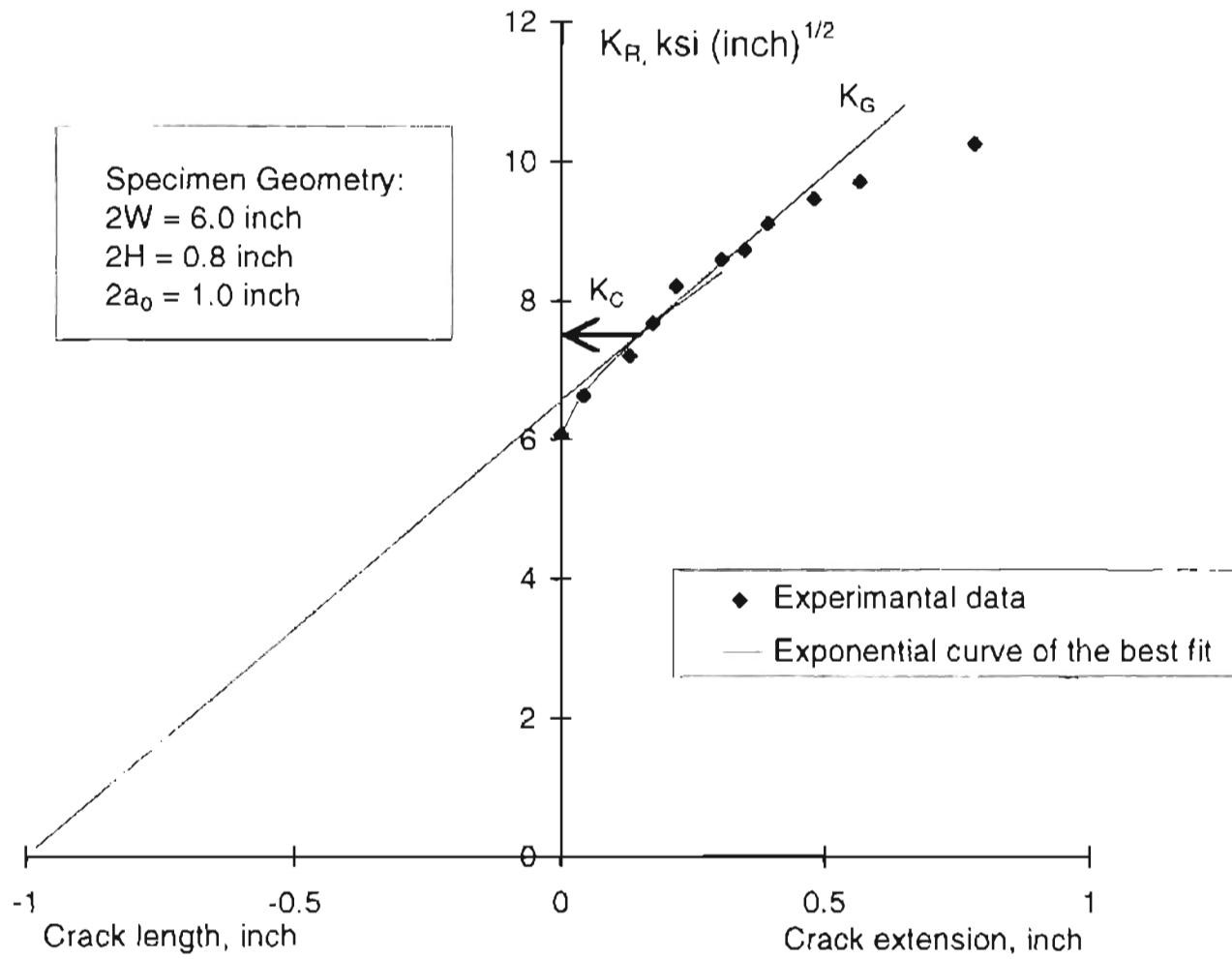
Figure 4.15.3: Crack growth resistance curve for a 200 gauge polyester film

Specimen Geometry:
2W = 6.0 inch
2H = 0.8 inch
$2a_0$ = 1.5 inch

K_R, ksi (inch)$^{1/2}$

K_C

K_G

◆ Experimental data

——— Experimental curve of the best fit

Crack length, inch

Crack extension, inch
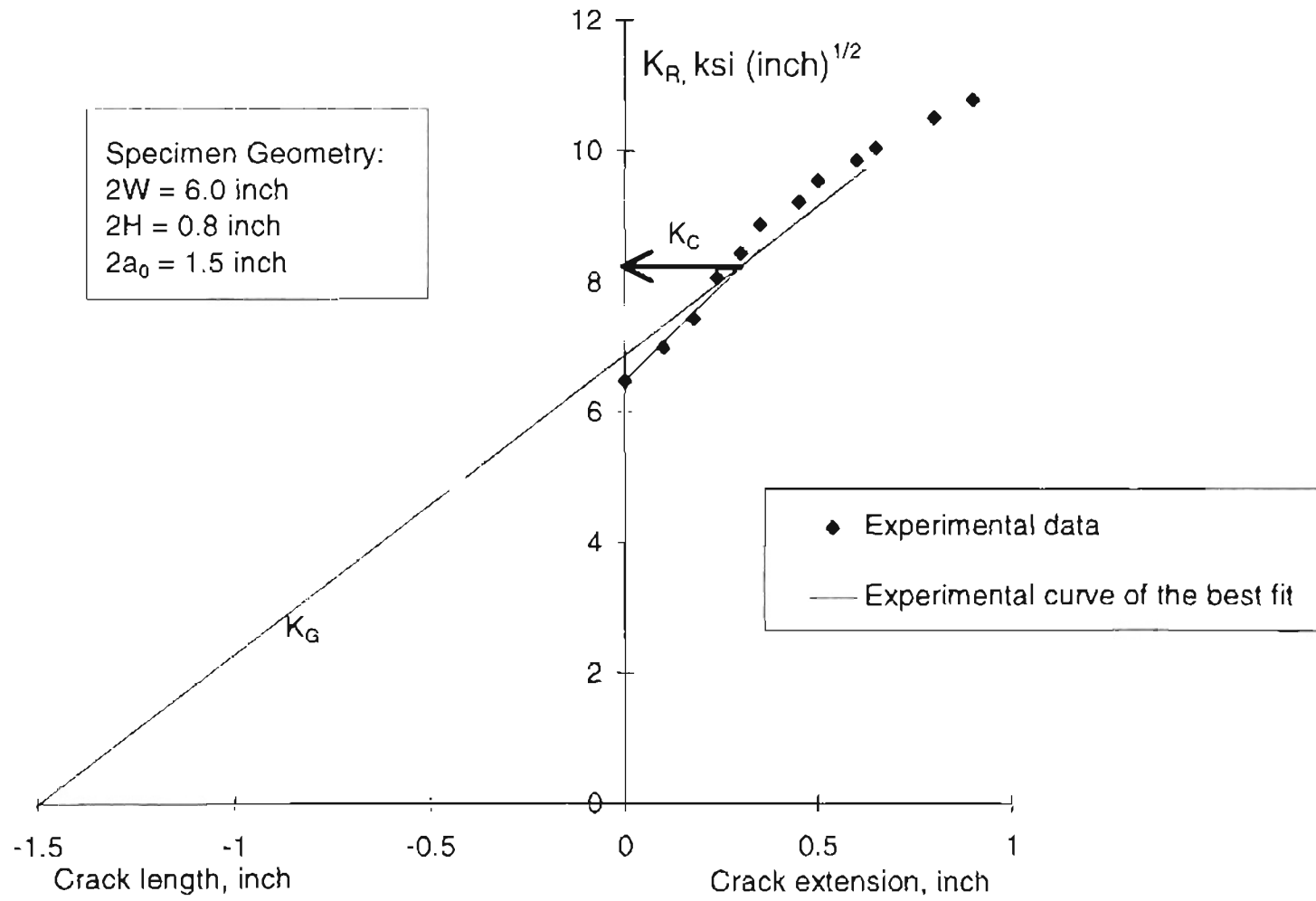
Figure 4.15.4: Crack growth resistance curve for a 200 gauge polyester film
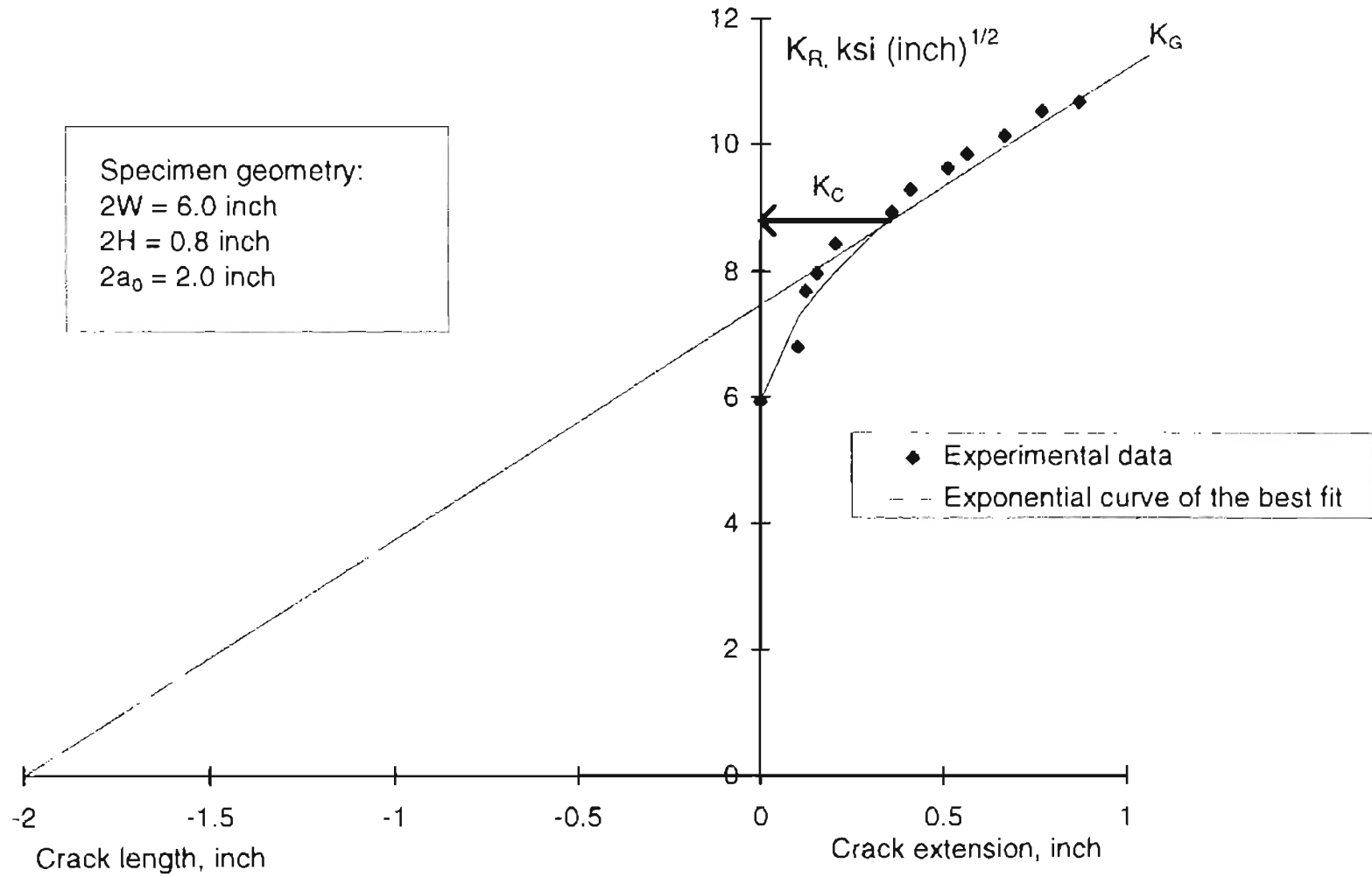
Figure 4.15.5: Crack growth resistance curve for a 200 gauge polyester film

K_R, ksi (inch)$^{1/2}$

Specimen geometry:
2W = 6.0 inch
2H = 0.8 inch
$2a_0$ = 3.0 inch

6.0

0.8 — 3.0

K_C

K_G

- Experimental data
— Exponential curve of the best fit

Crack length, inch

Crack extension, inch
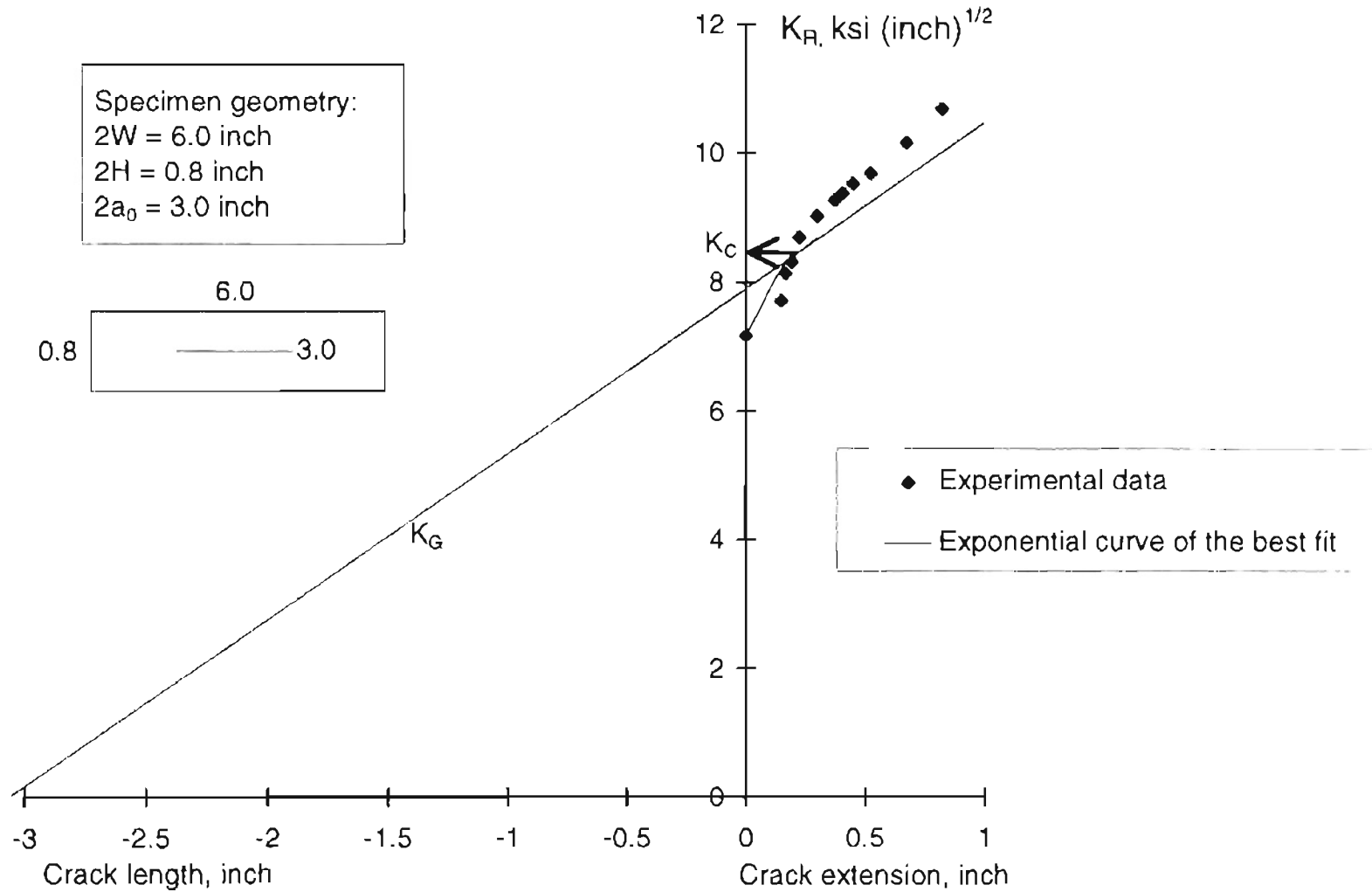
Figure 4.15.6: Crack growth resistance, K_R data for ICI 200 gauge polyester film specimens tested in MD, with different initial crack lengths (2a0).

Figure 4.16: K_R-curves for test run no. 5.

Figure 4.16.1: Crack growth resistance curve for a 92 gauge polyester film specimen.

Specimen geometry:
2W = 6.0 inch
2H = 1.25 inch
$2a_0$ = 1.0 inch

6.0

1.25

1.0

K_R, ksi (inch)$^{1/2}$

K_C

K_G

• Experimental data

—— Exponential curve of the best fit

Crack length, inch

Crack extension, inch

Figure 4.16.2: Crack growth resistance curve for a 92 gauge polyester film specimen.

K_R, ksi $(inch)^{1/2}$

Specimen geometry:
2W = 6.0 inch
2H = 1.25 inch
$2a_0$ = 2.0 inch

6.0

1.25   2.0

K_G

K_C

12
10
8
6
4
2
0

♦ Experimental data

——— Exponential curve of the best fit

-2   -1.6   -1.2   -0.8   -0.4   0   0.4   0.8
Crack length, inch   Crack extension, inch

Figure 4.17: K_R-curves for test run no. 6.

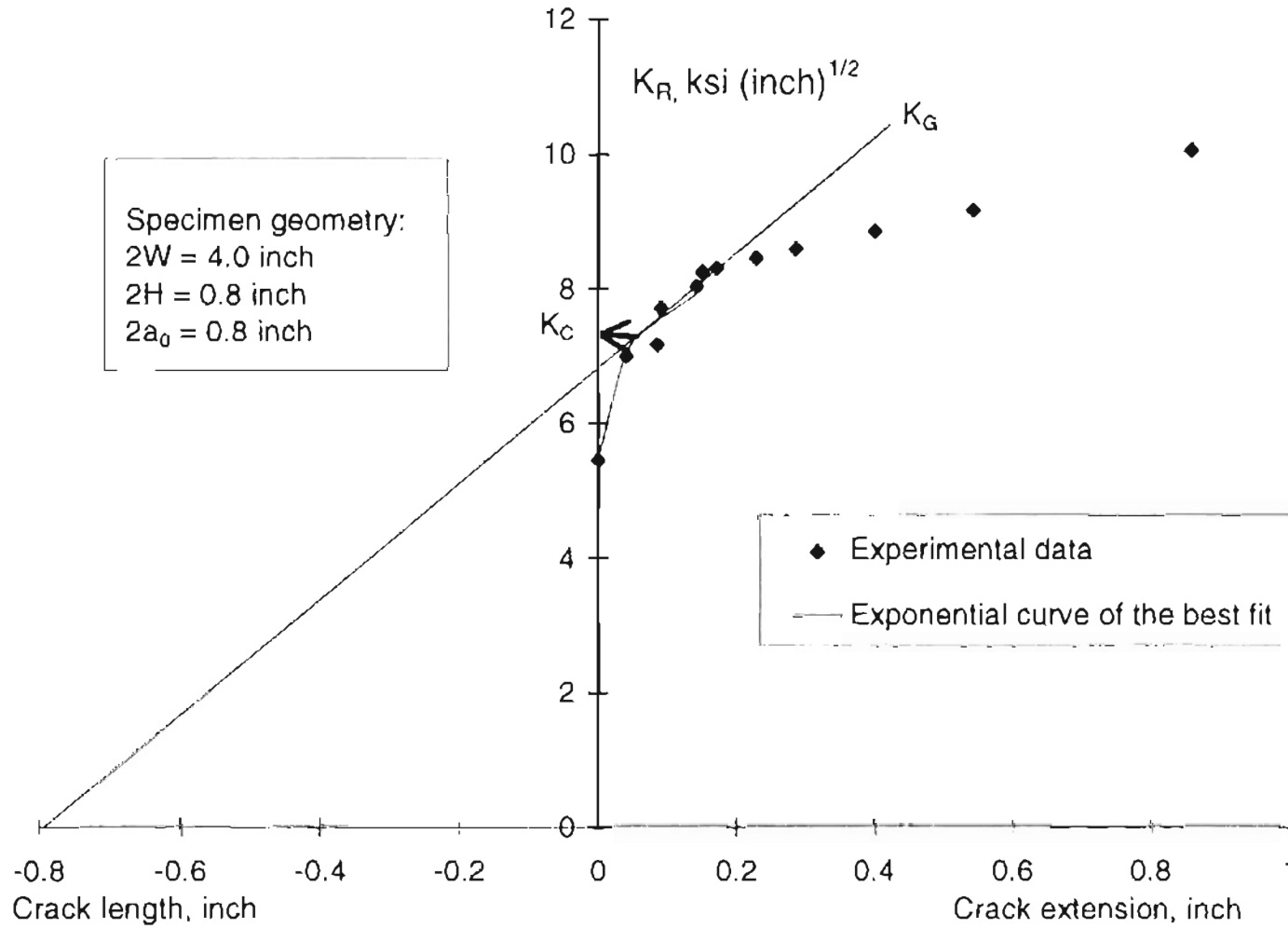Figure 4.17.1: Crack growth resistance curve for a 92 gauge polyester film specimen.

Specimen geometry:
2W = 6.0 inch
2H = 2.0 inch
$2a_0$ = 1.6 inch

6.0

2.0   1.6

K_R, ksi (inch)$^{1/2}$

K_G

K_c

12

10

8

6

4

2

0

• Experimental data

—— Exponential curve of the best fit

-1.6   -1.2   -0.8   -0.4   0   0.4   0.8

Crack length, inch   Crack extension, inch

141

Figure 4.17.2: Crack growth resistance curve for a 92 gauge polyester film specimen.

Specimen geometry:
2W = 6.0 inch
2H = 2.0 inch
$2a_0$ = 2.0 inch

K_R, ksi $(inch)^{1/2}$

K_C

K_G

♦ Experimental data

— Exponential curve of the best fit

Crack length, inch

Crack extension, inch

Figure 4.18: K_R-curves for test run no. 7.

Figure 4.18.1: Crack growth resistance curve for a 92 gauge polyester film specimen.

Figure 4.18.2: Crack growth resistance curve for a 92 gauge polyester film specimen.

Figure 4.18.3: Crack growth resistance curve for a 92 gauge polyester film specimen.
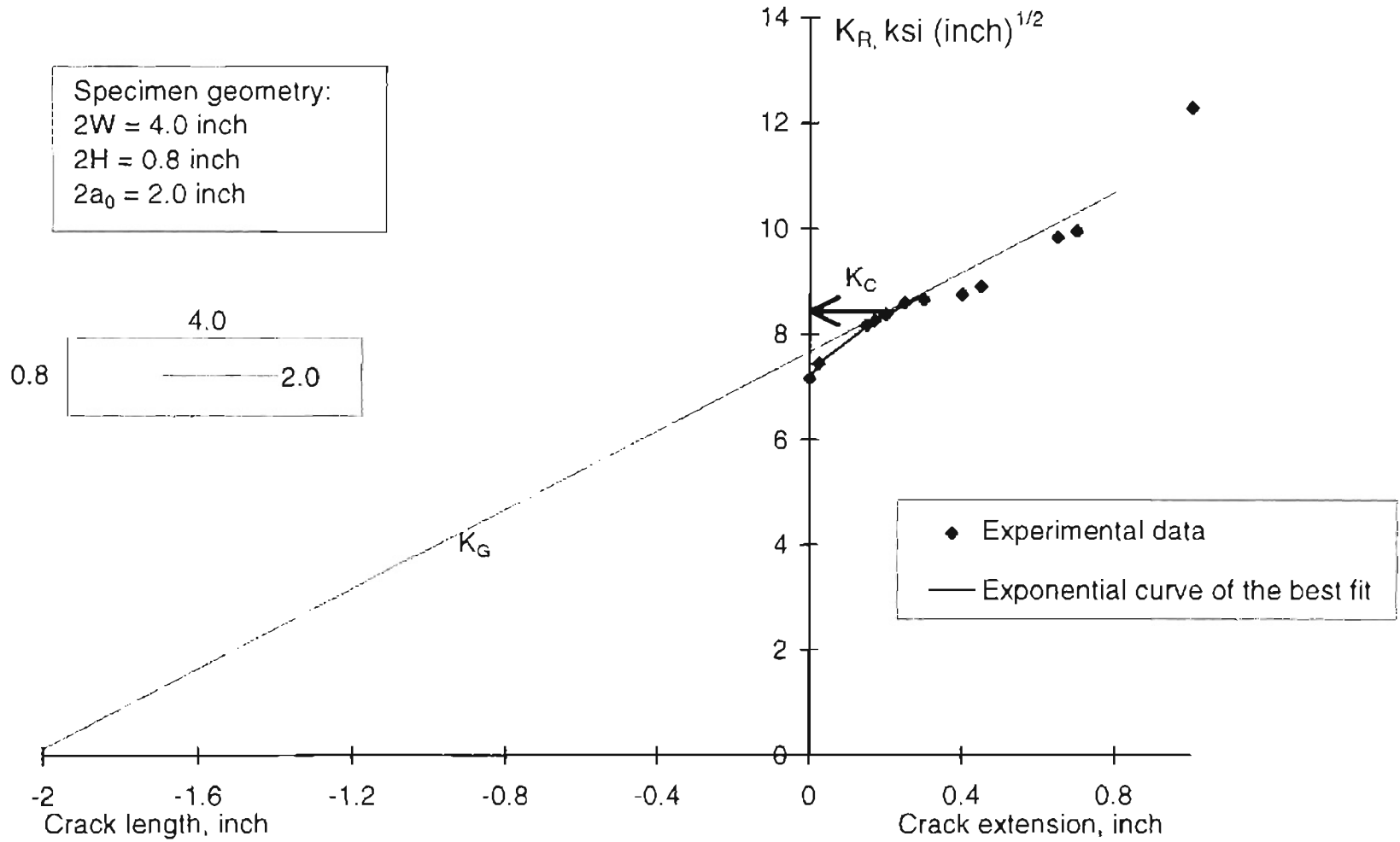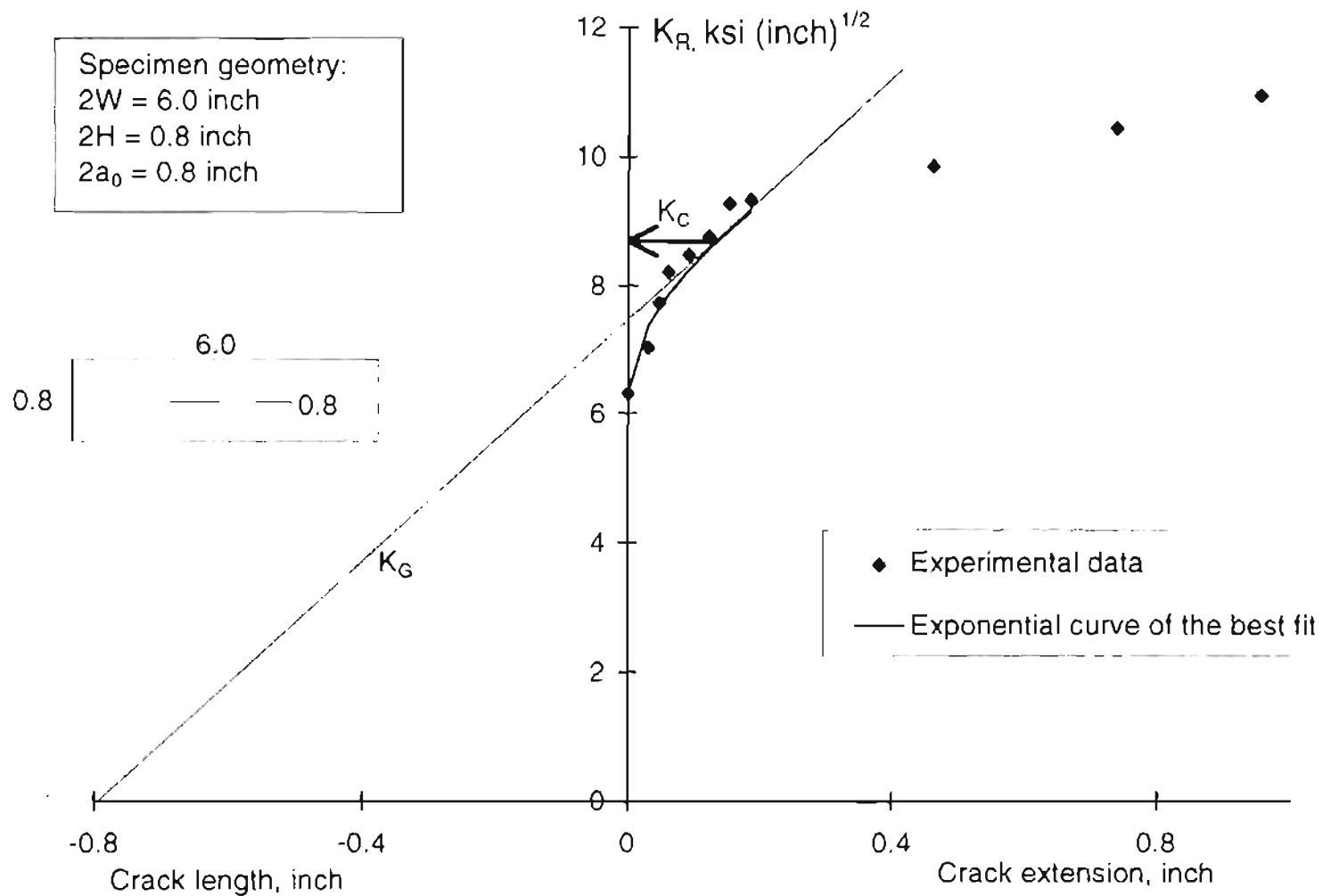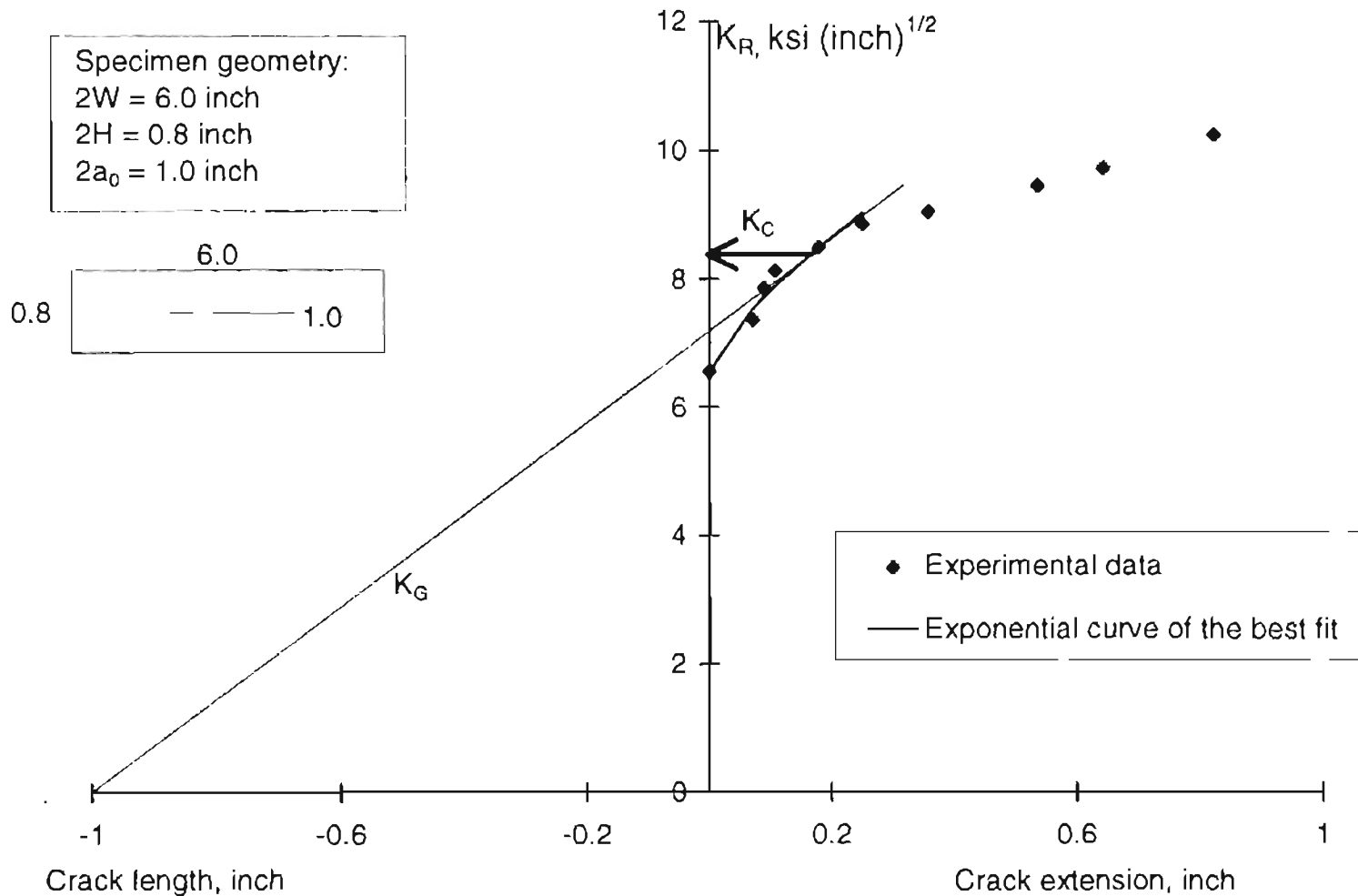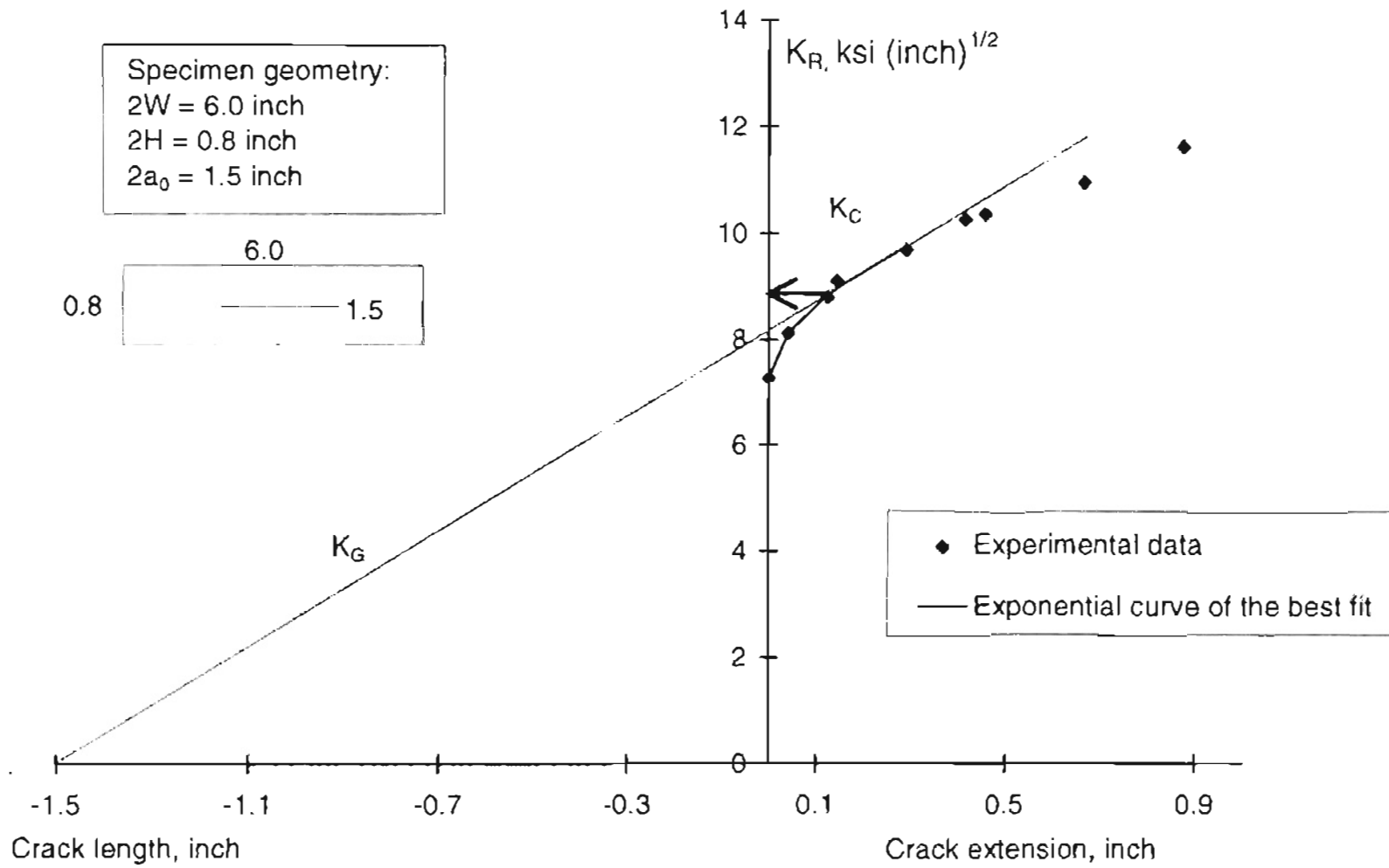
Specimen geometry:
2W = 8.0 inch
2H = 0.8 inch
$2a_0$ =2.0 inch

K_R, ksi (inch)$^{1/2}$

K_C

K_G

◆ Experimental data

— Exponential curve of the best fit

Crack length, inch

Crack extension, inch

Figure 4.18.4: Crack growth resistance curve for a 92 gauge polyester film specimen.

Specimen geometry:
2W = 8.0 inch
2H = 0.8 inch
$2a_0$ =2.5 inch

8.0

0.8

2.5

K_R, ksi (inch)$^{1/2}$

12

10

K_C

8

6

4

K_G

2

• Experimental data

—— Exponential curve of the best fit

-2.5   -2.1   -1.7   -1.3   -0.9   -0.5   -0.1   0.3   0.7

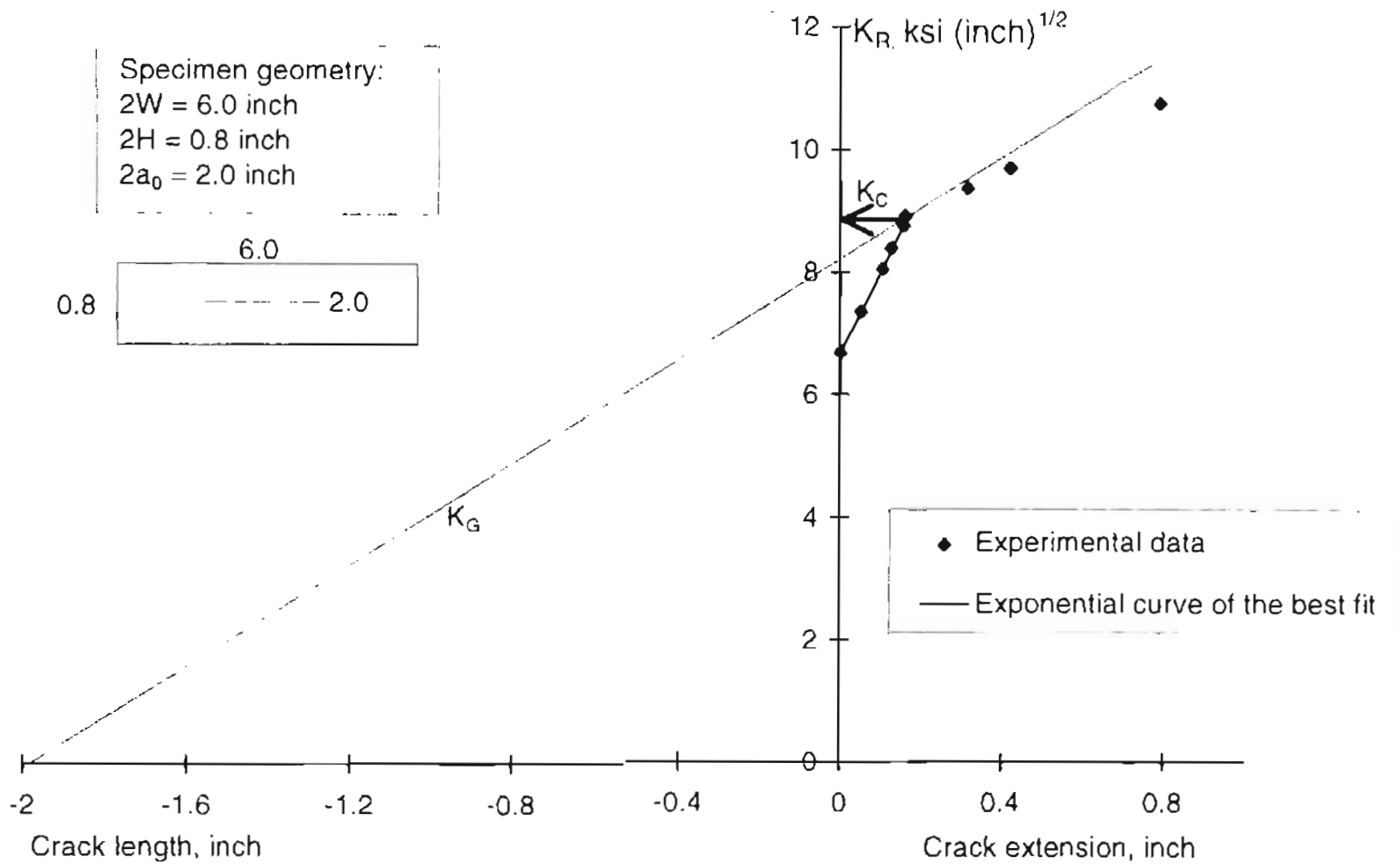Crack length, inch

Crack extension, inch

147

Figure 4.18.5: Crack growth resistance curve for a 92 gauge polyester film specimen.

Figure 4.19: K_R-curves for test run no. 8.

Figure 4.19.1: Crack growth resistance curve for a 92 gauge polyester film specimen.

Specimen geometry:
2W = 8.0 inch
2H = 1.25 inch
$2a_0 = 1.0$ inch

8.0

1.25 — 1.0

K_R, ksi (inch)$^{1/2}$

12

K_C

10

8

6

K_G

4

2

0

♦ Experimental data

— Exponential curve of the best fit

-1   -0.6   -0.2   0.2   0.6   1

Crack length, inch

Crack extension, inch

Figure 4.19.2: Crack growth resistance curve for a 92 gauge polyester film specimen.

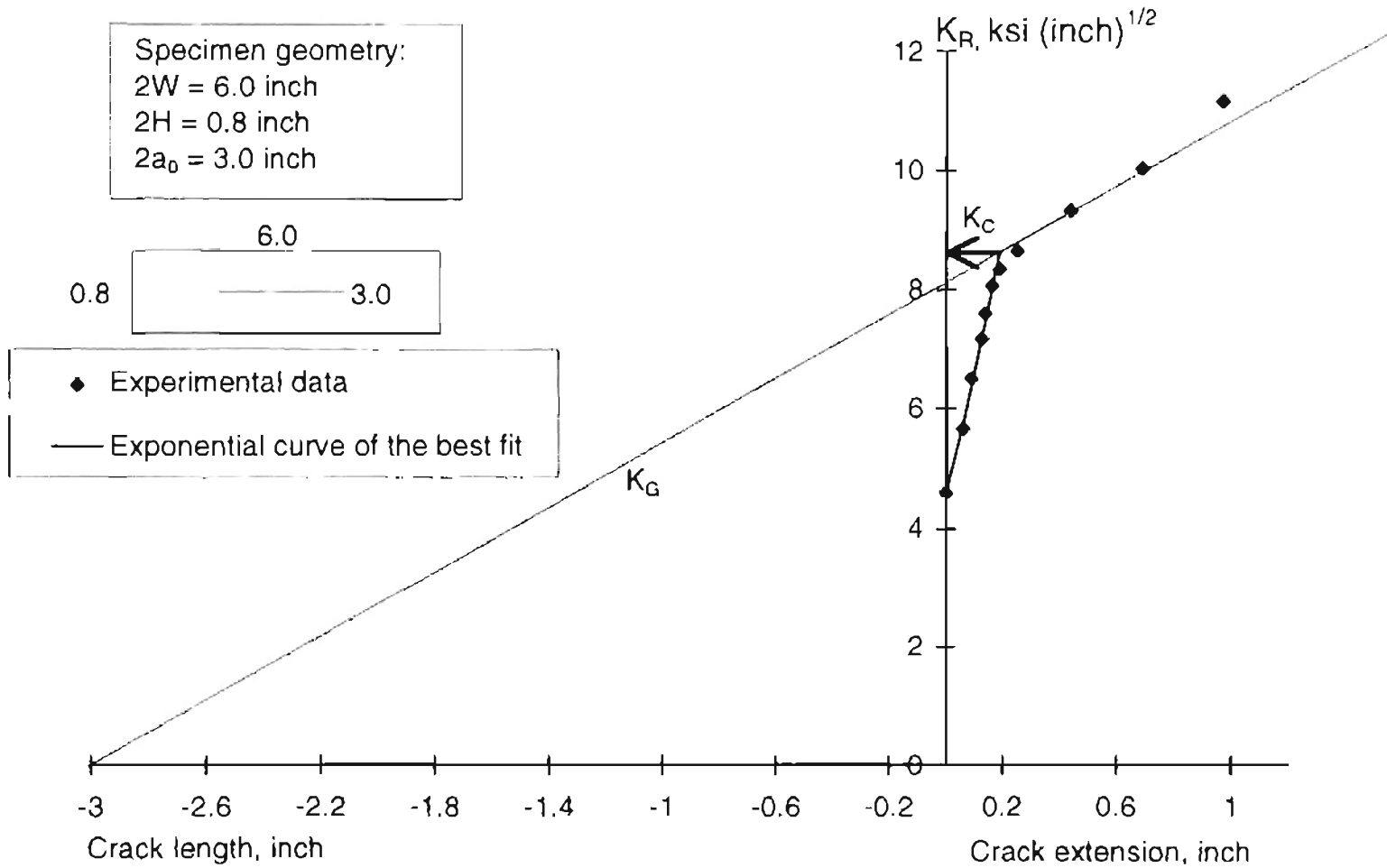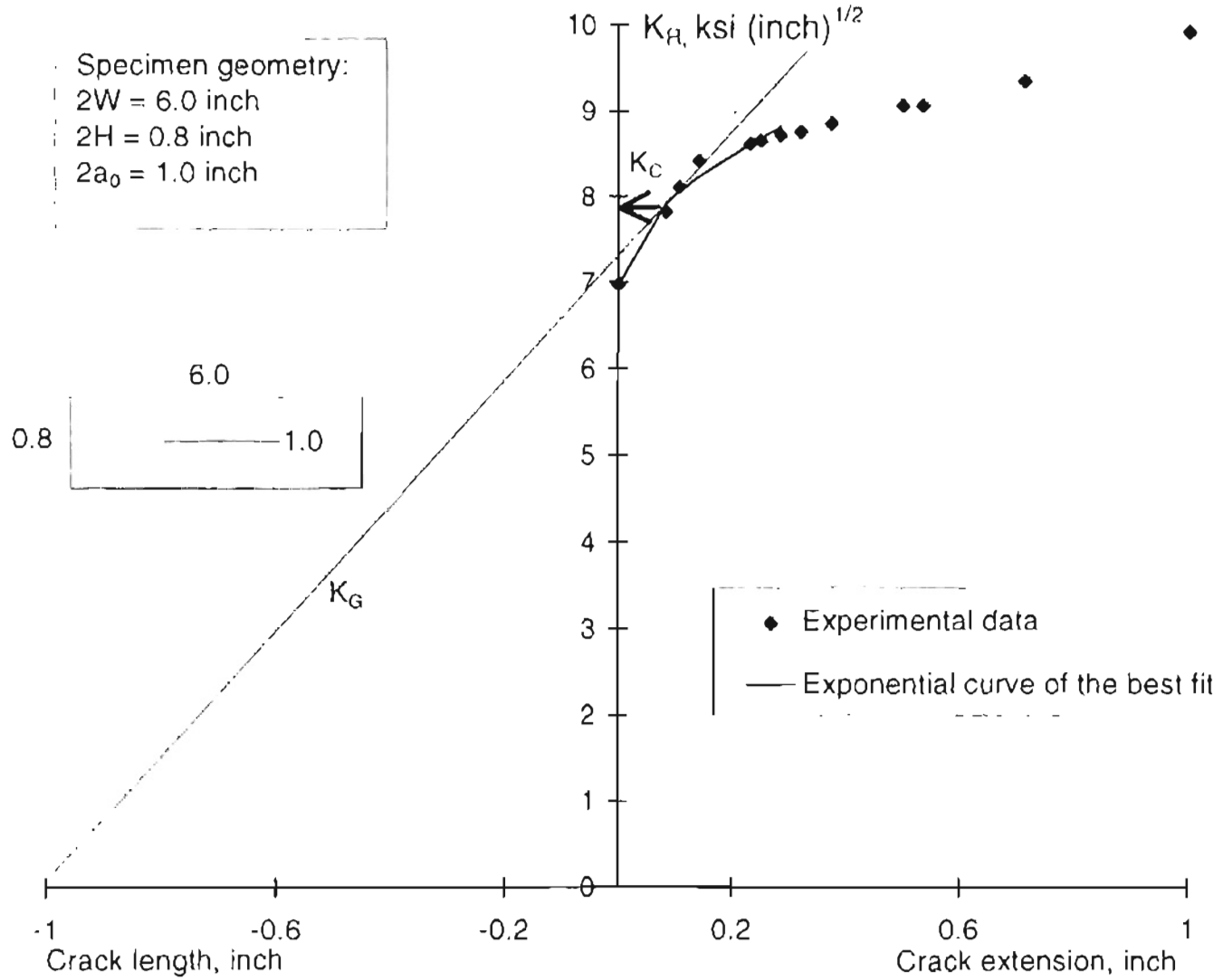Figure 4.19.3: Crack growth resistance curve for a 92 gauge polyester film specimen.
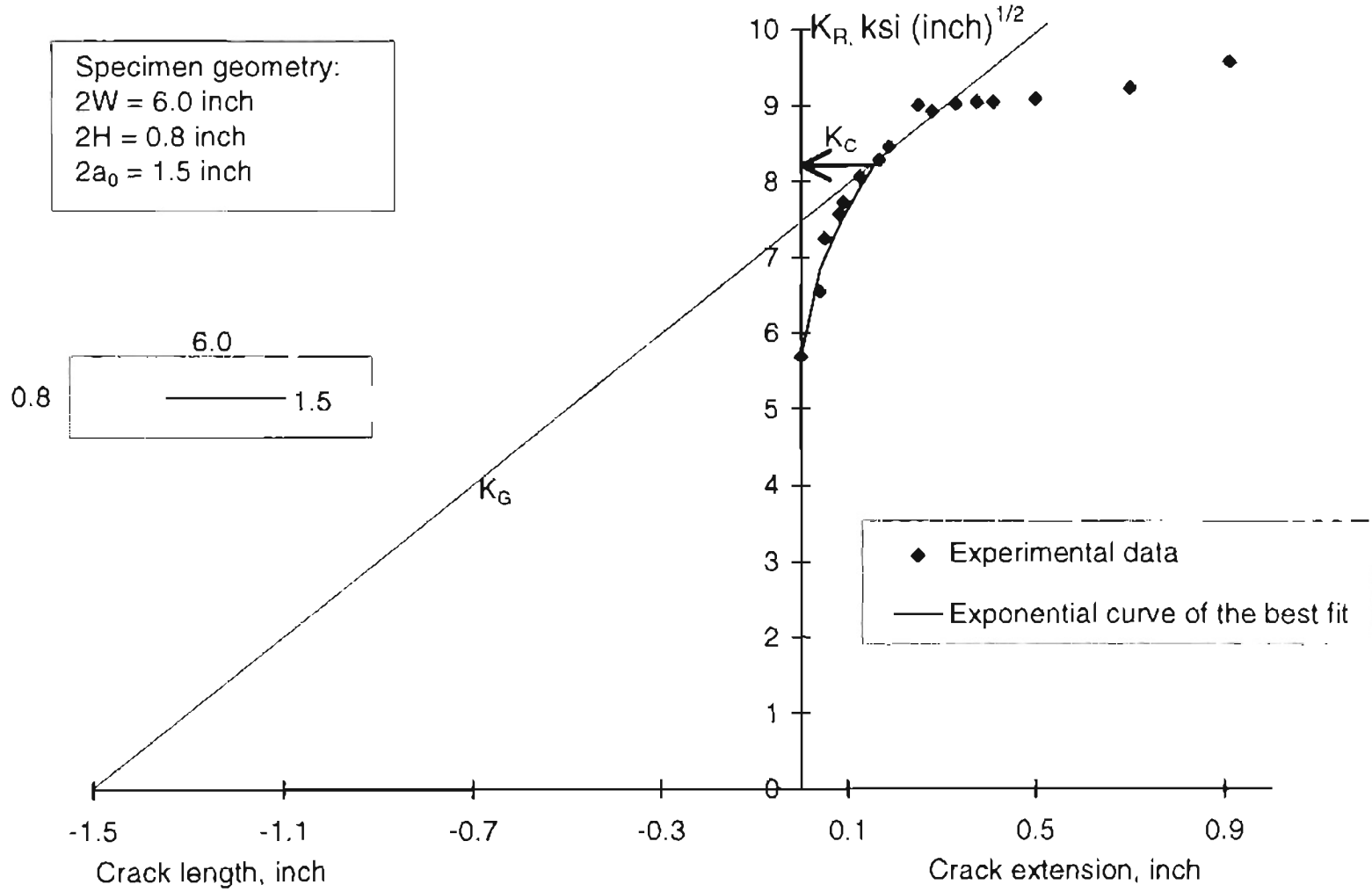
Specimen geometry:
2W = 8.0 inch
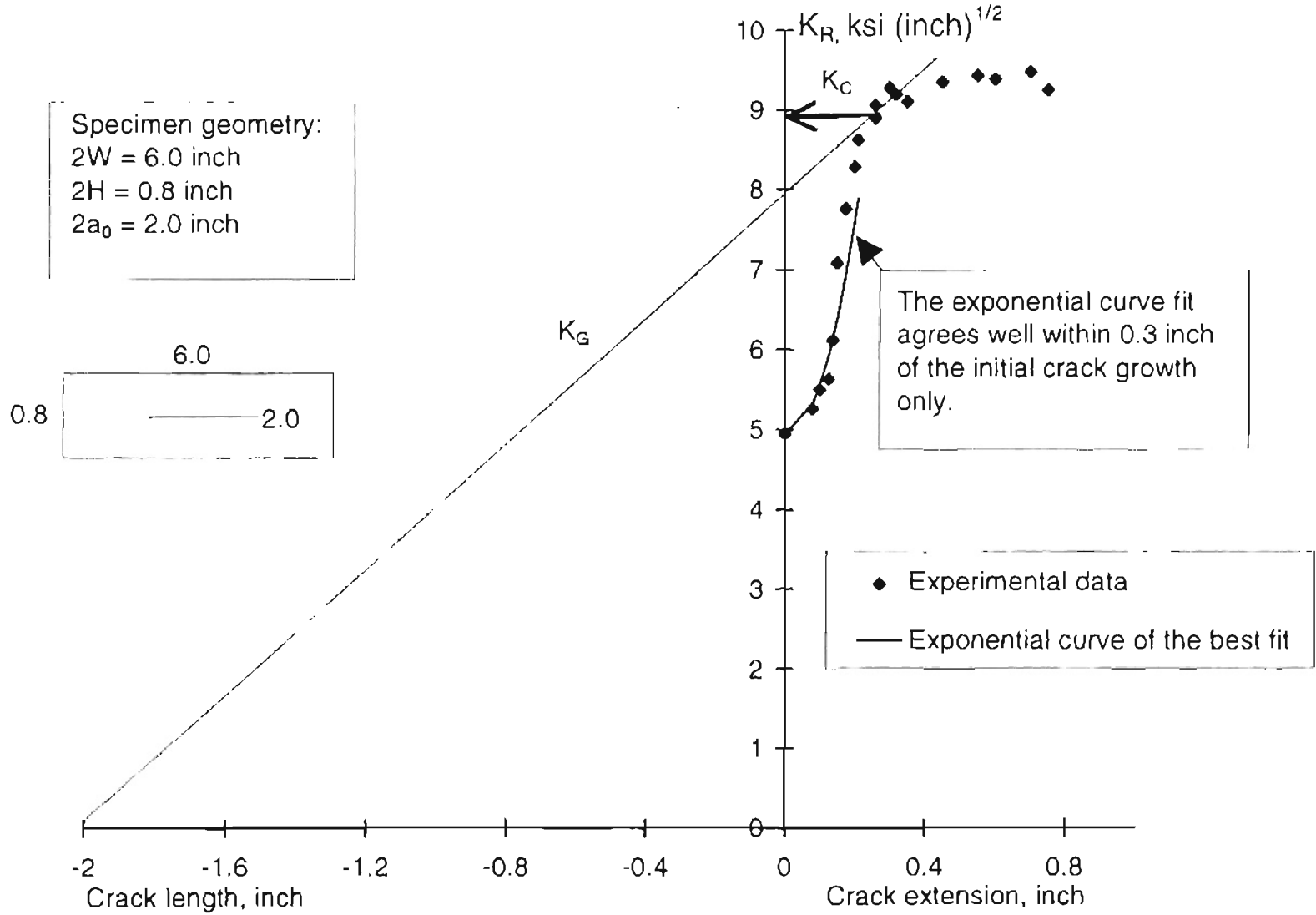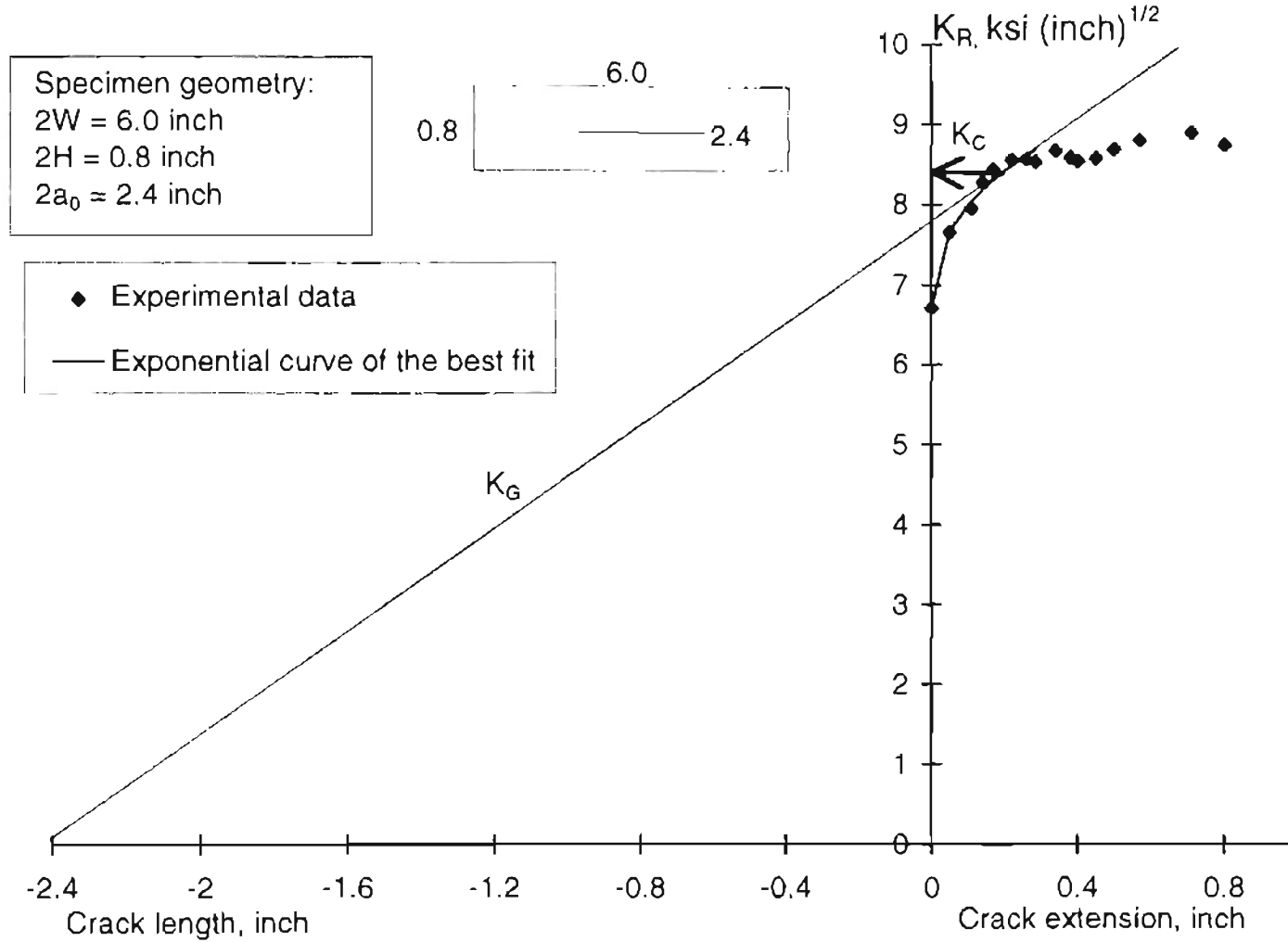2H = 1.25 inch
$2a_0$ = 3.0 inch

8.0

1.25   3.0

♦ Experimental data

— Exponential curve of the best fit

K_G

K_R, ksi (inch)$^{1/2}$

K_C

Crack length, inch

Crack extension, inch

Figure 4.20: K_R-curves for test run no. 9.

Figure 4.20.1: Crack growth resistance curve for a 92 gauge polyester film specimen.

K_R, ksi (inch)$^{1/2}$

Specimen geometry:
2W = 8.0 inch
2H = 2.0 inch
2a$_0$ =1.0 inch

K_C

K_G

8.0

2.0

1.0

♦ Experimental data

—— Exponential curve of the best fit

14

12

10

8

6

4

2

0

-1   -0.6   -0.2   0.2   0.6   1

Crack length, inch

Crack extension, inch

154

Figure 4.20.2: Crack growth resistance curve for a 92 gauge polyester film specimen.

Specimen geometry:
2W = 8.0 inch
2H = 2.0 inch
$2a_0$ =2.0 inch

8.0

2.0

2.0

K_R, ksi (inch)$^{1/2}$

K_C

K_G

- Experimental data
- Exponential curve of the best fit

14
12
10
8
6
4
2
0

-2   -1.6   -1.2   -0.8   -0.4   0   0.4   0.8

Crack length, inch

Crack extension, inch

Figure 4.21: K_R-curves for test run no. 10.

Figure 4.21: Crack growth resistance curve for a 92 gauge polyester film specimen.

Specimen geometry:
2W = 8.0 inch
2H = 3.0 inch
$2a_0$ = 2.0 inch

K_R, ksi (inch)$^{1/2}$

K_C

K_G

Experimental data

Exponential curve of the best fit

Crack length, inch

Crack extension, inch

157

Figure 4.22: K_R-curves for test run no. 11.

Figure 4.22.1: Crack growth resistance curve for a 92 gauge polyester film specimen.

Specimen geometry:
2W = 12.0 inch
2H = 0.8 inch
$2a_0$ = 0.8 inch

K_R, ksi $(inch)^{1/2}$

K_C

K_G

- Experimental data
- Exponential curve of the best fit

Crack length, inch

Crack extension, inch

Figure 4.22.2: Crack growth resistance curve for a 92 gauge polyester film specimen.

Specimen geometry:
2W = 12.0 inch
2H = 0.8 inch
$2a_0 = 1.5$ inch

K_R, ksi (inch)$^{1/2}$

K_C

K_G

♦ Experimental data

—— Exponential curve of the best fit

Crack length, inch

Crack extension, inch

Figure 4.22.3: Crack growth resistance curve for a 92 gauge polyester film specimen.

Specimen geometry:
$2W = 12.0$ inch
$2H = 0.8$ inch
$2a_0 = 2.0$ inch

K_R, ksi (inch)$^{1/2}$

K_C

K_G

♦ Experimental data

—— Exponential curve of the best fit

10

8

6

4

2

0

-2   -1.6   -1.2   -0.8   -0.4   0   0.4   0.8

Crack length, inch

Crack extension, inch

Figure 4.22.4: Crack growth resistance curve for a 92 gauge polyester film specimen.

Specimen geometry:
2W = 12.0 inch
2H = 0.8 inch
$2a_0$ =3.0 inch

◆ Experimental data

—— Exponential curve of the best fit

K_R, ksi $(inch)^{1/2}$

K_C

K_G

Crack length, inch

Crack extension, inch
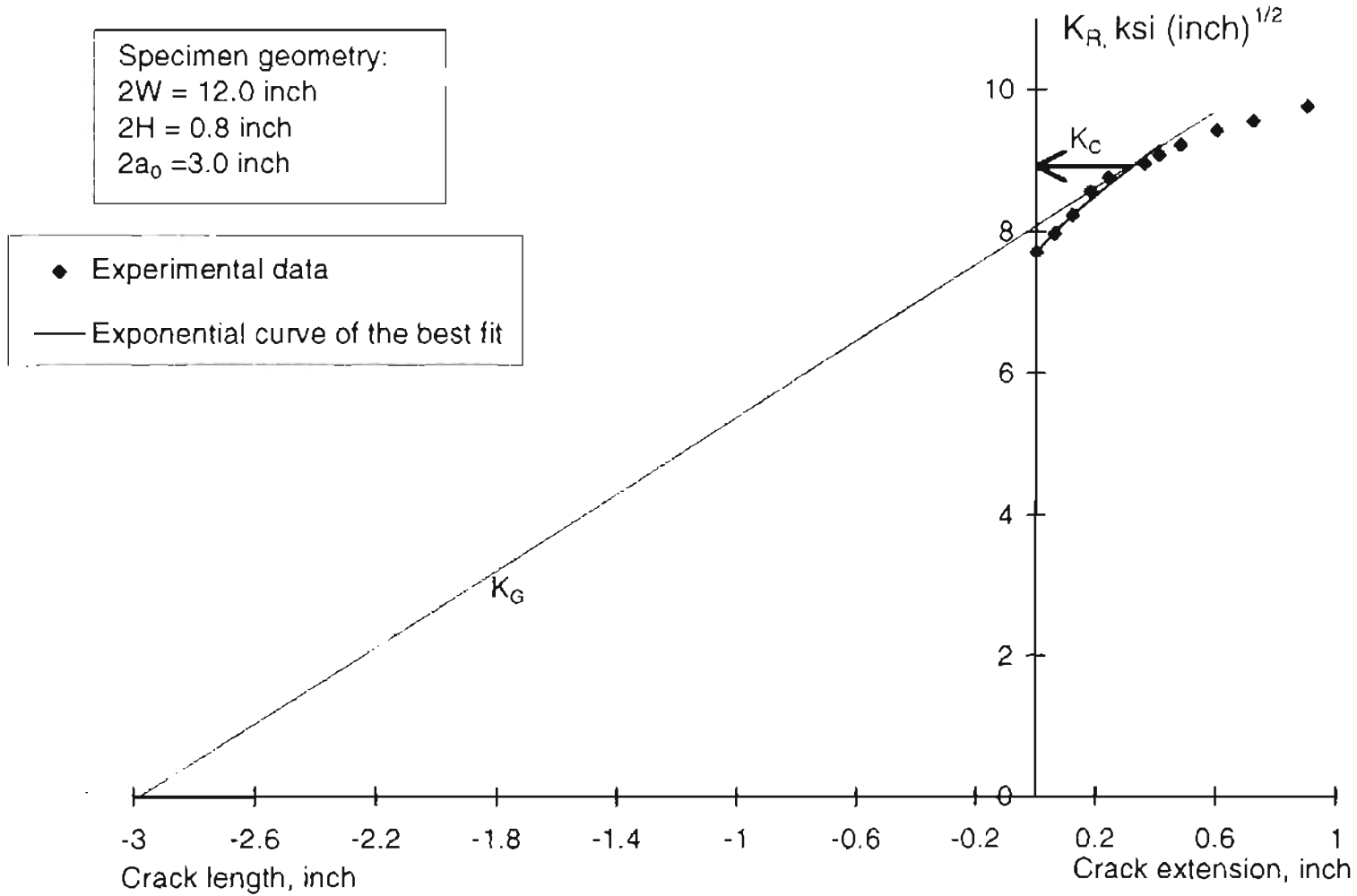
Figure 4.22.5: Crack growth resistance curve for a 92 gauge polyester film specimen.

Specimen geometry:
2W = 12.0 inch
2H = 0.8 inch
$2a_0$ = 4.0 inch

◆ Experimental data

—— Exponential curve of the best fit

K_R. ksi (inch)$^{1/2}$

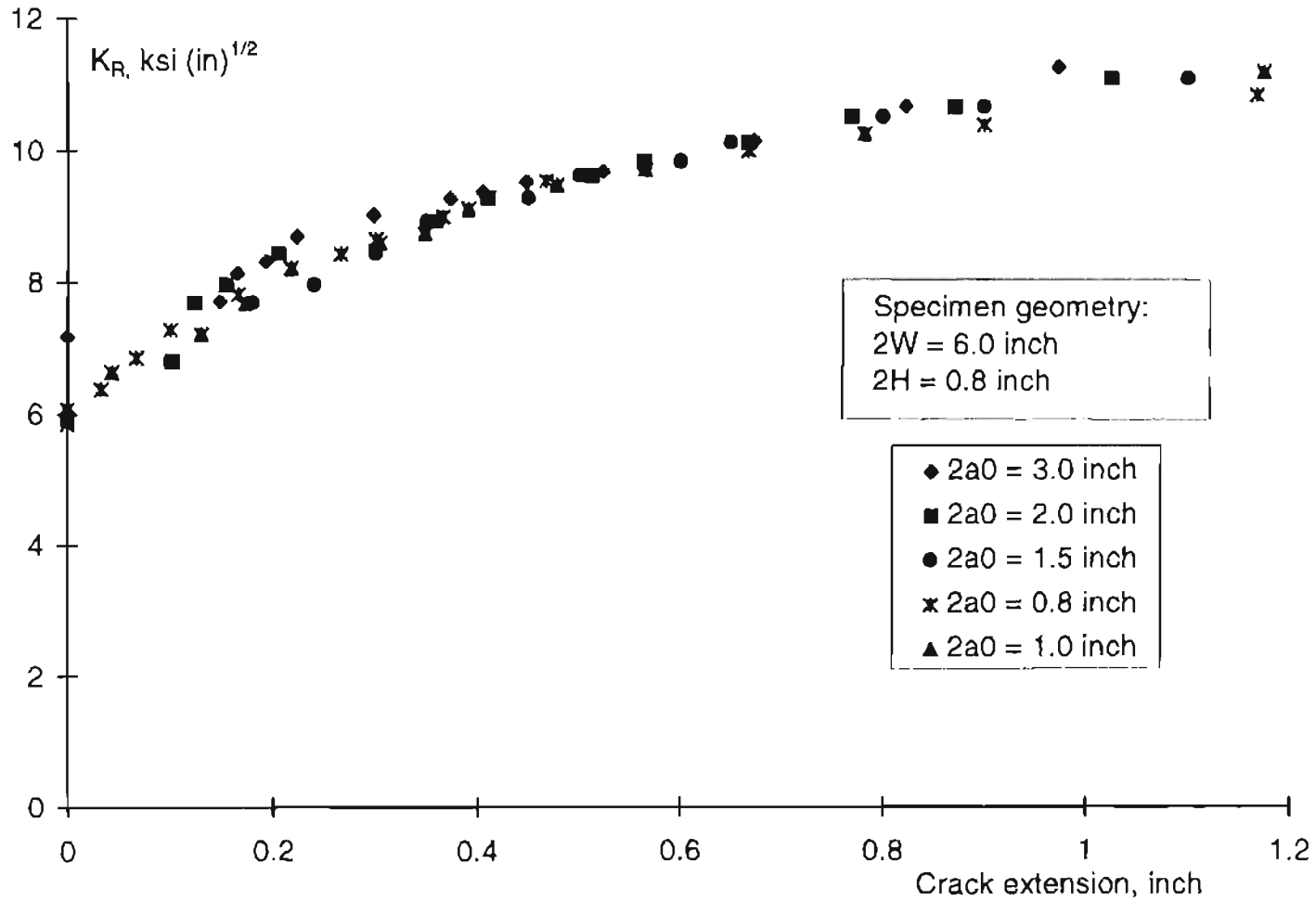K_C

K_G

Crack length, inch

Crack extension, inch
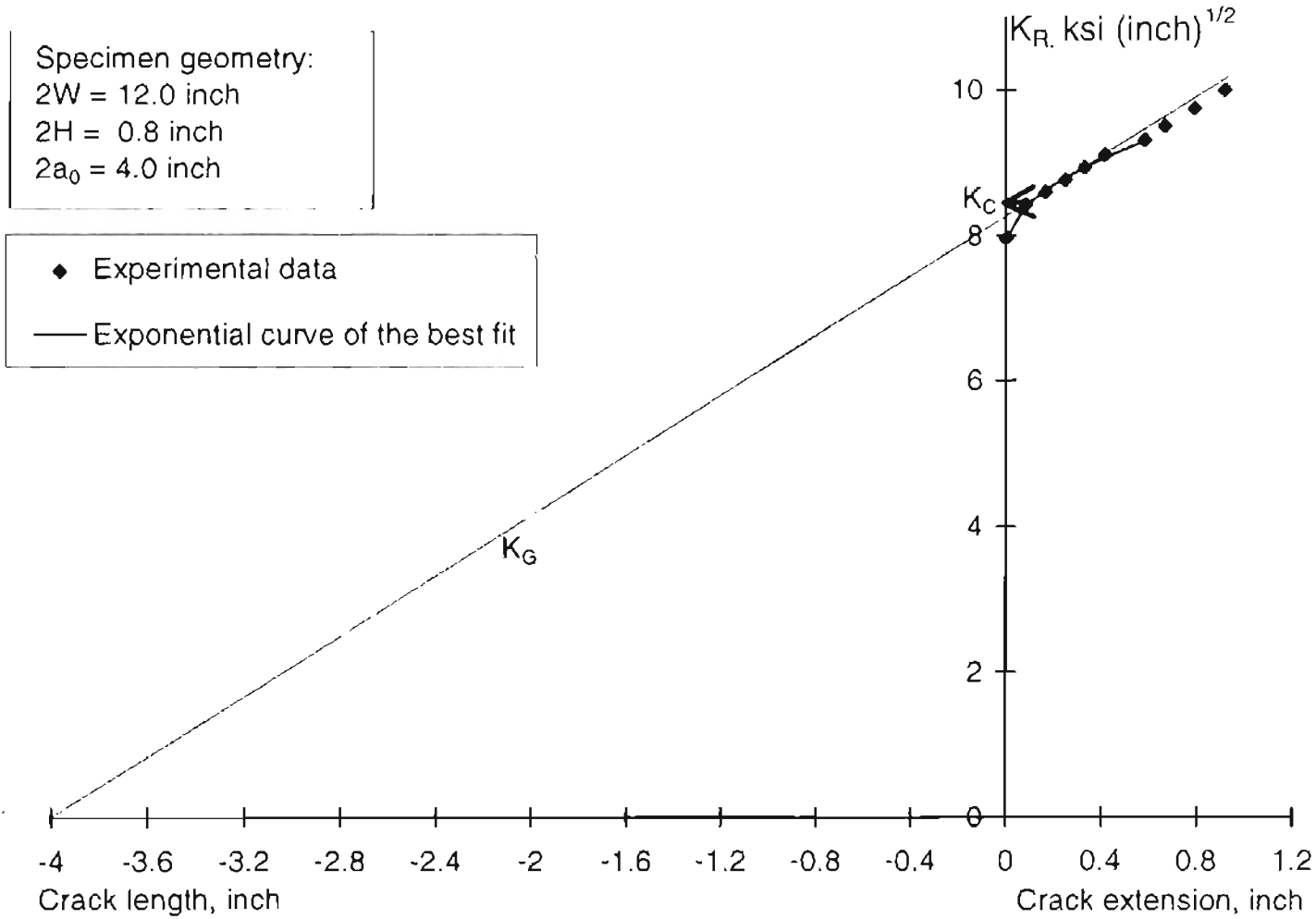
Figure 4.23: K_R-curves for test run no. 12.

Figure 4.23.1: Crack growth resistance curve for a 92 gauge polyester film specimen.
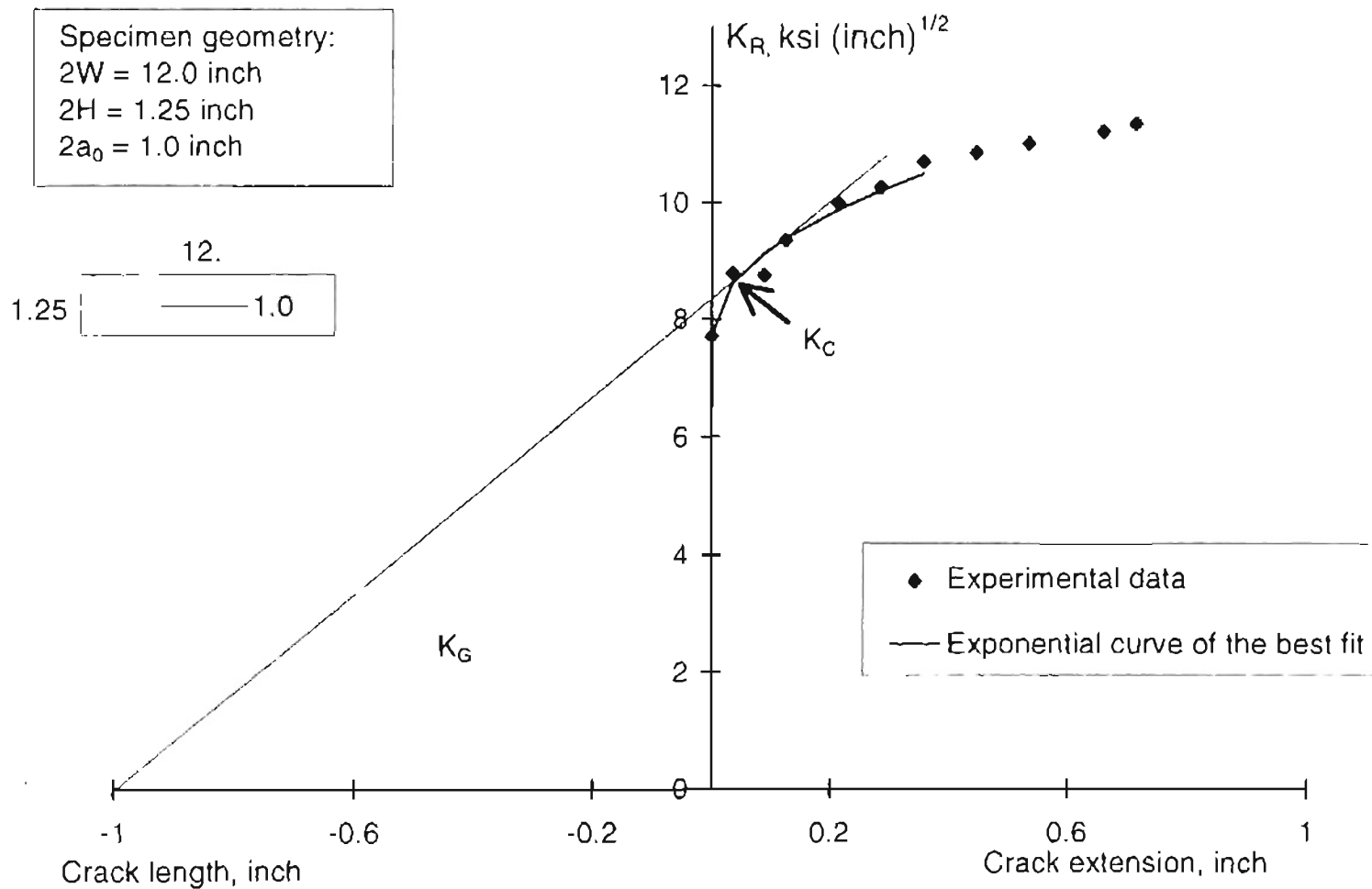
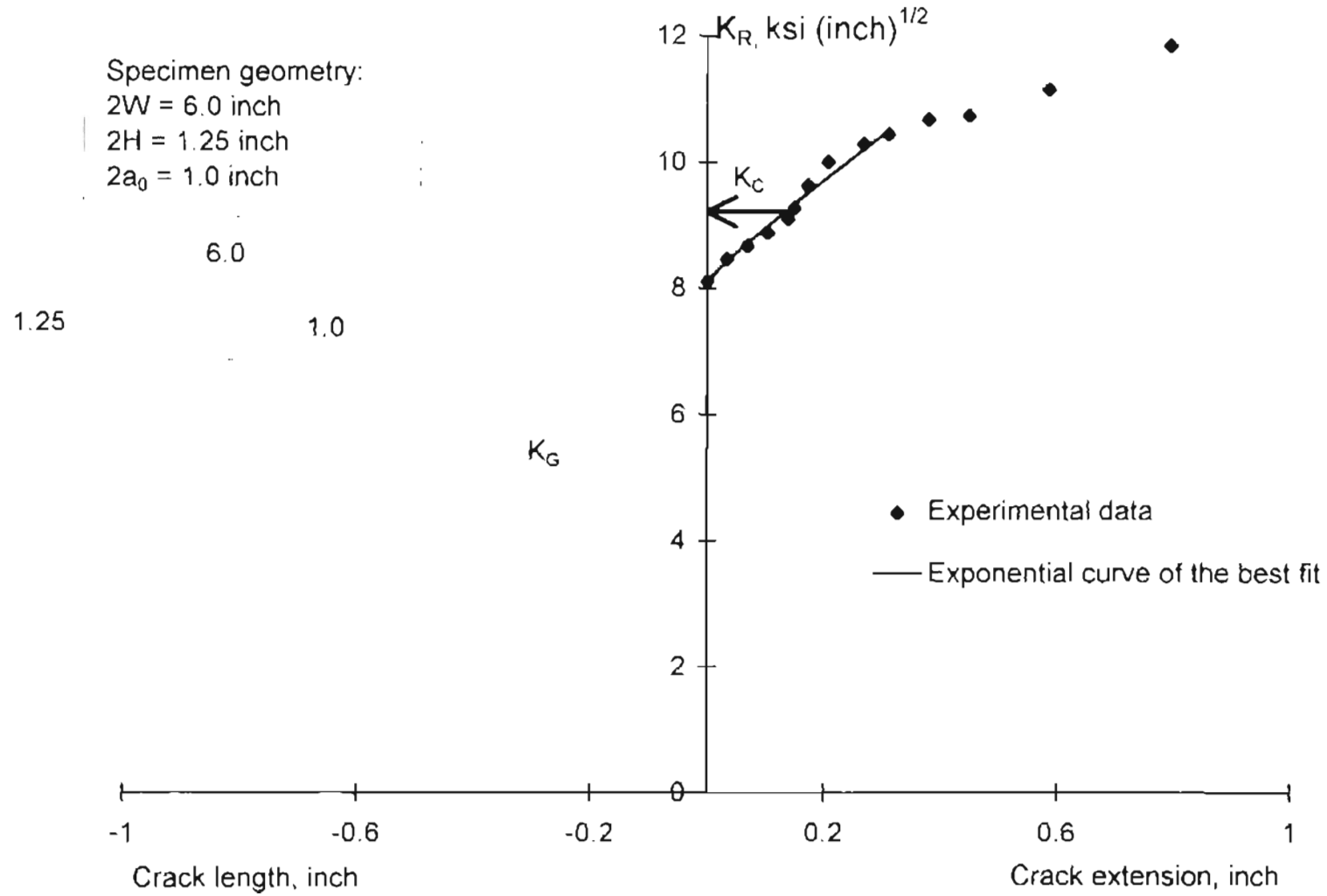Figure 4.23.2: Crack growth resistance curve for a 92 gauge polyester film specimen.
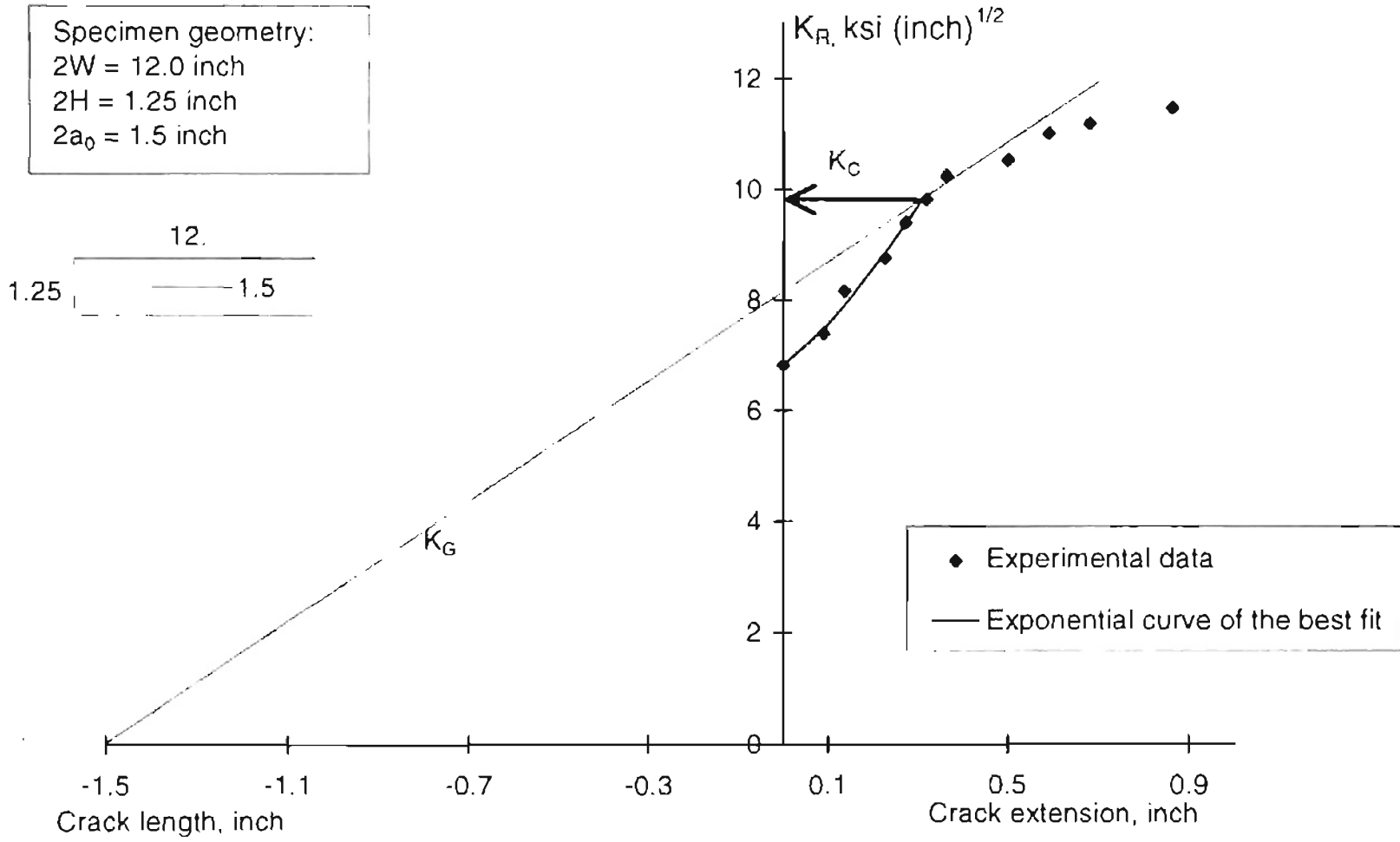
Figure 4.23.3: Crack growth resistance curve for a 92 gauge polyester film specimen.
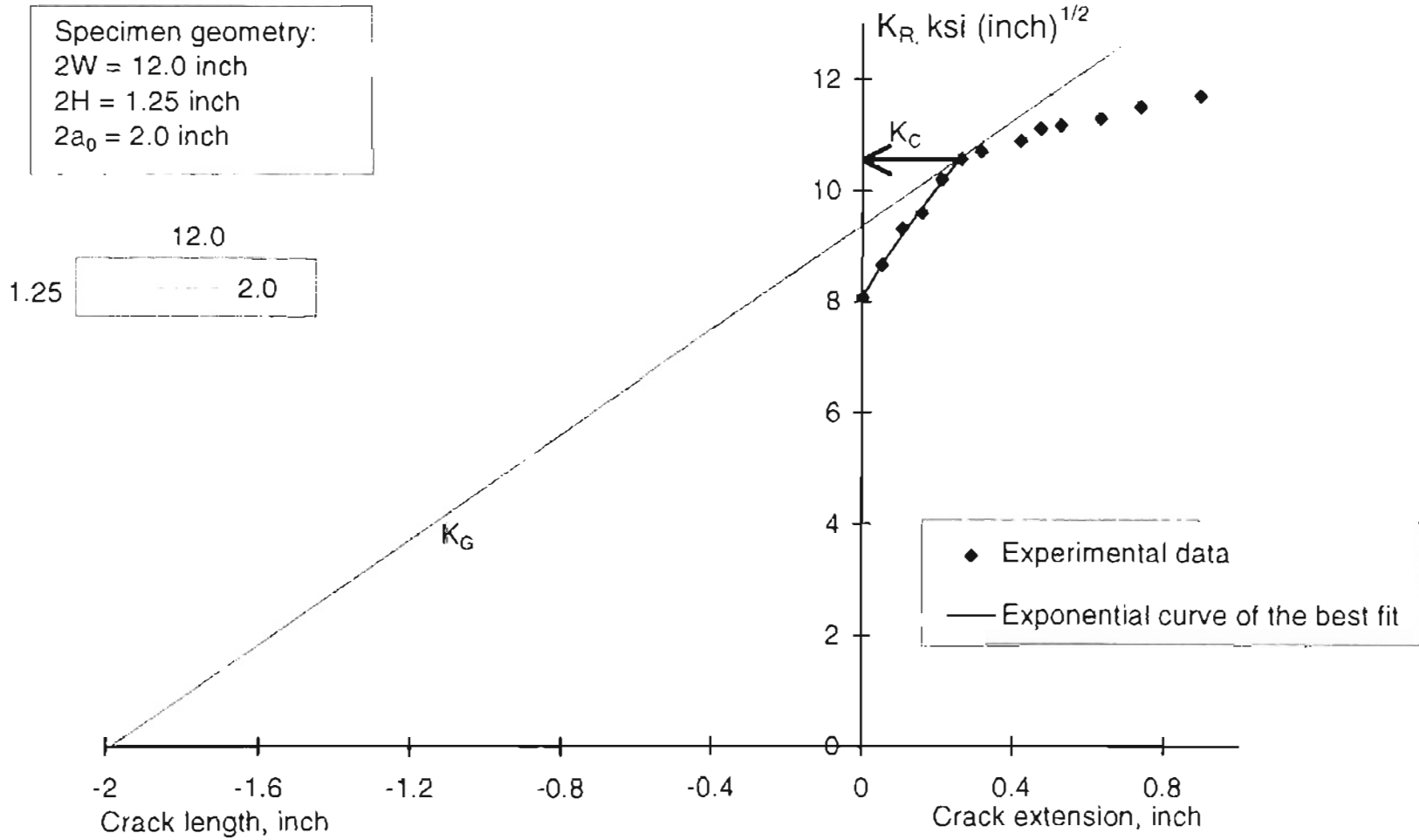
Figure 4.23.4: Crack growth resistance curve for a 92 gauge polyester film specimen.
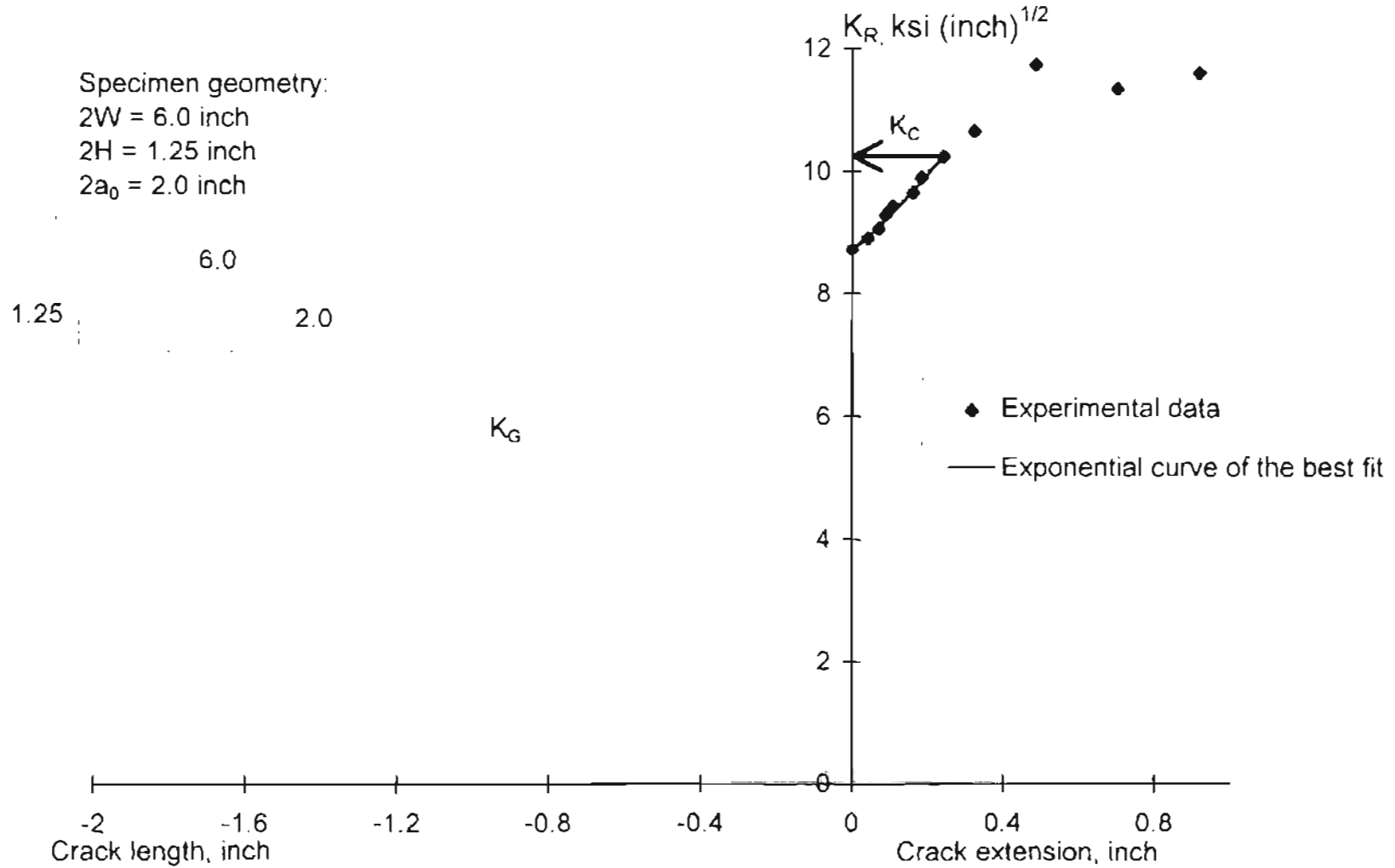

Specimen geometry:
2W = 12.0 inch
2H = 1.25 inch
$2a_0$ = 4.0 inch

12.

1.25   — 4.0

♦ Experimental data

—— Exponential curve of the best fit

K_R, ksi $(inch)^{1/2}$

K_C

K_G

Crack length, inch

Crack extension, inch
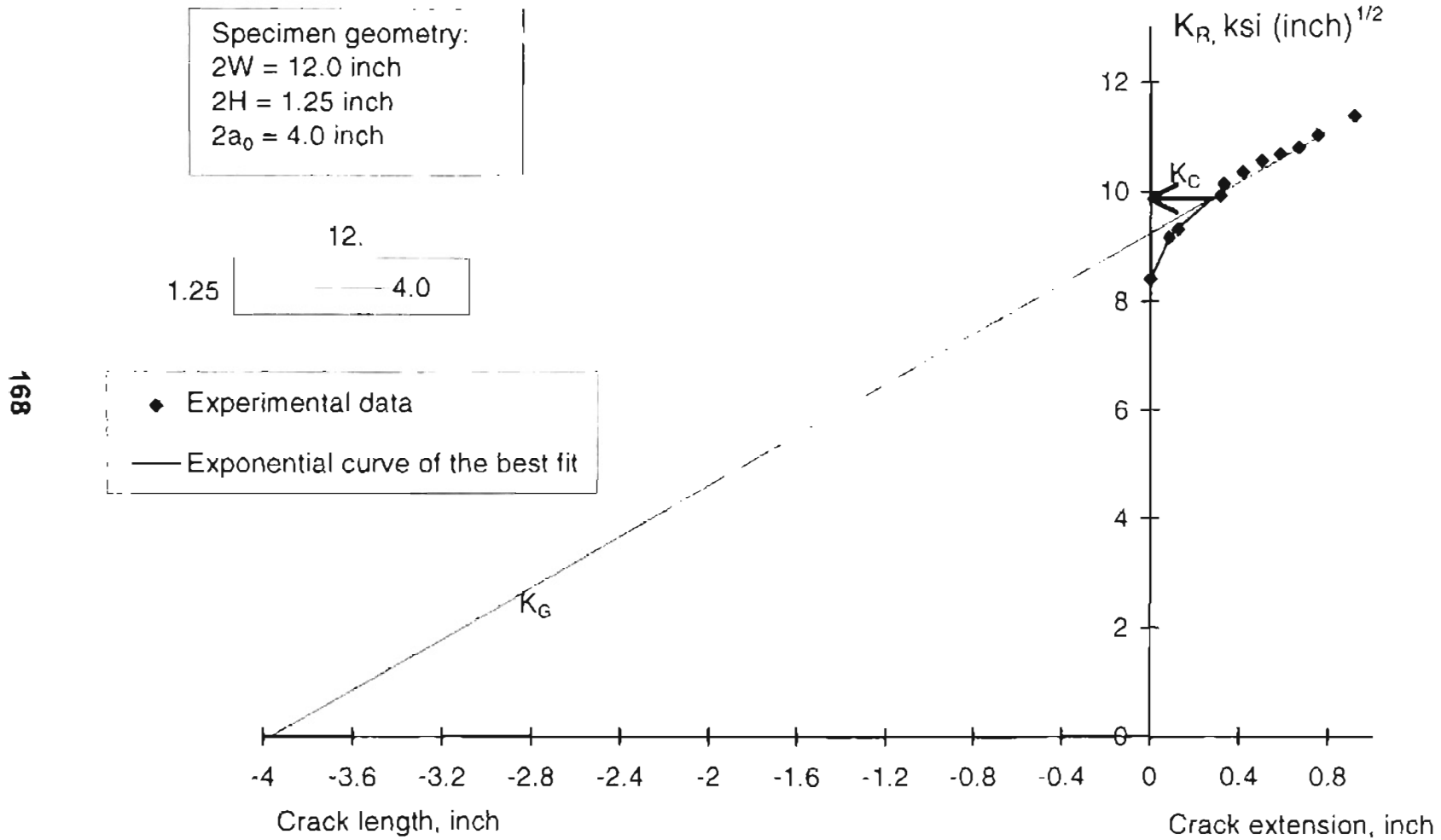
Figure 4.23.5: Crack growth resistance data for 92 gauge polyester film specimens with different initial crack lengths (2a), tested in MD.

K_R, ksi (inch)$^{1/2}$

12.0

1.25 — — 2a

♦ 2a = 4.0 inch
■ 2a = 2.0 inch
♦ 2a = 1.5 inch
+ 2a = 1.0 inch

Crack extension, inch
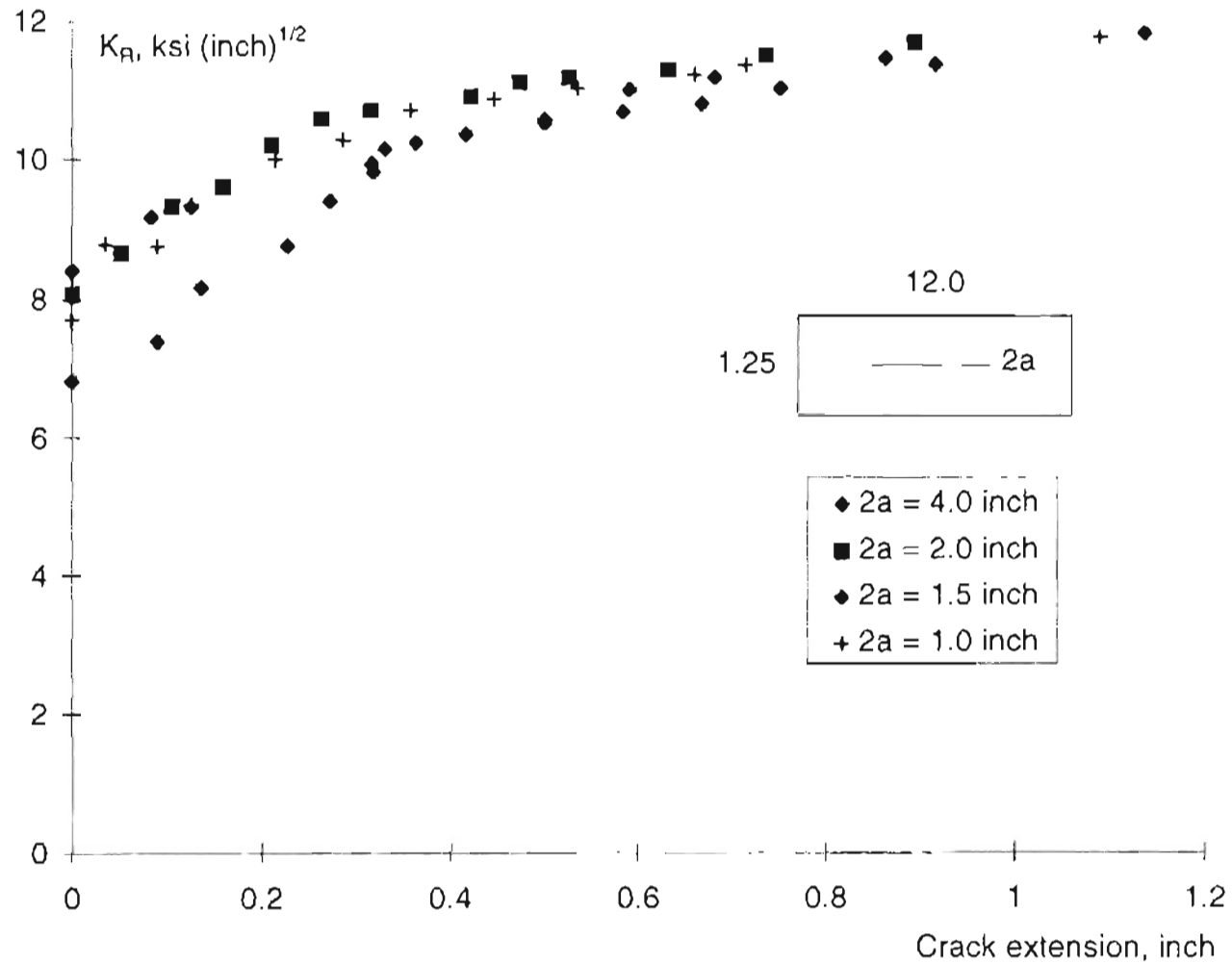
Figure 4.24: K_R-curves for test run no. 13.

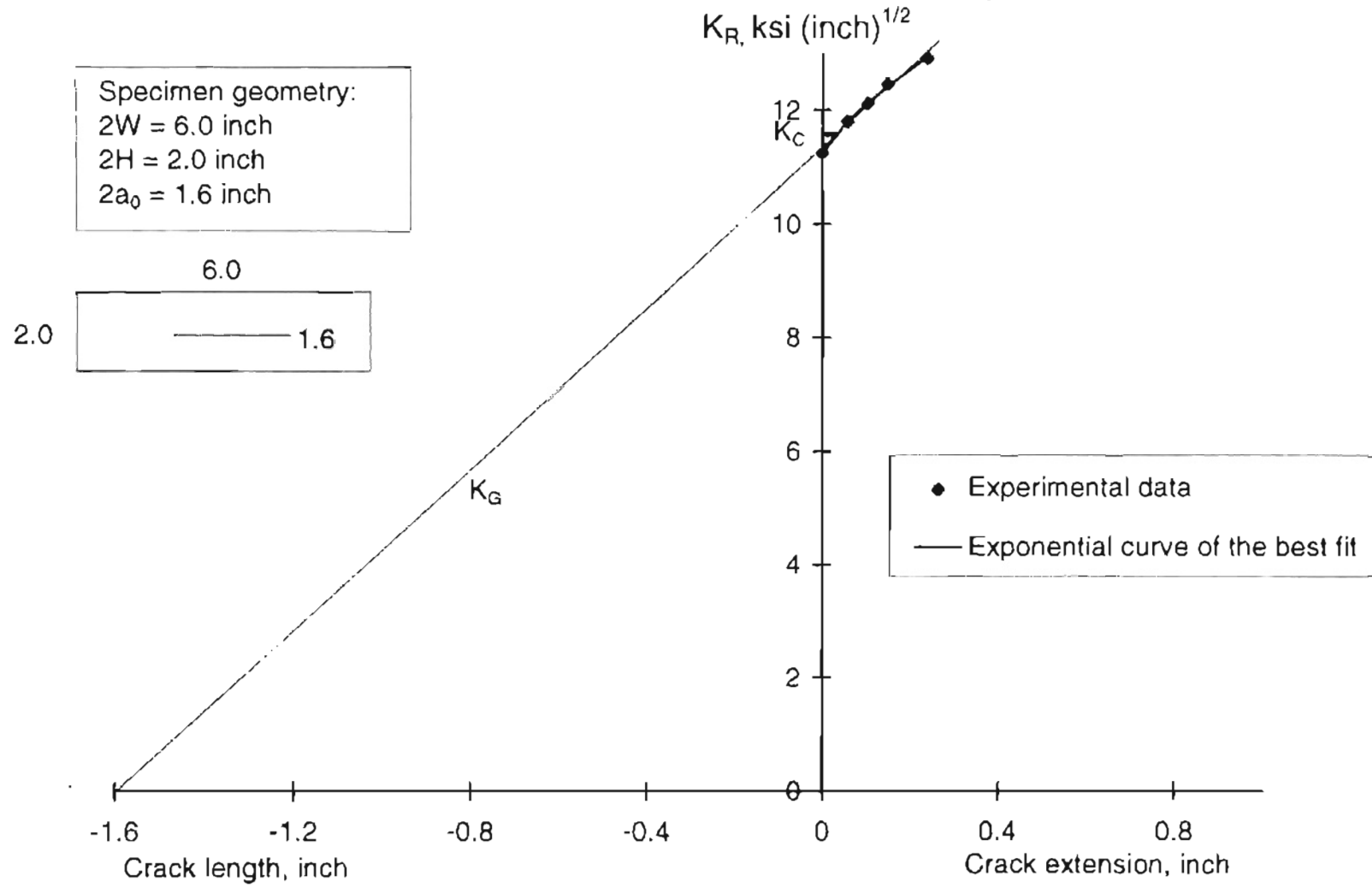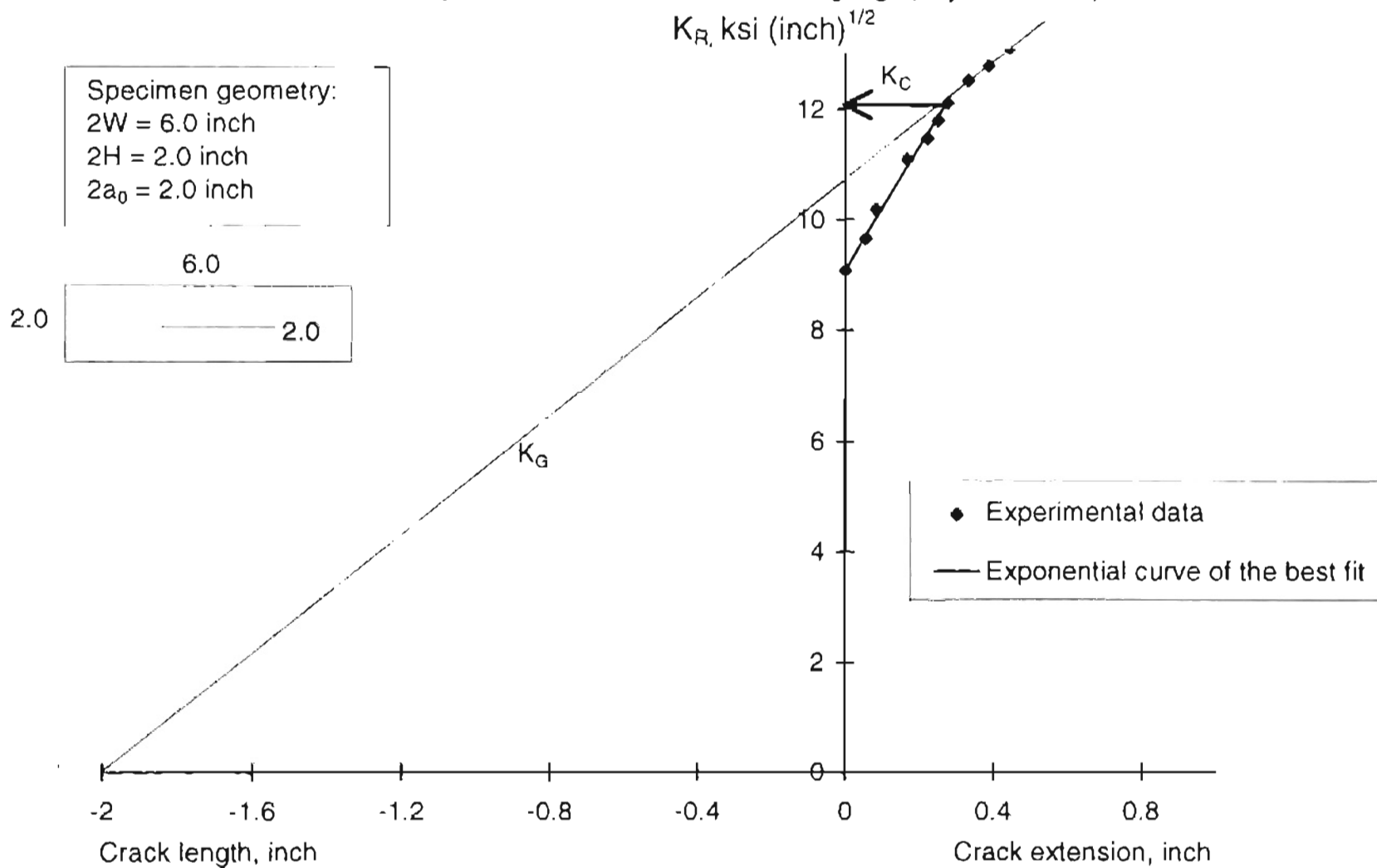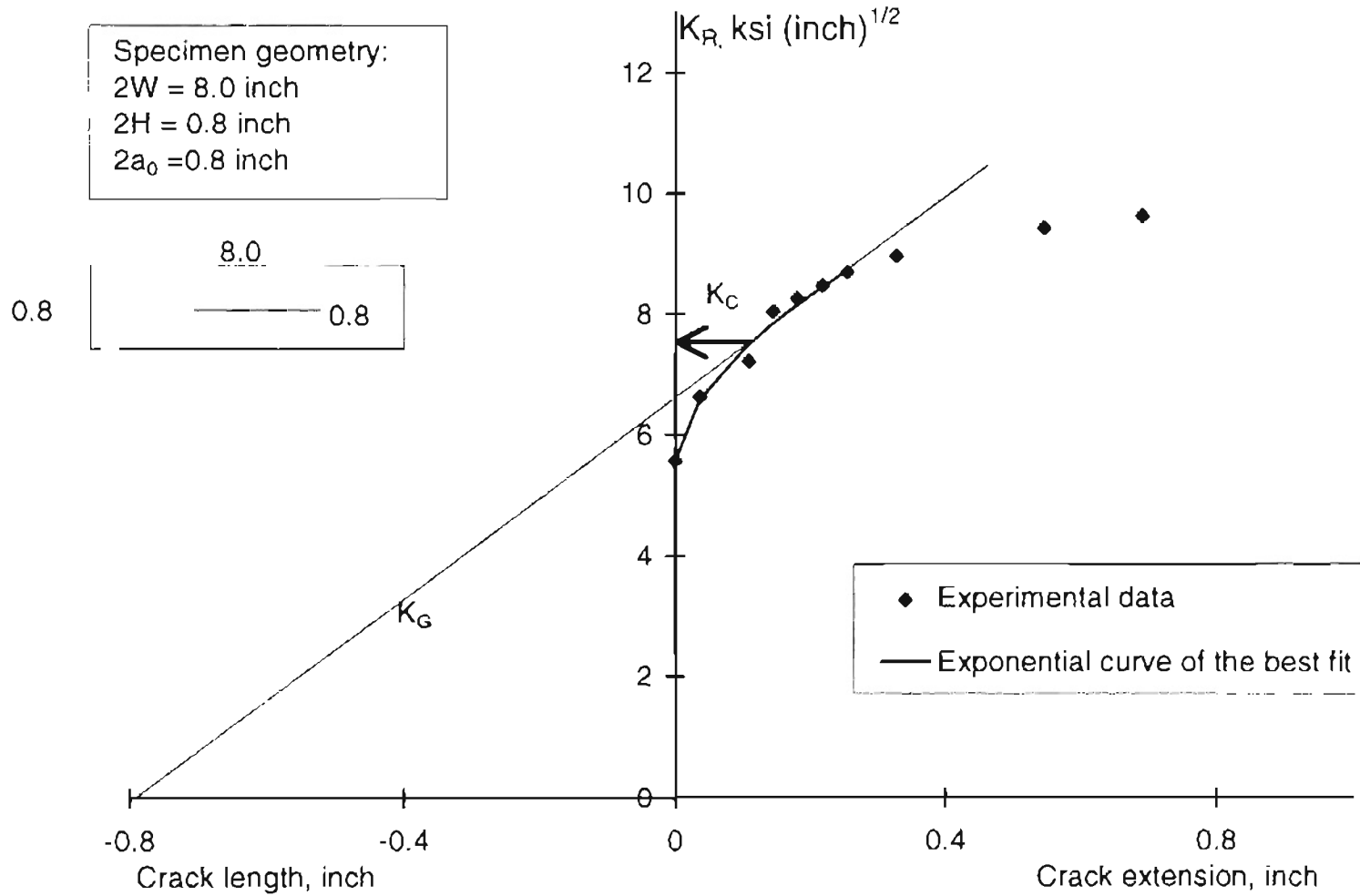Figure 4.24.1: Crack growth resistance curve for a 92 gauge polyester film specimen tested in CD.
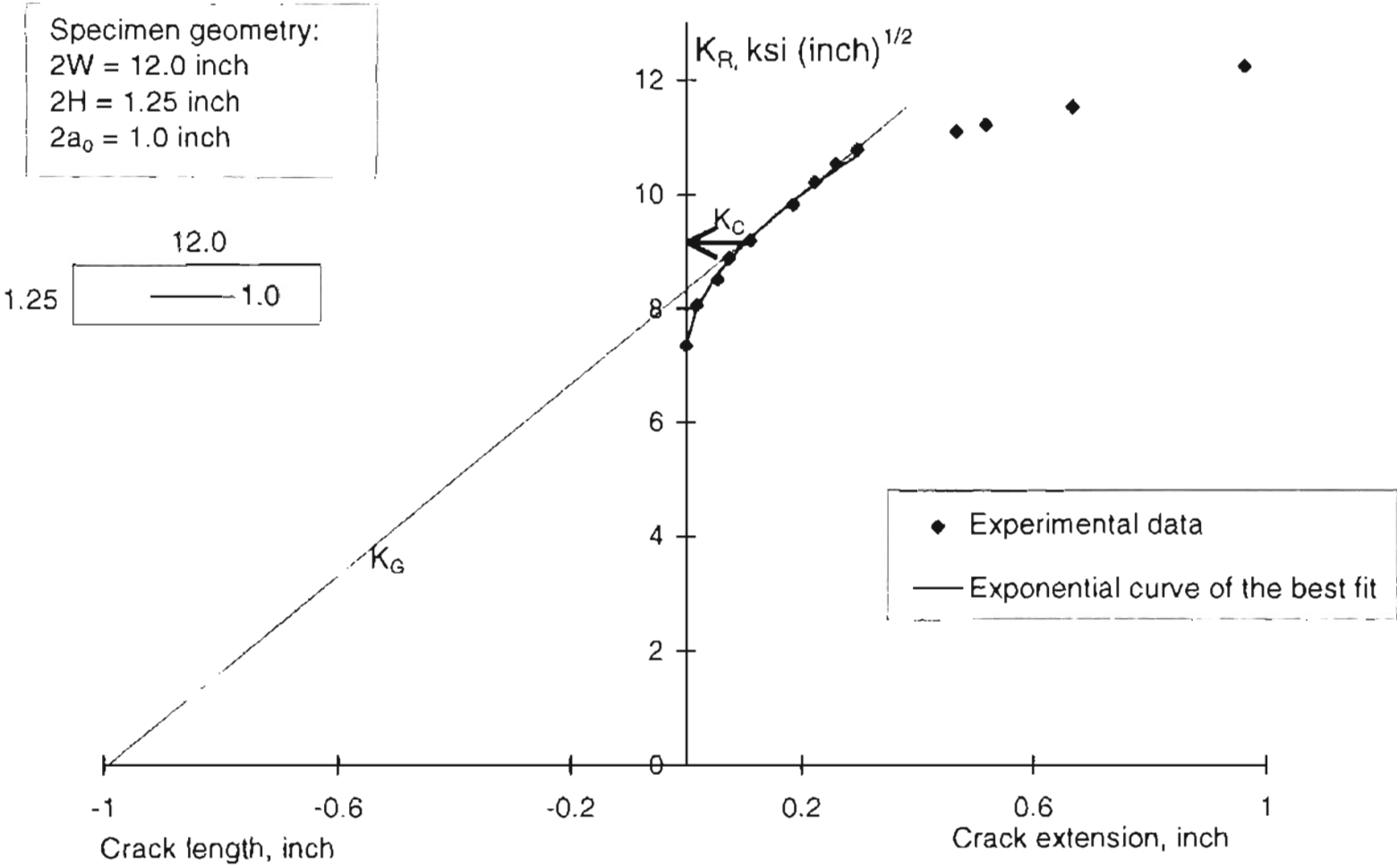
Figure 4.24.2: Crack growth resistance curve for a 92 gauge polyester film specimen tested in CD.

Specimen geometry:
2W = 12.0 inch
2H = 1.25 inch
$2a_0$ = 1.5 inch

K_R ksi $(inch)^{1/2}$

K_C

K_G

♦ Experimental data

—— Exponential curve of the best fit
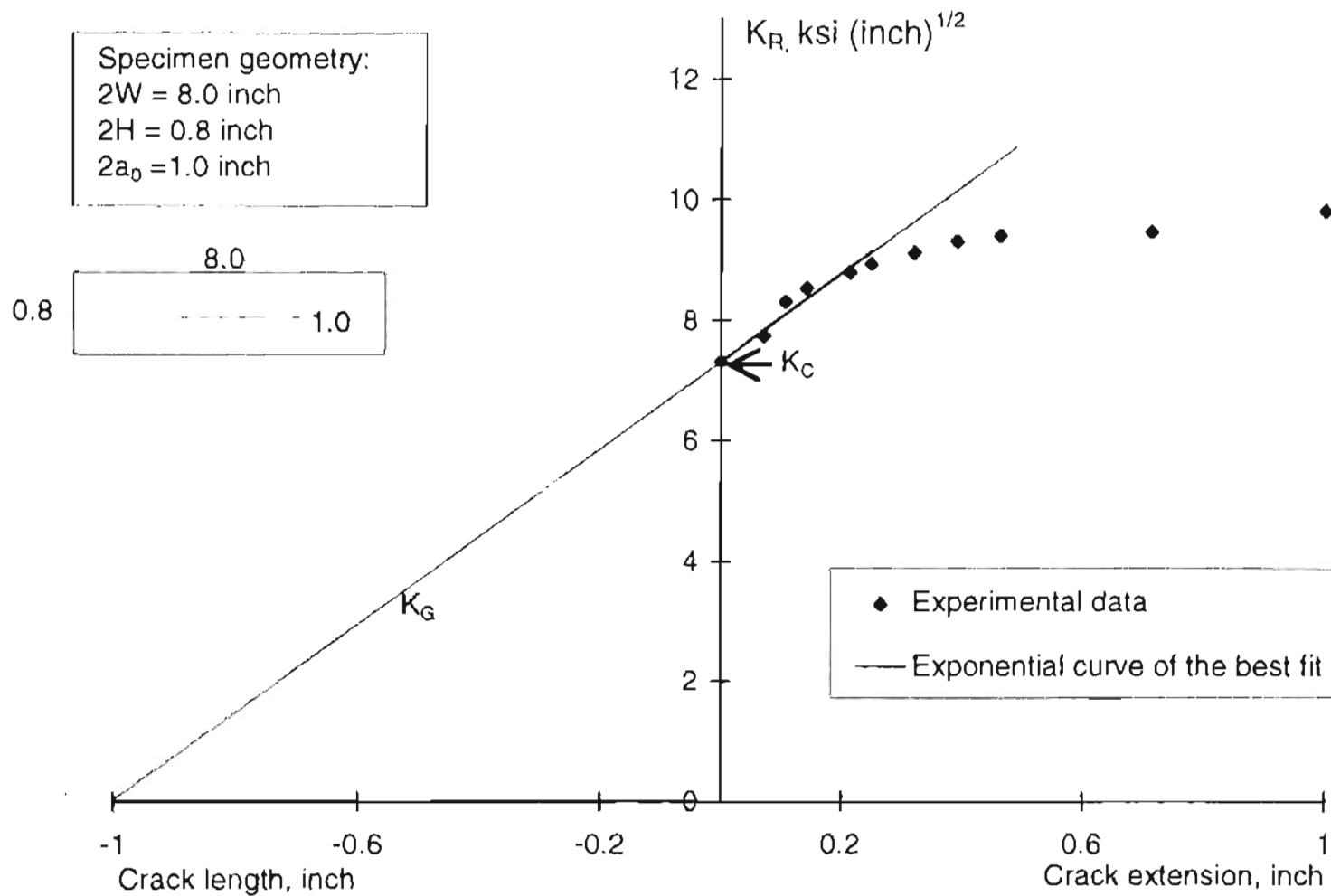
Crack length, inch

Crack extension, inch
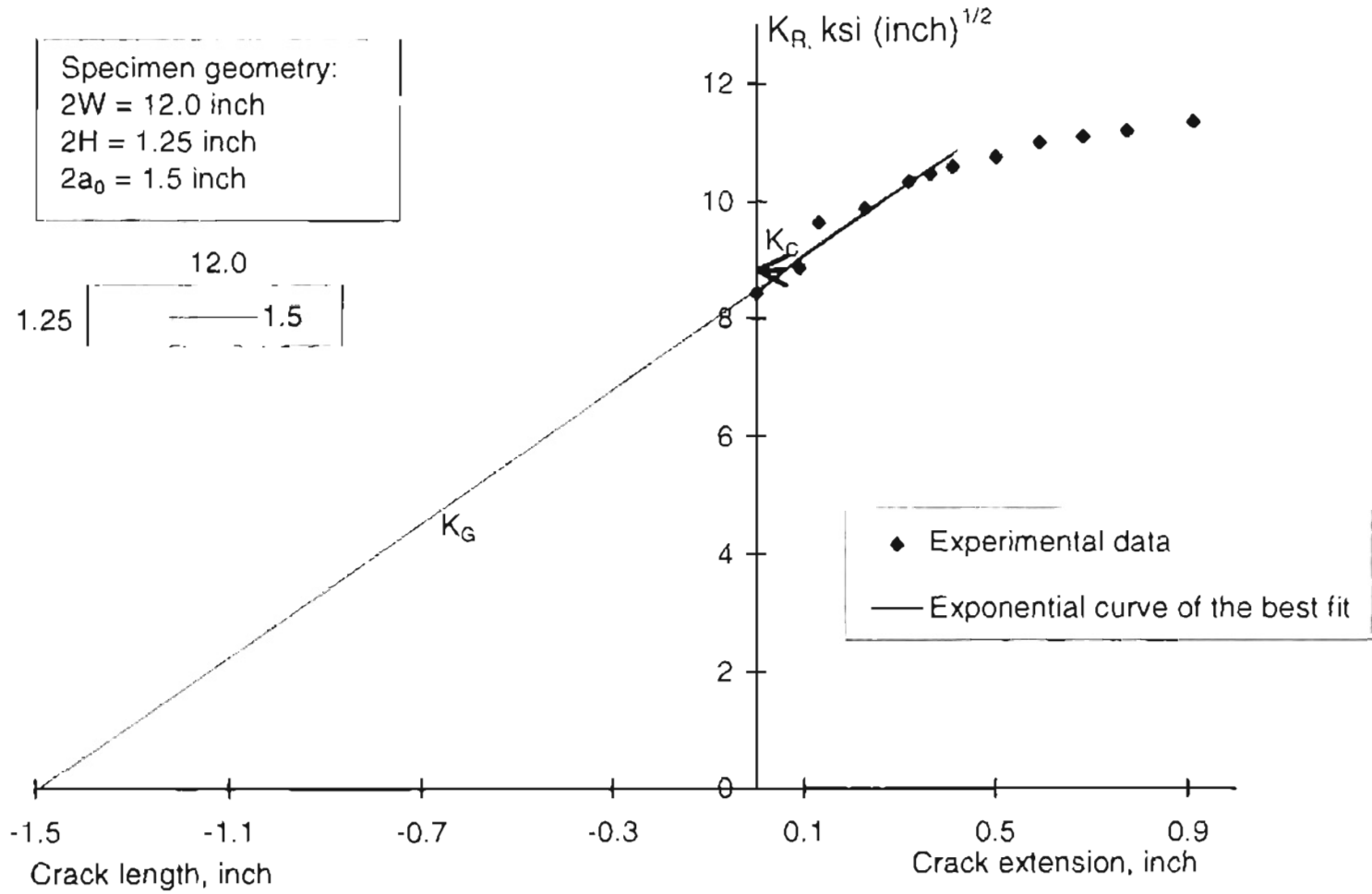
Figure 4.24.3: Crack growth resistance curve for a 92 gauge polyester film specimen tested in CD.
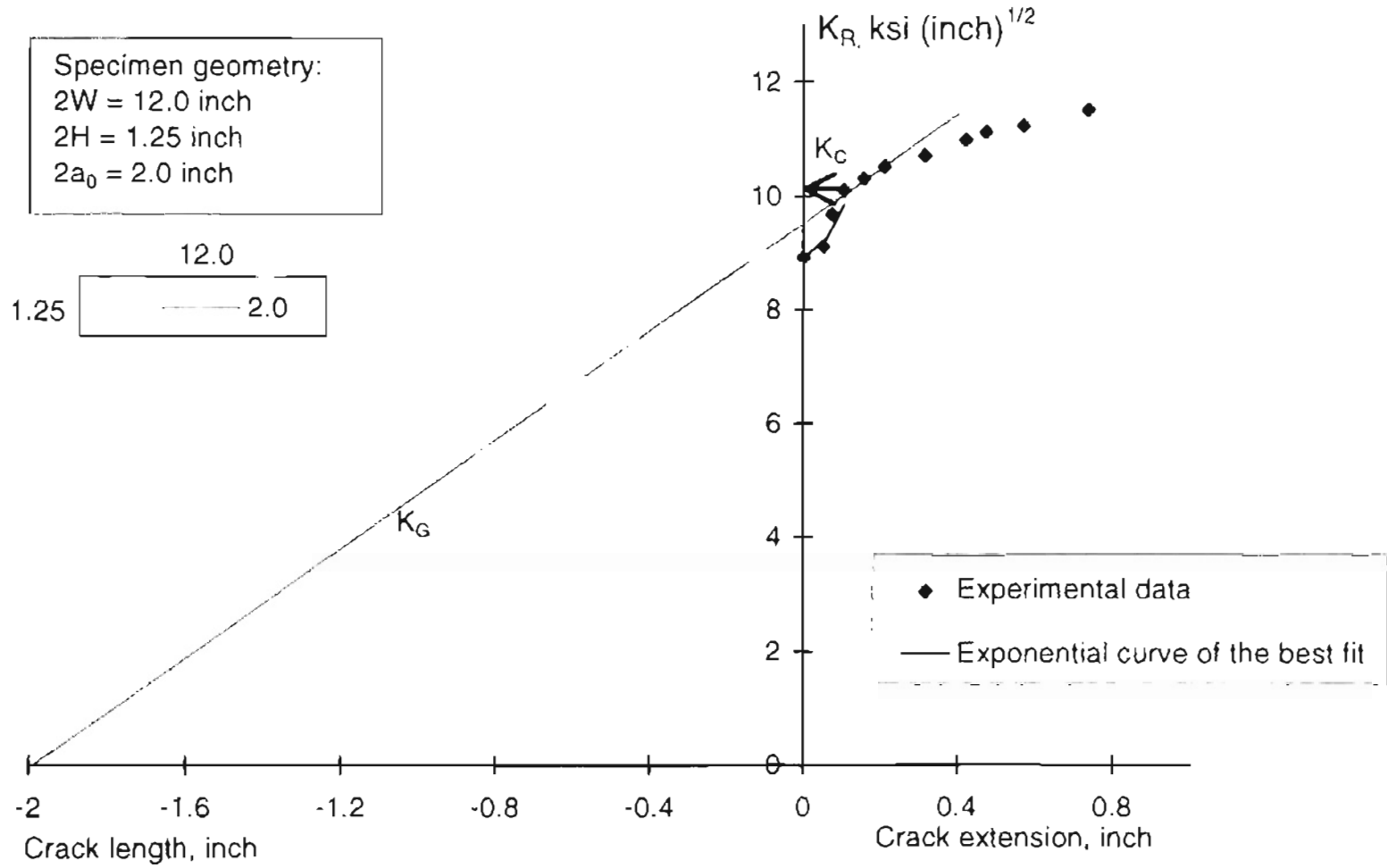
Figure 4.24.4: Crack growth resistance curve for a 92 gauge polyester film specimen tested in CD.

Specimen geometry:
2W = 12.0 inch
2H = 1.25 inch
$2a_0$ = 1.5 inch

12.0

1.25 ----4.0

◆ Experimental data

—— Exponential curve of the best fit

K_G

K_R, ksi $(inch)^{1/2}$

K_C

Crack length, inch

Crack extension, inch

174
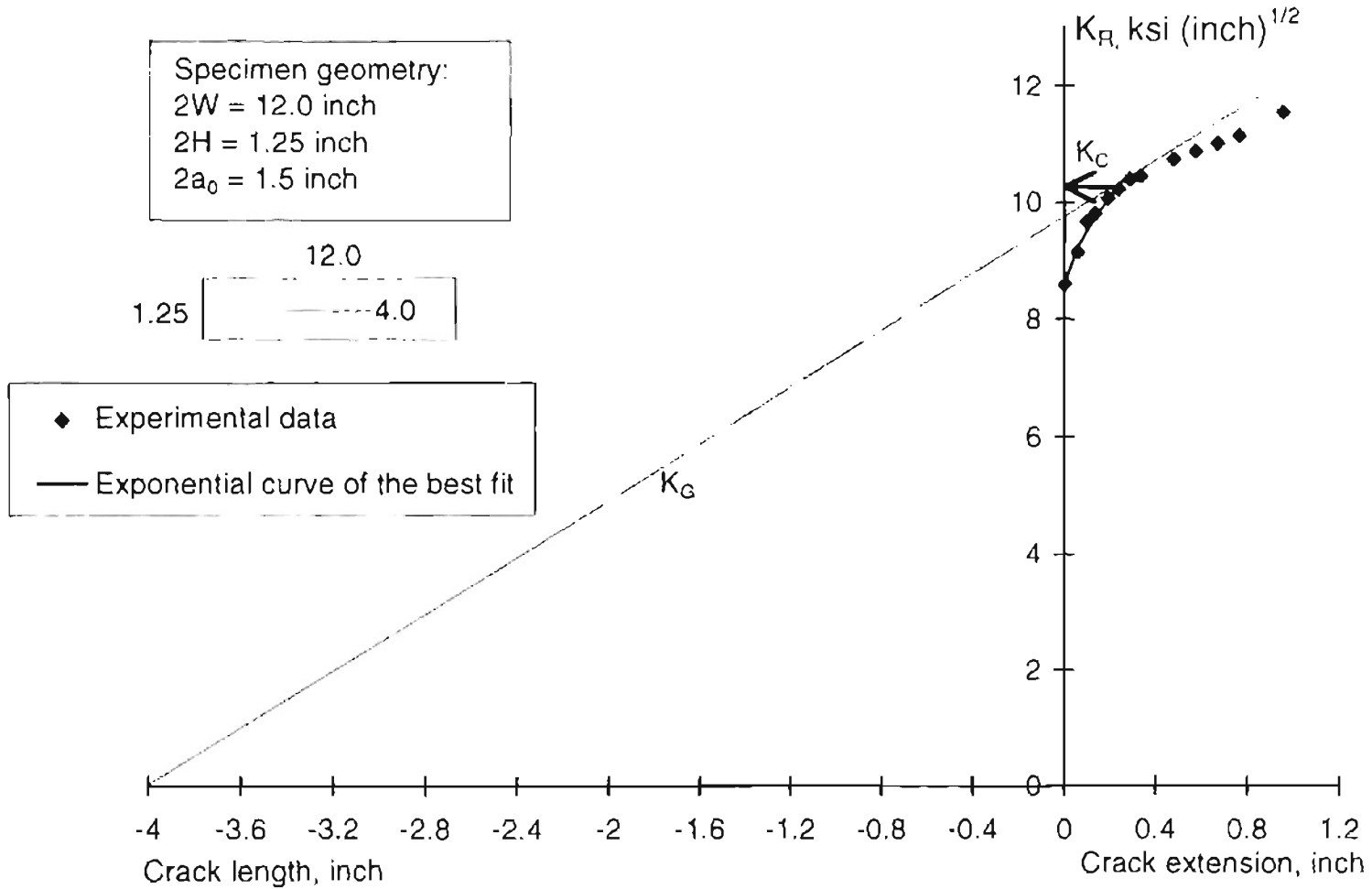
Figure 4.25: K_R-curves for test run no. 14.

Figure 4.25.1: Crack growth resistance curve for a 92 gauge polyester film specimen.
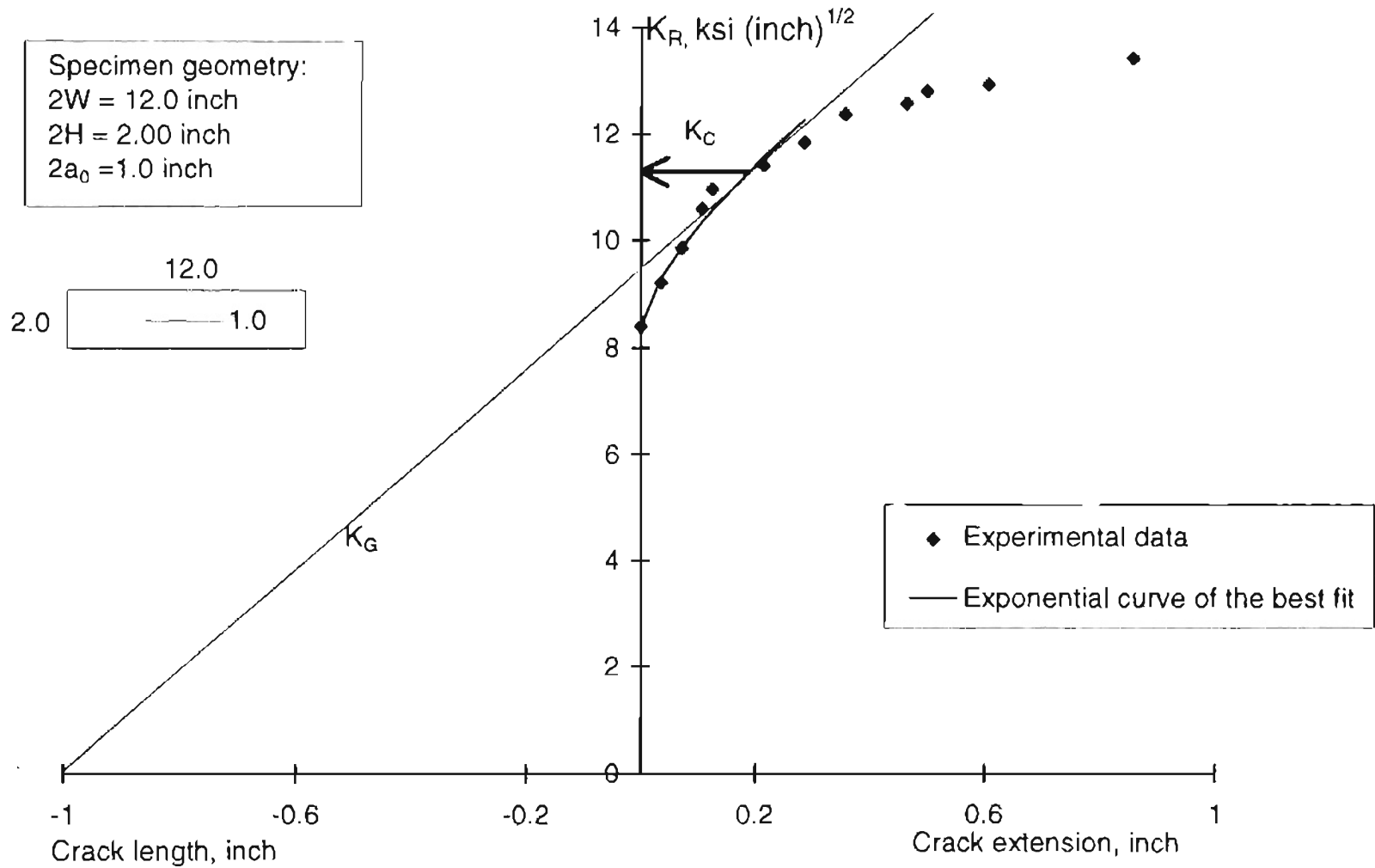
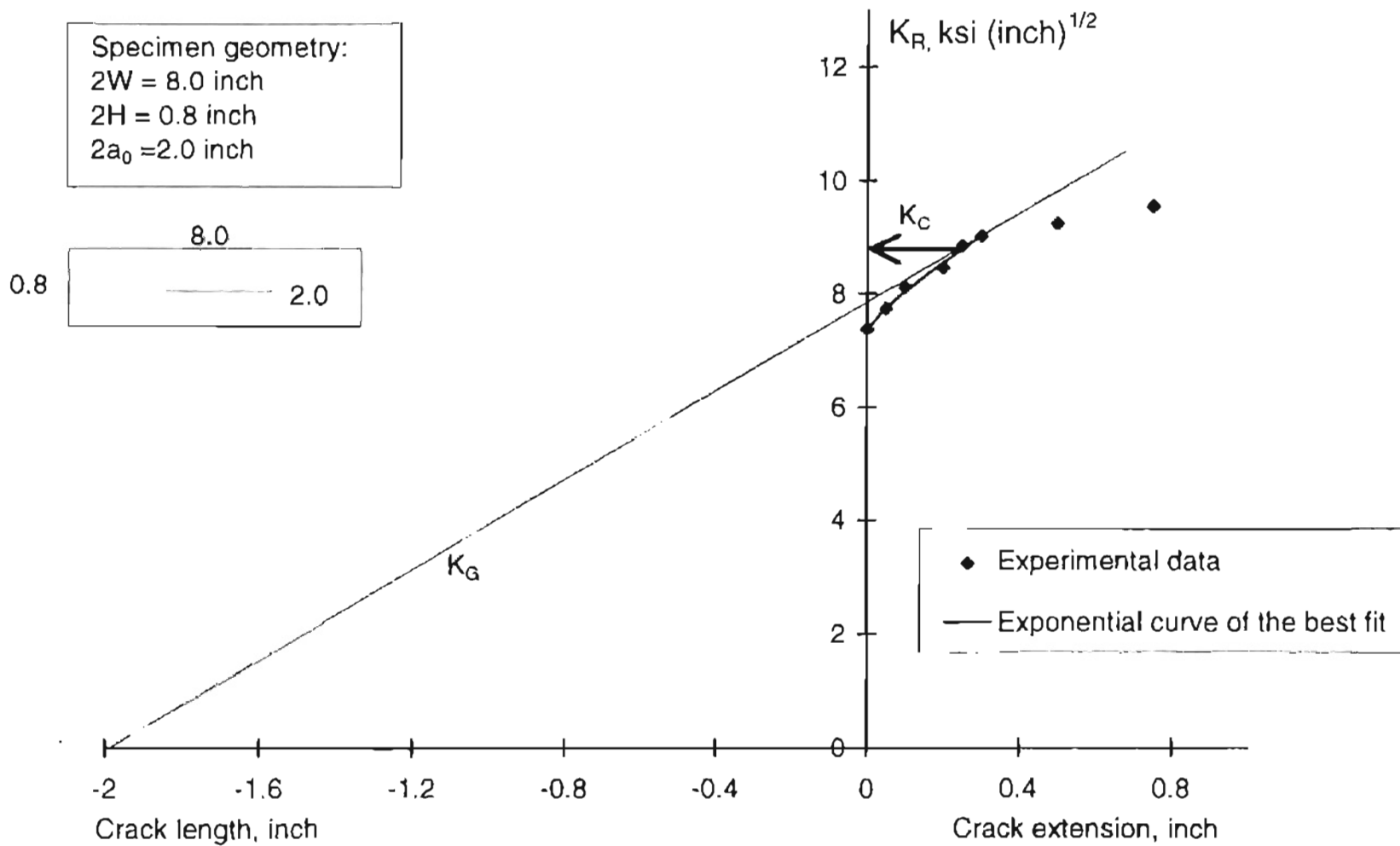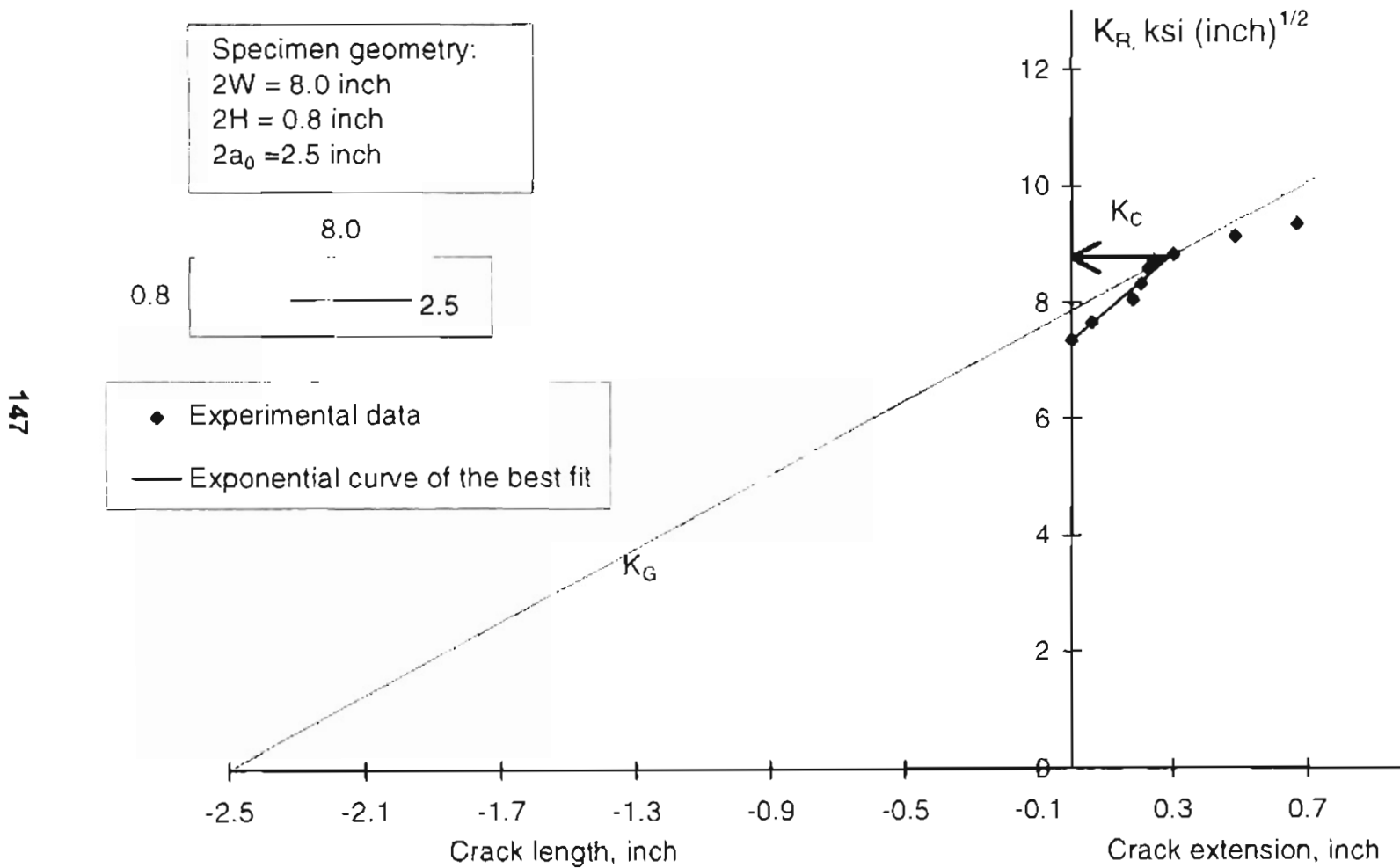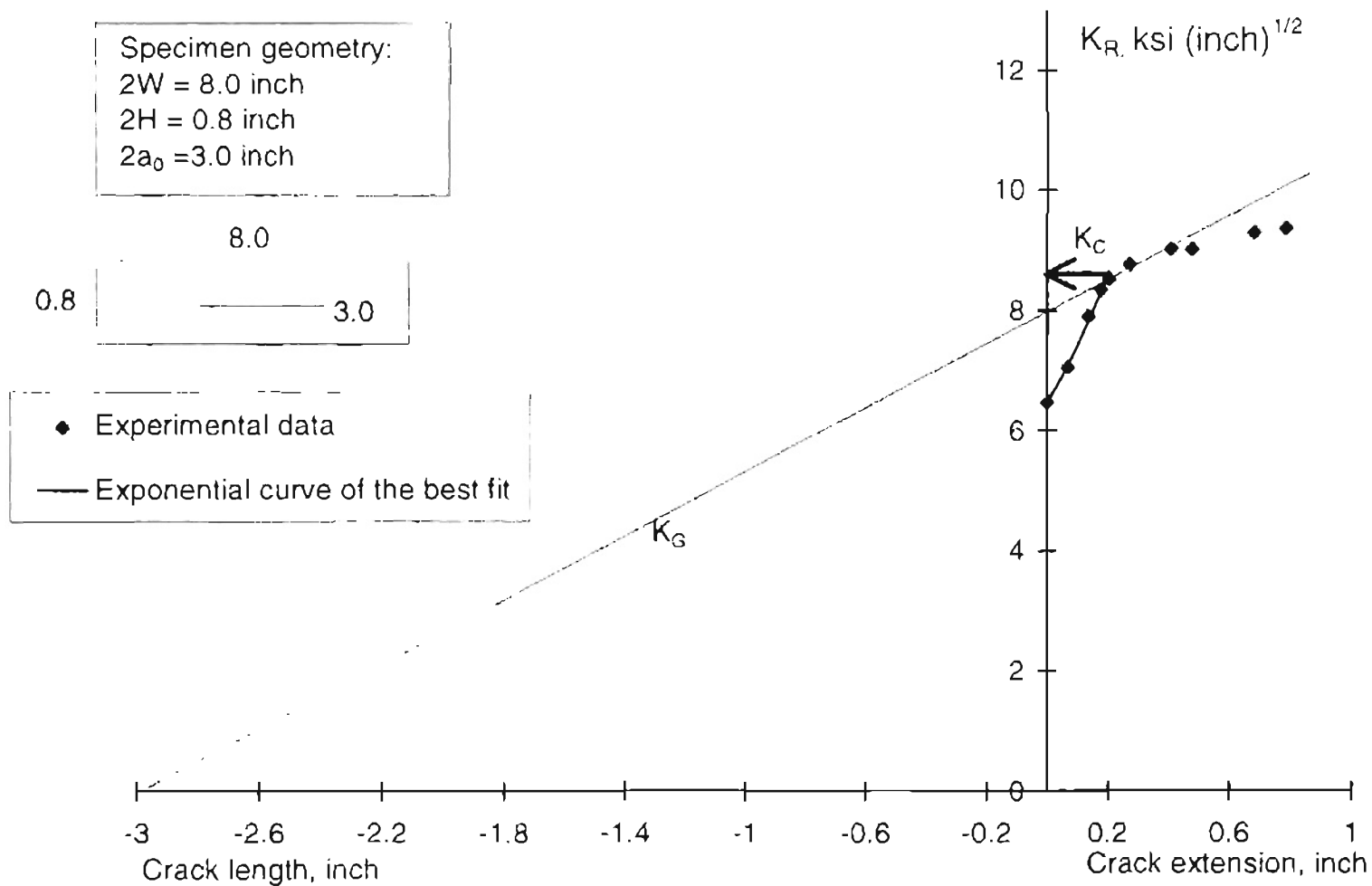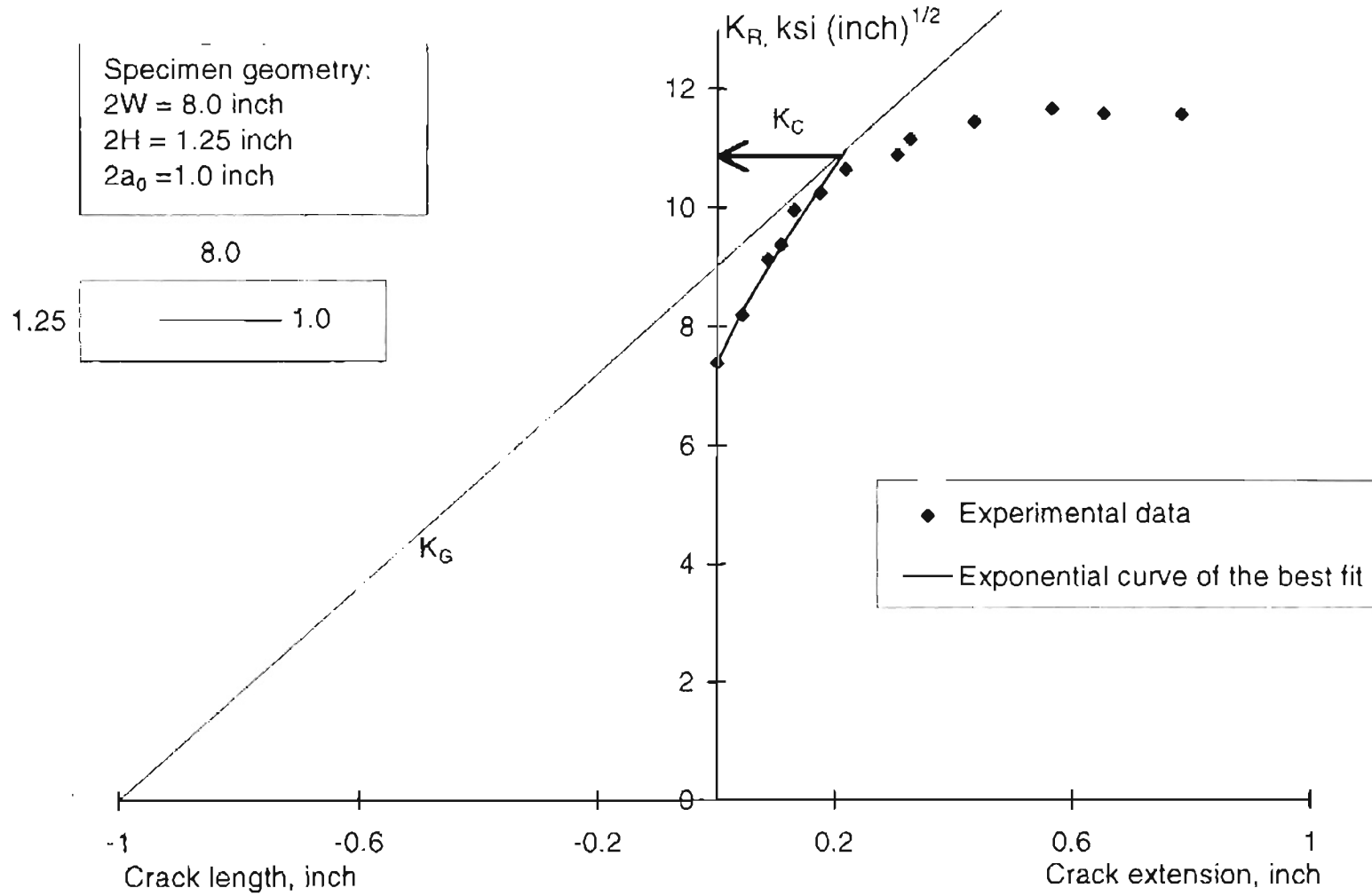Figure 4.25.2: Crack growth resistance curve for a 92 gauge polyester film specimen.

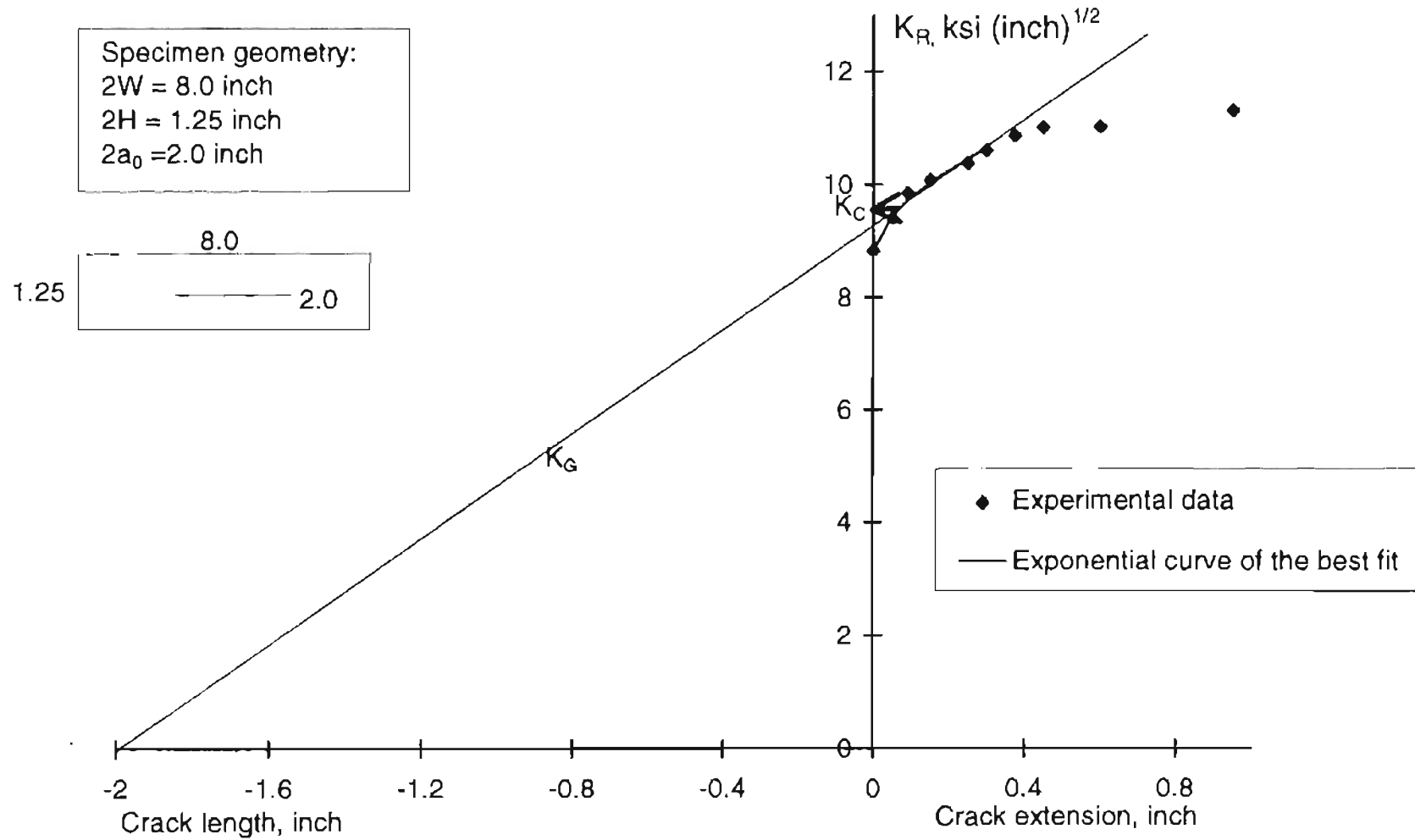Specimen geometry:
2W = 12.0 inch
2H = 2.00 inch
$2a_0$ = 1.5 inch

K_{R}, ksi $(\text{inch})^{1/2}$

K_c

K_G

Experimental data

Exponential curve of the best fit

Crack length, inch

Crack extension, inch
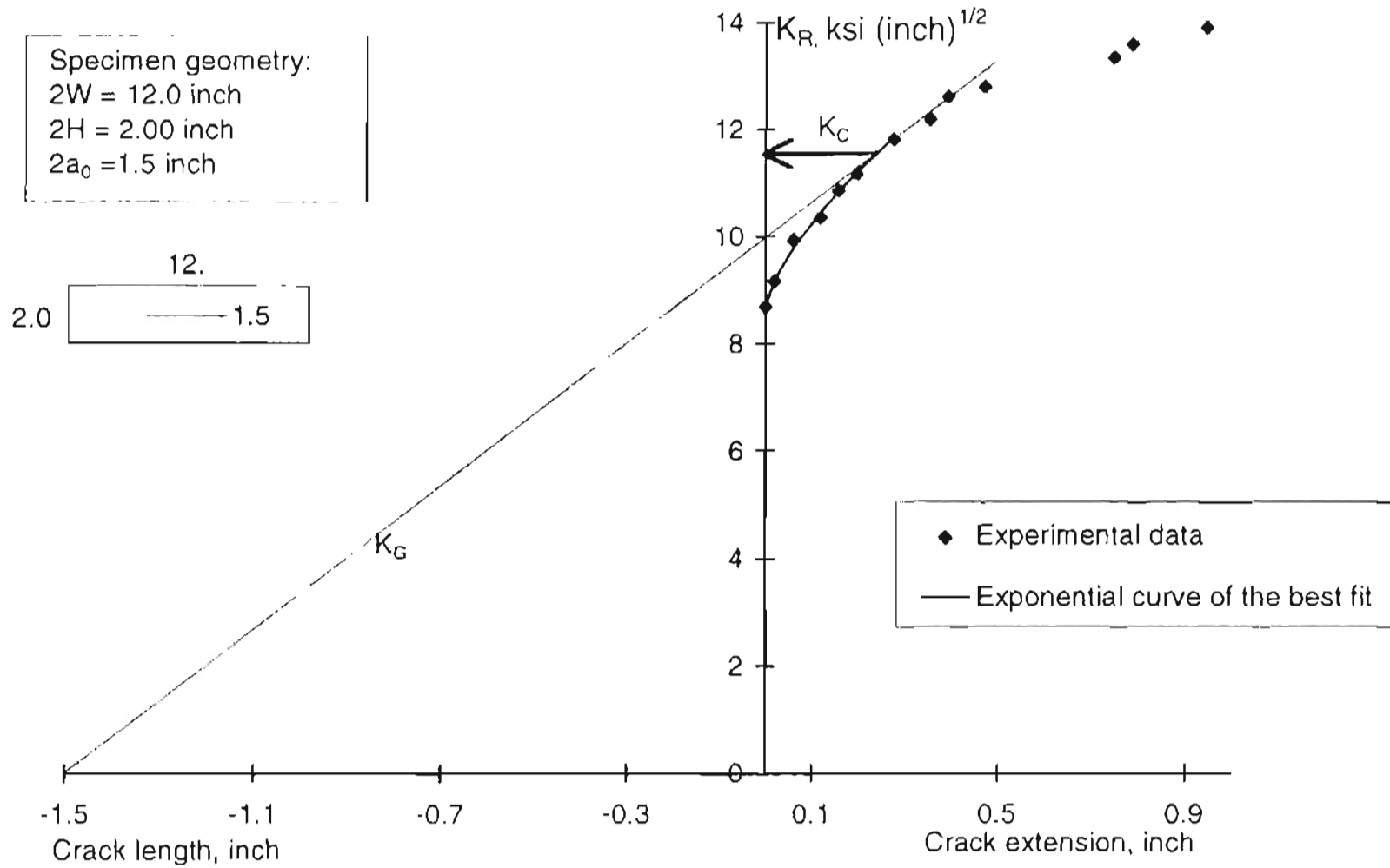
Figure 4.25.3: Crack growth resistance curve for a 92 gauge polyester film specimen.

Specimen geometry:
2W = 12.0 inch
2H = 2.0 inch
$2a_0$ = 2.0 inch

12.

2.0   2.0

K_G

K_R, ksi (inch)$^{1/2}$

14

K_C

12

10

8

6

4   ♦ Experimental data

        —— Exponential curve of the best fit

2

0

-2   -1.6   -1.2   -0.8   -0.4   0   0.4   0.8

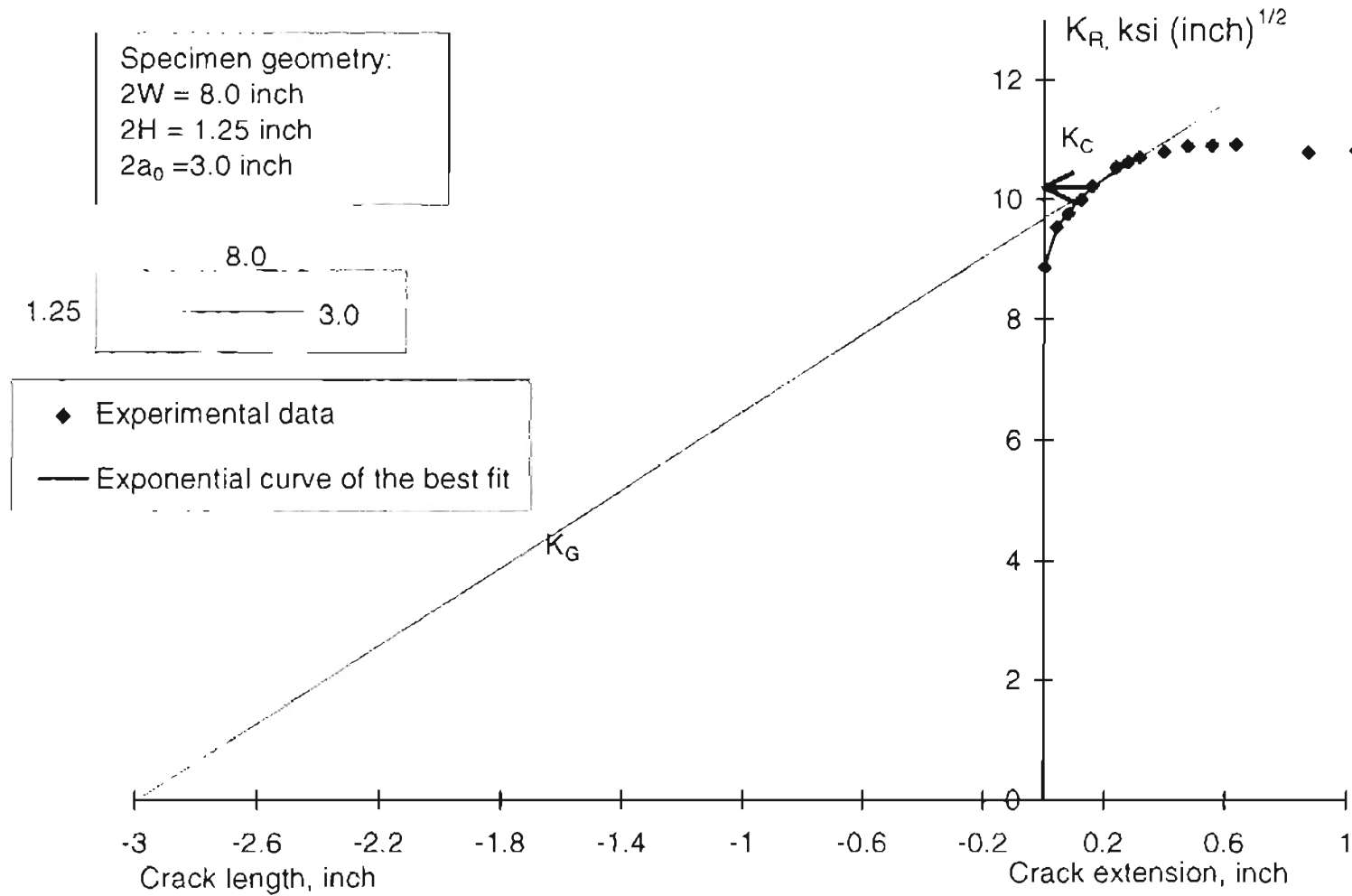Crack length, inch   Crack extension, inch

178
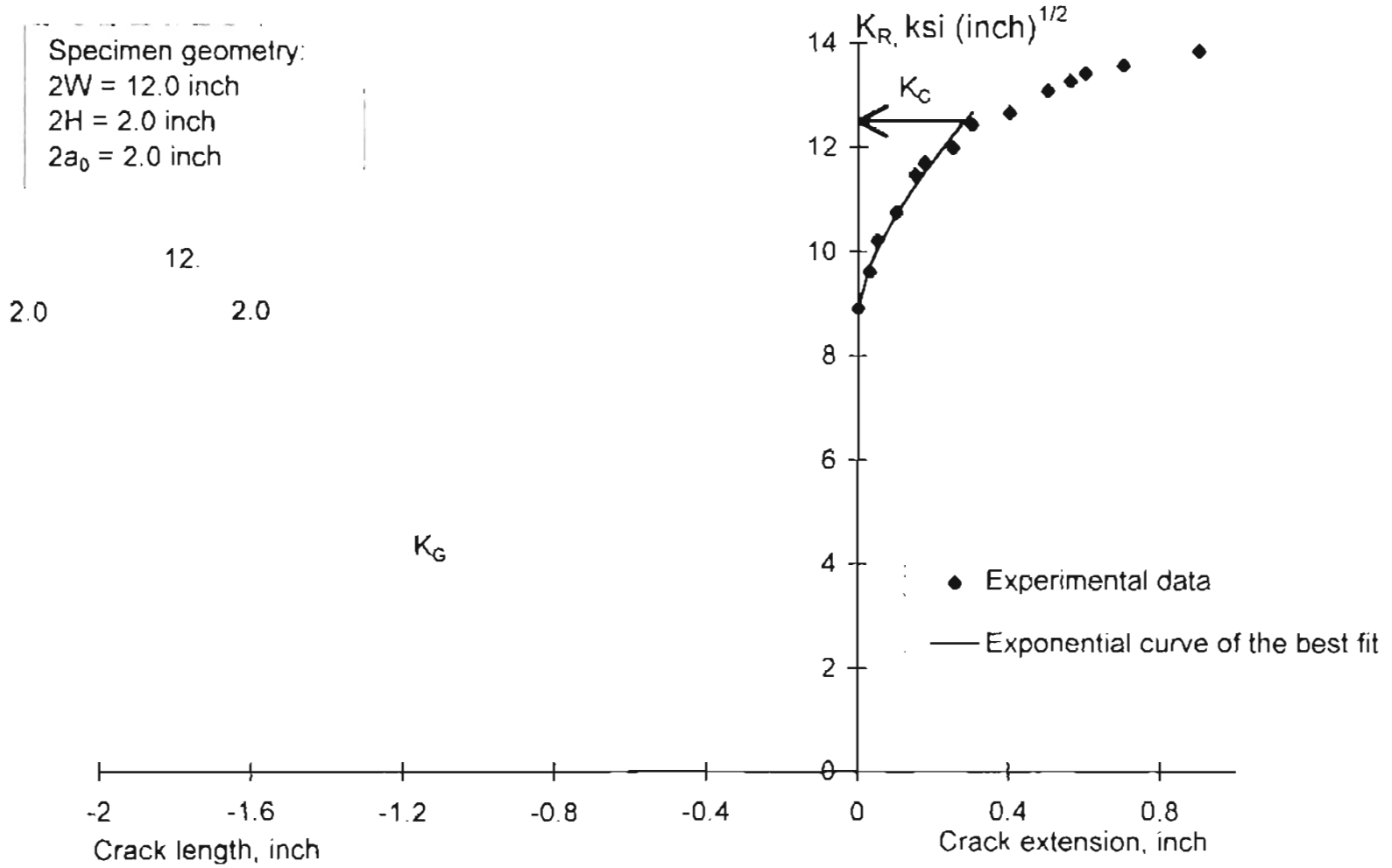
Figure 4.26: K_R-curves for test run no. 15.

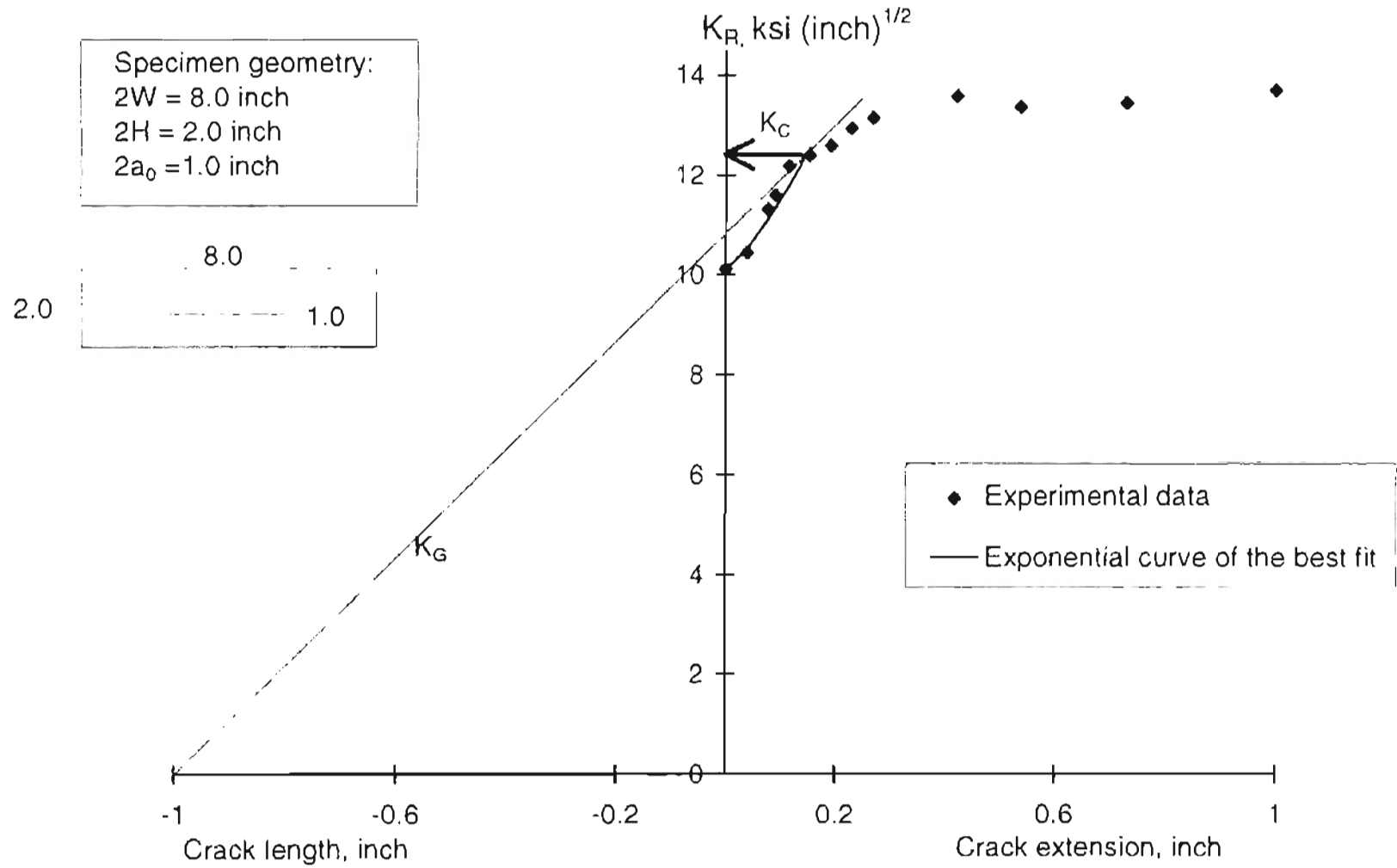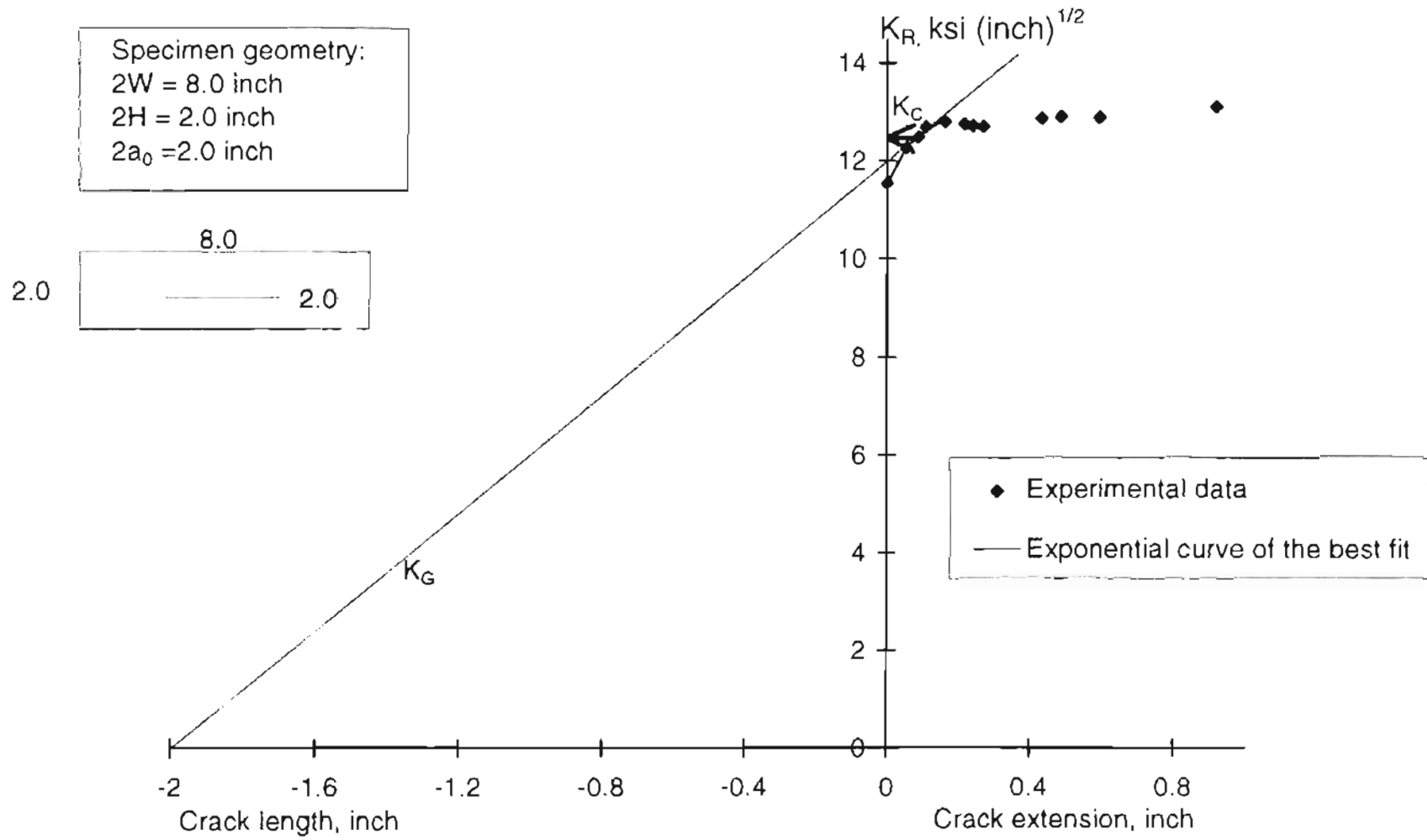Figure 4.26: Crack growth resistance curve for a 92 gauge polyester film specimen.
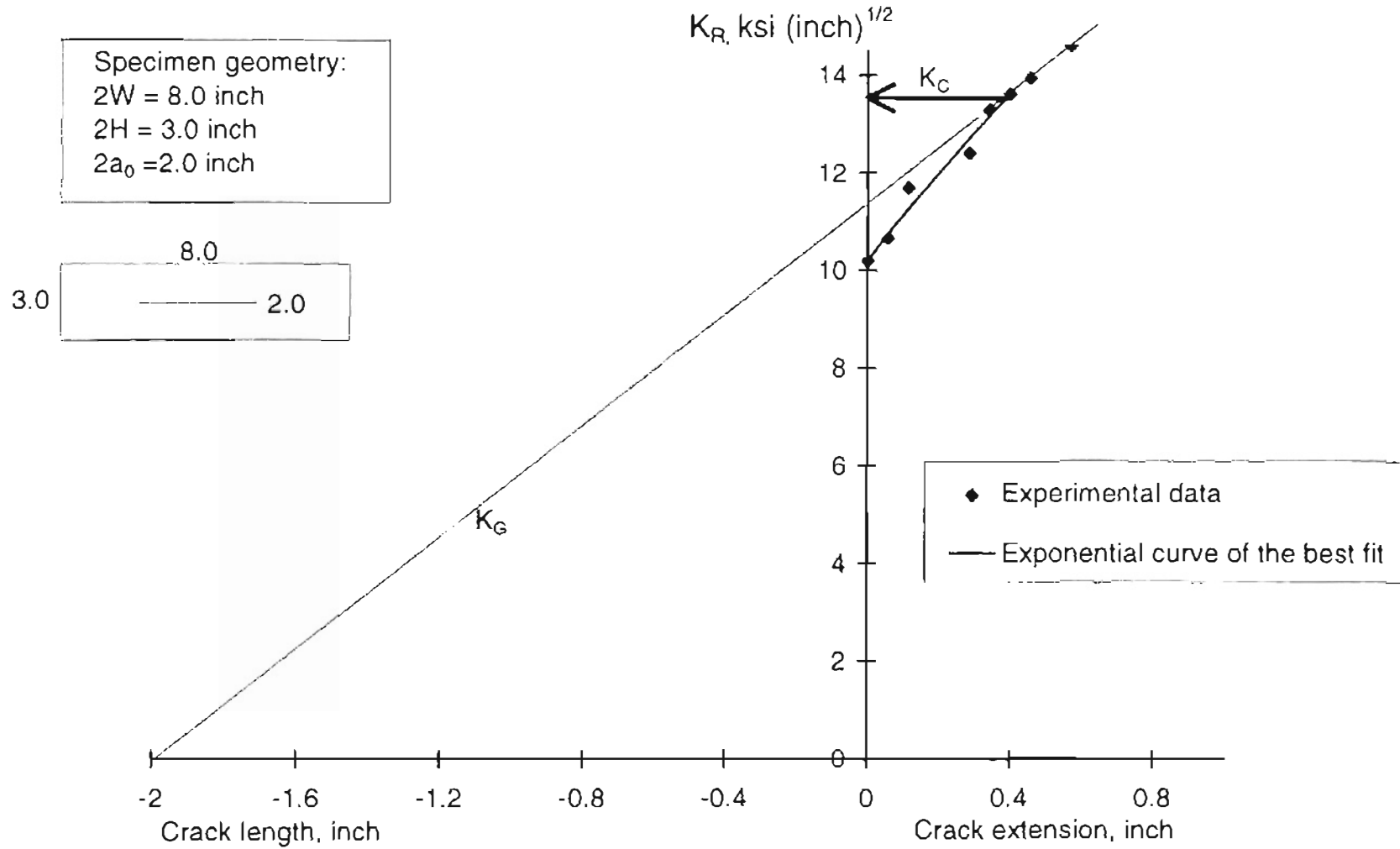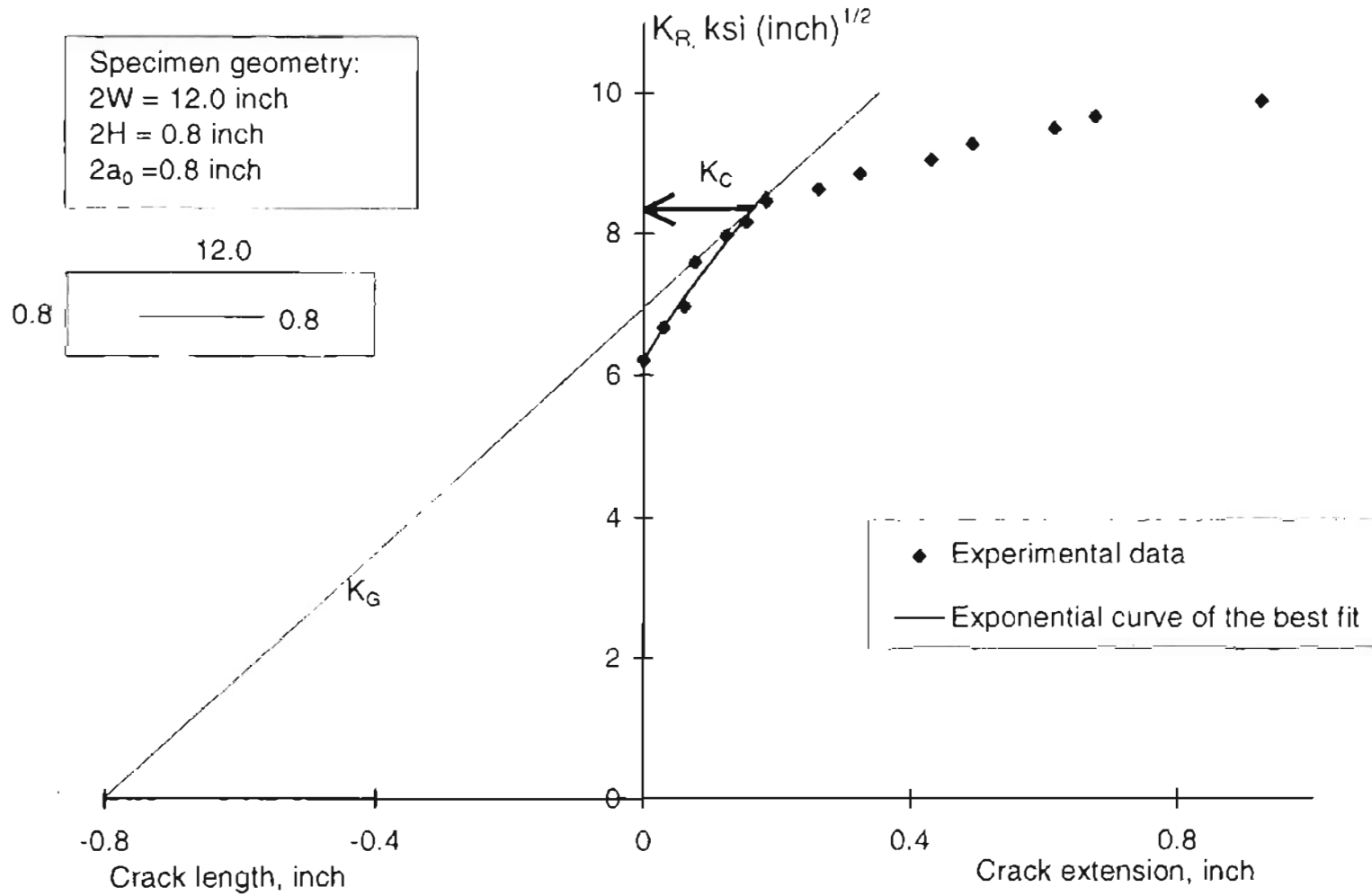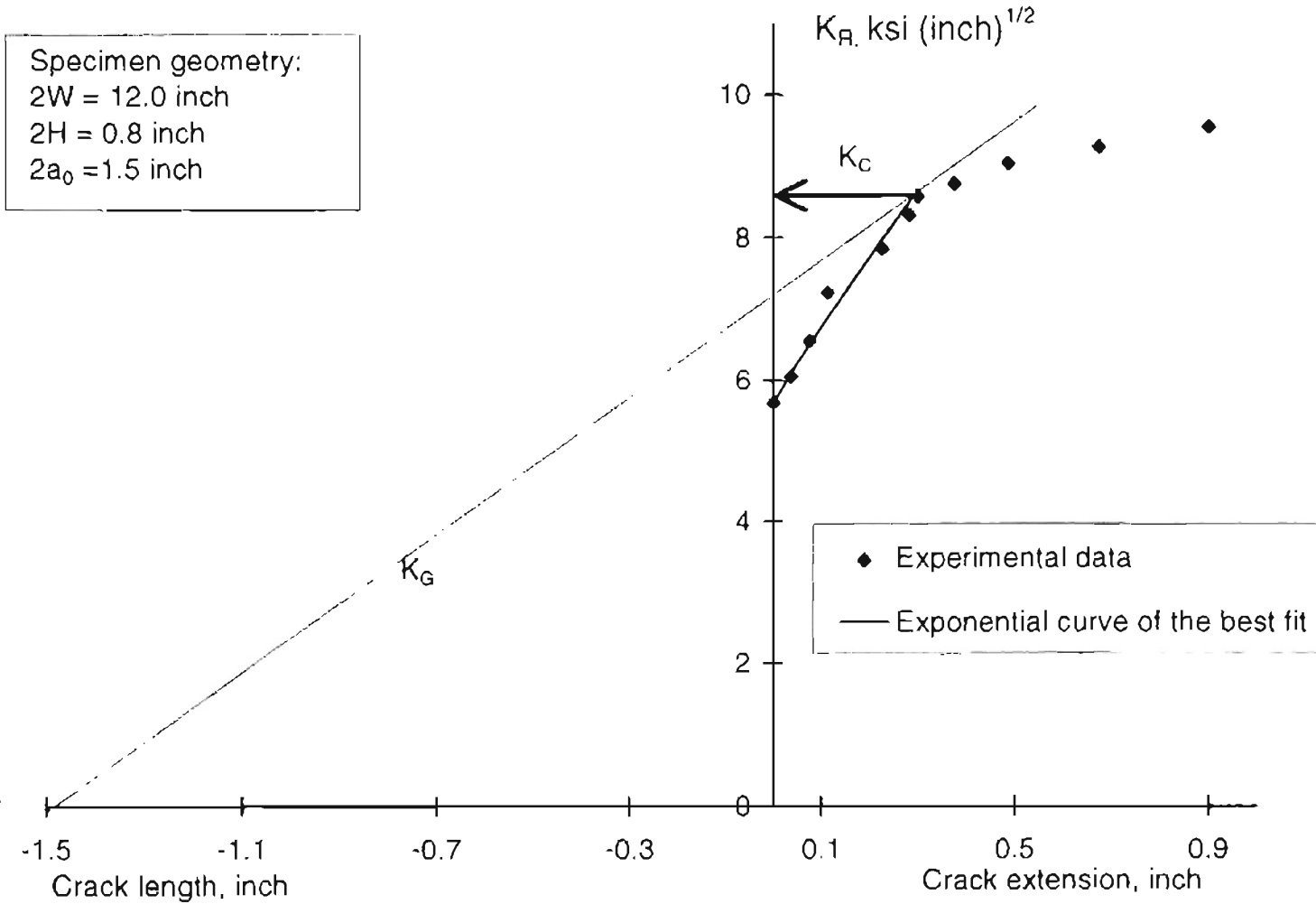
Specimen geometry:
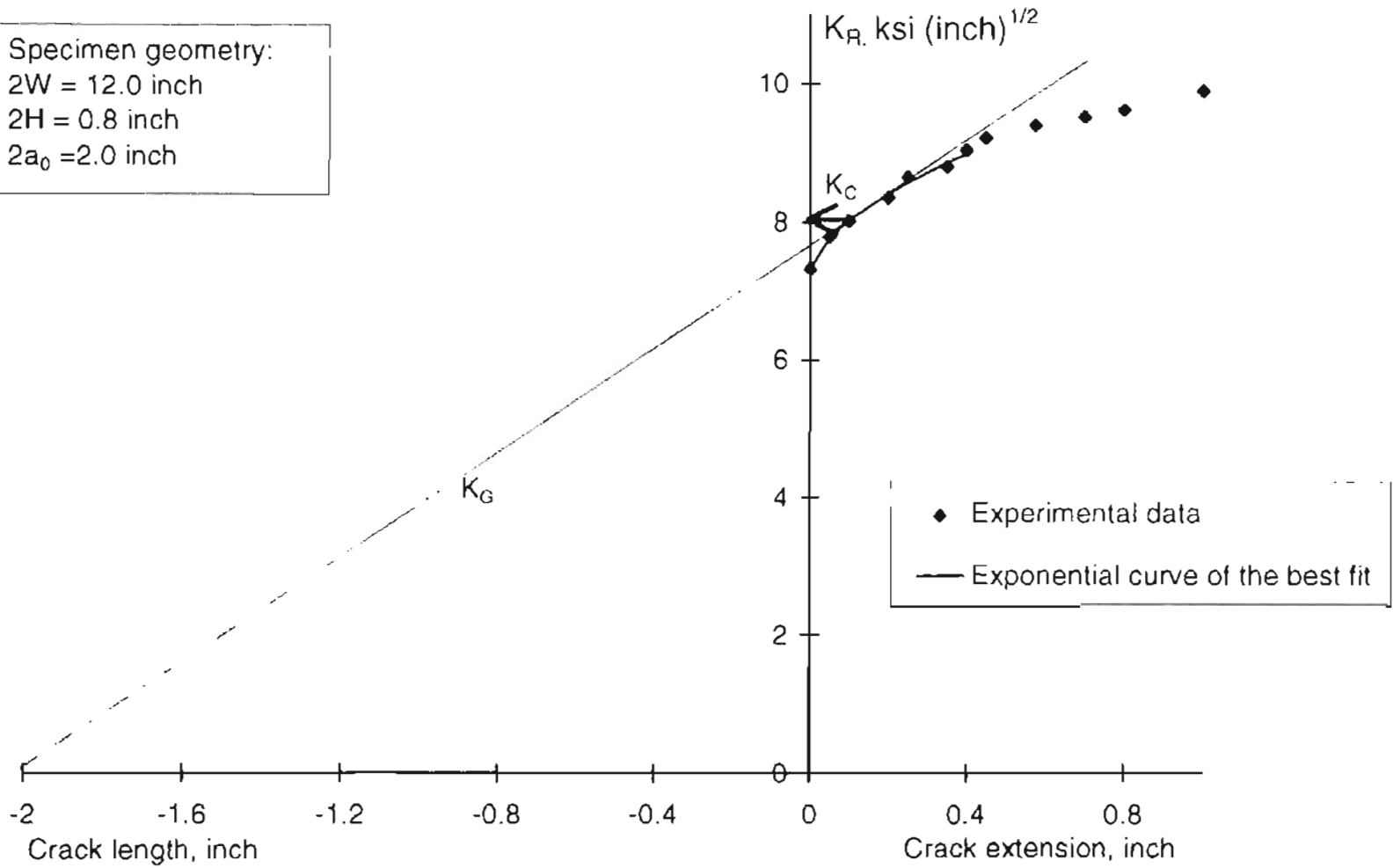$2W = 12.0$ inch
$2H = 3.0$ inch
$2a_0 = 2.0$ inch

♦ Experimental data

—— Exponential curve of the best fit

K_R, ksi $(inch)^{1/2}$

K_C

K_G

Crack length, inch

Crack extension, inch
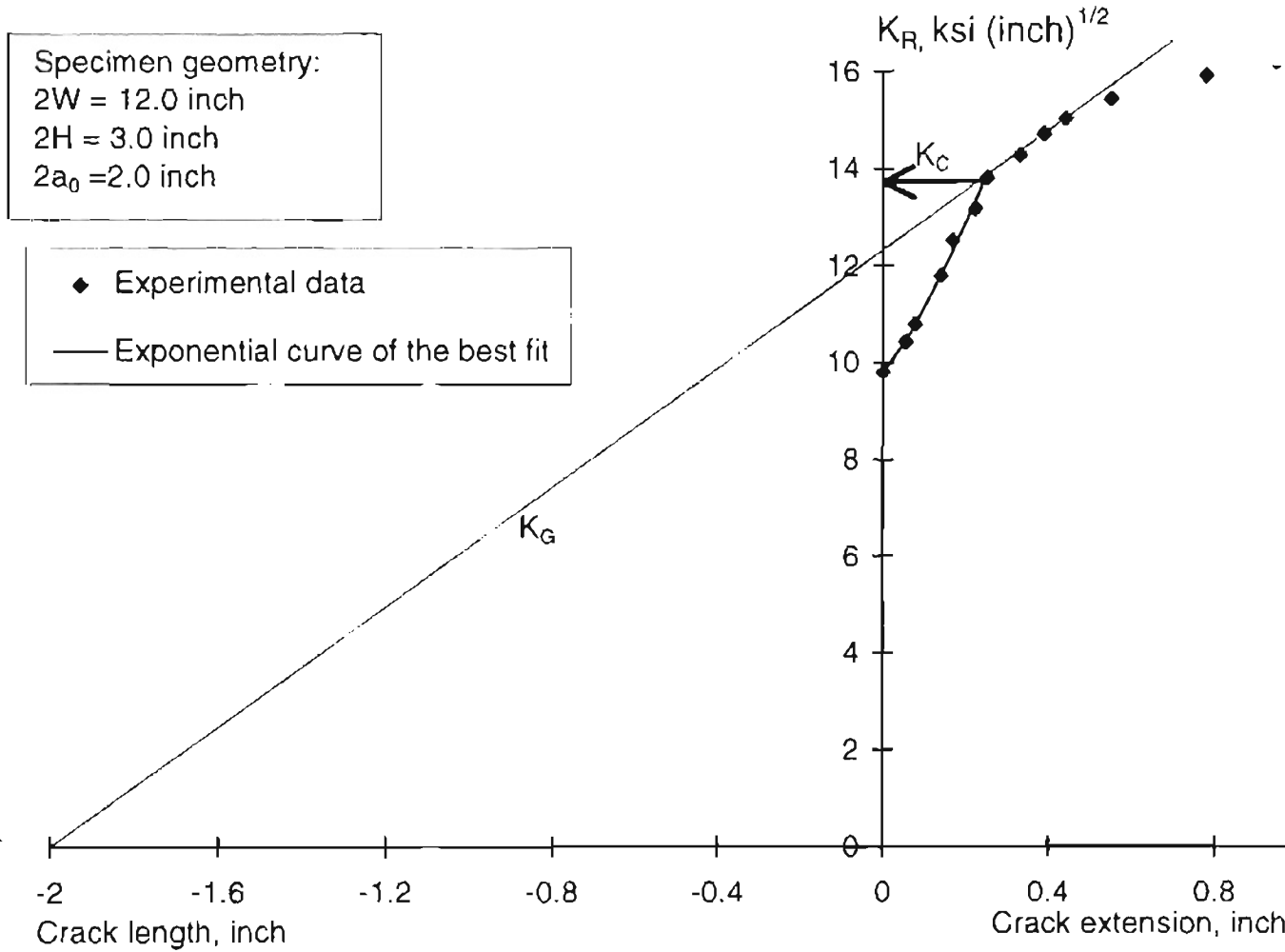
Table 4.1 lists estimated K_0, and K_C values for all the fifteen test runs. The information about the geometrical constraints in effect, is included for the better understanding of the estimates. The test runs are numbered as in Table 3.2. The thickness values, B, of the polyester films are taken as given by the manufacturer. For the standard width specimens (6 and 12 inch), no tolerances are specified here, as the width of the film roll supplied is the width of the test specimen. For non-standard width (4 and 8 inch) specimens, 2W (Column 3, Table 4.1) was measured accurately to 0.001 inch, using a precision dial caliper. The accuracy of specimen height, 2H (Column 4, Table 4.1), depends on the accuracy of the hole locations in the holding plates (Chapter 3, Figure 3.7). The hole location was determined accurately to 0.001 inch. The size and location of the crack lengths, $2a_0$ (Column 5, Table 4.1), were measured accurately to 0.01 inch using a precision dial caliper, and a metric inch scale. As detailed in Chapter 3, the use of cardboard templates aided in improving the consistency of measurements.

Determination of initiation fracture toughness, K_0

Table 4.1 lists estimated values of initiation fracture toughness, K_0. Inconsistencies in reported values, and higher estimation of the initiation fracture toughness resulted due to difficulty in the exact identification of the initial crack growth. Therefore, the lowest estimate of K_0 for a particular test run establishes the upper limit for initiation fracture toughness. Table 4.2 lists the lowest initiation fracture toughness values estimated for the test runs 1 to 15.

For a 48 gauge polyester film (Test run 2), the lowest observed value is 4.5 ksi $(inch)^{1/2}$ (4.9 MPa $(m)^{1/2}$). The spread of K_R data plots, Figures 4.14.6, 4.15.6, and 4.23.5, for the test runs 3, 4, and 12, clearly show the lowest K_R value obtainable at $\Delta a = 0$. Figures 4.14.6, 4.15.6 indicate 5.0, and 6.7 ksi $(inch)^{1/2}$ as the lowest K_0 values for a 92 gauge polyester film specimens of the test runs 3, and 4 respectively. Figure 4.23.5 give 5.9 ksi $(inch)^{1/2}$ as the lowest K_0 estimate for a 200 gauge polyester film. It appears that the initiation fracture toughness is maximum for a 200 gauge polyester film. The trend suggests an increase in the initiation fracture toughness with increasing thickness. However, the values reported here, being the upper limits, the above statement should be taken cautiously.

As discussed in Chapter 3, K_0 is independent of the specimen thickness, and has a constant value for a particular material. Therefore, the lowest value of the K_0 obtained of all the test runs, i.e. $K_O = 4.5$ ksi $(inch)^{1/2}$ (4.9 MPa $\sqrt{m}$), in general, can be considered nearest to the initiation fracture toughness value for ICI polyester films of 48, 92 and 200 gauges.

Determination of plane stress fracture toughness, K_C

A novel technique of establishing an approximate tangency point (K_G, K_R) by constructing a geometrical straight line passing through ($2a_0$, 0) and (K_G, K_R), has been used to estimate K_C values shown in Table 4.1. The range of possible variation in K_C is explained here with the help of Figures 4.15.2 and 4.22.1.

Figure 4.15.2 is a K_R-curve for a 200 gauge polyester film specimen having 2W = 6.0, 2H = 0.8, and $2a_0$ = 1.0 inch. The established (K_G, K_R)

tangency point can vary approximately between 7.2 to 7.8 ksi $(inch)^{1/2}$. The value of K_C considered in Table 4.1 is 7.4 ksi $(inch)^{1/2}$.

Figure 4.22.1 is a K_R-curve for a 92 gauge polyester film specimen having $2W = 12.0$ inch, $2H = 0.8$ inch, and $2a_0 = 0.8$ inch. The established (K_G, K_R) tangency point can vary approximately between 8.2 to 8.5 ksi $(inch)^{1/2}$. The value of K_C considered in Table 4.1 is 8.4 ksi $(inch)^{1/2}$. The ranges of variation for all the test runs are listed in Column 11 of Table 4.1.

The values listed in Table 4.1 are by no means, symmetrical with respect to the range of variation discussed here. The (K_G, K_R) tangency point for a particular curve is obtained by looking at the plot area of interest at twice the magnification of that of the shown in Figures 4.12-4.26.

Table 4.2 lists the average estimates of K_C based on two schemes. Scheme (a) is the average of K_C values obtained for those specimens only, which satisfied all the geometrical constraints considered. This include CST specimen geometry constraints as suggested by Cotterell et al. [19,20], (1) $W/H > 5$, (2) $a_0 > 0.8H$, and the crack length constraint, $2a_0 < 2w/3$, as suggested by the Feddersen approach. Scheme (b) averages Scheme (a) estimates of K_C for the specimens having same width. For Scheme (a), K_C is assumed approximately constant for the range of crack lengths included in the average estimate. For Scheme (b), the effect of W/H ratio on K_C is neglected. Table 4.2 is created to present a clear picture of the range of K_C values obtained through the CST test, which meet the geometrical constraints suggested in the literature, for valid plane stress fracture testing.

Table 4.1: K_O and K_C estimates for test runs 1 to 15.

Test run	B inch	2W inch	2H inch	$2a_0$ inch	W/H	a_0/H	Is $2a_0 < 2W/3$?	K_O ksi (inch)$^{1/2}$	K_C ksi (inch)$^{1/2}$	Range of K_C variation
1	0.00092	4.0	0.8	0.8	5	1	YES	5.4	7.3	7.2-7.6
				1.2		1.5	YES	5.0	8.2	8.0-8.2
				2.0		2.5	NO	7.0	8.3	8.3-8.6
2	0.00048	6.0	0.8	0.8	7.5	1	YES	6.1	8.6	8.6-9.0
				1.0		1.25	YES	6.5	8.4	8.0-9.0
				1.5		1.875	YES	7.2	8.6	8.5-9.5
				2.0		2.5	NO	6.67	8.8	8.8-9.5
				3.0		3.75	NO	4.53	8.6	8.5-9.0
3	0.00092	6.0	0.8	1.0	7.5	1.25	YES	7.0	8.0	7.9-8.2
				1.5		1.875	YES	5.8	8.2	8.2-8.8
				2.0		2.5	NO	5.0	8.8	8.6-9.2
				2.4		3.0	NO	6.7	8.4	8.2-8.7
				3.0		3.75	NO	7.3	8.0	7.8-8.4

Test run	B inch	2W inch	2H inch	2a₀ inch	W/H	a₀/H	Is 2a₀ < 2W/3?	K_O ksi (inch)$^{1/2}$	K_C ksi (inch)$^{1/2}$	Range of K_C variation
4	0.002	6.0	0.8	0.8	7.5	1.0	YES	5.9	6.8	6.8-7.5
				1.0		1.25	YES	6.0	7.4	7.1-7.8
				1.5		1.87	YES	6.4	8.2	8.2-8.4
				2.0		5	NO	6.0	8.6	8.5-8.7
				3.0		2.5	NO	7.0	8.4	8.2-8.5
						3.75				
5	0.00092	6.0	1.25	1.0	4.8	0.8	YES	8.0	9.2	8.5-9.5
				2.0		1.6	NO	8.7	10.0	10.0-10.2
6	0.00092	6.0	2.0	1.6	3.0	0.8	YES	11.1	11.5	11.0-12.4
				2.0		1.0	NO	9.0	12.0	12.0-12.5
7	0.00092	8.0	0.8	0.8	10	1.0	YES	5.6	7.5	7.5-8.5
				1.0		1.25	YES	--	7.2	7.2-9.0
				2.0		2.5	YES	7.2	8.6	8.6-9.0
				2.5		3.12	YES	7.2	8.6	8.4-8.6
				3.0		3.75	NO	6.3	8.5	8.2-8.7
8	0.00092	8.0	1.25	1.0	6.4	0.8	YES	7.4	10.6	10.4-10.8
				2.0		1.6	YES	8.6	9.3	9.3-10.5
				3.0		2.4	NO	8.6	10.2	10.0-10.7

186

Test run	B inch	2W inch	2H inch	$2a_0$ inch	W/H	a_0/H	Is $2a_0 < 2W/3$?	K_O ksi (inch)$^{1/2}$	K_C ksi (inch)$^{1/2}$	Range of K_C variation
9	0.00092	8.0	2.0	1.0	4.0	0.5	YES	10.0	12.4	12.4-13.0
				2.0		1.0	YES	11.7	12.4	12.2-13.0
10	0.00092	8.0	3.0	3.0	2.67	1.0	NO	10.2	13.5	13.2-14.2
11	0.00092	12	0.8	0.8	15.0	1.0	YES	6.2	8.4	8.2-8.6
				1.5		1.875	YES	5.8	8.5	8.5-8.7
				2.0		2.5	YES	7.2	8.0	7.8-8.5
				3.0		3.75	YES	7.8	8.8	8.5-9.1
				4.0		5.0	NO	7.9	8.4	8.4-9.0
12	0.00092 MD	12.0	1.25	1.0	9.6	0.8	YES	7.8	8.5	8.5-9.5
				1.5		1.2	YES	6.7	9.8	9.8-10.3
				2.0		1.6	YES	8.0	10.5	10.5-10.7
				4.0		3.2	NO	8.2	9.8	9.8-10.4
13	0.00092 CD	12.0	1.25	1.0	9.6	0.8	YES	7.2	9.0	8.8-10.2
				1.5		1.2	YES	8.2	8.6	8.4-10.0
				2.0		1.6	YES	8.8	10.1	9.8-10.5
				4.0		3.2	NO	8.5	10.2	10.0-10.5

Test run	B inch	2W inch	2H inch	$2a_0$ inch	W/H	a_0/H	Is $2a_0 < 2W/3$?	K_O ksi $(inch)^{1/2}$	K_C ksi $(inch)^{1/2}$	Range of K_C variation
14	0.00092	12.0	2.0	1.0	6.0	0.5	YES	8.2	11.0	10.5-12.0
				1.5		0.75	YES	8.4	11.5	11.0-12.0
				2.0		1.0	YES	8.8	12.4	12.4-12.5
15	0.00092	12.0	3.00	2.0	4.0	0.67	YES	9.9	13.8	13.8-14.8

Table 4.2: The lowest K_O and average K_C estimates

(a)

Test run	B inch	2W inch	2H inch	Lowest K_O ksi $(inch)^{1/2}$	Average K_C ksi $(inch)^{1/2}$
1	0.00092	4.0	0.8	5.0	7.75
2	0.00048	6.0	0.8	4.53	8.53
3	0.00092	6.0	0.8	5.0	8.1
4	0.002	6.0	0.8	5.9	7.46
7	0.00092	8.0	0.8	5.6	7.97
8	0.00092	8.0	1.25	8.4	9.95
11	0.00092	12.0	0.8	5.8	8.42
12 MD	0.00092	12.0	1.25	6.7	9.6
13 CD	0.00092	12.0	1.25	7.2	9.23
14	0.00092	12.0	2.0	8.2	12.4

Table 4.2 (contd.): Average K_C estimates based on the specimen width

(b)

	Average estimates based on the specimen width	ksi inch)$^{1/2}$
1	Average K_C for 48 gauge, 6 inch wide, ICI polyester film specimen	8.53
2	Average K_C for 92 gauge, 4 inch wide, ICI polyester film specimen	7.75
3	Average K_C for 92 gauge, 6 inch wide, ICI polyester film specimen	8.1
4	Average K_C for 92 gauge, 8 inch wide, ICI polyester film specimen	8.96
5	Average K_C for 92 gauge, 12 inch wide, ICI polyester film specimen (MD)	10.14
6	Average K_C for 92 gauge, 12 inch wide, ICI polyester film specimen (CD)	9.23
7	Average K_C for 200 gauge, 6 inch wide, ICI polyester film specimen	7.46

4.4 Geometrical effects on K_C

Effect of specimen thickness, B

The value of K_C depends on thickness, decreasing gradually to a limiting lower value of K_{IC}. The effect of sheet thickness is related to the gradual transition from plane stress to plane strain. There is no generally accepted quantitative model of the thickness effect on fracture toughness [23].

The test runs 2, 3, and 4 were made using 48, 92 and 200 gauge polyester film specimens having similar geometry. The K_C values decreases with the increasing thickness as summarized in Table 4.3. For the 200 gauge polyester film, the K_C values obtained are the lowest.

These observations agree with the general behavior discussed above, and also with the trend of decreasing K_{plat} with increasing thickness for Kapton polyimide films, as observed by Cotterell et al. [20]. Cotterell et al. [19,20] did not provide K_C values for the same.

Among the three different thickness of polyester films tested, the 200 gauge polyester film was found most convenient to utilize as test specimens. This was because of minimum web defects.

Table 4.3: K_C estimates for 48, 92, and 200 gauge polyester film specimens having similar geometry

Test run	B inch	2W inch	2H inch	$2a_0$ inch	K_C ksi (inch)$^{1/2}$	Average K_C ksi (inch)$^{1/2}$
2	0.00048	6.0	0.8	1.0	8.4	8.53
				1.5	8.6	
				2.0	8.8	
				3.0	8.6	
3	0.00092	6.0	0.8	1.0	8.0	8.1
				1.5	8.2	
				2.0	8.8	
				3.0	8.0	
4	0.002	6.0	0.8	1.0	7.4	7.46
				1.5	8.2	
				2.0	8.6	
				3.0	8.4	

Effect of specimen width, 2W

Broek [22] suggests that, the K_C depends on the specimen width, and is lower for the narrow specimens, and gradually increases to a constant value beyond a certain specimen width.

The trend of increasing K_C with the increasing width can be clearly observed in Table 4.1, and Table 4.2. For a 92 gauge polyester film specimens having $2W = 4.0$, 6.0, 8.0, and 12.0 inch, the average K_C values are 7.75, 8.1, 8.96 and 10.14 ksi $(inch)^{1/2}$ respectively, as shown in Table 4.2.

Effect of initial crack length, $2a_0$

The behavior of the K_C-$2a_0$ curve, due to moving K_R-curve, and increasing curvature of the K_G line has been discussed in Section 3.6.

The results for test runs 1, 5, 6, and 14 show an increase in K_C values with increasing initial crack lengths up to $2a_0 = 2$ inch.

The K_C values for the test run 9 are constant for the two initial crack lengths (1.0 and 2.0 inch) investigated.

The results for the test runs 3, 4, and 12 show an increase in the K_C values with the initial crack lengths up to $2a_0 = 2.0$ inch, and a slight decrease then onwards. The actual decrease may be more, as the curved K_G line tends to lower the (K_G, K_R) tangency point.

The general trend is, an increase in K_C with increasing initial crack lengths up to $2a_0 = 2.0$ inch. The minimum and maximum initial crack lengths investigated here are 0.8 and 4.0 inch respectively. The minimum size was selected based on the accuracy requirements. The maximum size was limited by

the image resolution of the camcorder used for video imaging. To record 1 inch of total crack growth for larger crack lengths ($2a_0$ = 3.0, and 4.0 inch), the high resolution obtained for shorter crack lengths ($2a_0$ = 0.8-2.5 inch) with the close up view had to be sacrificed.

The observations mentioned above agree in general, with the behavior of the K_C-$2a_0$ curve, as discussed in Section 3.6. In the literature about the CST test, the crack sizes used for testing were found less than one third of the total width of the specimen as suggested by Feddersen. However, this constraint was never examined explicitly, for polymer films. For the test results of polyester films reported here, the specimens not satisfying the Feddersen's constraint, seem to give K_C estimates well within the range described by those specimens which do meet the same (Table 4.1). It appears that the Feddersen's size constraint may be relaxed for the plane stress fracture testing of polyester films. Moreover, larger crack lengths are favored for K_R-curve testing, as the amount of stable crack growth obtainable increases with larger initial crack lengths. Initial crack lengths larger than 4.0 inch should be investigated for further developments.

Effect of W/H ratio

The effect of the W/H ratio is patterned in Table 4.4. In general, increasing the W/H ratio has a tendency to lower K_C, which is counteracted by the increasing width. The width of the specimen does not pose any constraint. The height is the limitation. Under the 'no slip' conditions established, the minimum height of the specimen investigated here is 0.8 inch. This was

193

determined by practical limitations such as an accurate location of the center crack, and the design of the grip plates and holding plates.

As seen from Table 4.1, for the narrower specimens (2W = 4 and 6 inch), W/H ≥ 4.0 gave consistent K_C estimates. The largest possible W/H ratio selected for the narrower specimen is 7.5, which is limited by the specimen height of 0.8 inch.

The smallest W/H ratio investigated is 2.67 for the test run 10 (2W = 8, and 2H = 3.0 inch). This test specimen showed visible crack buckling and the value of K_C obtained, has no significance.

For wider specimens (2W = 8.0, and 12.0 inch), W/H ratios less than 5.0 have the effect of producing higher K_C estimates (Refer to K_C values reported for the test runs 9, 10, 14, and 15 in Table 4.1). W/H ratios, near to 10, can be observed to give consistent K_C results for the wider specimens (2W = 8.0, and 12.0 inch), (Refer to K_C values reported for the test runs 7, 11, 12 and 13 in Table 4.1). For the test run 11, employing the largest W/H ratio of 15, the consistency of the K_C values reported for a 92 gauge polyester film specimen should be noted (Table 4.1). Therefore, the use of wider specimens having W/H ≥ 10, is recommended here.

Table 4.4: Effect of the W/H ratio on K_C

	W/H ratio	2W	2H	Average K_C ksi $(inch)^{1/2}$
1	2.67	8.0	3.0	13.5
2	3.0	6.0	2.0	11.5
3	4.0	8.0	2.0	12.4
		12.0	3.0	13.8
4	4.8	6.0	1.25	9.2
5	5.0	4.0	0.8	7.75
6	6.0	12.0	2.0	12.4
7	6.4	8.0	1.25	9.95
8	7.5	6.0	0.8	8.1
9	9.6 MD	12.0	1.25	9.6
	9.6 CD	12.0	1.25	9.23
10	15	12.0	0.8	8.425

Effect of specimen orientation

The test runs 12, and 13 were performed on the 92 gauge polyester film test specimens of similar geometry, in MD, and in CD (Table 4.1). Noting the range of possible variation in the K_C estimates, plane stress fracture toughness of a biaxially oriented polyester film appears to be same in MD and CD. The average estimates for the test runs 12, and 13, are $K_{C(MD)} = 9.6$ ksi (inch)$^{1/2}$ (10.5 MPa $\sqrt{m}$), and $K_{C(CD)} = 9.2$ ksi (inch)$^{1/2}$ (10.1 MPa $\sqrt{m}$), as listed in Table 4.2.

4.5 Significance of experimentally obtained K_0 and K_C values

As discussed, (1) K_C values for polyester films show considerable variation with the specimen geometry, and (2) The test specimens showing crack buckling provide incorrect estimation of K_C. The variation of K_C with the specimen width, 2W, and the W/H ratio, suggest presence of sizable plastic zone. It appears that the plastic zone is not entirely dominated by the K-field, and the size of the plastic zone cannot be assumed negligible in case of polyester films. Therefore, J-integral analysis is recommended for the improved analysis.

For engineering purposes such as the development of web defect inspection system, the initiation fracture toughness, K_0, is a more plausible predictor of web defects described by the mode-I fracture, rather than the plane stress fracture toughness, K_C. The K_0 value regards the whole material, and forms a criterion independent of the material thickness and specimen geometry. The precise estimation of K_0 would make it unnecessary to establish the

instability point, K_c, which is subjected to geometrical variations under plane stress conditions.

4.6 Some practical observations on plane stress fracture testing of metallic foils, papers, and ductile polymer films

In general, the CST specimen geometry is suitable for the plane stress fracture testing of any thin materials. The approach of analysis can be selected based on the size of the plastic zone. In what follows, practical issues mainly related with the design of the test grip fixture and optimization of the test variables such as displacement rate, introducing a sharp crack, and gripping technique are addressed.

Metallic foils

The test specimens ($2W = 8.0$, $2H = 1.25$, and $2a_0 = 5.0$ inch) made of Reynolds® Extra Heavy Duty Wrap aluminum foil were fracture tested at the displacement rate of 0.04 inch/minute. The peak load values obtained (about 38 lb.—average of 5 test runs on similar specimens) were same in MD and CD. With only six readings for the total of 2 inch of crack growth, six data points were obtained for constructing the K_R-curve. The crack growth measurements were made by a visual inspection method (i.e. by stopping the crosshead movement at the desired, and marked value of crack extension, and noting the load value). Though the method described has a low accuracy, K_c was roughly estimated as 9.0 ksi $(\text{inch})^{1/2}$.

However, the thickness dependence of K_c seems to disqualify the above mentioned value for the aluminum foil. In the manufacture of aluminum foil, the industry recognizes a thickness or gauge tolerance of plus or minus 10 percent. Therefore, a roll of Standard Reynolds Wrap aluminum foil will occasionally be as light as 0.00063 inch or as heavy as 0.00077 inch; a roll of Heavy Duty Reynolds Wrap aluminum foil will occasionally be as light as 0.0009 inch or as heavy as 0.0011 inch; and a roll of Extra Heavy duty Reynolds wrap aluminum foil will occasionally be as light as 0.00135 inch or as heavy as 0.00163 inch [51].

Aluminum foils have low elasticity, which contributes to one of the valuable packaging features of the foil —its 'deadfold' property (i.e. when it is folded, it stays put, and does not untwist or unfold) [52]. However, this 'deadfold' property proved disadvantageous for the CST test specimen preparation.

Though aluminum foil test specimens behave well under the CST test conditions, the total of 20 % of variation in the thickness makes them unsuitable for the determination of plane stress fracture toughness.

Precision metal shim stocks are manufactured to much less variation (2%) in the thickness. Attempts were made to test aluminum shim stock (B = 0.001, 2W = 6.0, 2H = 0.8, and $2a_0$ = 1.0 inch), and brass shim stock specimens (B = 0.001, 2W = 12.0, 2H = 1.25, and $2a_0$ = 1.0 inch). Difficulties in introducing a sharp crack, and the sudden onset of instability made these attempts unsuccessful. Instead of the razor slicing technique used, which damaged the crack edges, the die pressing technique should be investigated for introducing sharper initial cracks [10,11]. The sudden onset of instability may be explained

198

by the increase in critical stress caused by the bluntness of the crack (Figure 3.17). Fracture testing of shim stock materials also calls for the improvement in the CST test grip fixture to minimize the handling abuse.

Papers

Paper specimens prepared from the copier paper, and wax paper sheets as supplied, and not prepared according to the requirements of the standard test method [2] were examined for the plane stress fracture testing. Paper materials are easy to cut and mark, which aid the specimen preparation. The testing was done at room temperature (23°C). Though the displacement rate of 1 mm/minute (0.04 inch/minute) employed was lower than those reported in similar fracture studies (3 to 5 mm/minute), these attempts went completely unsuccessful. Stable crack growth could not be attained. The paper specimens fractured at random locations such as inside the grip plates, and near the edges. Those which did not show abnormal behavior, fractured suddenly and completely, making it impossible to record crack growth. Fracture testing of paper materials calls for the improvement in overall control of the test conditions as discussed in Section 2.4.

Ductile polymer films

Test specimens (2W = 6.0, 2H = 1.25, 2.0, and $2a_0$ = 1.0 inch) made of polyethylene films were fracture tested successfully at the displacement rates of 0.2, 0.1, 0.05, and 0.04 inch/minute. Considerable crack blunting was observed. This seems to put further limitations on the specimen height, and the range of

initial crack lengths, for the CST testing of ductile polymer films. No other

reportable measurements were made.

CHAPTER 5

CONCLUSIONS

The conclusions from this study are as follows:

1. The CST test specimen geometry eliminates buckling problems without the use of anti-buckling plates.

2. The peak load values for polyester film specimens are approximately 120-150% of the crack initiation load values.

3. It was difficult to identify the instant of initial crack growth. This resulted in higher estimates of initiation fracture toughness, K_0. Therefore, the lowest value of K_0 observed on the K_R-curve for a particular test specimen, has been established as the upper limit.

4. K_0 values obtained for polyester films show an increase with the increase in film thickness (B). The upper limits of K_0 obtained for 48, 92 and 200 gauge polyester film specimens, are 4.5, 5.0, and 5.9 ksi $(\text{inch})^{1/2}$ respectively.

5. If K_0 is considered independent of the specimen thickness, and having a constant value for a particular material, the lowest observed value, $K_0 = 4.5$ ksi $(\text{inch})^{1/2}$, can be reported as the nearest to the initiation fracture toughness of the polyester film.

6. K_C for polyester film specimens, decreases with increasing film thickness (B).

7. K_C increases with increasing the specimen width (2W).

8. Feddersen's initial crack length constraint $2a_0 < 2W/3$, can be relaxed for the plane stress fracture testing of polyester films. Consistent K_C values have

been obtained with the initial crack lengths of half the size of the specimen width.

9. The change in the K_C values observed by increasing the initial crack lengths, agrees with the general behavior of the K_C-$2a_0$ curve. The general trend is, an increase in K_C with increasing initial crack lengths up to $2a_0 = 2.0$ inch.

10. Increasing the W/H ratio has a tendency to lower K_C. Narrower specimens (2W = 4.0 and 6.0 inch) give consistent K_C values with W/H $\geq$ 4 For wider specimens (2W = 8.0 and 12.0 inch), W/H < 5 have the effect of producing higher K_C value for a particular test specimen. For consistent K_C results, wider specimens having W/H $\geq$ 10, are recommended.

11. For the CST test geometry, the specimen height (2H) is the size limitation.

12. Biaxially oriented 92 gauge polyester film has nearly same K_C in MD and CD.

13. For polyester films tested, it appears that the plastic zone is not completely dominated by the K-field, and the size of the plastic zone cannot be assumed negligible. Therefore, J-integral methods are suggested for the improved analysis.

14. For engineering purposes, the initiation fracture toughness, K_0, is a more plausible predictor of web defects described by the mode-I fracture, rather than the plane stress fracture toughness, K_C.

CHAPTER 6

FURTHER WORK

The focus of the further work should be towards the development of the standard test method for the plane stress fracture testing of very thin materials. The CST test method discussed here, is promising. The scope and limitations of this test, should be probed further using the very best in fracture testing technology. The ideas presented here, is an attempt to put the existing status of the research in perspective.

Scope of the CST test

The CST test geometry is suitable for measurements of the plane stress fracture toughness, K_c, and the crack growth resistance (as attempted here), fatigue, or time dependent fracture. Cotterell et al. [19] favors the use of the CST specimen geometry particularly for fatigue of time-dependent studies, because the stress intensity is constant, and independent of the crack length, if displacement control is used.

Upgrade the fracture testing apparatus

To better the accuracy of the basic measurements, and to expand the investigation possibilities, the fracture testing apparatus developed for this work, should be upgraded. The design of the CST test grip fixture should be further modified to increase the ease of the specimen preparation. Quick connect-disconnect features should be developed to reduce the time of specimen

preparation. Instead of using bolts for applying the grip pressure, spring controlled, or pneumatic arrangement could give better control, eliminate 'walking' of the grip plates, reduce the time for specimen preparation, and in general, improve the test performance. Use of dedicated instrumentation for such fracture studies, has already been reported [5]. High resolution camera, and carefully arranged illumination conditions, can give accurate crack growth data. The author recommends using a horizontal tensile testing arrangement over a conventional vertical testing arrangement for two reasons. First, the horizontal testing scheme increases the material tester's overall control over the test conditions, including the specimen preparation, and therefore, improves the overall test accuracy. Second, this is more convenient for the microscopic examinations of the crack growth behavior.

For anisotropic sheet materials, such as polymer films and paper materials, biaxial stress tests approximate real loading well. Reference [49] describes an attempt to develop a biaxial tensile testing machine and a non-disturbing displacement method. Such a development can be researched. Use of novel techniques, such as IT (infra red thermography) can be investigated for plane stress fracture testing of very thin materials such as papers, and polymer films, as discussed in Chapter 2.

Test various thin materials

This work examined the applicability of the CST test to polyester film specimens using LEFM. Repeatability, and limitations of the results presented here, should be further investigated. The next logical step is to apply the same

test methodology for ductile polymer films. Papers, and metallic foils, can also be fracture tested by improving the test performance (Section 3.5).

Improve analysis tools

The CST specimen geometry is suitable for the plane stress fracture testing of any thin materials. The analysis approach depends on the size of the plastic zone described by the particular material. J-integral analysis has been successfully employed by Tielking for polyethylene films [21] (Chapter 2, and 3). Fracture testing of ductile polymer films using J-integral analysis can be investigated. Test results obtained through CST geometry can be compared with those obtained by the popular EWF approach for DENT specimen geometry.

The constraints and the expression for K_R values were developed using finite element analysis [19,20]. An expression for the crack driving force K_G, can be developed to verify the approximate establishment of the tangency point (K_G, K_R) attempted for this work.

Investigate the dominant effects on fracture toughness measurements such as moisture, temperature, strain rate, and viscoelasticity

Various dominant effects on the fracture toughness measurements, listed above, and others, can be studied. This work discusses the short time crack growth resistance. Time dependent fracture of the polymer films demands considerable research effort.

REFERENCES

1   ASTM standard (1)E 399-90: Test methods for plane-strain fracture toughness of metallic materials, Vol. 3.01, and (2) D 5045-93: Test methods for plane-strain fracture toughness and strain energy release rate of plastic materials, Vol. 8.03. ASTM annual book of standards, ASTM, Philadelphia, PA, 1995.

2   (1) T 402 om-93: Standard conditioning and testing atmosphere for paper, board, pulp handsheets, and related products, and (2)T 414 om-88: Internal tearing resistance of paper (Elmendorf type method), TAPPI test methods 1994-95, TAPPI press, Atlanta, GA, 1994.

3   ASTM standard D 1004-94a: Initial tear resistance of plastic film and sheeting, and (2) D 1922-94a: Standard test method for propagation tear resistance of plastic films and thin sheeting by pendulum method, Vol. 8.01, ASTM annual book of standards, ASTM, Philadelphia, PA, 1995.

4   Briston, J.H., and Katan, L.L., "Plastics films," John Wiley & Sons, NY, 1974, Chapter 8 & 9.

5   Klemann, B.M., and DeVilbiss, T., "The fracture toughness of thin polymeric films," Polymer engineering and science, Vol. 36, No. 1, 1996, pp. 126-134.

6   Smith, R.D., "Roll and web defect terminology," TAPPI press, Atlanta, GA, 1995.

7   Ainsworth, J. H., "Paper the fifth wonder," Thomas printing and publishing Co., Ltd., 3rd revision, Library edition, 1967.

8   Biermann, C.B., "Essentials of pulping and paper making," Academic press, Inc., 1993, Chapter 7, pp. 158-189.

9   Bichard, D.W., "Physical testing: A fresh look at old habits," TAPPI journal, Vol. 79, No. 10, 1996, pp. 199-202.

10 Seth, R.S., Robertson, A.G., Mai, Y.W., and Hoffmen, J.D., "Plane stress fracture toughness of paper," TAPPI journal, Vol. 76, No. 2, 1993, pp. 109-116.

11   Seth, R.S., "Measurement of in-plane fracture toughness of paper," <u>TAPPI journal</u>, Vol. 78, No. 10, 1995, pp. 177-183.

12   Seth, R.S., "Optimizing reinforcement pulps by fracture toughness," <u>TAPPI journal</u>, Vol. 79, No. 1, 1996, pp. 170-178.

13   Page, D.H., and Seth, R.S., "The problem of pressroom runnability," <u>TAPPI Journal</u>, Vol.65, No. 8, 1982, pp. 92-95.

14   Moilanen, P., and Linqdvist, U., "Web defect inspection in the printing press research under the Finnish technology program," <u>TAPPI journal</u>, Vol. 79, No. 9, 1996, pp. 88-94.

15   Popelar, S.F., Popelar, C.H., and Kener, V.H., "Time dependent fracture of polyimide films," <u>Journal of electronic packaging</u>, Vol. 115, September 1995, pp. 264-269.

16   Hinkley, J.A., and Mings, S.L., "Fracture toughness of polyimide films," <u>Polymer</u>, Vol. 31, 1990, pp. 75-77.

17   Kilwon, Cho, Lee, Daeho, and Lee, M.S., "Fracture behavior of thin polyimide films," <u>Polymer</u>, Vol. 38, No. 7, 1997, pp. 1615-1623.

18   Han, Patricia, "<u>Tensile testing</u>," ASM publication, OH, 1993.

19   Cotterell, B., Sim, M.C., Amruthraj G. and Teoh, S.H., "A fracture test method for mode I fracture of thin metal materials," <u>Journal of testing and evaluation</u>, Vol. 24, No. 5, 1996, pp. 316-319.

20   Cottrell, B., Sim, M.C., Amruthraj, G., and Teoh, S.H., "The crack growth resistance of polyimide film," <u>Journal of materials science</u>, Vol. 31, 1996, pp. 291-295.

21   Tielking, J.T., "A fracture toughness test for polymer film," <u>Polymer testing</u>, Vol. 12, 1993, pp. 207-220.

22   Broek D., "<u>Elementary engineering fracture mechanics</u>," 4th edition, Martinus Nijhoff publishers, Dordrecht, Netherlands, 1986.

23   Ewalds, H.L., and Wanhill, R.J.H., "<u>Fracture mechanics</u>", Edward Arnold publishers, 1984.

24   Dixon, J.R., and Strannigan J.S., "Stress distribution in thin sheets with central slits," <u>Fracture</u>, 1969, pp. 105-108.

25   "Permeability and other film properties of plastics and elastomers," Plastics Design Library, NY, 1995.

26   Tada, H., Paris, P.C., and Irwin, G.R., "The stress analysis of cracks handbook," Del Research Corporation, Hellertown, PA, 1973.

27   Rice, J.R., "A path independent integral and the approximate analysis of strain concentration by notches and cracks," Journal of applied mechanics, Vol. 35, 1968, pp. 379-386.

28   Begley, J.A., and Landis, J.D., "The J-integral as a fracture criterion," Fracture toughness, ASTM STP 514, 1972, pp. 1-23.

29   ASTM standards (1) E 813-89: J_{ic}, a measure of fracture toughness and (2) E 1152-87: J-R curves determination, Vol. 3.01, ASTM annual book of standards, ASTM, Philadelphia, PA, 1995.

30   Cotterell, B., Mai, Y.W., Horluck, R. and Vigna, G., "The essential work of plane stress ductile fracture of linear polyethylenes," Polymer engineering & science, Vol. 27, No. 11, 1987, pp. 804-809.

31   Levita, G., Parisi, L., Marchetti, A., and Bartomelmmei, L., "Effect of thickness on the specific essential work of fracture of rigid PVC," Polymer engineering & science, Vol. 36, No. 20, 1996, pp. 2534-2541.

32   Karger-Kocsis, J., and Cziigang, T., "On the essential and non-essential work of fracture of biaxial-oriented filled PET film," Polymer, Vol. 37, No. 12, 1996, pp. 2433-38.

33   Hashemi, S., "Fracture toughness evaluation of ductile polymeric films," Journal of materials science, Vol. 32, No. 6, 1997, pp. 1563-1573.

34   Broberg, K. B., "Critical review of some theories in fracture mechanics," International Journal of Fracture Mechanics, Vol. 4, 1968, pp. 11-19.

35   Broberg, K.B., "On stable crack growth," Journal of the Mechanics and Physics of Solids, Vol. 23, 1975, pp. 215-237.

36   Cotterell, B., and Redell, J.K., "The essential work of plane stress ductile fracture," International journal of fracture, Vol. 13, 1977, pp. 267-277.

37   Mai, Y.W., and Cotterell, B., "Effect of specimen geometry on the essential work of plane stress ductile fracture," Engineering fracture mechanics, Vol. 21, No. 1, 1985, pp. 123-128.

38   Reynolds, A.P., "Comparison of R-curve methodologies for ranking the toughness of aluminum alloys," Journal of testing & evaluation, Vol. 24, No. 6, 1996, pp. 406-410.

39   Haynes, N.J., and Gangloff, R.P., "High resolution R-curve characterization of the fracture toughness of thin sheet aluminum alloys," Journal of testing & evaluation, Vol. 25, No. 1, 1997, pp. 82-98.

40   Marks, R.E., and Murakami Koji, "Handbook of physical and mechanical testing of paper and paperboard," Vol. 1, Marcel Dekker, INC., New York, NY, 1983, Chapter 4.

41   Seth, R.S., Barbe, M.C., Williams, J.C.R., and Page, D.H., "The strength of wet webs: a new approach," TAPPI journal, Vol. 65, No. 8, 1982, pp. 92-95.

42   Swienhart, D.E., and Broek, D., "Tenacity, fracture mechanics, and unknown coater web breaks," TAPPI journal, Vol. 79, No. 2, 1996, pp. 233-237.

43   Tanaka, A., Otsuka, Y., and Yamauchi, T., "In-plane fracture toughness testing using thermography," TAPPI journal, Vol. 88, No. 7, 1997, pp. 222-226.

44   Hertzberg, R.W., "Deformation and fracture mechanics of engineering materials," John Wiley & Sons, Inc., 1996, Chapter 6.

45   Klemann, B.M., Devilbiss, T., and Koutsky, J.A., "Fracture toughness and mechanical properties of Poly(n-Pentyl-n-Alkylsilanes)," Polymer engineering and science, Vol. 36, No. 1, 1996 pp. 135-145.

46   Hashemi, S., and Williams, J.G., "A fracture toughness study on low density and linear low density polyethylenes," Polymer, Vol. 27, March 1986, pp. 384-392.

47   "Instron Models 4201 and 4202, Operator's guide," Instron Corporation, Canton, MA., 1990.

48   "Canon VM-E708, 8 mm video camera & recorder, Instructions manual," Canon U.S.A, New York, NY., 1993.

49   Urruly, J., Huchon, R., and Pouget, J., "Development of a biaxial tensile testing machine and a non-disturbing displacement method," TAPPI journal, Vol. 79, NO.3, March 1996, pp. 283-89.

50   ASTM Standard E 561-94: Standard practice for R-curve determination, <u>ASTM annual book of standards</u>, Vol. 3.01, ASTM, Philadelphia, PA, 1995.

51   Personal communication, Reynolds metal company, Richmond, VA.

52   Oswin, C.R., "<u>Plastic films and packaging</u>," John Wiley & Sons, 1975.

VITA

Kalrav Buch

Candidate for the Degree of

Master of Science

Thesis: A CONSTRAINED SHORT TENSION TEST FOR PLANE
STRESS FRACTURE TOUGHNESS TESTING OF THIN
MATERIALS

Major Field: Mechanical Engineering

Biographical

Personal Data: Born in Amdavad, Gujarat, India, September 20, 1973,
the son of Jay and Bakula Buch.

Education: Graduated from Gujarat College, Amdavad, India in March
1990; received Bachelor of Engineering in Mechanical Engineering
with distinction from L. D. College of Engineering, Gujarat University,
Amdavad, India in October 1994; Completed the requirements for
the Master of Science degree with a major in Mechanical
Engineering at Oklahoma State University in May 1998.

Experience: Teaching Assistant for Material science. Department of
Mechanical and Aerospace Engineering, Oklahoma State University,
January 1996 to December 1997; Lecturer in Mechanical
Engineering, College of Hi-Tech Engineering, Amdavad, India,
December 1994 to December 1995.

Professional Memberships: American Society of Metals, American
Society of Mechanical Engineers and The Minerals, Metals and
Materials Society.